Describing and Evaluating Media Roughness Contributions to Granular Media Filtration

by

Chao Jin

A thesis

presented to the University of Waterloo

in fulfillment of the

thesis requirement for the degree of

Doctor of Philosophy

in

Civil Engineering

Waterloo, Ontario, Canada, 2014

AUTHOR'S DECLARATION

I hereby declare that I am the sole author of this thesis. This is a true copy of the thesis, including any required final revisions, as accepted by my examiners.

I understand that my thesis may be made electronically available to the public.

Abstract

The transport and fate of particles including microorganisms during physico-chemical filtration in natural and engineered aquatic environments remains essential for effective and sustainable drinking water treatment and wastewater reclamation, as well as understanding and assessing the risk of environmental contamination of water supplies. The development of models to predict particle deposition by physico-chemical filtration has been ongoing since the 1960's. What is now considered classical colloid filtration theory (CFT) was developed in the 1970's to predict particle removal during granular media filtration used for drinking water treatment. More recently, CFT has been applied to various applications related to subsurface particle and microbial transport and fate, including riverbank filtration, aquifer storage and recovery, bioremediation, and assessment of contaminant transport and fate. Significant discrepancies between predictions of particle deposition from current CFT models and experimental observations have been reported. While several model variations of CFT have been reported, models focusing on integration of impacts of collector surface geometry and physically-based mechanisms such as hydrodynamics have been rarely reported.

The overall goal of this work was to describe and evaluate the contribution of media grain (collector) surface roughness on particle removal by physico-chemical filtration. Four phases of experiments were conducted to investigate the impacts of surface roughness on particle deposition in porous media and parallel plate systems. Bench scale "proof of concept" experiments (Phase I) were conducted using small filtration columns, two sizes of colloidal particles (1.0 and 4.5 μm diameter polystyrene microspheres), two sizes of glass beads (0.71 to 0.85 mm and 0.5 to 0.595 mm), and three different levels of surface roughness. The experiments demonstrated that surface roughness not only enhanced particle deposition, but also decreased it. Classic colloid filtration theory, chemical heterogeneity, and hydrophobicity fail to explain this non-linear, non-monotonic impact of surface roughness on particle deposition; particularly decreased deposition resulting from increased surface roughness. The results indicated the existence of a minimum particle deposition efficiency

that is unique to each combination of sizes of colloidal particle, collector, and collector roughness. To verify this research finding, particle deposition experiments were conducted using a parallel plate chamber (Phase II) to further confirm and characterize the contribution of surface roughness to particle deposition. The impacts of different nano-scale quartz surface roughness sizes (10, 20, 50, 200 and 400 nm) on deposition kinetics of three sizes (0.55, 0.985 and 1.765 μm) of polystyrene microspheres suspended in 100 mM KCl were examined. A non-linear, non-monotonic relationship between surface roughness and particle deposition flux was again observed. A critical roughness size associated with a minimum deposition flux was identified for the experimental conditions investigated.

A numerical model approach incorporating the effect of surface roughness on flow field profile, hydrodynamic retardation functions, and DLVO interaction energy was developed for a parallel plate chamber system (Phase III). Key physical and chemical properties of the flow field, colloids and the modified rough surface were precisely measured and utilized in the simulation. Changes to the flow field, the hydrodynamic retardation functions, and the DLVO interaction energy due to the presence of nano-scale collector surface roughness were implemented in the developed model. The numerical solutions obtained using the developed model had excellent agreement with the experimental results obtained in research Phase II. This work provided a mathematical framework that was more applicable to real practice by including the effect of the collector surface roughness on particle deposition. The importance of the gravity effect was identified, underscoring the importance of precise measurements of particle size and density for model development.

The verified model framework developed for a parallel plat chamber in Phase III was extended to spherical geometry and utilized to simulate particle deposition behavior in porous media in Phase IV. Functions that were validated in Phase III for the flow field profile, the hydrodynamic retardation functions, and the DLVO interaction energy were utilized. Various operational scenarios including particle size, loading rate and ionic strength were investigated. The Phase IV results could also be used to explain experimental results observed in the porous media experiments (Phase I). It was found that the presence of nano-scale surface roughness was able to improve the particle deposition on spherical collectors;

the enhancement became more significant when roughness element height increased. Overall, this work demonstrated that nano-scale surface roughness and associated hydrodynamics can impact on particle deposition. These impacts can and should be incorporated into predictive mathematical models of clean bed colloidal particle deposition.

Acknowledgements

The final completion of this thesis would have been impossible without the support of several individuals and institutions. First and foremost, I would like to thank my Ph.D supervisor, Dr.Monica Emelko and Dr. Carolyn Ren for giving me the opportunity to work under their guidance. I greatly appreciate the support and encouragement that I was given during the last five years. Their guidance has helped me gradually grow into a capable research and a professional.

I would also like to thank the other members of my advisory committee for their support and interest in this work. My sincere thanks go to Dr. James Craig for providing numerical modeling advices. I greatly appreciate Dr. Hyung-Sool Lee's suggestions on practical application of my research. I would also like to thank my external examiner Dr. Zhongchao Tan and Dr. Ronald Harvey whose comments and suggestions were truly appreciated.

The financial support from National Sciences and Engineering Research Council, the American Water Association Research Foundation, the University of Waterloo and China Scholarship Council made this research possible.

This work would have also been impossible without the support of Dr. Tom Glawdel from the Waterloo Microfluidics lab. I am indebted to you for your commitment to this work and suggestions from the perspective of fluid mechanics. You insights and perspectives were instrumental to the full completion of my research objectives.

I would also like to express my appreciation to Dr. Maria Mesquita, who provided meaningful discussion towards to my research at early stage and constantly supported me on the experiments during my entire studies. Her assistance on English writing and presenting during my comprehensive exam was invaluable and her outlook on life and research was truly motivating.My whole experience would not have been rewarding without the help of Dr. Alexander Wong in Department of Systems Design Engineering who helped me with the computer coding for image numeration and Dr. Cui Bo in Department of Electrical and Computer Engineering who assisted me for the chip fabrication. Great thanks to Dr. Stefano

Normani who is always willing to help out and his continued willingness to provide suggestions on a variety of issues ranging from trajectory analysis code to constellation.

My gratitude to my fellow colleagues in civil engineering, Alex H.S. Chik, Andrew WT Wong, Kate Geng, Mark Spanjers, Nicole MeLellan and Leslie Gray and also the colleagues in Waterloo Microfluidics lab who provided valuable input with regards to my work: Zeyad Almutairi, Mostafa Shameli, Cody Chen and Ning Qin. Many thanks to Peng Peng in Centre for Advanced Materials Joining who helped me with numbers of experiments. It was great pleasure to work with you and discuss the academic issues towards to future research. I would also like to acknowledge the support of several individuals who spent hundreds hours helping me with the particle numerations, Justin Kim. Guoshu Bin, Kathy Hui, Darrell Cheng and Jessica Mcleod.

I would like to express my appreciation to all the staff members in Civil engineering department. Whenever I had a technical or administrative question, the civil fellows were always willing to help me out. I am indebted to Trey Ridgway, Mark Sobon, Mark Merlau who helped with the experimental set-up, dealing with the “Dangerous HF acid” and also Paul Thompson and Kevin Rampersad who supported me on the computing issues. Thanks a lot to Victoria Tolton whose smile and support really helpful for all the administrative issues.

Pursing a PhD degree in English is a long and very often frustrating, lonely and repetitive journey especially to an international student who is 10000 miles away from home. I would like to extend my thanks to several friends that I met during my study and made my life more enjoyable, Shunhao Ni, Qi Sun, Lei Liu, Chenyi Liu and Junjie Zhao.

I am deeply grateful to all my family members whose support is truly appreciated. I would especially like to my wife Dr.Weiwei Du(杜惟玮) whose love, support, and company has been one of the greatest sources of strength for me. Without your cheer and encouragement, I will never go this far from all perspectives.

Finally, my sincere gratitude is extended to my parents Guoxiang Jin(金国祥) and Xin He (何鑫) who have been always behind me all the way.

Table of Contents

List of Figures

List of Tables

Chapter 1
Introduction

1.1 Granular media filtration for water treatment

Granular media filtration (GMF) has been used for thousands of years as a separation process to remove small colloidal particles from fluids (1). In natural environments, colloids are fine particles in the size range of 10 nm to ~10μm and include silicate clays, Fe and Al oxides, mineral precipitates, humic materials and pathogenic microorganisms such as viruses, bacteria and protozoa (2).The presence and accumulation of colloids in water supplies can impact human health and drinking water treatment system operation (3-5). It has been estimated that over half of the global outbreaks of waterborne disease have been caused by the contamination of drinking water supplies with pathogenic bacteria and or viruses, which are bio-colloids (6, 7). Colloids can also accelerate the transport of heavy metals, recalcitrant synthetic organics and nutrients through porous and fractured media (4, 8-11).

Increasingly stringent regulations necessitate a multi-barrier approach to protect drinking water from chemical and biological contamination (USEPA, 2000; IESWTR 1998; LT2ESWTR). To achieve this ultimate goal, treatment technologies for colloidal particle removal should be resilient, meaning they can consistently provide high quality finished water to protect public health To be sustainable, treatment technologies should also be cost-effective for application in both large- and small-sized communities. GMF, that is engineered and chemically assisted or naturally occurring in the subsurface, is one of few technologies that can concurrently achieve these objectives (12, 13).

GMF can effectively achieve up to 5 log (99.999%) removal (or more) of colloidal particles, including some pathogens, from water (14-16). Several types of GMF systems are used during contemporary drinking water treatment, they include: rapid sand filtration (deep bed, multi-media, dual media), biological filtration, and riverbank filtration (12, 17). Operational conditions (e.g., chemical pre-treatment, water chemistry, hydraulic loading rate, backwash strategies *etc.*) and filter design (e.g., media type, size, hardness, density, uniformity *etc.*) can affect colloid removal by filtration(12). A thorough understanding of filter design and

operation effects on process performance is critical to ensuring optimal filtration performance and maximal protection of public health by provision of consistently safe drinking water.

The concept of single collector efficiency (η) quantitatively describes the colloid removal efficiency of a single grain of a filtration medium (i.e., a collector). This concept has been applied to the study of various natural filtration scenarios in the subsurface (e.g., fractures(18-20) and karst(21, 22), the vadose zone(1, 23, 24) and riverbank filtration(25)) to quantitatively describe the migration behavior of colloids. This concept has also been applied to several aspects of: wastewater treatment (26, 27), wastewater reuse (28), landfill leachate treatment (29), magnetic separation of particles (30), chemical-mechanical planarization in the semiconductor industry (31), and surface treatments for polishing (32), as well as magnetic separation of submicron particles (30), particle transport during oil extraction (33, 34), particle cycling in marine chemistry studies (35, 36), and particle transport in the lungs(37). Accordingly, the importance of developing accurate tools for quantitatively describing colloid removal and deposition on surfaces such as filtration media extends well beyond water treatment applications, which are the focus of the present investigation.

Since the first theoretical studies of GMF in the 1930s(1), four types of modeling approaches have been developed to describe particle deposition during GMF: macroscopic models (1), Eulerian models (38, 39), Lagrangian models (40-42) and regression models (43-45). Macroscopic models are not predictive in nature and are limited to specific systems operating under well-defined conditions because they are fitted models; accordingly, they are not commonly used(1, 46). Eulerian and Lagrangian models both describe colloid deposition behavior by simulating the forces/interactions exerted on colloids with numerical formulations; however, Eulerian models describe particle concentration in time and space. In contrast, Lagrangian models describe individual particle trajectory; they describe the colloid deposition behavior by simulating the forces/interactions exerted on colloids with numerical formulations(47, 48). Both of these two methods are predicative in nature, but require extensive computing capacity. The most commonly used models for describing colloid deposition during GMF are regression models developed as the best fit to numerical solutions

from either Eulerian or Lagrangian models. These models involve numerical simulation, but are much less computationally demanding than Eulerian and Lagrangian models and can yield reasonable approximations of observed data in most cases. Accurate and reliable solutions for these models depend on fundamental understanding of the forces/interaction/mechanisms that act upon on colloidal particles during the physico-chemical filtration process.

Deviations between experimental observations and existing filtration theory predictions have been extensively reported (5, 47, 49, 50). Several mechanisms have been suggested to explain the discrepancies between numerical models and experimental results including chemical heterogeneity (51, 52), short range forces (53), surface roughness (54, 55), and hydrophobicity (56). The majority of current theoretical explanations focus changes in DLVO interaction energy to help explain particle deposition behavior on surfaces such as porous media; however, significant discrepancies between numerical models and experimental results remain common. Other factors that can also influence particle deposition behavior on surfaces such as porous media include physical aspects of the system, such as changes in the flow field, hydrodynamic effects, and physical entrapment. Among these, media surface roughness is one key system attribute that merits further investigation (47, 57-61).

1.2 Research objectives

The overall goal of this research was to describe and evaluate the contribution of granular media roughness to particle removal. While this goal has numerous application areas, it is discussed here in the context of drinking water treatment. This knowledge can ultimately improve models for optimizing colloidal particle removal by filtration and enable their incorporation into practical filter design and operation strategies or assessments of colloid and nano-particle fate and transport in the subsurface. Specific objectives in pursuit of this research goal were:

1) To define granular filtration media “surface roughness” conceptually to categorize various types of media roughness (e.g., smooth or rough media).

2) To design and commission a bench-scale filtration system for evaluating granular media particle removal performance and for determining the impacts of media surface roughness parameters on filtration process.

3) To develop a mathematical model for physico-chemical filtration that includes the contributions of nano-scale roughness to particle deposition on granular media.

4) To experimentally validate the developed mathematical model for physico-chemical filtration that includes the contributions of nano-scale roughness to particle deposition on granular media.

5) To compare the outcomes from the mathematical model for physico-chemical filtration that includes the contributions of nano-scale roughness to those obtained by existing models for particle deposition on granular media.

1.3 Research approach

To meet these research objectives, four phases of investigation were conducted. These were:

Phase I. Proof-of concept investigation: Bench-scale column tests using packed media of the same material, but with different surface roughness were conducted at identical operating conditions to definitively demonstrate that different scales of surface roughness can impact particle deposition behaviour. Model colloids (polystyrene microspheres) were suspended in a high ionic strength (100mM KCl) solution to maximize deposition potential by minimizing electrostatic double layer thickness around the particles and exclude the impact of electrostatic interactions with the collector surface.

Phase II. Verification experiments: Particle deposition experiments were conducted using a parallel plate chamber to further confirm and characterize the contribution of surface roughness to particle deposition. Model colloids (polystyrene microspheres) suspended in a high ionic strength (100mM KCl) solution and plates fabricated with patterned nano-scale roughness were used in these experiments. The use of parallel plates enabled detailed analytical description of

the flow profile in the chamber. Extensive quality assurance and control efforts ensured that other factors such as chemical heterogeneity and hydrophobicity on the collector surface as well as physical trapping, blocking and particle aggregation did not contribute to experimental observations and were excluded from the data interpretation. The contribution of roughness to particle deposition was incontrovertibly demonstrated and quantified by avoiding confounding mechanisms such as the complex effects of flow, physical trapping (staining and wedging), chemical heterogeneity and hydrophobicity.

Phase III. Numerical simulations for particle deposition in parallel plate chamber: Particle deposition in the parallel plate chamber (observed during Phase II) was numerically simulated. Key physical and chemical properties of the flow field, colloids and the modified rough surface were precisely measured and utilized in the simulation. Changes to the flow field, hydrodynamic retardation functions and DLVO interaction energy due to the presence of nano-scale roughness were implemented in the developed model. The contribution of each component on particle deposition was evaluated individually and collectively. A numerical framework was developed in Phase III that can provide a platform to verify the numerical simulation outcomes by comparing to the experimental result from Phase II with improved understanding of deposition mechanisms.

Phase IV. Numerical simulations for particle deposition in porous media: Particle deposition in spherical geometry was simulated. The Phase III simulations demonstrated that the numerical expressions of flow field, hydrodynamic retardation functions and DLVO interaction energy curves could be modified to account for nano-scale surface roughness. These modifications were utilized during Phase IV to quantitatively investigate the contributions of media surface roughness on particle deposition on spherical collectors at water quality conditions that are favourable for particle deposition (i.e. high ionic strength). The work in Phase IV demonstrates the importance of incorporating surface roughness into the Convection-Diffusion equation, with accurate representation of its associated impacts on the flow field,

hydrodynamic retardation, and DLVO forces. The impacts of operational conditions including particle size, particle loading rate (i.e., approach velocity), and background electrolyte solution on particle deposition were evaluated at several roughness sizes. The outcome obtained in Phase IV can be used to better explain the non-linear, non-monotonic relationship between roughness size and particle deposition.

1.4 Thesis structure

This thesis is comprised of eight chapters. A comprehensive literature review is presented in Chapter 2. The forces, interactions and mechanisms impacting particle deposition behavior are discussed. This is followed by a critical review of existing filtration models that have been utilized to describe particle deposition during granular media filtration. Potential reasons for the discrepancy between model solutions and empirical observations are discussed. Factors that affect particle deposition on surfaces are briefly introduced. Knowledge regarding the effect of surface roughness on particle deposition is then summarized.

Experimental results obtained from the porous media (Phase I) and parallel plate (Phase II) experimental investigations are elaborated upon in Chapter 3 and 4, respectively. A model incorporating the effect of surface roughness on particle deposition is developed for the parallel plate chamber in Chapter 5 (Phase III) and verified with the data presented in Chapter 4. The verified model framework is then utilized and adjusted to simulate spherical geometry (Phase IV); the adjusted model is presented in Chapter 6. Various operational scenarios are investigated using this model and are also illustrated in Chapter 6, where they are used to explain the results observed in the porous media experiments (Phase I). Chapters 3 through 6 are presented in a paper format. Chapter 7 summarizes the conclusions and contributions from this thesis work. Research implications and further recommendations are presented in Chapter 8.

1.5 Nomenclature

a_c : collector radius [m]

b : thickness of fluid shell surrounding the collector [m]

ε : overall porosity of packed media [-]

r : center-to-center distance between the approaching particle and collector [m]

V_r : radial particle velocity components [m/s]

V_θ : tangential particle velocity components [m/s]

ψ : Stokes stream function for flow field [-]

u, v,w : velocity components on the direction of x,y,z in Cartesian coordinate [m/s]

V_{avg} : the average flow velocity [m/s]

b : half channel height in parallel plate chamber [m]

z : vertical distance to the bottom surface in parallel plate chamber [m]

i , j : different components of contact bodies for VDW force calculation

A : Hamaker constant [J]

$A_{collector-colloid-water}$: modified Hamaker constant between collector, colloid and water [J]

$A_{collector-colloid}$: modified Hamaker constant between collector and colloid [J]

$A_{water-water}$: Hamaker constant between water and water [J]

$A_{colloid-colloid}$: Hamaker constant between colloid and colloid [J]

h : separation distance [m]

H : dimensionless separation distance [-]

k_b : Boltzmann constant [J/K]

T : absolute temperature [K]

ψ : electrostatic potential of flat surface,

ρ : density of fluid [kg/m^3]

ε_{Vacuum} : permittivity of the dielectric medium of vacuum

ε_0 : permittivity of the dielectric medium of water [C/Vm]

u_i : chemical potential [J]

u_i^0 : standard chemical potential at 273K [J]

z_i : the valence of ion *I*

n_i : number of ions of type *i* per unit volume

κ: Debye-Hückel length [m]

ψ_1 and ψ_i : chemical potentials of the two spheres [V]

ψ_S and ψ_P : chemical potentials of sphere and plates [V]

h: absolute distance between particle and target surface [m]

H : dimensionless distance normalized by the particle radius [-]

ρ_p and ρ_w : densities of colloidal particle and fluid [kg/m^3]

g : gravitational acceleration vector [m/s^2]

$E(h)$: interaction energy per unit area between two flat plates [J/m2]

$F(h)$: applied force between two spheres [N]

F_{Lift} : shear lift force,

μ :dynamic viscosity of fluid [Ns/m^2]

v : kinematic viscosity of fluid [m^2/s]

$G = du_1 / dy$: wall-normal gradient of the streamwise fluid velocity [m/s^2]

$U_s = v_1 - u_1$: difference in the instantaneous streamwise velocity between the center of particle and fluid [m/s]

l : distance between particle center and wall [m]

$\kappa = a_p / l$

$\Lambda = a_p U_s / G$

$\mathrm{Re} = \gamma_0 a_p{}^2 / v$: dimensionless number of inertia effect over viscosity [-]

$\gamma_0 = u / H$: dimensionless flow velocity [-]

$f_1(H)$ $f_2(H)$ $f_3(H)$ and $f_4(H)$: hydrodynamic retardation functions [-]

D_∞ is the Stoke-Einstein diffusion coefficient [m^2/s]

C: particle concentration [particle/m^3]

Sh: dimensionless Sherwood number [-]

$\overline{Sh}$: average Sherwood number [-]

$\vec{j}$: particle flux vector [mol/m^{2}s]

δ: dimensionless location of perfect sink boundary location [-]

$Gr = \frac{\vec{F}_g * a_p}{k_b T}$: dimensionless gravity force [-]

$DLVO = -\frac{d\Psi}{dy} * \frac{a_p}{k_b T}$: dimensionless DLVO force [-]

$z^* = \frac{z}{a_p}$: dimensionless vertical distance [-]

$x^* = \frac{x}{b}$: dimensionless distance along the flow direction [-]

$a_p^* = \frac{a_p}{b}$:dimensionless particle radius [-]

$c^* = \frac{c}{c_\infty}$: dimensionless particle concentration [-]

$N_R = \frac{a_p}{r}$: scaled particle ratio [-]

$V_r = \frac{v_r}{U}$: scaled radial velocity component [-]

$V_\theta = \frac{v_\theta}{U}$: scaled tangential velocity component [-]

$N_{Pe} = \frac{2Ua_p}{D_\infty}$:scaled Pelect number

$N_R = d_p / d_c$: ratio of convection over diffusion

$N_{VDW} = 4\pi {a_p}^4 (\rho_p - \rho_f) g / 3k_B T$: ratio of VDW force over thermal energy

$N_A = \frac{A}{12\pi {a_p}^2 U}$: ratio of combined influence VDW force and fluid velocity on particle deposition

$N_{Gr} = \frac{2}{9} \frac{{a_p}^2 (\rho_p - \rho_f) g}{\mu U}$:ratio of stokes particle setting velocity over approaching velocity

$N_{Lo} = A/9\pi\mu a_P^2 U$: Dimensionless VDW force number

$N_{DL} = \kappa a$: dimensionless EDLO force parameter

$N_{diff} = v_{pdiff} d_f / De$: dimensionless Diffusiophoresis number

F^{VDW} : VDW force between approaching particle and collector [N]

U^{VDW} : VDW interaction energy between approaching particle and contact surface [kT]

$F_G^* = \frac{F_G a_p}{kT}$: scaled gravity number

$\Phi = \frac{\varphi}{k_B T}$: scaled interaction energy

$J^*\left(H_\delta, \theta\right)$:dimensionless deposition flux

$\eta = \frac{I}{\pi a_c^2 Uc}$: single collector efficiency

η_D : single collector efficiency of transport by diffusion

η_I : single collector efficiency of transport by interception

η_G : single collector efficiency of transport by sedimentation due to gravity

α is the attachment efficiency

$\lambda = \lambda_0 F(a, \sigma)$: filter coefficient (m^{-1})

λ_0: initial value of filter coefficiency (m^{-1})

$F(\alpha, \sigma)$: the fitting function of filter coefficient

v_s : superficial liquid velocity (m/s)

$V_\theta^{'}(r)$: modified radial velocity component,

r_{slip} : dimensionless slip-length

m : particle mass for trajectory analysis

m^*: virtual mass for trajectory analysis

F_{VDW} : VDW force

F_{EDL} : EDL force

F_{Short} : short range force

F_{Short} : Brownian motion force

F_{drag} : drag force

Q : the reaction rate for particle deposition

t: the reaction time for particle deposition

r_{slip} : dimensionless slip-length

$r_{Roughness}$:dimensionless roughness length

F_{slip} : modified hydrodynamic force using slip boundary condition

$F_{no-slip}$: hydrodynamic force using no-slip boundary condition

F_{new} : modified hydrodynamic force using slip length for approximation

$F_i(h)$: modified hydrodynamic retardation functions using slip length

GMF: Granular media filtration

DI: Derjaguin's integration

SEI: surface element integration

VDW: Van der Waals force

EDL: Electrostatistic double layer force

SWTR: Surface Water Treatment Rule

GAC: granular active carbon

HHF approximation: Hogg-Healy-Fuerstenau expression for DLVO interaction energy

DLVO: the name for interfacial force after Derjaguin and Landau, Verwey and Overbeek.

USEPA : the US Environmental Protection Agency

SWTR : the Surface Water Treatment Rule

IESWTR : the Interim Enhanced Surface Water Treatment Rule

LT1ESWTR: the long-term 1 Enhanced Surface Water Treatment Rule

LT2ESWTR: the long-term 2 Enhanced Surface Water Treatment Rule

1.6 References

1. Tien, C. and Ramarao, B.V. *Granular filtration of aerosols and hydrosols.* Access Online via Elsevier: 2011; .

2. Mccarthy, J.F. and Zachara, J.M. Subsurface Transport of Contaminants - Mobile Colloids in the Subsurface Environment may Alter the Transport of Contaminants. *Environ. Sci. Technol.* **1989,** *23* (5), 496-502.

3. Schijven, J.F. and Hassanizadeh, S.M. Removal of viruses by soil passage: Overview of modeling, processes, and parameters. *Crit. Rev. Environ. Sci. Technol.* **2000,** *30* (1), 49-127.

4. Emelko, M.B.; Huck, P.M.; Coffey, B.M. A review of Cryptosporidium removal by granular media filtration. *Journal American Water Works Association* **2005,** *97* (12), 101-+.

5. Tufenkji, N. Modeling microbial transport in porous media: Traditional approaches and recent developments. *Adv. Water Resour.* **2007,** *30* (6-7), 1455-1469; 10.1016/j.advwatres.2006.05.014.

6. Keswick, B.H. and Gerba, C.P. Viruses in Groundwater. *Environ. Sci. Technol.* **1980,** *14* (11), 1290-1297.

7. Rochelle, P. and Clancy, A. The evolution of microbiology in the drinking water industry. *Journal American Water Works Association* **2006,** *98* (3), 163-+.

8. Harvey, R.W. and Garabedian, S.P. Use of Colloid Filtration Theory in Modeling Movement of Bacteria through a Contaminated Sandy Aquifer. *Environ. Sci. Technol.* **1991,** *25* (1), 178-185.

9. Penrose, W.R.; Polzer, W.L.; Essington, E.H.; Nelson, D.M.; Orlandini, K.A. Mobility of Plutonium and Americium through a Shallow Aquifer in a Semiarid Region. *Environ. Sci. Technol.* **1990,** *24* (2), 228-234.

10. Ryan, J.N. and Elimelech, M. Colloid mobilization and transport in groundwater. *Colloids and Surfaces A-Physicochemical and Engineering Aspects* **1996,** *107*, 1-56.

11. Sunnotel, O.; Lowery, C.J.; Moore, J.E.; Dooley, J.S.G.; Xiao, L.; Millar, B.C.; Rooney, P.J.; Snelling, W.J. Cryptosporidium. *Lett. Appl. Microbiol.* **2006,** *43* (1), 7-16; 10.1111/j.1472-765X.2006.01936.x.

12. Crittenden, J.C.; Trussell, R.R.; Hand, D.W.; Howe, K.J.; Tchobanoglous, G. *MWH's Water Treatment: Principles and Design.* Wiley. com: 2012; .

13. Edzwald, J.K. *Water Quality & Treatment: A Handbook on Drinking Water*. McGraw-Hill New York: 2011; .

14. Betancourt, W.Q. and Rose, J.B. Drinking water treatment processes for removal of Cryptosporidium and Giardia. *Vet. Parasitol.* **2004,** *126* (1–2), 219-234; http://dx.doi.org/10.1016/j.vetpar.2004.09.002.

15. Rose, J.B.; Dickson, L.J.; Farrah, S.R.; Carnahan, R.P. Removal of pathogenic and indicator microorganisms by a full-scale water reclamation facility. *Water Res.* **1996,** *30* (11), 2785-2797.

16. Emelko, M.B. Removal of viable and inactivated Cryptosporidium by dual- and tri-media filtration. *Water Res.* **2003,** *37* (12), 2998-3008; http://dx.doi.org/10.1016/S0043-1354(03)00113-1.

17. DeNovio, N.M.; Saiers, J.E.; Ryan, J.N. Colloid movement in unsaturated porous media: Recent advances and future directions. *Vadose Zone Journal* **2004,** *3* (2), 338-351.

18. Zheng, Q.; Dickson, S.E.; Guo, Y. Differential transport and dispersion of colloids relative to solutes in single fractures. *J. Colloid Interface Sci.* **2009,** *339* (1), 140-151; 10.1016/j.jcis.2009.07.002.

19. Li, B.; Jiang, Y.; Koyama, T.; Jing, L.; Tanabashi, Y. Experimental study of the hydro-mechanical behavior of rock joints using a parallel-plate model containing contact areas and artificial fractures. *Int. J. Rock Mech. Min. Sci.* **2008,** *45* (3), 362-375; 10.1016/j.ijrmms.2007.06.004.

20. Rodrigues, S. and Dickson, S. A Phenomenological Model for Particle Retention in Single, Saturated Fractures. *Groundwater* **2013,** .

21. McCarthy, J.F. and McKay, L.D. Colloid transport in the subsurface. *Vadose Zone Journal* **2004,** *3* (2), 326-337.

22. Vesper, D.J. and White, W.B. Metal transport to karst springs during storm flow: an example from Fort Campbell, Kentucky/Tennessee, USA. *Journal of Hydrology* **2003,** *276* (1), 20-36.

23. Edzwald, J.K. Principles and applications of dissolved air flotation. *Water Science and Technology* **1995,** *31* (3), 1-23.

24. Berkowitz, B. Characterizing flow and transport in fractured geological media: A review. *Adv. Water Resour.* **2002,** *25* (8), 861-884.

25. Tufenkji, N.; Ryan, J.N.; Elimelech, M. The promise of bank filtration. *Environ. Sci. Technol.* **2002,** *36* (21), 422A-428A.

26. Çeçen, F. *Activated carbon for water and wastewater treatment: Integration of adsorption and biological treatment.* Wiley. com: 2011; .

27. Bouwer, E.J. Theoretical investigation of particle deposition in biofilm systems. *Water Res.* **1987,** *21* (12), 1489-1498.

28. Redman, J.A.; Grant, S.B.; Olson, T.M.; Estes, M.K. Pathogen filtration, heterogeneity, and the potable reuse of wastewater. *Environ. Sci. Technol.* **2001,** *35* (9), 1798-1805.

29. Gounaris, V.; Anderson, P.R.; Holsen, T.M. Characteristics and environmental significance of colloids in landfill leachate. *Environ. Sci. Technol.* **1993,** *27* (7), 1381-1387.

30. Moyer, C.; Natenapit, M.; Arajs, S. Filtration of submicron particles by spheres in HGMS. *J Magn Magn Mater* **1986,** *61* (3), 271-277.

31. Matijević, E. and Babu, S. Colloid aspects of chemical–mechanical planarization. *J. Colloid Interface Sci.* **2008,** *320* (1), 219-237.

32. Lu, Z.; Ryde, N.P.; Babu, S.; Matijevic, E. Particle adhesion studies relevant to chemical mechanical polishing. *Langmuir* **2005,** *21* (22), 9866-9872.

33. Minssieux, L.; Nabzar, L.; Chauveteau, G.; Longeron, D.; Bensalem, R. Permeability damage due to asphaltene deposition: Experimental and modeling aspects. *Oil & Gas Science and Technology* **1998,** *53* (3), 313-327.

34. Lawal, K.A.; Vesovic, V.; Boek, E.S. Modeling Permeability Impairment in Porous Media due to Asphaltene Deposition under Dynamic Conditions. *Energy Fuels* **2011,** *25* (12), 5647-5659.

35. Honeyman, B. and Santschi, P. A Brownian-pumping model for oceanic trace metal scavenging: Evidence from Th isotopes. *J. Mar. Res.* **1989,** *47* (4), 951-992.

36. Quigley, M.S.; Santschi, P.H.; Guo, L.; Honeyman, B.D. Sorption irreversibility and coagulation behavior of< sup> 234</sup> Th with marine organic matter. *Mar. Chem.* **2001,** *76* (1), 27-45.

37. Hofmann, W. Modelling inhaled particle deposition in the human lung—a review. *J. Aerosol Sci.* **2011,** *42* (10), 693-724.

38. Elimelech, M. and Song, L. Theoretical investigation of colloid separation from dilute aqueous suspensions by oppositely charged granular media. *Separations Technology* **1992,** *2* (1), 2-12; http://dx.doi.org.proxy.lib.uwaterloo.ca/10.1016/0956-9618(92)80001-T.

39. Song, L.; Johnson, P.; Elimelech, M. Kinetics of Colloid Deposition Onto Heterogeneously Charged Surfaces in Porous-Media. *Environ. Sci. Technol.* **1994,** *28* (6), 1164-1171; 10.1021/es00055a030.

40. Payatake.Ac; Tien, C.; Turian, R.M. Trajectory Calculation of Particle Deposition in Deep Bed Filtration .1. Model Formulation. *AICHE J.* **1974,** *20* (5), 889-900.

41. Rajagopalan, R. and Tien, C. Trajectory Analysis of Deep-Bed Filtration with Sphere-In-Cell Porous-Media Model. *AICHE J.* **1976,** *22* (3), 523-533.

42. Ma, H.L.; Pedel, J.; Fife, P.; Johnson, W.P. Hemispheres-in-Cell Geometry to Predict Colloid Deposition in Porous Media (vol 43, pg 8573, 2009). *Environ. Sci. Technol.* **2010,** *44* (11), 4383-4383; 10.1021/es1009373 ER.

43. Tufenkji, N. and Elimelech, M. Correlation equation for predicting single-collector efficiency in physicochemical filtration in saturated porous media. *Environ. Sci. Technol.* **2004,** *38* (2), 529-536; 10.1021/es034049r.

44. Rajagopalan, R. and Tien, C. Single Collector Analysis of Collection Mechanisms in Water Filtration. *Can. J. Chem. Eng.* **1977,** *55* (3), 246-255.

45. Nelson, K.E. and Ginn, T.R. New collector efficiency equation for colloid filtration in both natural and engineered flow conditions. *Water Resour. Res.* **2011,** *47* (5).

46. Jegatheesan, V. and Vigneswaran, S. Deep bed filtration: Mathematical models and observations. *Crit. Rev. Environ. Sci. Technol.* **2005,** *35* (6), 515-569; 10.1080/10643380500326432 ER.

47. Elimelech, M.; Jia, X.; Gregory, J.; Williams, R. *Particle deposition & aggregation: measurement, modelling and simulation.* Butterworth-Heinemann: 1998; .

48. Masliyah, J.H. and Bhattacharjee, S. *Electrokinetic and colloid transport phenomena.* John Wiley & Sons: 2006; .

49. Johnson, W.P.; Tong, M.; Li, X. On colloid retention in saturated porous media in the presence of energy barriers: The failure of alpha, and opportunities to predict eta. *Water Resour. Res.* **2007,** *43* (12), W12S13; 10.1029/2006WR005770.

50. Tufenkji, N. and Elimelech, M. Breakdown of colloid filtration theory: Role of the secondary energy minimum and surface charge heterogeneities. *Langmuir* **2005,** *21* (3), 841-852; 10.1021/la048102g.

51. Nazemifard, N.; Masliyah, J.H.; Bhattacharjee, S. Particle deposition onto charge heterogeneous surfaces: Convection-diffusion-migration model. *Langmuir* **2006,** *22* (24), 9879-9893; 10.1021/la061702q ER.

52. Nazemifard, N.; Masliyah, J.H.; Bhattacharjee, S. Particle deposition onto micropatterned charge heterogeneous substrates: Trajectory analysis. *J. Colloid Interface Sci.* **2006,** *293* (1), 1-15; 10.1016/j.jcis.2005.06.033 ER.

53. Hoek, E.M.V. and Agarwal, G.K. Extended DLVO interactions between spherical particles and rough surfaces. *J. Colloid Interface Sci.* **2006,** *298* (1), 50-58; 10.1016/j.jcis.2005.12.031.

54. Henry, C.; Minier, J.; Lefevre, G.; Hurisse, O. Numerical Study on the Deposition Rate of Hematite Particle on Polypropylene Walls: Role of Surface Roughness. *Langmuir* **2011,** *27* (8), 4603-4612; 10.1021/la104488a.

55. Huang, X.F.; Bhattacharjee, S.; Hoek, E.M.V. Is Surface Roughness a "Scapegoat" or a Primary Factor When Defining Particle-Substrate Interactions? *Langmuir* **2010,** *26* (4), 2528-2537; 10.1021/la9028113 ER.

56. Tang, H.; Cao, T.; Liang, X.; Wang, A.; Salley, S.O.; McAllister,James,,II; Ng, K.Y.S. Influence of silicone surface roughness and hydrophobicity on adhesion and colonization of Staphylococcus epidermidis. *Journal of Biomedical Materials Research Part a* **2009,** *88A* (2), 454-463; 10.1002/jbm.a.31788.

57. Scott, D.J. Cryptosporidium and Particle Removal from Low Turbidity Water by Engineered Ceramic Media Filtration. **2008,** .

58. Vinogradova, O.I. and Belyaev, A.V. Wetting, roughness and flow boundary conditions. *Journal of Physics-Condensed Matter* **2011,** *23* (18), 184104; 10.1088/0953-8984/23/18/184104.

59. Johnson, W.P.; Li, X.; Yal, G. Colloid retention in porous media: Mechanistic confirmation of wedging and retention in zones of flow stagnation. *Environ. Sci. Technol.* **2007,** *41* (4), 1279-1287; 10.1021/es061301x.

60. Johnson, W.P.; Ma, H.L.; Pazmino, E. Straining Credibility: A General Comment Regarding Common Arguments Used to Infer Straining As the Mechanism of Colloid

Retention in Porous Media. *Environ. Sci. Technol.* **2011,** *45* (9), 3831-3832; 10.1021/es200868e ER.

61. Bradford, S.A.; Torkzaban, S.; Walker, S.L. Coupling of physical and chemical mechanisms of colloid straining in saturated porous media. *Water Res.* **2007,** *41* (13), 3012-3024; 10.1016/j.watres.2007.03.030.

Chapter 2

Literature review

A literature review focused on granular media filtration (GMF) follows. Starting with the general history of GMF, Section 2.1 summarizes the significance of filtration and the factors used to describe it. To further describe particle deposition on filtration media, Section 2.2 introduces the fundamental steps of transport and attachment/detachment and describes the associated mechanisms. Section 2.3 builds on the previous section and presents detailed description of colloid transport mechanisms and the equations that describe flow field profiles in parallel plate and porous media systems. Section 2.4 and Section 2.5 detail the fundamental interfacial and hydrodynamic forces that govern the fate (i.e. attachment/ detachment on surfaces) of particles suspended in solution. Theoretical models describing particle deposition rate (efficiency) on surfaces are introduced in Section 2.6. In Section 2.7, factors that influence particle deposition on surfaces are summarized. Section 2.8 concludes with a comprehensive review of the current understanding surface roughness contributions to particle deposition on surfaces.

2.1 Introduction

Regarded as a 'robust technology' for removing colloids and waterborne pathogens from water supplies, GMF has been widely used a critical component of the multi-barrier approach to protect drinking water from chemical and biological contaminants(1). Contaminants including metal oxides/precipitates, humic materials and pathogenic microorganisms can be generally considered as "colloidal particles" because they occur in the size range of 10 nm to 10 μm(2, 3). The presence and accumulation of colloids in water supplies can impact human health by introducing water pathogens and sediment-associated heavy metals and nutrients, thereby challenging effective maintenance of drinking water treatment systems(4-6).

Regulations related to drinking water filtration have changed considerably over recent history. In 1852 GMF was first recommended for the treatment of water in London;

specifically, it was suggested that river water supplies should be filtered before municipal distribution(7). In 1989, responding to congressional mandates in the United States (Safe Drinking Water Act Amendments, 1986), the Surface Water Treatment Rule (SWTR) was enacted in recognition that chemical disinfection alone is not effective in the removal of protozoa such as *Giardia lamblia* and *Cryptosporidium parvum*. It required mandatory GM of surface waters and groundwater under the influence of surface water. Stringent regulations for treated water quality continue to be implemented to protect human health from waterborne disease(8). In the United States, the US Environmental Protection Agency (USEPA) promulgated the Surface Water Treatment Rule(SWTR) regulated that treatment plants required to achieved 3-log cyst removal or inactivation (USEPA, 1989). In 1998, the Interim Enhanced Surface Water Treatment Rule (IESWTR) was promulgated to control water quality. In 2000 and 2002, the long-term 1 and long-term 2 Enhanced Surface Water Treatment Rule (LT1ESWTR and LT2ESWTR) were implemented to improve control of microbial pathogens such as *Cryptosporidium* and *E.coli* and 2-year monitoring program is needed to determine the treatment requirements.

Despite of the emergence of alternative technologies such as membranes, UV, and nano-filtration, GMF is still utilized as a relatively robust, affordable, and arguably "green" technology for the treatment of drinking water(7). Various operational factors (*e.g.* filter cycle run time, head loss development, media selection, backwash protocol, *etc.*) can affect filtration performance (7). Comprehensive understanding of filtration processes is required to achieve optimal particle removal performance and establish feasible operational strategies for maintaining process performance. Several operational factors that affect particle removal by filtration have been identified and are summarized in Table 2-1.

Table 2-1. Operational factors affecting particle removal performance in filtration

Factors	Description	Consideration/effect	References
Chemical pretreatment	➢ Coagulation, flocculation, clarification, pH adjustment, charge neutralization	➢ Destabilize particles by compressing the thickness of double layer around the particle / collector or charge reversal	(7, 9-12)
Loading rate	➢ hydraulic shear forces	➢ High or unstable flow rate can deteriorate effluent water quality	(9, 13-15)
Backwashing	➢ Typically an up-flow wash of filtration media with or without media fluidization and/or air or surface scour.	➢ Extend the filter run time by removing all the clogged/ attached particles	(1, 16-18)
Ripening	➢ Initial period of filter operation during which particle removal by filtration shows significant improvement ➢ Effluent turbidity may peak and then decrease until pseudo steady-state performance is achieved ➢ Two separate turbidity peaks (associated with backwash remnants and non-attachment to filter media surfaces) may be present	➢ Remove up to 90% particles ; ➢ Improve overall particle removal by developing favorable surface site for attachment ➢ Prolong filter run cycle	(19-23)

Media type is also important for optimizing particle removal during filtration. It fundamentally affects filter design and operation(22). A number of media–associated factors affect particle removal by GMF and their impacts have been demonstrated at bench-, pilot- and full-scales. These factors include media type, size, size distribution, shape, density, hardness, porosity and surface roughness (Table 2-2)(7, 24-26). Quantitative measurement or description of many of these factors (e.g., size, size distribution, density and hardness) has been standardized; however, standard methods for describing media roughness, shape, and porosity are not presently available.

Filter media characterization and selection for design heavily rely on anecdotal knowledge of filter performance. Accordingly, much of GMF design is empirically based, with very limited consideration of fundamental processes that govern particle removal. Empirical

recommendations are often constrained for specific filter designs or localized water qualities. Improved theoretical explanation of particle removal mechanisms is therefore critical to understanding and optimizing filtration process design and performance; particularly in treatment scenarios without chemical pre-treatment, such as riverbank filtration and aquifer storage and recovery, where the subsurface is relied upon for its natural filtration capacity.

Table 2-2. Media characteristics influencing filtration performance

Factors	Description	Measurement	Reference
Type	➢ Several materials are commonly used in engineered filtration: silica sand, anthracite coal, garnet, granular active carbon (GAC), engineered ceramic media, etc.	➢ Standard methods for sampling, testing ,placement and packing (AWWA B100-96) ➢ Specific standards for GAC (AWWA B604-90.)	(7, 12, 16)
Size	➢ Effective size (ES): the media grain diameter at which 10 percent of the media (d_{10}) within the distribution are smaller by weight. Typically used in engineered filtration. d_{50} is often used to describe porous media in the subsurface. ➢ In engineered filtration, it is typically considered that media depth should be ~1000X larger than media size	➢ Standard sieve analysis: American Society for Testing and Materials Standard Test C136-92.	(27-29)
Size distribution	➢ Uniformity coefficient (UC): d_{60}/ d_{10}.	➢ Standard sieve analysis: American Society for Testing and Materials Standard Test C136-92.	(7, 30)
Shape	➢ Can be described as prolate/ oblate, angular and round. ➢ The ratio of surface area of an equal volume sphere to surface of grain is sometimes used ➢ Shape indictor, sphericity, associated equation (Phi) and angularity are main factors	➢ No standardized method for evaluation.	(7, 12, 31)
Density	➢ No direct influence on filtration performance; however, it does affect backwashing.	➢ ASTM standard Test C128-93.	(1, 7)
Hardness	➢ Indicator of long-term performance capacity.	➢ MOH hardness numbers ➢ hard to apply to small media grain) ➢ Standard measurement for GAC abrasion resistance (AWWA Standard B604-90)	(7)
Porosity	➢ The ratio of void volume to total bed volume. ➢ Related to head loss, backwash flow rate ➢ Affected by grain sphericity, angularity and media type	➢ No standardized methods for evaluation.	(7, 32)
Roughness	➢ No quantitative definition ➢ Represent a combined effect of media numbers, size, density and surface asperity ➢ Coarse media normally provides better removal performance than smooth media	➢ No standardized method for evaluation.	(7)

2.2 The process of physico-chemical filtration

Physico-chemical filtration should not be confused with straining, which is a size exclusion process. Particle removal by physico-chemical filtration has been described as a process that involves two distinct steps: ***transport*** of particles to media grain or "collector" surfaces and ***attachment*** of the particles on collector surfaces. A possible third step may also be included when considering filtration performance over time: ***detachment*** of particles from collector surfaces(33, 34). In suspension, colloids move along fluid streamlines and are transported to the vicinity of collector surfaces(1, 34). Particles can attach to collector surfaces if the net force on the approaching particles is attractive. Particle attachment to collectors is sometimes reversible; in these cases, detachment may occur(20, 35, 36). Figure 2-1 illustrates particle transport, attachment, and detachment during physico-chemical filtration in granular media.

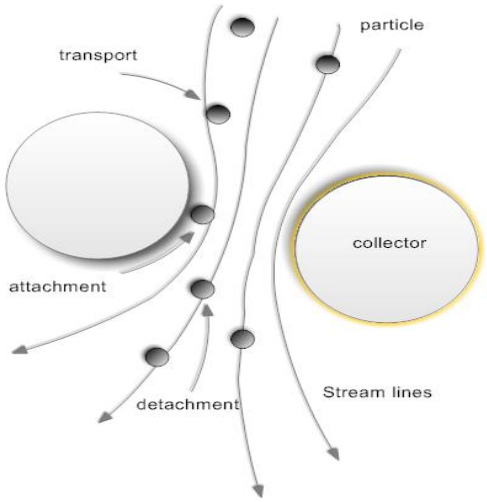

Figure 2-1. Schematic representation of physico-chemical filtration after Amirtharajah (1988)(19)

2.2.1 Particle Transport

Colloidal particle removal from a fluid suspension requires particle transport to within a close distance of a collector surface(33, 37). Summarized in Table 2-3, diffusion, interception (or convection), sedimentation, inertia and hydrodynamics are all mechanisms that contribute to this process(33, 34, 38). In water treatment, diffusion, interception/convection and sedimentation are regarded as the dominant mechanisms that govern particle migration behavior.

Table 2-3. Mechanisms for colloid transport to collector surfaces during physico-chemical filtration

Mechanism	Schematic	Definition	Considerations	Reference
Diffusion	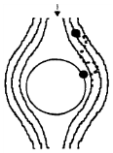	➢ Random motion of small particles brought on by thermal effects	➢ Primary mechanism in granular media filtration; ➢ Effective for particles which are smaller than 1μm	(34, 39, 40)
Interception	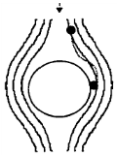	➢ When a particle is close enough to a collector	➢ Akin to straining but valid for small particles	(19, 33, 41)
Sedimentation	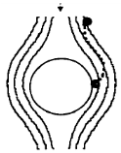	➢ Vertical transport of colloid due to the net force of gravity and buoyant weight on particles	➢ Most significant for large particles (> 1 um in diameter)	(33, 42)
Inertia	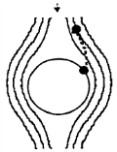	➢ Particles deviate from streamlines because of resistance to change in their state of motion (inertia) and contact a collector	➢ Can been ignored in water treatment model due to the relative slow flow motion	(43, 44)
Hydrodynamics	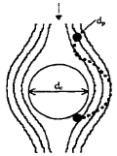	➢ Additional force between colloid and collectors caused by non-uniform shear distributions and complex flow patterns	➢ Definition of the effect of hydrodynamics on particle transport is difficult due to the complexity of media pore geometry; ➢ Not addressed in existing filtration theory	(45, 46)

2.2.2 Particle Attachment and Detachment

When particles are transported to the vicinity of collector surfaces, the net force exerted on the approaching particles determines if particle attachment will occur(47). These particle-solid interfacial forces/interactions include short range forces, long range forces, gravity, and hydrodynamic interactions(33). The consequence of net attractive forces is attachment of the colloid to the collector surface and removal from the bulk suspension(48, 49). Detachment occurs when other, "pull-off" forces (*e.g.*, hydrodynamic forces, Born forces, hydration forces *etc*.)(35, 36, 50) overcome attractive forces, resulting in particle migration back to the bulk suspension. Colloids can experience a repetitive process of capture and release or attachment and detachment, on porous media in packed beds. In later stages of particle deposition in a packed bed (when substantial particle deposition has already occurred within the bed), particle-particle interactions such as attachment between particles, simultaneous detachment, and blocking of deposition sites can also occur; however, those are beyond the scope of the present investigation, which focuses on the early stages of particle deposition on surfaces (i.e, "clean bed" filtration) from dilute particle suspensions.

2.3 Flow velocity profiles

2.3.1 Flow fields in porous media

Understanding and description of the flow field that carries particles to collector surfaces is critical to thorough quantitative description of colloidal particle deposition behavior (i.e. physico-chemical filtration) on different kinds of surfaces(51). In GMF, it is challenging to provide realistic numeric description of flow fields (i.e., fluid streamlines) around collectors. This challenge is attributable to the complexity of flow fields in packed media beds(52). Accordingly, assumptions are made to approximate flow fields around collectors in these systems. During the past 50 years, various theoretical models have been established to describe these flow field profiles(34, 46, 52-55); several key theoretical models for describing flow fields in porous media systems are summarized in Table 2-4.

Table 2-4. Representation of porous media as an assembly of collectors

Model	Schematic	Descriptions	Ref
Isolated sphere	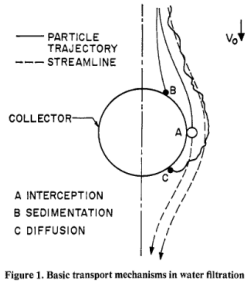 Figure 1. Basic transport mechanisms in water filtration Adapted from Yao and O'Melia (1971)	➢ Convection-Diffusion (C-D) based Model ➢ Valid at favorable conditions for deposition (i.e., high ionic strength), thereby assuming attachment efficiency is equal to unity ➢ Assumes particle is fixed in space and not affected by neighboring particles ➢ First microscopic model (C-D) to describe the filtration process ➢ Uses sum of analytical solutions to approximate numerical solution ➢ Uses single collector efficiency (η) to determine particle removal efficiency of collector (i.e. a single media grain)	(34)
Constricted tube	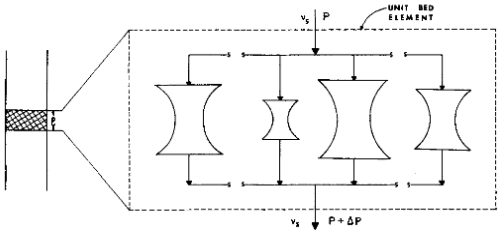 Fig. 1. Schematic representation of a unit bed element. Adapted from Tien and Payatakes (1979)	➢ Trajectory based model ➢ Packed bed considered as an array of pores, each of which is connected with its neighboring pores through narrow channels ➢ Channel walls possess axial symmetry ➢ First Lagrangian model to describe the filtration process ➢ Packed bed was decomposed to a unit bed element (UBE) with determined length to describe the particle removal efficiency	(56, 57)

Table 2-4(Continued). Representation of porous media as an assembly of collectors

Happel's sphere-in-cell	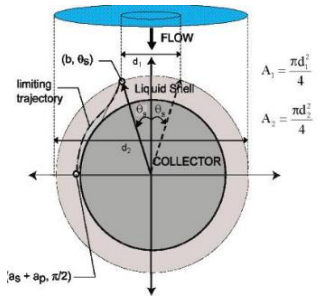 Adapted from Nelson and Ginn (2005)	➢ Most commonly used for C-D based or trajectory based models ➢ Packed bed represented as an assemblage of uniform cells ➢ Each cell contains a solid sphere with a liquid envelope whose thickness is related to overall media porosity ➢ Particles in the surrounding suspension have equal opportunities to access all unit collectors at the same vertical level from the inlet of filter ➢ Particle removal is represented by single collector efficiency (η)	(58, 59)
Dense cubic packing	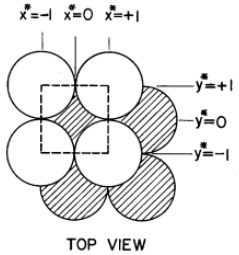 Adapted from Snyder and Stewart (1966)	➢ Commonly used in aerosol applications ➢ Trajectory based model with analytical solutions for flow field ➢ Single spherical media forms a square lattice in each plane ➢ Analytical solution is available for creeping flow	(55, 60)
Hemisphere-in-cell	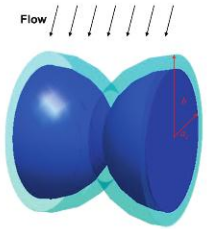 Adapted from Ma and Johnson (2009)	➢ Trajectory based model ➢ Uses two hemispheres with a liquid envelope to represent the packed media, including grain to grain contact points ➢ Similar to the Happel's sphere-in-cell model, but physically "stackable" for unit cells ➢ Uses overall porosity to determine liquid envelope thickness ➢ Potentially could be used at unfavorable conditions for deposition	(52)

In above mentioned geometric representations of porous media, Happel's sphere-in-cell model is the most widely known and commonly utilized model to represent packed bed geometry as an assemblage of uniform cells, each containing one collector/media grain. The advantages of Happel' sphere-in-cell model are that a) each cell has an individual flow velocity profile around the collector(53, 59) that can be described with an analytical solution; b) it includes the concept of a fluid envelope around the solid collector that reasonably describes the realistic physical conditions of the fluid; and c) the solutions obtained from the model can be scaled up from one single collector to an entire packed bed without further assumptions. In this model, the packed media are generally regarded as perfectly smooth spheres and are assembled for form a bed using a simple cubic packing scheme(1, 51, 61). The collectors are assumed to be enveloped by a shell of fluid, the thickness of which (b) is related to the overall porosity (ε) of the packed media and described by.

$$b = a_c(1-\varepsilon)^{1/3} \tag{2-1}$$

in which b is the thickness of fluid shell surrounding the collector, a_c is the collector radius and ε is the overall bed porosity. When dealing with an incompressible fluid at steady state creeping flow (i.e. Stoke's flow) conditions (i.e., when inertial forces are negligible), the fluid velocity field can be determined for the sphere, using spherical coordinates and the following boundary conditions(53)

$$E^4\psi = 0 \tag{2-2}$$

$$V_r = 0 \qquad \text{when } r = a_c + b \tag{2-3}$$

$$\mu\left(\frac{\partial V_r}{r\partial\theta} + \frac{\partial V_\theta}{\partial V_r} - \frac{V_\theta}{r}\right) = 0 \qquad \text{when } r = a_c + b \tag{2-4}$$

where r is the center-to-center distance between the approaching particle and collector, V_r and V_θ are the radial and tangential particle velocity components, and ψ is the Stokes stream function. The flow field velocity can then be represented by

$$v_r = \frac{-1}{r^2 sin\theta}\frac{\partial \psi}{\partial \theta} \tag{2-5}$$

$$v_\theta = \frac{1}{r sin\theta}\frac{\partial \psi}{\partial r} \tag{2-6}$$

Applying non-slip boundary conditions on the collector surface, the analytical solution for the stream function satisfying Equation 2-2 can be written as the follows(1):

$$\psi = A\left[k_1\left(\frac{a_c}{r}\right) + k_2\left(\frac{r}{a_c}\right) + k_3\left(\frac{r}{a_c}\right)^2 + k_4\left(\frac{r}{a_c}\right)^3\right] \tag{2-7}$$

Where

$$A = Ua_c^{\,2}/2 \tag{2-8}$$

$$p = a_c / b = (1-\varepsilon)^{1/3} \tag{2-9}$$

$$w = 2 - 3p + 3p^5 - 2p^6 \tag{2-10}$$

$$k_1 = 1/w \tag{2-11}$$

$$k_2 = -(3+2p^5)/w \tag{2-12}$$

$$k_3 = (2+3p^5)/w \tag{2-13}$$

$$k_4 = -p^5/w \tag{2-14}$$

The stream function in Equation 2-7 is only valid within the envelope of thickness *b* that surrounds the sphere/collector in the model. Once the particle is outside of the envelope (Happel's fluid shell), Equation 2-7 cannot describe the flow field(53) due to the violations of assumed boundary conditions.

2.3.2 Flow fields in parallel plate chambers

Flow fields in porous media are complex; therefore, none of models in Table 2-4 are able to realistically represent flow velocity profiles in these systems (62). The geometric representation of collectors in packed beds affects predicted particle deposition performance(52, 63). This makes it difficult to distinguish the impact of flow field on particle deposition from the impact of other factors such as surface roughness, chemical heterogeneity, *etc.* (64, 65). Different experimental configurations such as parallel plates can be used to overcome the confounding effect of representation of packed bed geometry(66, 67). Parallel plate chambers offer several advantages over packed beds of porous media. These include: a) action of the same forces (Van der Waals, electrostatic double layer, *etc.*) upon the colloidal particles (but at different flow condition) (66, 68); b) ease of control, monitoring, and analysis (69-71); and c) availability of analytical solutions for flow field profiles(66). The fluid velocity profile and associated transport of a colloidal particle in a parallel plate chamber is depicted in Figure 2-2. In this system, flow can be assumed to be laminar, incompressible and steady. Ignoring entrance effects, a no-slip boundary condition can be applied at the bottom of chamber.

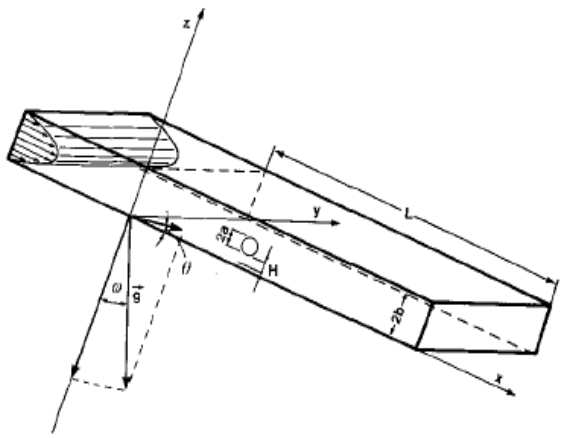

Figure 2-2. Schematic representation of a parallel plate chamber (66)

When the plate surface is chemically homogenous and smooth, a completely parabolic velocity profile is developed and can be expressed by

$$u = \frac{3}{2} V_{avg} \frac{z}{b}\left(2 - \frac{z}{b}\right) \tag{2-15}$$

$$v = 0 \tag{2-16}$$

$$w = 0 \tag{2-17}$$

where u, v,w represent the velocity components in the x,y,z directions in Cartesian coordinates, V_{avg} is the average flow velocity, b is the half channel height and z is the vertical distance to the bottom surface.

2.4 Interfacial forces

Once colloidal particles are transported to the vicinity of collector surfaces, forces exerted upon the particles will govern their attachment to and potential detachment from collector surfaces (1, 34). These forces are universal in natural and engineered environments(33) and include DLVO forces (the sum of Van der Waals and electrostatic double layer forces), short-range forces, gravity, and the shear lift force. These forces are comprehensively discussed below.

2.4.1 Van der Waals force

When two colloidal particles are in close proximity to one another, there is always an attractive force between them. It is caused by spontaneous electric and magnetic polarization and is commonly called the London van der Waals force (VDW)(34). Essentially, it is a force between dipoles. A microscopic approach developed by Hamaker (1937) has been traditionally used to assess the magnitude of the VDW force(72-74). In this approach, the interactions between particles and surfaces can be estimated by summation of the pairwise combinations of the interactions between the atoms/molecules of which they are composed(51, 67, 75). The VDW force can be calculated as

$$F^{VDW} = \nabla\left(\sum_{i}^{j} U^{VDW}\right) = \sum_{i}^{j} -\frac{A}{6h_i^2 k_b T} \tag{2-18}$$

where F^{VDW} is the VDW force, U^{VDW} is the VDW interaction energy, *i* and *j* are the different components of interacting bodies, *A* is the Hamaker constant, *h* is the separation distance, k_b is the Boltzmann constant and *T* is temperature.

During GMF, a dilute suspension of colloidal particles in water flows around collector surfaces. The associated calculation of the VDW interaction described by Equation 2-18 requires modification of the Hamaker constant, which can be approximated as(29, 76)

$$A_{collector-colloid-water} = (A_{collector-colloid}^{1/2} - A_{water-water}^{1/2})(A_{colloid-colloid}^{1/2} - A_{water-water}^{1/2}) \qquad (2\text{-}19)$$

where $A_{collector-colloid-water}$ is the modified Hamaker constant and $A_{collector-colloid}$, $A_{water-water}$ and $A_{colloid-colloid}$ are the original Hamaker constants between each of the interacting bodies in the system. Obtaining an exact value of the Hamaker constant for water treatment and other such applications is difficult because of the polar nature of water and the confounding interaction with ionic strength. In practice, the Hamaker constant is commonly selected from the range of 10^{-21} to 10^{-19} J so that it best fits experimental data(51).

The Hamaker method is able to provide relatively accurate estimation of VDW forces at short separation distances(75). When the separation distance is large (~100 nm), a retardation effect leads to a reduced interaction; in these cases, the Hamaker method overestimates the VDW interaction due to the electromagnetic nature of VDW(73, 77, 78). To represent the retarded VDW force, a correction factor $f(_P)$ is introduced to the Hamaker expressions(78). The analytical expressions of VDW interaction energy (un-retarded and retarded functions) for sphere-sphere and sphere-infinite plate geometries according to Equation 2-18 are summarized in Table 2-5. These analytical solutions are only valid for simple geometries such as spheres, flat plates, *etc*(33). If the shape of the particle and/or collector is irregular, these solutions are not valid and different numerical methods such as the Derjaguin approximation(79) and surface element integration(80, 81) should be used in the calculation; some of these analytical expressions are also provided in Table 2-5.

Table 2-5. Analytical formulas for un-retarded and retarded VDW interaction energy (33)

Expression	Applied condition
$U_{Sphere-sphere}^{VDW} = -\frac{A_{ij}}{6}[\frac{2a_i a_j}{R_{ij}^2-(a_i+a_j)^2} + \frac{2a_i a_j}{R_{ij}^2-(a_i+a_j)^2+4a_i a_j} + \ln(\frac{R_{ij}^2-(a_i+a_j)^2}{R_{ij}^2-(a_i+a_j)^2+4a_i a_j})]$	➢ Sphere to sphere; ➢ Un-retarded
$U_{Sphere-plate}^{VDW} = -\frac{Aa_P}{12h}$	➢ Sphere to infinite plate; ➢ Un-retarded
$U_{Sphere-sphere}^{VDW} = -\frac{Aa_i a_j}{6(a_i+a_j)h}\frac{1}{(1+11.12h/\lambda)}$	➢ Sphere to sphere; ➢ Retarded; ➢ $h<\lambda/\pi$, $h<<a_i$
$U_{Sphere-plate}^{VDW} = -\frac{Aa_P}{12h}\frac{1}{(1+14h/\lambda)}$	➢ Sphere to infinite plate; ➢ Retarded
$U_{Sphere-sphere}^{VDW} = -\frac{Aa_i a_j}{6(a_i+a_j)h}\left[1-\frac{bh}{\lambda}\ln(1+\frac{\lambda}{bh})\right]\frac{h}{S}$	➢ Rough sphere and b=5.32; ➢ Retarded

2.4.2 Electrostatic double layer force

Colloidal particles and media grain collectors are typically charged in both natural and engineered filtration applications (82). When charged colloidal particles suspended in electrolytic solutions (e.g., fine sediments suspended in river water) approach collectors, their individual double layers overlap and electrostatic forces are exerted on both the particle and the collector(83). To quantitatively describe the electrostatic double layer force (EDL), the well-known Poisson-Boltzmann equation has to be solved either numerically or analytically with assumptions (i.e. linear approximation for charge distribution)(83).

When a charged element (e.g., a colloidal particle) is immersed in a dielectric medium (e.g., water), the strength of the electric field can be significantly reduced because molecular dipoles tend to align to balance the electric field. Permittivity (ε) describes how an electric field affects, and is affected by, a dielectric medium. The ion distribution and spatial distribution of chemical potential can be quantitatively described by the Poisson equation, which is (83-85)

$$\Delta\psi = \nabla^2\psi = -\frac{\rho}{\varepsilon_0} \tag{2-20}$$

where the ψ is the electrostatic potential of a flat surface, ρ is the density of fluid and ε_0 is the permittivity of the dielectric medium. Because the electric and diffusion forces on ions must be balanced, the electro-chemical potential of ions on the particle can be described by

$$\nabla\mu_i = -z_i e\nabla\psi \tag{2-21}$$

$$\mu_i = \mu_i^0 + kT\ln n_i \tag{2-22}$$

$$n_i = n_i^0 \exp(\frac{-z_i e\psi}{k_b T}) \tag{2-23}$$

where u_i is chemical potential and z_i is the valence of ion *I*, where n_i is the number of ions of type *i* per unit volume, k_b is the Boltzmann constant ,T is the absolute temperature, u_i^0 is the standard chemical potential at 273K and e is the charge of electron . It should be constant

everywhere. Assuming that the electrostatic and chemical potentials are constant on the plane parallel to the charged surface, Equation 2-21 can be simplified to the one dimensional expression

$$\frac{d\mu_i}{dx} = -z_i e \frac{d\psi}{dx} \tag{2-24}$$

Given the definition of chemical potential for flat surfaces, Equation 2-20 can be analytically solved by integrating Equations 2-22 through 2-24 from a point in the bulk solution where ψ =0 and $n_i = n_i^0$.

Given the volume charge density in the neighborhood of colloidal surface described as

$$\rho = \sum_i n_i z_i e \tag{2-25}$$

The complete Poisson-Boltzmann equation, which has been successfully used to define the electric potential distribution in the diffuse ionic layer adjacent to a subject with charged surface(83), can be expressed as

$$\nabla^2 \psi = -\frac{1}{\varepsilon} \sum_i n_i^0 z_i e \exp(\frac{-z_i e \psi}{k_b T}) \tag{2-26}$$

The partial differential equation (PDE) in Equation 2-26 can be solved analytically. When ψ is small (*i.e.* $z_i e\psi << k_b T$), the exponential term can be approximated using the relation that $e^{-x} = 1 - x$ when x is small (Debye-Hückel approximation). κ is commonly called inverse Debye-Hückel length and is described by

$$\kappa = \left[\frac{e^2 \sum n_i^0 z_i^2}{\varepsilon k_b T} \right]^{1/2} \tag{2-27}$$

$$\psi = \psi_0 e^{-\kappa x} \tag{2-28}$$

Equation 2-26 can be represented using the full formula of chemical potentials as

$$\tanh(ze\psi / 4k_b T) = \tanh(ze\psi_0 / 4k_b T) \exp(-\kappa x) \tag{2-29}$$

Representative curves for the linear-approximation and fully developed electric potential for the double layer in one-dimensional space are plotted in Figure 2-3 where the y axis ($\Delta\phi^*$) represents the dimensionless electric potentials and the x axis (y^*) represents the dimensionless distance away from the collector surface. In Figure 2-3, the solid lines are the linearized solution for the electric potentials whereas the dots are the full solutions for Equation 2-29. When the electric potential is small, the linear approximation reasonably represents the fully developed electric potential distribution. When the electric potential is greater than 25.2 mV, the Debye-Hückel approximation overestimates the potentials(86).

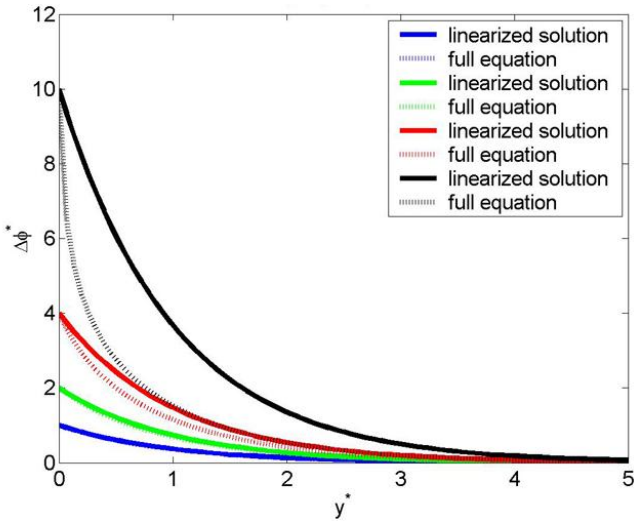

Figure 2-3. Representative curves of linearized and fully developed Poisson-Boltzmann equation for electric potential distribution (83)

Using the Debye-Hückel approximation, the EDL force between a sphere and flat surface (U_{PS}^{EDL}) and two spheres (U_{ij}^{EDL}) can be expressed respectively by(75)

$$U_{PS}^{EDL} = \pi\varepsilon\varepsilon_0 a_p [2\psi_P\psi_S \ln(\frac{1+\exp(-\kappa H)}{1-\exp(-\kappa H)}) + (\psi_P^2 + \psi_S^2)\ln(1-\exp(-2\kappa H))] \quad (2\text{-}30)$$

$$U_{ij}^{EDL} = \frac{\pi\varepsilon\varepsilon_0 a_i a_j}{(a_i + a_j)} [2\psi_i\psi_j \ln(\frac{1+\exp(-\kappa H)}{1-\exp(-\kappa H)}) + (\psi_i^2 + \psi_j^2)\ln(1-\exp(-2\kappa H))] \quad (2\text{-}31)$$

where *s* and *p* represent the sphere and plate, *i* and *j* represent the two different spheres, ψ_1 and ψ_i are the respective chemical potentials of the two spheres and *h* and *H* are the true and dimensionless surface-to-surface distance. ψ_S and ψ_P are the chemical potentials of the sphere and plate respectively.

The analytical solutions of the Debye-Hückel approximation for the electrostatic double layer interaction (Equation 2-30 and 2-31) have often been used improperly(33, 87) because the conditions under which the approximation is valid have been disregarded; specifically, the linear approximation is only valid when chemical potentials are within the range of ± 25.2 mV(88, 89). If the chemical potential exceeds this range, the EDL interaction calculated by the Debye-Hückel approximation is overestimated by several orders of magnitude and the region of the EDL force is affected significantly(75).

2.4.3 Short range forces/interactions

Short range forces are a group of interfacial forces that had been introduced to interpret the discrepancy between experimental results and theoretical calculations for colloidal stability, deposition and adhesion in engineered and natural environmental systems (90). They include the Born repulsive force(20), hydration effects(46, 91), hydrophobic interactions(92-94),steric interactions(95), polymer bridging(33), and Lewis acid–based interactions(90). These forces have been recognized for a long time, but their exact nature has not yet been firmly established. The presence of these forces is also not as universal as the VDW and EDL forces and is highly dependent on particle and collector characteristics (materials, adsorption, hydrophobicity, *etc.*)(67) and the aquatic environment(33). Universal quantitative descriptions that account for all these of forces/interactions are not currently available. It is believed, however, that all the short-range forces are only effective within 5 nm from the collector surface (67, 96, 97) and that most of them are repulsive forces. Table 2-6 summarizes the details of these forces.

Table 2-6. Short range forces/interactions of the colloids and target surface

Forces	Description	Characteristics	Reference
Born force	➢ Overlap of atom electron clouds	➢ Repulsive short range force; ➢ Effective at small inter-atomic distances	(20)
Hydration	➢ Water molecules strongly bind to surfaces containing hydration groups	➢ Repulsive short range force; ➢ i.e. hydroxyl(-oh) group	(46)
Hydrophobic effect	➢ Attractive force that exists between hydrophobic surfaces	➢ Attractive short range force; ➢ Decrease exponentially with distance.	(98, 99)
Steric interaction	➢ Occurs when colloids are coated with macromolecules	➢ Short range force; ➢ Can be attractive/ repulsive -depends on the polymer-solvent interaction	(95, 100)
Lewis acid–base interaction	➢ The formation of hydrogen bonds during the hydrolysis process	➢ Usually repulsive force ➢ Can be represented by the Gibbs energy of acid-base free energy per unit area	(90, 101)
Polymer bridging	➢ More than one uncoupled polymer aggregated together	➢ Usually charged and repulsive from each other ➢ Stability highly related to ionic strength	(7, 33)

2.4.4 Gravity

The gravity effect is well understood for colloid transport and attachment on surfaces. It relies on the relative density between suspended colloidal particles and their total volume. It can be numerically represented as the net effect of gravity and buoyancy forces on the particles suspended in the solution and expressed as

$$\vec{F}_G = \frac{4}{3}\pi a_p^3(\rho_p - \rho_w)\vec{g} \qquad (2\text{-}32)$$

where the a_p is the particle diameter, ρ_p and ρ_w are the colloidal particle and fluid densities and g is the gravitational acceleration vector(66).

2.4.5 Interaction energy Integration

Commonly reported in the literature, the effect of all the forces on the colloid can be numerically represented as the interaction energy, the integral of specific force over distance(34, 67, 75, 102). The net force exerted on a colloidal particle can be defined as the derivative of the overall interaction energy over distance (Equation 2-33). Different numerical methodologies are used to calculate the interaction energy, including Derjaguin's integration (DI)(79) and surface element integration (SEI) methods(81). The applied for $F(h)$ can be described by

$$F(h) = \frac{\partial E(h)}{\partial h} \qquad (2\text{-}33)$$

where $E(h)$ is the interaction energy per unit area between two flat plates and h is the separation distance.

The DI method is an approximate solution for total interaction energy in which the target objects (approaching particle/sphere and surface/plate) are regarded as a series of parallel concentric rings; each concentric ring is a flat plate with certain width. The total interaction energy is calculated by integrating the plate–plate (ring–ring) interaction energies over the

area of the leading face(s) of the curved surface(s) of the two rings (75, 79). It can be represented as

$$U_{DI} = f(a)\int_{D}^{\infty} E(h)dh \qquad (2\text{-}34)$$

where U_{DI} is the interaction energy, $f(a)$ is parameter for different shape and D is the minimum separation distance.

The DI method is able to provide good approximation of the overall interaction energy when the thickness of the double layer is much smaller than the object (81). The energy, $E(h)$ decays with distance quickly enough so that its contribution to U_{DI} is insignificant in the area some distance away from the point of the closest approach of the two rings. In other words, all of the interaction energy is from a small region around the point of closest approach; surface curvature is ignored.

Proposed for systems described by complicated geometry, the SEI approach is a more general form of the DI method(81, 88, 103-105). It computes the total interaction energy between two bodies by numerically integrating the interaction energy per unit area between opposing differential planar elements over the entire surfaces. It can handle both protrusions and depressions on a surface and is accurate when the double layer thickness is comparable to the scale of the objects. Using the SEI method, the interaction energy for realistic surface features can be calculated. The major disadvantage of the SEI method is that significantly more computationally intensive than the DI method(80, 105, 106).

2.4.6 DLVO theory

The classical theory of colloidal stability developed by Derjaguin, Landau, Verwey, and Overbeek, collectively known as the DLVO theory, is typically used in CFT models to describe the interactions between particles and media grain (collector) surfaces(86, 107, 108). Within the framework of DLVO theory, all of the above-mentioned forces are regarded as interfacial forces between the colloidal particle and the collector surface. Their contributions on particle deposition (or particle destabilization) are additive. They can be combined

together and numerically represented by the total interaction energy between the approaching colloidal particle and the collector surface as a function of separation distance(77, 89, 109).

Originally, classic DLVO theory only accounted for the impacts from VDW and EDL forces (long range forces), which are only valid when the separation distance is relatively large(75). More recently, extended DLVO theory has been developed and includes the contributions of short-range forces on particle deposition or stability in addition to traditional total interaction energy(90). The total interaction (U^{Total}) is then expressed as the sum of the long- and short-rang forces by

$$U^{Total} = U^{VDW} + U^{EDL} + \sum U^{Short} \tag{2-35}$$

$$F^{Total} = \frac{\partial U^{Total}}{\partial h} \tag{2-36}$$

where U^{VDW} is the VDW interaction, U^{EDL} is the EDL interaction, U^{Short} is the short-range interactions, F^{Total} is the net force exerted on colloidal particle and h is the separation distance.

Representative curves of DLVO interaction (the sum of VDW and EDL force only) are shown in Figure 2-4. The EDL force decreases exponentially with increasing separation distance, whereas the VDW force decreases slowly with distance. When a particle is very close to the collector surface, a primary energy minimum exists where the attractive VDW force is dominant. Here, the total interaction energy is negative and the particle will attach to the collector surface, thus being removed from the bulk suspension. When the separation distances between particles and collectors are a few nanometers, an energy barrier is present. Colloids that have been attached on collector surfaces have to overcome this energy barrier to migrate from collector surfaces back to the bulk suspension (43, 110). If separation distance increases up to 5 nm, the net interaction energy will decrease to a negative value and the net forces on particles will be attractive. The peak of this negative net interaction energy is the secondary minimum. When separation distances increase from here, total interaction energy will be negative, but relatively small (111, 112).

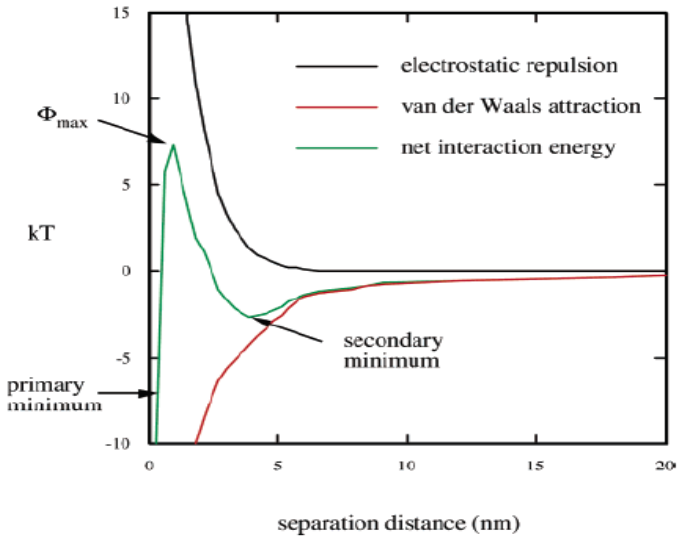

Figure 2-4. Typical interaction energy curves between particle and media surface at unfavorable conditions

The net interaction energy between colloids and collector surfaces is highly dependent on aquatic chemistry. Two types of interaction energy curves are presented in Figure 2-5: unfavorable and favorable conditions for deposition. In natural environments, colloids and filtration media (*e.g.*, sand, clay, *etc*.) typically possess a net negative charge at neutral pH and low ionic strength (3)(3). The energy barrier, the presence of which can "slow" down colloid attachment, then emerges a few nanometers away from the collector surface(113). Accordingly, this aquatic condition is considered "unfavorable". At unfavorable conditions, colloid deposition rates are relatively slow, because colloids have to overcome energy barriers to deposit on collectors (46, 55). An interaction energy curve at unfavorable conditions is shown in Figure 2-5(a). In contrast, in engineered filtration systems operated after optimal coagulation, favorable conditions are commonly present, at which colloid deposition rates are relatively fast(34). Due to the high ionic strength in these systems, the double layer around the collectors is compressed extensively. An interaction energy curve at favorable conditions is shown in Figure 2-5(b), with no energy barrier between the colloid and collector surfaces(43).

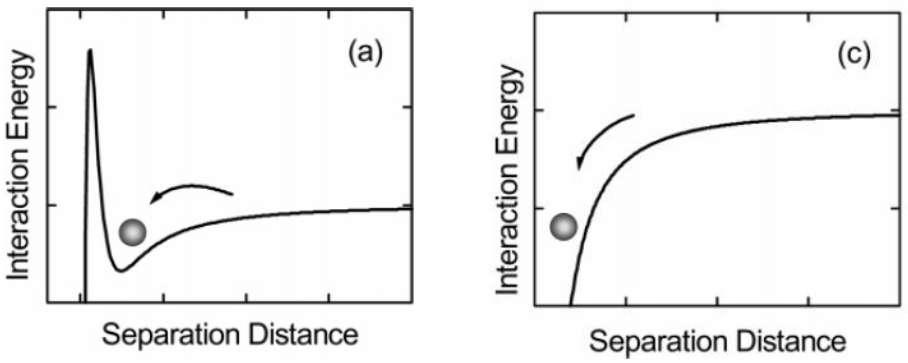

Figure 2-5. Schematic representation of net interaction energy between a particle and plat plate at favorable and unfavorable conditions (43)

2.5 Hydrodynamic mechanisms

In addition to interfacial forces, hydrodynamic effects caused by flow streams and wall effects associated with flow velocity changes near collector surfaces also impact colloidal particle deposition. Accordingly, the shear lift force and hydrodynamic retardation effects must also be considered when describing particle deposition on collector surfaces.

2.5.1 Shear lift force

Saffman 1965, 1968 first introduced the shear lift force, which is caused by velocity gradients in bulk flow(114, 115). When a particle is moving through a viscous liquid with a velocity component different from uniform shear, the particle will experience a lift force perpendicular to the flow direction due to inertia in the viscous flow. It can be represented by

$$F_{Lift} = -6.46\mu a_p^2 U_s \,\mathrm{sgn}(G)\left[\frac{|G|}{\nu}\right]^{1/2} \tag{2-37}$$

where F_{Lift} is the shear lift force, μ is the dynamic viscosity, ν is the kinematic viscosity, a_p is the particle radius, $G = du_1 / dy$ is the wall-normal gradient of the streamwise fluid velocity, $U_s = v_1 - u_1$ is the difference in the instantaneous streamwise velocity between the center of the particle and the fluid.

The derived Equation 2-37 reasonably describes the shear lift force in the bulk solution but overestimates the shear lift force at small separation distances. After Saffman's work, Cox and co-workers (116, 117), McLaughlin and co-worker(118-120) derived a theoretical form of shear lift force that considered wall effects and was applicable when the distance between the particle and collector surface was comparable to the particle radius(121); it is described by

$$\begin{aligned} F_{lift} = \rho a_p^2 U_s (&1.17716 + 0.216\kappa - 0.7292\kappa^2 + 0.4854\kappa^3 \\ &-(3.2397\kappa^{-1} + 1.145 + 2.084\kappa - 0.9059\kappa^2)\Lambda \\ &+(2.0069 + 1.0575\kappa - 2.4007\kappa^2 + 1.3174\kappa^3)\Lambda^2 \end{aligned} \quad (2\text{-}38)$$

where *l* is distance between the particle center and wall and $\kappa = a_p / l$, $\Lambda = a_p U_s / G$.

The Shear lift force estimated by Equation 2-38 is generally smaller than that derived by Saffman (1968) and is the same as the Saffman force when the particle is far from the collector surface. By accounting for wall effects, the shear lift force formula is more applicable to modeling and predicting particle deposition in various natural and engineered environments(121).

O'Neil (1968)(122) and Leighton and Acrivos (1985)(123) extended the studies of shear lift force to include inertial effects when colloidal particles contacted but did not fully attach to collector surfaces. When a particle is under a simple shear flow at condition of small Reynolds number (i.e., Re < 0.1), the shear lift force can be determined by

$$F_{lift} = 9.22\mu a_p \,\mathrm{Re}\gamma_0 \quad (2\text{-}39)$$

$$\mathrm{Re} = \gamma_0 a_p{}^2 / \nu \quad (2\text{-}40)$$

where *Re* is Reynolds number, $\gamma_0 = u / H$ is the dimensionless flow velocity and *H* is the distance from collector surface.

Colloidal particles suspended in a flowing solution constantly experience a shear lift force that always "lifts" them from target surfaces. Although it might be relatively small compared to other forces at certain circumstances, the shear lift force still should be considered,

especially in porous media systems like packed beds even the *Re* is still small. Notably, it has been recently found that the shear lift force on approaching particles can be significantly enhanced by collector surface roughness(124).

2.5.2 Hydrodynamic retardation effect

Other than the shear lift force, colloidal particles also experience a retardation effect as a result of hydrodynamic disturbances generated by the presence of bounding walls. In the vicinity of collector surfaces, where particle attachment takes place, the velocity field of an approaching particle will be altered. First developed by Brenner and co-workers (1961, 1967 and 1968), the dimensionless hydrodynamic retardation functions $f_1(H)$, $f_2(H)$ and $f_3(H)$ are employed to describe deviations in particle velocity from bulk fluid motion by

$$u_x = f_3(H)u \tag{2-41}$$

$$u_z = f_1(H)\, f_2(H)v \tag{2-42}$$

where H is the dimensionless surface-to-surface distance(122, 125-127). The modified diffusion tensor between the approaching particle and the surface are described by $f_1(H)$ and $f_4(H)$.(66, 74)

$$D_x = f_4(H)D_\infty \tag{2-43}$$

$$D_z = f_1(H)D_\infty \tag{2-44}$$

where D_∞ is the Stokes-Einstein diffusion coefficient.

As described in Equation 2-41 to 2-44, the tangential and perpendicular velocity components are retarded due to the presence of a bounding wall/surface. For the purpose of particle attachment in this thesis work, as the distance between the particle and target surface decreases, approaching particles experience hydrodynamic resistance and it becomes harder to get closer to the collector surface(33). Precise description of the hydrodynamic retardation

functions is important, especially when *H* is approaching zero for attachment and infinity for detachment(1, 87). Analytical solutions have been developed to numerically represent the hydrodynamic retardation effect(53, 125-128); however, it their use is computationally intensive. To overcome the disadvantages of using the full analytical solution, simplified analytical functions valid only at the asymptotic limits have also been developed. Alternatively, numerical methods have also been commonly utilized(33, 52, 61). Universal functions that are precise over the entire domain, but also require some computational capacity are still lacking in the literature.

2.6 Filtration theory

Ideally, filtration theory should be able to predict the transport and fate of various particles including bacteria, viruses and protozoa, as well as colloid-bounded pollutants in porous media. Historically, four basic approaches have been utilized to describe particle transport and deposition in porous media. They include: Eulerian models(33), Lagrangian models(1, 129, 130) macroscopic models(41), and regression models(61, 131, 132). Eulerian models use a simplified geometric representation of porous media; the spatial distribution and probability density of colloidal particles in time and space is quantitatively evaluated under the influence of various forces/interactions(51). Lagrangian models, which are developed based on Newton's second law, consider each individual colloidal particle's behavior or "trajectory" at the microscopic level(47). The macroscopic or "phenomenological" approach combines mass balance with an empirical rate expression to model particle removal and estimate headloss(55). Aiming to avoid laborious mathematical calculations and acquire empirical equation, regression models have been developed to best fit the numerical solutions of Eulerian or Lagrangian models at various operational conditions(131). The quantitative formulations, numerical solutions and applications of these models are comprehensively reviewed below. The limitations of these models are discussed with a focus on model ability to describe impacts of granular media surface characteristics on filtration performance.

2.6.1 Eulerian approach

Determined from the conservation law, the mass transport of particles in dilute suspensions can be expressed as

$$\frac{\partial c}{\partial t} + \nabla \cdot J = Q \tag{2-45}$$

where J is the particle flux vector, Q is particle reaction rate, c is particle concentration and t is reaction time. At steady state without additional chemical reactions, the general convection-diffusion equation for mass transfer due to diffusion, convection and external forces can be expressed as

$$\nabla \cdot (\boldsymbol{u}C) = \nabla \cdot (D \cdot \nabla C) - \nabla \cdot \left(\frac{\boldsymbol{D} \cdot \boldsymbol{F}}{kT} C \right) \tag{2-46}$$

qhere T is the absolute temperature, k_b is the Boltzmann constant, c is the particle concentration, D is the diffusion tensor, and F is the external force. The convection-diffusion equation as shown in Equation 2-46 describes the particle distribution in time and space and can be solved numerically when the flow velocity field, diffusion tensor and external forces and associated boundary conditions are all known.

To conduct numerical simulations using equation 2-46, several mathematical criteria and assumptions must be met. Explicit formulas of Equation 2-46 need to be dimensionless to reduce the numbers of variables and decrease computing demands. In porous media, which are represented by spherical geometry, the formulae also need to be converted from spherical coordinates to Cartesian coordinates to facilitate simulation. It is also critical to appropriately define boundary conditions in the simulation domain so that the partial differential equations can be properly solved. A perfect sink boundary condition is commonly implemented on collector surfaces and assumes that if particles are located close enough to collector surfaces, they can attached and simultaneously removed from the simulation domain. A cut-off distance ranging from 0.4 nm to 1 nm at favorable conditions for deposition has been

assumed and utilized(51, 52, 133). It is also assumed that when particle is far away from the contact surface, the concentration of colloid is equal to the bulk concentration.

2.6.2 Lagrangian approach

The Lagrangian approach, commonly referred to as "trajectory analysis," involves determining particle deposition rates from particle trajectories. By knowing all the elaborated forms of all force vectors exerted upon particles and their associated streamlines, the trajectories can be determined using Newton's second law. First proposed for aerosol deposition in the 1930's(134, 135), the concepts of trajectory analysis were first applied to water filtration in the 1970s(130). Various models have been developed using different geometric representations; they are summarized in Table 2-7.

The general equation describing particle migration through a flowing fluid around a collector surface can be written as

$$(m+m^*)\frac{du}{dt} = F_{VDW} + F_{EDL} + F_{Short} + F_{Gr} + F_B + F_{Lift} + F_{drag} \quad (2\text{-}47)$$

where m is the particle mass, m^* is the virtual mass, and u is the transit velocity vector. On the right side of Equation 2-47, a list of all potential forces is presented, including VDW forces (F_{VDW}) and EDL forces (F_{EDL}), short range forces (F_{Short}), gravity (F_{Gr}), Brownian motion (F_B), shear lift force(F_{Lift}) and drag forces (F_{drag}).

Results from trajectory analysis should be the same as those obtained by solving the convection-diffusion equation. In contrast to the Eulerian approach, trajectory analysis is able to describe the behavior of individual particles and enables calculation of the overall deposition rate by statistical analysis after simulation; of course, the deposition behaviors of a large number of particles must be calculated to make meaningful conclusions. The numerical solutions associated with trajectory analysis are substantially more computationally intensive and time consuming compared to Eulerian, convection-diffusion based approaches(52); however, they can also be applied to more complicated surface geometric features and localized physical/chemical heterogeneity mapping(104, 136). Existing models commonly

utilize simplified geometry to approximate realistic flow conditions and physical/chemical properties; however, the interactions between neighboring collectors and the dynamic repetitive processes of attachment and detachment between particles and collectors are rarely represented. Nonetheless, the framework of trajectory analysis enables the development of numerical solutions to describe particle deposition in more complicated geographic situations.

2.6.3

2.6.4 Macroscopic models

Macroscopic modeling approaches are empirical and developed based on experimental data for specific deposition rates. The mathematical formulations of macroscopic models are based on the mass balance for a differential element of depth in a filter, which can be generally expressed as

$$\text{Mass accumulation} = \text{mass flux in} - \text{mass flux out} \pm \text{reactions} \tag{2-48}$$

Macroscopic models do not focus on the accumulation of particles on single collectors, but rather evaluate mass accumulation of different elements. A simplified one-dimensional model that represents a suspension flowing through porous media is shown in Figure 2-6.

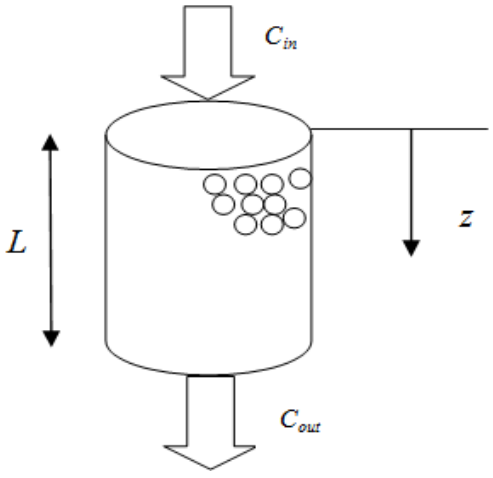

Figure 2-6. Schematic representation of a suspension flow through porous media

Combined with mass balance (Equation 2-48), the specific deposition rate can be expressed as

$$\frac{\partial \sigma}{\partial t} = \lambda v_s c \tag{2-49}$$

where c is the particle concentration (mg/L), z is the axial distance in filter (m), σ is the specific deposition mass of accumulated particles per filter bed volume (mg/L), λ is the filter coefficient (m^{-1}), v_s is the superficial liquid velocity (m/s), and t is the filter run time (s). It should be noted that the relationship between colloid concentration in the bulk suspension (c) and colloid deposition (σ) follows first order kinetics(1, 55, 137).

Determination of λ is the key step for macroscopic model simulation, because the other parameters can be measured experimentally. For homogeneous media, the initial value of λ is considered constant as λ_0. The filter coefficient λ changes over time and depth due to the capture of colloidal particles by collector surfaces. Particle removal efficiency increases with depth and is dependent on particle size(138). The value of λ, as shown in Equation 2-49, can be expressed as a function of λ_0 and $F(\alpha, \sigma)$, which is a function of α (the parameter vector characteristic of filtration) and σ (Tien, 2007). The filter coefficient λ can be described as

$$\lambda = \lambda_0 F(a, \sigma) \tag{2-50}$$

The accuracy of the macroscopic approach depends on the validity of the expressions for the function $F(\alpha, \sigma)$, which are determined from experimental data. The uncertainties of the model will increase when improper expressions of $F(\alpha, \sigma)$ are employed. None of the expressions are predictive in nature; this is partially because the parameters used in macroscopic models do not account for filter media characteristics. Variations in water quality and operational parameters are also ignored in these approaches. Different factors that may govern the particle deposition process (*e.g.*, diffusion, hydrodynamic interactions) are also absent in macroscopic modeling approaches. Macroscopic models have to be solved numerically and associated filter coefficients are site specific; accordingly, such models are not widely utilized(1, 135, 139).

2.6.5 Regression models

In filtration modeling, the key goal is to determine the filter coefficient λ, defined in Equation 2-51. It can be described by the single collector efficiency (η) based on mass conservation in a controlled volume as described by

$$\lambda = \frac{3}{2}\frac{(1-\varepsilon)}{d_c}\alpha\eta_0 \tag{2-51}$$

where α is the attachment efficiency and η_0 is the overall deposition efficiency,

Different than the macroscopic models that are pure fitting without predictive capacity, regression based models have been widely developed. The physico-chemical parameters used in the models represent different mechanisms such as diffusion, convection, sedimentation and hydrodynamics. Assuming individual contributions from each mechanism can be added together to estimate particle deposition rates, regression models are able to best fit the numerical solutions from convection-diffusion equation or trajectory analysis, avoiding laborious mathematical calculation.

Firstly proposed by Yao and O'Melia (1971)(34), analytical solutions for diffusion, interception and gravity are utilized to represent the overall deposition efficiency for a single collector. The single collector efficiency can be approximated as

$$\begin{aligned}\eta_0 &= \eta_D + \eta_I + \eta_G \\ &= 0.9\left(\frac{k_B T}{4\mu a_p a_c U}\right)^{2/3} + \frac{3}{2}\left(\frac{a_p}{a_c}\right)^2 + \frac{2}{9}\frac{{a_p}^2(\rho_p - \rho_f)g}{\mu U}\end{aligned} \tag{2-52}$$

where η_D is transport by diffusion, η_I is transport by interception, and η_G is transport by sedimentation due to gravity. These transport/deposition mechanisms are represented by power functions of multiple dimensionless parameters that consist of physico-chemical filtration parameters. The exact numerical forms for each individual term are obtained by performing a multiple linear regression analysis between relevant dimensionless parameters over a wide range of parameter values. Table 2-7 summarizes several existing filtration models.

Table 2-7. Existing models for single collector efficiency after Yao's work 1971

Models	Formulations	Notes	Ref
Yao and O'Melia,1971	$\eta = 4A_s^{1/3}N_{Pe}^{-2/3} + \frac{3}{2}N_R^2 + N_G$	➢ Eulerian based model using Happel's cell geometry ➢ The Happel' correction factor *As* for the porosity is included ➢ Valid for favorable condition ➢ VDW,EDL and hydrodynamic interaction were not included	(34, 140)
Rajapopalan and Tien, 1976	$\eta \approx 0.72A_sN_{Lo}^{1/8}N_R^{15/8} + 0.0024A_sN_G^{1.2}N_R^{-0.4} + 4A_s^{1/3}N_{Pe}^{-2/3}$	➢ Lagrangian based model using Happel's sphere geometry ➢ Lubrication effect due to the resistance of an incompressible fluid and VDW force is accounted ➢ Valid when $N_R \le 0.18$ and $N_{Lo} > 0$ ➢ Contain a hidden variable which assume the porosity is 0.39 of the packed bed	(47)
Rajapopalan and Tien, 1982	$\eta = \gamma^2(4A_s^{1/3}N_{Pe}^{-2/3} + A_sN_{Lo}^{1/8}N_R^{15/8} + 0.00338A_sN_G^{1.2}N_R^{-0.4})$	➢ Developed in Happel's sphere geometry ➢ Correct the hidden variable in their former work ➢ Correction factor γ^2 was introduced to reflect the concept of single collector efficiency	(141)
Cushing, 1998	$\eta = 0.029N_{L_0}^{0.012}N_R^{0.023} + 0.48N_G^{1.8}N_R^{-0.38}$	➢ Lagrangian based model using Array of sphere geometry ➢ VDW, EDL, Hydrodynamic and drag forces were considered ➢ Inertia and Brownian motion was neglected ➢ Presented as dimensionless groups in the format of power functions	(55)

Table 2-7(Continued). Existing models for single collector efficiency after Yao's work 1971

Tufenkji and Elimelech,2004	$\eta_0 = 2.4A_s^{1/3}N_R^{-0.081}N_{Pe}^{-0.715}N_{vDw}^{0.052} + 0.55A_sN_R^{1.675}N_A^{0.125} + 0.22N_R^{-0.24}N_G^{1.11}N_{vdW}^{0.053}$	➢ Eulerian based model using Happel's cell geometry ➢ VDW, gravity and hydrodynamic Brownian motion were considered in the model ➢ EDL, Drag force and shear lift force were not included ➢ Presented as dimensionless groups in power functions format	(131)
Long and Hilpert, 2009	$\eta_0 = (15.56 \pm 0.21)\frac{(1-\varepsilon)^3}{\varepsilon^2}N_{Pe}^{-0.65\pm0.023}N_R^{-0.19\pm0.03} + 0.55A_sN_R^{1.675}N_A^{0.125} + 0.22N_R^{-0.24}N_G^{1.11}N_{vdW}^{0.053}$	➢ Eulerian based model using random packing geometry for diffusion ➢ Happel's sphere geometry for interception and sedimentation ➢ Superposition of numerical solution for diffusion (no hydrodynamic retardation) ➢ Using TE model for the interception and sedimentation	(142)
Ma and Johnson, 2009	$\eta \approx \gamma^2\left[\begin{array}{l} 2.3A_s^{1/3}N_R^{-0.08}N_{P_e}^{-0.65}N_A^{0.052} + \\ 0.55A_s^{1.8}N_A^{0.15} + 0.2N_R^{-0.1}N_G^{1.1}N_A^{0.053}N_{Pe}^{0.053}\end{array}\right]$	➢ Lagrangian based model using Hemisphere-in-cell geometry to account the effect of grain to grain contact ➢ VDW, EDL, Shear lift, hydrodynamic, drag forces and Brownian motion were introduced ➢ Have the potential to be used in the presence of energy barrier for un-favorable condition	(143)
Nelson and Ginn, 2011,	$\eta \approx \gamma^2\left[\begin{array}{l} 2.4A_s^{1/3}\left(\frac{N_{Pe}}{N_{Pe}+16}\right)^{0.75}N_{Pe}^{-0.68}N_{Lo}^{-0.015}N_G^{0.8} + \\ A_sN_{Lo}^{1/8}N_R^{15/8} + 0.7\left(\frac{N_G}{N_G+0.9}\right)N_GN_R^{-0.05}\end{array}\right]$	➢ Lagrangian based model using Happel's sphere geometry ➢ Attachment efficiency was always smaller than 1.0 by introducing a correction factor to serve as a governor for diffusion and sedimentation	(61)

Table 2-7(Continued). Existing models for single collector efficiency after Yao's work 1971

Chang et al, 2012	$\eta_0 = A_s(1-\varepsilon)^{2/3} N_{Lo}^{1/8} N_R^{15/8} + 4(1-\varepsilon)^{2/3} A_s^{1/3} N_{Pe}^{-2/3} + 1.866 A_s^{1.591} (1-\varepsilon)^{4.531} N_{Diff}^{-0.312} N_{Pe}^{-0.312}$	➢ Lagrangian based model using sinusoidal constricted tube geometric structure ➢ Diffusiophoretic velocity (diffusiophoresis) was included using Brownian dynamics simulation method ➢ Valid for submicron particle at high ionic strength ➢ include equation for attachment efficiency	(144, 145)
Rodrigues and Dickson,2013	$f_r = N_Q^{-0.072} N_{IS}^{-0.065} N_{Pe}^{-0.09}$	➢ A Phenomenological model in single saturated fractures ➢ Effect of gravity, staining, ionic strength and geographic feature of fractures were included ➢ VDW, hydrodynamic and interception were not included.	(146)

Note: The dimensionless variables used in these regression models are presented in Table 2-8.

Table 2-8. Dimensionless parameters used in regression models for filtration

parameters	Forms	Physical interpretation
N_R	d_p/d_c	Size aspect ratio
N_{Pe}	Ud_c/D_∞	Ratio of convection over diffusion
N_{VDW}	A/k_BT	Ratio of VDW force over thermal energy
N_G	$4\pi a_p{}^4(\rho_p-\rho_f)g/3k_BT$	Ratio of gravity effect over thermal energy
N_A	$\frac{A}{12\pi a_p{}^2U}$	Ratio of combined influence of VDW forces and fluid velocity on particle deposition rate due to interception
N_{Gr}	$\frac{2}{9}\frac{a_p{}^2(\rho_p-\rho_f)g}{\mu U}$	Ratio of stokes particle setting velocity over approaching velocity
N_{Lo}	$A/9\pi\mu a_P^2U$	Dimensionless VDE force number
N_{DL}	κa	Electric double-layer force parameter
N_{diff}	$v_{pdiff}d_f/De$	Diffusiophoresis number

Among the regression models, Rajapopalan and Tien's (RT)(132) and Tufenkji and Elimelech's (TE)(131) models, which represent Lagrangian and Eulerian approaches respectively, represent two key milestones.

The RT and TE model are valid for clean beds, so that particle-particle interactions and blocking and straining effects are not relevant. The models utilize simplified geometry to represent flow conditions, without considering the interactions between different collectors. Numerical solutions are for favorable conditions for particle deposition, in absence of an energy barrier. Mechanisms for particle deposition processes are represented by power functions of multiple dimensionless parameters and contributions of these mechanisms are addictive.

Compared to TE model, the RT model overestimates the single collector efficiency for particles with sizes in the Brownian regime (<1 μm). When colloidal particle size is 1-2 μm, η calculated by the RT equation is 50% greater than the numerical solution (131). The primary

drawback of the RT model is that it does not physically account for the effect of hydrodynamics on particle deposition (3, 61, 143). The TE model does not directly introduce the effects of double layer forces on particles (65). The impacts of particle rotation and hydrodynamic retardation are only partly accounted for in the TE equation(147)..

Although existing regression models have been used extensively to describe idealized filtration processes, the limitations of these models still restrict their application to practice. These include:

a) Well established filtration models such as the Yao et al. (1971)(34), RT, and TE models are only valid for clean beds and do not accurately describe colloid deposition at unfavorable conditions for deposition.
b) Oversimplified geometric models of media have been used. The complexities of pore geometries and granular media properties are not quantitatively defined and evaluated. Physical mechanisms that may affect colloid deposition such as collector surface roughness are not incorporated(87).
c) The chemical heterogeneity of collector surfaces and non-uniformity of colloid and collector surface potentials are not taken into consideration in established filtration models (148)'(148).
d) Expressed as an empirical correlation function that contains a number of dimensionless terms (149), existing regression models are in a phenomenological form to predict of colloid transport behavior.

2.7 Influencing factors

It has been recognized that in addition to the forces and interactions introduced in the previous sections, mechanisms including surface roughness, chemical heterogeneity, physical trapping (straining and wedging) and secondary energy minimum may also significantly impact particle deposition behavior. This section will discuss the contribution of these factors to particle deposition.

2.7.1 Chemical heterogeneity

Chemical heterogeneity is defined as the microscopic non-uniformity of charge distribution (discrete charge effect) on colloids and collector surfaces (136, 150-152). Many investigations have demonstrated that chemical heterogeneity can significantly change DLVO interaction energy, thereby affecting particle deposition on surfaces(97, 147, 151, 153, 154). In several studies, colloidal particles were found to deposit on charged surfaces at unfavorable conditions for deposition, even when large energy barriers are present; moreover, the associated observed particle deposition rates were much higher than estimated by classic DLVO theory using average collector surface potentials (112,137,151,155-158). Chemical heterogeneity is believed to be one of the major factors causing such preferential deposition of particles on energetically favorable sites(33).

Although the importance of chemical heterogeneity of surfaces is recognized, it is not well represented by common parameters such as average chemical potential or distribution index. Song et al. (1994) and Adamczyk (1989) used Gaussian probability distributions have been used to describe patch-wise chemical heterogeneity(104, 159). They found that a small patch of heterogeneously charged surface could increase particle deposition by at least two orders of magnitude compared to deposition on homogenous surfaces. Elsewhere, it has been reported that low levels of chemical heterogeneity on collector surfaces substantially enhanced particle deposition at unfavorable conditions for deposition , while no significant changes in deposition were associated with low levels of chemical heterogeneity on collector surfaces at favorable conditions(89, 104, 136, 160, 161).

2.7.2 Straining, wedging and secondary minimum

Physical mechanisms such as secondary energy minima (111, 112, 151, 162), straining (24, 49, 63, 163-165) and wedging in grain-to-grain contact (166, 167) have also been utilized to help explain particle deposition phenomena. At unfavorable conditions for deposition, and with the presence of an energy barrier, the secondary energy minimum has been utilized to explain particle deposition phenomenon as a reversible process during which attached

particles were released to the bulk suspension as ionic strength decreased and re-attached to surfaces while ionic strength increased(111, 112, 162).

Such observations cannot be explained by the framework of classic DLVO theory, according to which attached particles are believed to be trapped and immobilized in the primary energy minimum due to short range forces. In contrast, particles trapped within the secondary energy minimum are further away from collector surfaces where the balance between attractive and repulsive forces exerted on them is affected by changes in ionic strength(151, 168). When ionic strength decreases, the repulsive (EDL) force becomes stronger than the attractive (VDW) force, thereby releasing particles from the secondary energy minimum. In contrast, when ionic strength increases, the energy barrier decreases and the attractive force enables particle attachment on surfaces. Straining is the entrapment of colloids in down-gradient pore throats that are too small to allow particle to pass through in the presence of an energy barrier. Straining is considered as applicable when the $d_{particle}/d_{50}$ is greater than 0.005 (169, 170). The process of wedging in grain-to-grain contact is caused by confinement between two bounding surfaces in the presence of an energy barrier (113, 167). Colloids can also be wedged within grain-to-grain contacts and then removed in flow stagnation zones. The difference between straining and wedging is that in straining, the size of the pore throats is smaller than that of the colloids, whereas in wedging they are larger.

2.8 Surface roughness

Collector surface roughness has been regarded as a key factor that affects particle deposition on surfaces and contributes to discrepancies between experimental observations and theoretical predictions of particle deposition. Numerous studies have been conducted to investigate the impact of roughness on particle deposition phenomenon within the framework of classic DLVO theory and have emphasized changes in interaction energy and other surface chemistry-related interactions(51, 69, 171-179). In contrast, physical interactions such as changes in flow fields, the hydrodynamic retardation, and shear lift have not been quantitatively integrated into this framework.

2.8.1 Description of surface roughness

Surface roughness can generally be described as the three- dimensional irregular topography of surfaces. At present, there is no standard approach for quantitatively describing surface roughness on granular filtration media or other surfaces, though several methods have been reported. "Hypothetical surface morphologies" utilize simple geometries such as spheres, hemi-spheres, cylindrical column or waves with periodic frequency to represent real roughness properties(25, 103, 173, 180). These approaches simplify surface topography so that it can be more readily implemented in quantitative models. The use of simplified surface morphologies is only relevant in some situations, however, because roughness size and spatial distribution on the surface may be somewhat random or more complex than can be described by simplified structures with periodic frequency.

Statistical parameters such as the arithmetic mean (R_a) and root mean square (R_q) of absolute values of surface topographic features such as height can also be used to describe collector surface roughness(174, 181-183). These metrics provide a 'bulk' description of surfaces without detailed information on the spatial arrangements/distributions of roughness elements(175). These parameters are only general descriptors of surface roughness because the same R_a and R_q values can be calculated and obtained from completely different types and/or distributions of surface features.

More recently, surface roughness has also been described using numerical metrics calculated by analysis of images obtained by atomic force microscopy (AFM) or scanning electron microscopy (SEM)(183). During these analyses, measurements are numerically converted to artificial surfaces via decomposition and integration using advanced mathematical approaches such as Fourier transformation(184, 185), Hilbert-Huang transform analysis(186) and fractal analysis(187-189). Although these types of surface roughness estimates are often believed to best represent real collector roughness features, these approaches are complicated and extremely computationally demanding. Accordingly, at present, no existing mathematical models that sufficiently describe surface roughness have been integrated into classic filtration modeling frameworks.

2.8.2 Impact of roughness on particle deposition

It is widely believed that surface roughness can enhance colloidal particle deposition. Table 2-9 summarized experimental studies observed in parallel plate chamber systems regarding the contribution of roughness on various materials with different roughness. Enhanced particle depositions due to the presence of surface roughness were observed within these conducted studies. In general, bigger scale and wider spread of roughness will result greater particle /microorganism deposition. Chemical related mechanisms were also found important to the deposition rate in parallel plate chamber system. However interpretations of the observed results using the classic DLVO theory were not successful.

Table 2-9. Impact of roughness on particle deposition in parallel plate chamber

Study	Selected particle	Selected surface	Major conclusions
Tamai and Suzawa, 1983(190)	Polymethyl methacrylate latex	Fabrics, polyacryloitrile, polyester and cotton	• Deposition rate on Vonnel fabric are not influenced by the change of interaction energy • pH and ionic strength have impacts on deposition rate on Nylon fabric but cannot be fully explained by the change of interaction energy • Colloidal particles preferably attached along the rougher surface grooves than on the smooth surface
Zan et al,2008(176)	mouse MC3T3-E1 *osteoblasts*	Chitonsan-based microsphere	• mouse MC3T3-E1 osteoblasts cells attached more on rough chitonsan-based surface compared to smooth
Vanhaecke et al,1990(94)	*Pseudomonas aeruginosa*	Stainless steel plate	• 120-grit-treated (Roughest) surface in general had the highest deposition of *P.aeruginosa* 848/25 • Chemical parameters such as ionic strength, pH, contact angle also had impacts on deposition rate
Chen et al,2010(69)	Fluorescent carboxylate-modified polystyrene latex microshphere	Bare and zeolite (ZSM-5) coated stainless steel and aluminum alloy	• Surface roughness from micro/macro-scale had a pronounced impact on deposition • Greater roughness resulted in higher colloidal deposition, even when roughness is 2 orders of magnitude smaller than colloids • Two exceptions were found that rough surface (ZSM-5 coated and unpolished aluminum surface) had less deposition than smoother surface

Table 2-9 (Continued). Impact of roughness on particle deposition in parallel plate chamber

Natasa Mitik-Dineva et al, 2009 (174)	*E. coli, P. aeruginosa, and S. aureus*	7105-PPA premium glass	• Nano-scale roughness positively contributed to bacteria deposition • The rate of *E.Coli* , *P.Aeruginosa* and *S.Aureus* can be increased 82%, 119% and 35% respectively • Hydrophobicity (alternatively Contact angle) also influenced the trend of deposition
Darbha et al, 2012 (191)	Latex colloids	Structured silicon surface	• Rough surface constantly provide greater deposition for different sized particle under various operational conditions • Particle rolling, dragging and lifting had been utilized to interpret the deposition phenomena
Darbha et al, 2012(192)	Polystyrene latex colloids	Granodiorite rock	• Highest deposition was found at walls of inter-granular pores with highest roughness area (Ra=500-2000nm) • 2 orders of lower deposition happened on smooth area (Ra<500 nm) • surface roughness enhanced particle deposition has been associated with smaller colloidal particle sizes

Enhanced particle deposition on rough surfaces is not limited to flat plate surfaces – it has also been reported for granular media filtration (i.e., packed bed) systems. In one study, smooth glass beads were coated with polypyrrole to create surface roughness, which resulted in a 180% increase in colloid deposition(193, 194). Shellenberger and Logan (2002) reported increased removal of colloidal (latex microspheres, *E. coli* and *Dechlorosoma sp KJ*.) particles during clean bed filtration, specifically noting 30-40% increases in particle deposition on rough surfaces at low ionic strength (0.01 mM KCl solution) and 50% increases in deposition at high ionic strength (100 mM KCl)(183). Other studies utilizing sand with a variety of grain sizes and surface roughness have also consistently demonstrated greater retention/deposition of colloidal particles on rough media; in this case, both at saturated and unsaturated conditions(175). Improved colloidal particle removal attributable to rough collector surfaces has also been reported during pilot-scale drinking water treatment investigations focusing on granular media filtration. Scott and Emelko (2008) evaluated *Cryptosporidium* oocyst and oocyst-size microsphere (~4.5um diameter) removal at various operational conditions. They reported that, depending on the exact operational conditions (*e.g.*, coagulation dose, loading rate, *etc*.), ceramic media engineered to have greater surface roughness than conventional anthracite media could achieve up to 1.25 $\log_{10}$ (~95%) higher colloidal microsphere removal/deposition and 0.31 $\log_{10}$ (~51%) higher oocyst removal(27).

While several studies have reported comparative increases in particle deposition and attributed them to collector surface roughness, the presence of surface roughness does not ensure higher colloid deposition relative to that achieved on otherwise comparable smooth surfaces. For example, while Morales and Tammo (2009) reported that surface roughness could increase particle removal by 20% when relatively small media (effective size of 0.3-0.4 mm) were used, no differences in particle deposition on smooth and rough 0.8-1.2 mm media were observed(175). Not only has a lack of differences in colloid deposition between otherwise similar rough and smooth media been reported occasionally(183); in some cases, less particle deposition has been reported on rough surfaces relative to otherwise similar smooth surfaces(69). For example, one investigation of the effects of nano-scale roughness on the deposition of bacteria on glass plates demonstrated 218% and 134% higher deposition

of *E. coli* and *P. aeruginosa* respectively on smooth plate surfaces relative to rough ones(174). Based on the experimental observation of above mentioned experiment, it seems like roughness could also negatively contribute to particle deposition which is contradictory to others observations in parallel plate chamber or packed column mentioned before.

Due to the complexities among different experiments, impacts of surface roughness on particle deposition still have not been quantitatively identified. Several reasons would contribute to explain this issue. One of reasons is that there is no quantitative distinguishment of the difference between microscale and macroscale roughness which could contribute to particle deposition differently. Measured statistical parameters, such as R_a, R_q and R_w are able to provide 'bulk descriptions' of roughness feature without classification. Surface with completely different roughness feature might result in same values of measured statistical roughness parameters. As a result, comparison between different experimental results could be difficult. Experiments with well controlled roughness feature in parallel plate chamber or packed beads column were rarely reported in the literature.

It is also changeling to decouple the roughness contribution from other chemical mechanisms which can also impact particle deposition. With different roughness features, hydrophobicity, chemical heterogeneity, pH, hydrodynamic behaviors and chemical potentials of selected deposition surface could be varied significantly. It is also changeling to distinguish the contributions from various physical related mechanisms from roughness including staining, wedging and grain to grain contact. Rigorous experimental studies which can identify the 'purely roughness impacts' and exclude confounding impacts from other chemical/physical-related mechanisms were still missing from reported literature. Overall, these above studies suggest that the impact of collector surface roughness on colloid deposition neither simple and nor monotonic; rather, it is likely non-linear and not monotonic and requires further elucidation.

2.8.3 Impact of roughness on DLVO interaction energy

The influence of surface roughness on interaction energy between collector surfaces and approaching particles has been studied extensively. According to classic DLVO theory, more attractive force exists between the colloids and collector surface, higher deposition flux should be expected. When surface roughness is available even at the level of a few hundreds nanometers, the interaction energy can be reduced substantially and the surface becomes more favorable to particle attachment.

Dabros et al (1977) derived the theoretical formula describing the VDW force between rough spheres and smooth collector surfaces(195). A radial mass distribution of surface irregularities was used in their model. Notably, the calculated VDW interaction energy decreases when surface roughness increases(195). Elimelech and O'Melia (1990) used the pairwise summation method to calculate the interaction energy between negatively charged particles and collector surfaces and estimated the height of the energy barrier at $212kT$ and $23kT$ for smooth and rough (20nm roughness represented by spheres) surfaces respectively; relative to the smooth surface, higher particle deposition on the rough surface at unfavorable conditions for deposition (i.e., low ionic strength) was attributed to this decrease in interaction energy barrier(171). Similar conclusions have been reported by others who have utilized surface element integration (SEI) methods to calculate the interaction energy between approaching particles and collector surfaces with nano-scale roughness using SEI methods(80, 90, 173, 196). Recently, Henry et al. (2011) used the pairwise summation method to estimate the interaction energy between nano- and macro-sized particles and parallel plate collector surfaces with nano-scale roughness(172, 180). They found that there was a critical roughness size that could reduce the energy barrier to a minimum value when the particle and collector were both negatively charged. The value of the critical roughness size depended on the particle size, roughness coverage and distribution on the surface.

Although achieved reasonable progress, several theoretical changelings and experimental limitations still constrain the effectiveness of current interpretations using DLVO theory. In most filtration studies, chemical potentials of colloidal particle and collector surface were

experimentally measured using Debye-Hückel approximation which requires the determined chemical potentials should not exceed $\pm$25.2 mV. However, in realistic practice especially at unfavorable conditions, the measured chemical potentials were mostly higher than 25 mV and therefore introduce bias into the determined data and overestimated the degree of energy barrier.

The classic DLVO theory only evaluate the impact of long range forces including VDW and EDL forces without the consideration of short range forces, chemical absorption and chemical hydrophobicity. Perfect sink boundary condition has been widely utilized into the explanation of attachment which assumes the particle will attach to the surface as long as it approaching to the primary energy minimum and simultaneously removed from the system. The cumulative impacts from attached particles as well as the detachment process were still not included into the DLVO theory. These assumptions are only valid within restrict conditions but not widely applicable with in practice, especially in water filtration. Fitting parameter, attachment efficiency (α) has to be introduced to explain the difference between theoretical interpretation and experimental results.

Current classic DLVO theory often fails to interpret the observed results when roughness is available. The changes on interaction energy can qualitatively describe the trend of deposition rate but not quantitatively. Explanations in the presence of large energy barrier and also the decreased deposition due to roughness presence is still changeling and further studies on DLVO theory, especially the chemical potentials changes due to roughness on colloids and target surface is highly needed.

2.8.4 Impact of roughness on flow field

Inclusion of surface roughness in quantitative models of colloid deposition (e.g., Eulerian approaches to solving the Convection-Diffusion Equation) necessitates modifications to the boundary conditions used to calculate the flow field. When target surfaces are assumed to be smooth, the no-slip boundary condition can be used to determine flow velocity. In contrast, for rough surfaces, a slip or partial-slip boundary condition must be used for accurate flow field calculation(197, 198). In these cases, the appropriate extent of the slip condition

depends on the height and total coverage of roughness elements, as well as surface hydrophobicity and chemical heterogeneity(199, 200). These modified boundary condition can be numerically described using two approaches: changing the no-slip boundary condition to slip (or partial slip), or shifting the original no-slip boundary from the top plane of surface roughness elements to an artificial plane (i.e., an effective target surface) located between the top and bottom of the roughness elements(201-203).The dimensionless distance between the artificial plane and the real surface normalized by the radius of the approaching particle is called "dimensionless slip length". When >50% of a surface is rough, the "effective target surface" can be considered as the plane at the bottom of the roughness elements and the velocity component of flow can be scaled down by dimensionless slip length as shown in Equations 2-53 and 2-54

$$V_{\theta}^{'}(r) = V_{\theta}(r + r_{slip}) \tag{2-53}$$

$$r_{slip} = r_{Roughness} / r_{particle} \tag{2-54}$$

in which $V_{\theta}^{'}(r)$ is the modified radial velocity component of flow and r_{slip} is the dimensionless slip-length(198, 201). When the $r_{Roughness}$ is equal to zero (i.e., no roughness on the collector surface) the velocity component is equal to that when the surface is smooth.

2.8.5 Impact of roughness on hydrodynamic retardation functions

In the vicinity of a surface, the velocity field and the force exerted on an approaching particle should be modified to account for the hydrodynamic disturbances/retardation introduced by the surface/wall (i.e., wall effects). Hydrodynamic correction functions have been developed to describe wall effects and include necessary modifications to the velocity component of the flow field and the forces exerted on an approaching particle when both the particle and target surface are smooth and hydrophilic(53, 125-128). Surface roughness changes the hydrodynamic behavior of particles, however(204). First reported by Vinogradova et al. (1999) (197, 199, 200, 205), for a given distance from the target surface, the hydrodynamic retardation functions between an approaching particle and a rough surface are lower than

those between the same kind of particle and a smooth surface. Specifically, although the shape and behavior of the hydrodynamic retardation function over dimensionless distance were the same for these two scenarios, the curve shifted along the vertical dimensionless distance from the wall. The modified hydrodynamic retardation functions that account for these surface roughness-associated shifts can be represented by either of two mathematical approaches. One method is to apply the slip boundary conditions to derive a new retardation function that includes a correction factor, *f** such that

$$\frac{F_{slip}}{F_{no-slip}} \sim (1+\frac{9}{8}\frac{R}{h}) f^* \tag{2-55}$$

$$f^* = \frac{1}{4}\left(1+\frac{3h}{2b}\left[\left(1+\frac{h}{4b}\right)\ln\left(1+\frac{4b}{h}\right)-1\right]\right) \tag{2-56}$$

in which F_{slip} is the modified hydrodynamic force using the slip boundary condition, $F_{no-slip}$ is the hydrodynamic force using the no- slip boundary condition, *R* is the particle radius, *h* is the separation distance between the approaching particle and the surface and f^* is the correction factor(202).

Another approach for describing the modified hydrodynamic retardation functions by defining an effective target surface, as discussed above. Here, the rough surface is treated as a hydrodynamically equivalent smooth plane (i.e., a no-slip wall) located between the top and bottom of the surface roughness elements such that

$$\frac{F_{new}}{F_{no-slip}} \sim 1+\frac{9}{8}\frac{R}{h+r_{slip}} \tag{2-57}$$

$$r_{slip} = r_{roughness} / r_p \tag{2-58}$$

in which F_{new} represents the modified hydrodynamic force, r_{slip} is the dimensionless slip length obtained by normalizing the roughness size ($r_{roughness}$) by particle radius (r_p)(199, 200, 206). This modification is valid when roughness is smaller than the particle diameter(199,

206). As discussed above, when surface roughness is >50%, the effective target surface can be regarded as located on the bottom of roughness element so that

$$f_i(H) = f_{i-new}(H') = f_{i-new}(H + r_{slip}) \quad (2\text{-}59)$$

$$r_{slip} = r_{roughness} / a_p \quad (2\text{-}60)$$

where H is the dimensionless distance and $r_{roughness}$ is the absolute roughness size, a_p is particle radius, r_{slip} is the dimensionless slip length due to the presence of roughness, $f_i(H)$ is the original hydrodynamic retardation functions and f_{i-new} is the modified hydrodynamic retardation functions accounting the presence of surface roughness. For rough surfaces, the maximum hydrodynamic retardation effect is at $h = r_{slip}$. As necessary, the modified hydrodynamic correction function is the same as the function for smooth surfaces if $r_{roughness} = 0$.

2.8.6 Impact of roughness on Shear lift force

Surface roughness can change the magnitude of shear lift force(114, 115). When a particle is approaching to a target surface, the particle experiences a lift force perpendicular to the direction of oncoming flow; that force essentially "pushes" the particle away from the wall. The magnitude of this lift force depends on the relative transition velocity between the particle and the streamlines in the viscous flow. When a particle is resting on the surface, a shear lift force always exists, tending to drive the particle away from the wall; surface roughness can affect the magnitude that force(123). For example, during low *Re* experiments, the shear lift force was found to increase 3.6 times relative to that on a smooth surface when spheres were assembled to generate surface roughness on flat bottom surface (124, 207).

2.9 Summary

It is commonly recognized that collector surface roughness can impact particle deposition. To date, the effects of surface roughness on particle deposition have been predominantly described within the framework of classic DLVO theory with an emphasis on changes in

interaction energy and other surface chemistry-related interactions. Physical interactions such as changes in flow fields, hydrodynamic retardation, and shear lift must also be considered, however. Chemical heterogeneity, straining, wedging, the existence of a secondary energy minimum, and surface roughness have all been utilized to explain differences between observed and predicted/modeled particle deposition on surfaces; of these, surface roughness remains a clearly critical factor requiring further study and integration into models of particle deposition on surfaces.

2.10 References

1. Tien, C. and Ramarao, B.V. *Granular filtration of aerosols and hydrosols.* Access Online via Elsevier: 2011; .

2. McCarthy, J.F. and McKay, L.D. Colloid transport in the subsurface. *Vadose Zone Journal* **2004,** *3* (2), 326-337.

3. Schijven, J.F. and Hassanizadeh, S.M. Removal of viruses by soil passage: Overview of modeling, processes, and parameters. *Crit. Rev. Environ. Sci. Technol.* **2000,** *30* (1), 49-127.

4. Keswick, B.H. and Gerba, C.P. Viruses in Groundwater. *Environ. Sci. Technol.* **1980,** *14* (11), 1290-1297.

5. Rochelle, P. and Clancy, A. The evolution of microbiology in the drinking water industry. *Journal American Water Works Association* **2006,** *98* (3), 163-+.

6. Emelko, M.B. and Tufenkji, N. Transport and fate of colloids and microbes in granular aqueous environments. *Water Res.* **2010,** *44* (4), 1027-1027; 10.1016/j.watres.2010.02.005.

7. Crittenden, J.C.; Trussell, R.R.; Hand, D.W.; Howe, K.J.; Tchobanoglous, G. *MWH's Water Treatment: Principles and Design.* Wiley. com: 2012; .

8. Emelko, M.B.; Schmidt, P.J.; Reilly, P.M. Particle and Microorganism Enumeration Data: Enabling Quantitative Rigor and Judicious Interpretation. *Environ. Sci. Technol.* **2010,** *44* (5), 1720-1727; 10.1021/es902382a.

9. Logsdon, G.S. Effective management and operation of coagulation and filtration. *Water Air and Soil Pollution* **2000,** *123* (1-4), 159-166.

10. Gregory, D. and Carlson, K. Relationship of pH and floc formation kinetics to granular media filtration performance. *Environ. Sci. Technol.* **2003,** *37* (7), 1398-1403.

11. Kim, J.; Nason, J.A.; Lawler, D.F. Influence of surface charge distributions and particle size distributions on particle attachment in granular media filtration. *Environ. Sci. Technol.* **2008,** *42* (7), 2557-2562.

12. Emelko, M.B.; Huck, P.M.; Coffey, B.M. A review of Cryptosporidium removal by granular media filtration. *Journal American Water Works Association* **2005,** *97* (12), 101-+.

13. Logsdon, G.S.; Horsley, M.B.; Freeman, S.D.N.; Neemann, J.J.; Budd, G.C. Filtration processes - A distinguished history and a promising future. *Journal American Water Works Association* **2006,** *98* (3), 150-+.

14. Williams, G.J.; Sheikh, B.; Holden, R.B.; Kouretas, T.J.; Nelson, K.L. The impact of increased loading rate on granular media, rapid depth filtration of wastewater. *Water Res.* **2007,** *41* (19), 4535-4545.

15. Stevenson, D. Flow and filtration through granular media—the effect of grain and particle size dispersion. *Water Res.* **1997,** *31* (2), 310-322.

16. Emelko, M.B.; Huck, P.M.; Coffey, B.M.; Smith, E.F. Effects of media, backwash, and temperature on full scale biological filtration. *Journal American Water Works Association* **2006,** *98* (12), 61-73.

17. Raveendran, P. and Amirtharajah, A. Role of short-range forces in particle detachment during filter backwashing. *J. Environ. Eng.* **1995,** *121* (12), 860-868.

18. Moran, M.C.; Moran, D.C.; Cushing, R.S.; Lawler, D.F. Particle Behavior in Deep-Bed Filtration .2. Particle Detachment. *Journal American Water Works Association* **1993,** *85* (12), 82-93.

19. Amirtharajah, A. Some Theoretical and Conceptual Views of Filtration. *J. Am. Water Work Assoc.* **1988,** *80* (12), 36-46.

20. Amirtharajah, A. and Raveendran, P. Detachment of Colloids from Sediments and Sand Grains. *Colloids and Surfaces A-Physicochemical and Engineering Aspects* **1993,** *73*, 211-227.

21. O'Melia, C.R. and Ali, W. Role of Retained Particles in Deep Bed Filtration. *Progress in Water Technology* **1978,** *10* (5), 167-182.

22. O'Melia, C.R. Particles, pretreatment, and performance in water filtration. *J. Environ. Eng.* **1985,** *111* (6), 874-890.

23. Moran, D.C.; Moran, M.C.; Cushing, R.S.; Lawler, D.F. Particle Behavior in Deep-Bed Filtration .1. Ripening and Breakthrough. *Journal American Water Works Association* **1993,** *85* (12), 69-81.

24. Bradford, S.A.; Torkzaban, S.; Walker, S.L. Coupling of physical and chemical mechanisms of colloid straining in saturated porous media. *Water Res.* **2007,** *41* (13), 3012-3024; 10.1016/j.watres.2007.03.030.

25. Saiers, J.E. and Ryan, J.N. Colloid deposition on non-ideal porous media: The influences of collector shape and roughness on the single-collector efficiency. *Geophys. Res. Lett.* **2005,** *32* (21), L21406; 10.1029/2005GL024343.

26. Tong, M. and Johnson, W.P. Excess colloid retention in porous media as a function of colloid size, fluid velocity, and grain angularity. *Environ. Sci. Technol.* **2006,** *40* (24), 7725-7731; 10.1021/es061201r.

27. Scott, D.J. Cryptosporidium and Particle Removal from Low Turbidity Water by Engineered Ceramic Media Filtration. **2008,** .

28. Bradford, S.A.; Yates, S.R.; Bettahar, M.; Simunek, J. Physical factors affecting the transport and fate of colloids in saturated porous media. *Water Resour. Res.* **2002,** *38* (12), 63-1-63-12.

29. Bradford, S.A. and Torkzaban, S. Colloid transport and retention in unsaturated porous media: A review of interface-, collector-, and pore-scale processes and models. *Vadose Zone Journal* **2008,** *7* (2), 667-681; 10.2136/vzj2007.0092.

30. Yohe, T. and Getting, T. Effect of Low Uniformity Coefficient Anthracite on Dual-media Filtration. **1999,** .

31. Trussell, R.R.; Trussell, A.R.; Lang, J.S.; Tate, C.H. Recent developments in filtration system design. *AM.WATER WORKS ASSOC.J.* **1980,** *72* (12), 705-710.

32. Tiller, F. and Shirato, M. The role of porosity in filtration: VI. New definition of filtration resistance. *AICHE J.* **1964,** *10* (1), 61-67.

33. Elimelech, M.; Jia, X.; Gregory, J.; Williams, R. *Particle deposition & aggregation: measurement, modelling and simulation.* Butterworth-Heinemann: 1998; .

34. Yao, K.M.; Habibian, M.M.; O'Melia, C.R. Water and Waste Water Filtration - Concepts and Applications. *Environ. Sci. Technol.* **1971,** *5* (11), 1105-&.

35. Bergendahl, J.A. and Grasso, D. Mechanistic basis for particle detachment from granular media. *Environ. Sci. Technol.* **2003,** *37* (10), 2317-2322; 10.1021/es0209316.

36. Kim, J.K. and Lawler, D.F. Particle detachment during hydraulic shock loads in granular media filtration. *Water Science and Technology* **2006,** *53* (7), 177-184; 10.2166/wst.2006.222 ER.

37. Payatake.Ac; Tien, C.; Turian, R.M. Trajectory Calculation of Particle Deposition in Deep Bed Filtration .1. Model Formulation. *AICHE J.* **1974,** *20* (5), 889-900.

38. Tobiason, J.E. and O'Melia, C.R. Physicochemical Aspects of Particle Removal in Depth Filtration. *Journal American Water Works Association* **1988,** *80* (12), 54-64.

39. Clark, S.C.; Lawler, D.F.; Cushing, R.S. Contact Filtration - Particle-Size and Ripening. *Journal American Water Works Association* **1992,** *84* (12), 61-71.

40. Ives, K.J. Research on Deep Filters. *Transactions of the Institution of Chemical Engineers and the Chemical Engineer* **1965,** *43* (8), T238-&.

41. Ives, K.J. and Pienvich.V Kinetics of Filtration of Dilute Suspensions. *Chemical Engineering Science* **1965,** *20* (11), 965-&.

42. O'Melia, C.R. Particles, Pretreatment, and Performance in Water Filtration. *J. Environ. Eng. -ASCE* **1985,** *111* (6), 874-890.

43. Tufenkji, N. and Elimelech, M. Deviation from the classical colloid filtration theory in the presence of repulsive DLVO interactions. *Langmuir* **2004,** *20* (25), 10818-10828; 10.1021/la0486638.

44. Tien, C. and Payatakes, A.C. Advances in Deep Bed Filtration. *AICHE J.* **1979,** *25* (5), 737-759.

45. Ison, C.R. and Ives, K.J. Removal Mechanisms in Deep Bed Filtration. *Chem. Eng. Sci.* **1969,** *24* (4), 717-&.

46. Jegatheesan, V. and Vigneswaran, S. Deep bed filtration: Mathematical models and observations. *Crit. Rev. Environ. Sci. Technol.* **2005,** *35* (6), 515-569; 10.1080/10643380500326432 ER.

47. Rajagopalan, R. and Tien, C. Trajectory Analysis of Deep-Bed Filtration with Sphere-In-Cell Porous-Media Model. *AICHE J.* **1976,** *22* (3), 523-533.

48. Kim, J. and Lawler, D.F. Aspects of particle attachment in filtration. *5th World Water Congress: Drinking Water Quality and Treatment* **2006,** *6* (4), 125-134; 10.2166/ws.2006.898 ER.

49. Bradford, S.A. and Bettahar, M. Straining, attachment, and detachment of Cryptosporidium oocysts in saturated porous media. *J. Environ. Qual.* **2005,** *34* (2), 469-478.

50. Bergendahl, J. and Grasso, D. Prediction of colloid detachment in a model porous media: hydrodynamics. *Chemical Engineering Science* **2000,** *55* (9), 1523-1532.

51. Elimelech, M. and Song, L. Theoretical investigation of colloid separation from dilute aqueous suspensions by oppositely charged granular media. *Separations Technology* **1992,** *2* (1), 2-12; http://dx.doi.org.proxy.lib.uwaterloo.ca/10.1016/0956-9618(92)80001-T.

52. Ma, H.L.; Pedel, J.; Fife, P.; Johnson, W.P. Hemispheres-in-Cell Geometry to Predict Colloid Deposition in Porous Media (vol 43, pg 8573, 2009). *Environ. Sci. Technol.* **2010,** *44* (11), 4383-4383; 10.1021/es1009373 ER.

53. Happel, J. and Brenner, H. *Low Reynolds number hydrodynamics: with special applications to particulate media.* Springer: 1965; Vol. 1, .

54. Payatakes, A.C.; Rajagopalan, R.; Tien, C. Application of Porous-Media Models to Study of Deep Bed Filtration. *Can. J. Chem. Eng.* **1974,** *52* (6), 722-731.

55. Cushing, R.S. and Lawler, D.F. Depth filtration: Fundamental investigation through three dimensional trajectory analysis. *Environ. Sci. Technol.* **1998,** *32* (23), 3793-3801.

56. Payatakes, A.C.; Tien, C.; Turian, R.M. A new model for granular porous media: Part I. Model formulation. *AICHE J.* **1973,** *19* (1), 58-67.

57. Payatakes, A.C.; Tien, C.; Turian, R.M. A new model for granular porous media: Part II. Numerical solution of steady state incompressible Newtonian flow through periodically constricted tubes. *AICHE J.* **1973,** *19* (1), 67-76.

58. Elimelech, M. and Song, L. Deposition of Colloids in Porous-Media - Theory and Numerical-Solution. *ACS Symp. Ser.* **1992,** *491*, 26-39.

59. Nelson, K.E. and Ginn, T.R. Colloid filtration theory and the Happel sphere-in-cell model revisited with direct numerical simulation of colloids. *Langmuir* **2005,** *21* (6), 2173-2184; 10.1021/la048404i.

60. Snyder, L. and Stewart, W. Velocity and pressure profiles for Newtonian creeping flow in regular packed beds of spheres. *AICHE J.* **1966,** *12* (1), 167-173.

61. Nelson, K.E. and Ginn, T.R. New collector efficiency equation for colloid filtration in both natural and engineered flow conditions. *Water Resour. Res.* **2011,** *47* (5).

62. Johnson, W.; Li, X.; Tong, M. Colloid retention behavior in environmental porous media challenges existing theory. *Eos, Transactions American Geophysical Union* **2005,** *86* (18), 179-180.

63. Johnson, W.P.; Ma, H.L.; Pazmino, E. Straining Credibility: A General Comment Regarding Common Arguments Used to Infer Straining As the Mechanism of Colloid Retention in Porous Media. *Environ. Sci. Technol.* **2011,** *45* (9), 3831-3832; 10.1021/es200868e ER.

64. Tufenkji, N. and Elimelech, M. Response to comment on "Correlation equation for predicting single-collector efficiency in physicochemical filtration in saturated porous media". *Environ. Sci. Technol.* **2005,** *39* (14), 5496-5497; 10.1021/es050810g.

65. Rajagopalan, R. and Tien, C. Comment on "Correlation equation for predicting single-collector efficiency in physicochemical filtration in saturated porous media". *Environ. Sci. Technol.* **2005,** *39* (14), 5494-5495; 10.1021/es050309o ER.

66. Adamczyk, Z. and Vandeven, T.G.M. Deposition of Particles Under External Forces in Laminar-Flow through Parallel-Plate and Cylindrical Channels. *J. Colloid Interface Sci.* **1981,** *80* (2), 340-356; 10.1016/0021-9797(81)90193-4.

67. Adamczyk, Z. and Weronski, P. Application of the DLVO theory for particle deposition problems. *Adv. Colloid Interface Sci.* **1999,** *83* (1-3), 137-226; 10.1016/S0001-8686(99)00009-3.

68. Adamczyk, Z. Particle adsorption and deposition: role of electrostatic interactions. *Adv. Colloid Interface Sci.* **2003,** *100*, 267-347; 10.1016/S0001-8686(02)00062-3.

69. Chen, G.; Bedi, R.S.; Yan, Y.S.; Walker, S.L. Initial Colloid Deposition on Bare and Zeolite-Coated Stainless Steel and Aluminum: Influence of Surface Roughness. *Langmuir* **2010,** *26* (15), 12605-12613; 10.1021/la101667t.

70. Azeredo, J.; Pacheco, A.P.; Lopes, I.; Oliveira, R.; Vieira, M.J. Monitoring cell detachment by surfactants in a parallel plate flow chamber. *Water Science and Technology* **2003,** *47* (5), 77-82.

71. Vankooten, T.; Sshakenraad, J.; Vandermei, H.; Busscher, H. Development and use of a Parallel-Plate Flow Chamber for Studying Cellular Adhesion to Solid-Surfaces. *J. Biomed. Mater. Res.* **1992,** *26* (6), 725-738; 10.1002/jbm.820260604.

72. Hamaker, H. The London—van der Waals attraction between spherical particles. *physica* **1937,** *4* (10), 1058-1072.

73. Gregory, J. Approximate expressions for retarded van der waals interaction. *J. Colloid Interface Sci.* **1981,** *83* (1), 138-145; http://dx.doi.org/10.1016/0021-9797(81)90018-7.

74. Spielman, L.A. and Fitzpatrick, J.A. Theory for particle collection under London and gravity forces. *J. Colloid Interface Sci.* **1973,** *42* (3), 607-623.

75. Hogg, R.; Healy, T.W.; Fuersten.Dw Mutual Coagulation of Colloidal Dispersions. *Transactions of the Faraday Society* **1966,** *62* (522P), 1638-&; 10.1039/tf9666201638.

76. Israelachvili, J.N. *Intermolecular and surface forces: revised third edition.* Academic press: 2011; .

77. Walz, J.Y. and Sun, N. Effects of surface roughness on van der Waals and electrostatic contributions to particle-particle interactions and particle adhesion. *Particles of Surfaces 7: Detection, Adhesion and Removal* **2002,** , 151-169.

78. Clayfield, E.; Lumb, E.; Mackey, P. Retarded dispersion forces in colloidal particles—exact integration of the Casimir and Polder equation. *J. Colloid Interface Sci.* **1971,** *37* (2), 382-389.

79. Derjaguin, B.; Muller, V.; Toporov, Y.P. Effect of contact deformations on the adhesion of particles. *J. Colloid Interface Sci.* **1975,** *53* (2), 314-326.

80. Bhattacharjee, S.; Ko, C.H.; Elimelech, M. DLVO interaction between rough surfaces. *Langmuir* **1998,** *14* (12), 3365-3375.

81. Bhattacharjee, S. and Elimelech, M. Surface element integration: A novel technique for evaluation of DLVO interaction between a particle and a flat plate. *J. Colloid Interface Sci.* **1997,** *193* (2), 273-285.

82. Hunter, R.J. Foundations of colloid science (POD). **2000,** .

83. Hunter, R.J.; Hunter, R.J.; Hunter, R.J. *Zeta potential in colloid science : principles and applications.* London ; Toronto : Academic Press: London ; Toronto; London ; Toronto : Academic Press, 1981, 1981; .

84. Gouy, G. Constitution of the electric charge at the surface of an electrolyte. *J.phys* **1910,** *9* (4), 457-467.

85. Chapman, D.L. LI. A contribution to the theory of electrocapillarity. *The London, Edinburgh, and Dublin Philosophical Magazine and Journal of Science* **1913,** *25* (148), 475-481.

86. Verwey, EJ Evert Johannes Willem; Overbeek, J.T.G.; Overbeek, J Th Jan Theodoor Gerard *Theory of the stability of lyophobic colloids.* DoverPublications. com: 1999; .

87. Masliyah, J.H. and Bhattacharjee, S. *Electrokinetic and colloid transport phenomena.* John Wiley & Sons: 2006; .

88. Das, P.K. and Bhattacharjee, S. Finite element estimation of electrostatic double layer interaction between colloidal particles inside a rough cylindrical capillary: effect of charging

behavior. *Colloids and Surfaces A-Physicochemical and Engineering Aspects* **2005,** *256* (2-3), 91-103; 10.1016/j.colsurfa.2004.12.059 ER.

89. Kemps, J.A.L. and Bhattacharjee, S. Interactions between a solid spherical particle and a chemically heterogeneous planar substrate. *Langmuir* **2005,** *21* (25), 11710-11721; 10.1021/la051292q ER.

90. Hoek, E.M.V. and Agarwal, G.K. Extended DLVO interactions between spherical particles and rough surfaces. *J. Colloid Interface Sci.* **2006,** *298* (1), 50-58; 10.1016/j.jcis.2005.12.031.

91. Elimelech, M. Indirect Evidence for Hydration Forces in the Deposition of Polystyrene Latex Colloids on Glass Surfaces. *Journal of the Chemical Society-Faraday Transactions* **1990,** *86* (9), 1623-1624; 10.1039/ft9908601623.

92. Dorobantu, L.S.; Bhattacharjee, S.; Foght, J.M.; Gray, M.R. Analysis of Force Interactions between AFM Tips and Hydrophobic Bacteria Using DLVO Theory. *Langmuir* **2009,** *25* (12), 6968-6976; 10.1021/la9001237 ER.

93. Dorobantu, L.S.; Bhattacharjee, S.; Foght, J.M.; Gray, M.R. Atomic force microscopy measurement of heterogeneity in bacterial surface hydrophobicity. *Langmuir* **2008,** *24* (9), 4944-4951; 10.1021/la7035295 ER.

94. Vanhaecke, E.; Remon, J.P.; Moors, M.; Raes, F.; Derudder, D.; Vanpeteghem, A. Kinetics of Pseudomonas-Aeruginosa Adhesion to 304 and 316-L Stainless-Steel - Role of Cell-Surface Hydrophobicity. *Appl. Environ. Microbiol.* **1990,** *56* (3), 788-795.

95. Considine, R.F.; Drummond, C.J.; Dixon, D.R. Force of interaction between a biocolloid and an inorganic oxide: Complexity of surface deformation, roughness, and brushlike behavior. *Langmuir* **2001,** *17* (20), 6325-6335; 10.1021/la001459+.

96. Bradford, S.A.; Kim, H.N.; Haznedaroglu, B.Z.; Torkzaban, S.; Walker, S.L. Coupled Factors Influencing Concentration-Dependent Colloid Transport and Retention in Saturated Porous Media. *Environ. Sci. Technol.* **2009,** *43* (18), 6996-7002; 10.1021/es900840d.

97. Walz, J.Y. The effect of surface heterogeneities on colloidal forces. *Adv. Colloid Interface Sci.* **1998,** *74*, 119-168.

98. Ison, C.R. and Ives, K.J. Removal Mechanisms in Deep Bed Filtration. *Chemical Engineering Science* **1969,** *24* (4), 717-&.

99. Jegatheesan, V. and Vigneswaran, S. Surface coverage of filter medium in deep bed filtration: Mathematical modeling and experiments. *Sep. Sci. Technol.* **2000,** *35* (7), 967-987.

100. Jegatheesan, V. and Vigneswaran, S. Deep bed filtration: Mathematical models and observations. *Crit. Rev. Environ. Sci. Technol.* **2005,** *35* (6), 515-569; 10.1080/10643380500326432 ER.

101. Van Oss, C.; Good, R.; Chaudhury, M. The role of van der Waals forces and hydrogen bonds in "hydrophobic interactions" between biopolymers and low energy surfaces. *J. Colloid Interface Sci.* **1986,** *111* (2), 378-390.

102. Hermansson, M. The DLVO theory in microbial adhesion. *Colloids and Surfaces B-Biointerfaces* **1999,** *14* (1-4), 105-119.

103. Hoek, E.M.V.; Bhattacharjee, S.; Elimelech, M. Effect of membrane surface roughness on colloid-membrane DLVO interactions. *Langmuir* **2003,** *19* (11), 4836-4847; 10.1021/la027083c.

104. Nazemifard, N.; Masliyah, J.H.; Bhattacharjee, S. Particle deposition onto micropatterned charge heterogeneous substrates: Trajectory analysis. *J. Colloid Interface Sci.* **2006,** *293* (1), 1-15; 10.1016/j.jcis.2005.06.033 ER.

105. Eichenlaub, S.; Kumar, G.; Beaudoin, S. A modeling approach to describe the adhesion of rough, asymmetric particles to surfaces. *J. Colloid Interface Sci.* **2006,** *299* (2), 656-664; 10.1016/j.jcis.2006.03.010.

106. Das, P.K. and Bhattacharjee, S. Electrostatic double-layer interaction between spherical particles inside a rough capillary. *J. Colloid Interface Sci.* **2004,** *273* (1), 278-290; 10.1016/j.jcis.2003.10.003 ER.

107. Derjaguin, B. *Some results from 50 years' research on surface forces.* Springer: 1987; .

108. Derjaguin, B. and Landau, L. The theory of stability of highly charged lyophobic sols and coalescence of highly charged particles in electrolyte solutions. *Zh.Eksp.Teor.Fiz* **1941,** *11* (2), 802-821.

109. Das, P.K. and Bhattacharjee, S. Electrostatic double layer force between a sphere and a planar substrate in the presence of previously deposited spherical particles. *Langmuir* **2005,** *21* (10), 4755-4764; 10.1021/la047147e ER.

110. Tufenkji, N. and Elimelech, M. Breakdown of colloid filtration theory: Role of the secondary energy minimum and surface charge heterogeneities. *Langmuir* **2005,** *21* (3), 841-852; 10.1021/la048102g.

111. Hahn, M.W.; Abadzic, D.; O'Melia, C.R. Aquasols: On the role of secondary minima. *Environ. Sci. Technol.* **2004,** *38* (22), 5915-5924; 10.1021/es049746d.

112. Hahn, M.W. and O'Melia, C.R. Deposition and reentrainment of Brownian particles in porous media under unfavorable chemical conditions: Some concepts and applications. *Environ. Sci. Technol.* **2004,** *38* (1), 210-220; 10.1021/es030416n.

113. Johnson, W.P.; Pazmino, E.; Ma, H. Direct observations of colloid retention in granular media in the presence of energy barriers, and implications for inferred mechanisms from indirect observations. *Water Res.* **2010,** *44* (4), 1158-1169; 10.1016/j.watres.2009.12.014.

114. Saffman, P.G. Correction. *J. Fluid Mech.* **1968,** *31*, 624-&.

115. Saffman, P.G. Lift on a Small Sphere in a Slow Shear Flow. *J. Fluid Mech.* **1965,** *22*, 385-&; 10.1017/S0022112065000824.

116. Vasseur, P. and Cox, R.G. Lateral Migration of a Spherical-Particle in 2-Dimensional Shear Flows. *J. Fluid Mech.* **1976,** *78* (NOV23), 385-413; 10.1017/S0022112076002498.

117. Cox, R. and Hsu, S. The lateral migration of solid particles in a laminar flow near a plane. *Int. J. Multiphase Flow* **1977,** *3* (3), 201-222.

118. Mclaughlin, J.B. The Lift on a Small Sphere in Wall-Bounded Linear Shear Flows. *J. Fluid Mech.* **1993,** *246*, 249-265; 10.1017/S0022112093000114.

119. Cherukat, P. and Mclaughlin, J.B. The Inertial Lift on a Rigid Sphere in a Linear Shear-Flow Field Near a Flat Wall. *J. Fluid Mech.* **1994,** *263*, 1-18; 10.1017/S0022112094004015.

120. Cherukat, P.; McLaughlin, J.B.; Dandy, D.S. A computational study of the inertial lift on a sphere in a linear shear flow field. *Int. J. Multiphase Flow* **1999,** *25* (1), 15-33.

121. Wang, Q.; Squires, K.; Chen, M.; McLaughlin, J. On the role of the lift force in turbulence simulations of particle deposition. *Int. J. Multiphase Flow* **1997,** *23* (4), 749-763.

122. O'Neill, M.E. A Sphere in Contact with a Plane Wall in a Slow Linear Shear Flow. *Chemical Engineering Science* **1968,** *23* (11), 1293-&; 10.1016/0009-2509(68)89039-6.

123. Leighton, D. and Acrivos, A. The Lift on a Small Sphere Touching a Plane in the Presence of a Simple Shear-Flow. *Zeitschrift Fur Angewandte Mathematik Und Physik* **1985,** *36* (1), 174-178; 10.1007/BF00949042.

124. Derksen, J.J. and Larsen, R.A. Drag and lift forces on random assemblies of wall-attached spheres in low-Reynolds-number shear flow. *J. Fluid Mech.* **2011,** *673*, 548-573; 10.1017/S0022112010006403.

125. Brenner, H. The Slow Motion of a Sphere through a Viscous Fluid Towards a Plane Surface. *Chem. Eng. Sci.* **1961,** *16* (3-4), 242-251; 10.1016/0009-2509(61)80035-3.

126. Goldman, A.J.; Cox, R.G.; Brenner, H. Slow Viscous Motion of a Sphere Parallel to a Plane Wall .I. Motion through a Quiescent Fluid. *Chemical Engineering Science* **1967,** *22* (4), 637-&; 10.1016/0009-2509(67)80047-2.

127. Goldman, A.J.; Cox, R.G.; Brenner, H. Slow Viscous Motion of a Sphere Parallel to a Plane Wall .2. Couette Flow. *Chemical Engineering Science* **1967,** *22* (4), 653-&; 10.1016/0009-2509(67)80048-4.

128. Cox, R.G. and Brenner, H. The slow motion of a sphere through a viscous fluid towards a plane surface—II Small gap widths, including inertial effects. *Chemical Engineering Science* **1967,** *22* (12), 1753-1777; http://dx.doi.org/10.1016/0009-2509(67)80208-2.

129. Lawler, D.F. and Nason, J.A. Granular media filtration: old process, new thoughts. *Water Sci. Technol.* **2006,** *53* (7), 1-7; 10.2166/wst.2006.201.

130. O'Melia, C.R. and Stumm, W. Aggregation of Silica Dispersions by Iron(3). *J. Colloid Interface Sci.* **1967,** *23* (3), 437-&.

131. Tufenkji, N. and Elimelech, M. Correlation equation for predicting single-collector efficiency in physicochemical filtration in saturated porous media. *Environ. Sci. Technol.* **2004,** *38* (2), 529-536; 10.1021/es034049r.

132. Rajagopalan, R. and Tien, C. Single Collector Analysis of Collection Mechanisms in Water Filtration. *Can. J. Chem. Eng.* **1977,** *55* (3), 246-255.

133. Yang, J.L.; Bos, R.; Poortinga, A.; Wit, P.J.; Belder, G.F.; Busscher, H.J. Comparison of particle deposition in a parallel plate and a stagnation point flow chamber. *Langmuir* **1999,** *15* (13), 4671-4677; 10.1021/la981607k.

134. Albrecht, F. Theoretical investigations of dust deposition from flowing air and its application to the theory of the dust filter. *Physik.Z* **1931,** *32*, 48.

135. Tien, C. Hydrosol deposition in porous media: the effect of surface interactions. *Advanced Powder Technology* **2000,** *11* (1), 9-56.

136. Rizwan, T. and Bhattacharjee, S. Particle Deposition onto Charge-Heterogeneous Substrates. *Langmuir* **2009,** *25* (9), 4907-4918; 10#1021/la804075g ER.

137. Johnson, W.P. and Hilpert, M. Upscaling colloid transport and retention under unfavorable conditions: Linking mass transfer to pore and grain topology. *Water Resour. Res.* **2013,** *49* (9), 5328-5341.

138. Darby, J.L. and Lawler, D.F. Ripening in Depth Filtration - Effect of Particle-Size on Removal and Head Loss. *Environ. Sci. Technol.* **1990,** *24* (7), 1069-1079.

139. Bradford, S.A.; Simunek, J.; Bettahar, M.; Van Genuchten, M.T.; Yates, S.R. Modeling colloid attachment, straining, and exclusion in saturated porous media. *Environ. Sci. Technol.* **2003,** *37* (10), 2242-2250; 10.1021/es025899u.

140. Logan, B.E.; Jewett, D.G.; Arnold, R.G.; Bouwer, E.J.; O'Melia, C.R. Clarification of Clean-Bed Filtration Models. *Journal of Environmental Engineering-Asce* **1995,** *121* (12), 869-873.

141. Krishnaiah, D.; Sarkar, S.; Rajagoplan, R.; Tien, C.; Pfeffer, R.; Tardos, G. Letters to the editor. *AICHE J.* **1982,** *28* (5), 871-872; 10.1002/aic.690280544.

142. Long, W. and Hilpert, M. A Correlation for the Collector Efficiency of Brownian Particles in Clean-Bed Filtration in Sphere Packings by a Lattice-Boltzmann Method. *Environ. Sci. Technol.* **2009,** *43* (12), 4419-4424; 10.1021/es8024275 ER.

143. Ma, H.; Pedel, J.; Fife, P.; Johnson, W.P. Hemispheres-in-Cell Geometry to Predict Colloid Deposition in Porous Media. *Environ. Sci. Technol.* **2009,** *43* (22), 8573-8579; 10.1021/es901242b.

144. Chang, Y.; Cheng, W.; Tseng, H.; Liao, K. New correlation equations for predicting filter coefficient ratio of submicron particles at high ionic strength when the diffusiophoretic effect is considered. *Colloid Polym. Sci.* **2012,** *290* (9), 801-816.

145. Keh, H.J. and Jan, J.S. Boundary Effects on Diffusiophoresis and Electrophoresis: Motion of a Colloidal Sphere Normal to a Plane Wall. *J. Colloid Interface Sci.* **1996,** *183* (2), 458-475; 10.1006/jcis.1996.0569.

146. Rodrigues, S. and Dickson, S. A Phenomenological Model for Particle Retention in Single, Saturated Fractures. *Groundwater* **2013,** .

147. Tufenkji, N. and Elimelech, M. Reply to comment on breakdown of colloid filtration theory: Role of the secondary energy minimum and surface charge heterogeneities. *Langmuir* **2005,** *21* (23), 10896-10897; 10.1021/la051621e.

148. Kim, J.; Nason, J.A.; Lawler, D.F. Influence of surface charge distributions and particle size distributions on particle attachment in granular media filtration. *Environ. Sci. Technol.* **2008,** *42* (7), 2557-2562.

149. Rockhold, M.L.; Yarwood, R.R.; Selker, J.S. Coupled microbial and transport processes in soils. *Vadose Zone Journal* **2004,** *3* (2), 368-383.

150. Adamczyk, Z.; Nattich, M.; Wasilewska, M.; Zaucha, M. Colloid particle and protein deposition—electrokinetic studies. *Adv. Colloid Interface Sci.* **2011,** *168* (1), 3-28.

151. Tufenkji, N. and Elimelech, M. Breakdown of colloid filtration theory: Role of the secondary energy minimum and surface charge heterogeneities. *Langmuir* **2005,** *21* (3), 841-852; 10.1021/la048102g.

152. Nazemifard, N.; Masliyah, J.H.; Bhattacharjee, S. Particle deposition onto micropatterned charge heterogeneous substrates: Trajectory analysis. *J. Colloid Interface Sci.* **2006,** *293* (1), 1-15; 10.1016/j.jcis.2005.06.033.

153. Zembala, M. Electrokinetics of heterogeneous interfaces. *Adv. Colloid Interface Sci.* **2004,** *112* (1-3), 59-92; 10.1016/j.cis.2004.08.001.

154. Elimelech, M.; Chen, J.Y.; Kuznar, Z.A. Particle deposition onto solid surfaces with micropatterned charge heterogeneity: The "hydrodynamic bump" effect. *Langmuir* **2003,** *19* (17), 6594-6597; 10.1021/la034516i.

155. Li, X.Q. and Johnson, W.P. Nonmonotonic variations in deposition rate coefficients of microspheres in porous media under unfavorable deposition conditions. *Environ. Sci. Technol.* **2005,** *39* (6), 1658-1665; 10.1021/es048963b.

156. Hull, M. and Kitchene.Ja Interaction of Spherical Colloidal Particles with Planar Surfaces. *Transactions of the Faraday Society* **1969,** *65* (563P), 3093-&.

157. Bowen, B. and Epstein, N. Fine Particle Deposition in Smooth Parallel-Plate Channels. *J. Colloid Interface Sci.* **1979,** *72* (1), 81-97; 10.1016/0021-9797(79)90184-X.

158. Vaidyanathan, R. and Tien, C. Hydrosol Deposition in Antigranulocytes Media Under Unfavorable Surface Conditions. *Chemical Engineering Science* **1991,** *46* (4), 967-983.

159. Song, L.; Johnson, P.; Elimelech, M. Kinetics of Colloid Deposition Onto Heterogeneously Charged Surfaces in Porous-Media. *Environ. Sci. Technol.* **1994,** *28* (6), 1164-1171; 10.1021/es00055a030.

160. Nazemifard, N.; Masliyah, J.H.; Bhattacharjee, S. Particle deposition onto charge heterogeneous surfaces: Convection-diffusion-migration model. *Langmuir* **2006,** *22* (24), 9879-9893; 10.1021/la061702q ER.

161. Bhattacharjee, S.; Ryan, J.N.; Elimelech, M. Virus transport in physically and geochemically heterogeneous subsurface porous media. *J. Contam. Hydrol.* **2002,** *57* (3-4), 161-187.

162. Kuznar, Z.A. and Elimelech, M. Direct microscopic observation of particle deposition in porous media: Role of the secondary energy minimum. *Colloids and Surfaces A-Physicochemical and Engineering Aspects* **2007,** *294* (1-3), 156-162; 10.1016/j.colsurfa.2006.08.007 ER.

163. Bradford, S.A.; Simunek, J.; Bettahar, M.; van Genuchten, M.T.; Yates, S.R. Significance of straining in colloid deposition: Evidence and implications. *Water Resour. Res.* **2006,** *42* (12), W12S15; 10.1029/2005WR004791.

164. Li, X.Q.; Johnson, W.P.; Lin, C.L. Direct observation of particle straining using X-ray microtomography. *Abstracts of Papers of the American Chemical Society* **2005,** *229*, 109-COLL.

165. Bradford, S.A.; Bettahar, M.; Simunek, J.; van Genuchten, M.T. Straining and attachment of colloids in physically heterogeneous porous media. *Vadose Zone Journal* **2004,** *3* (2), 384-394.

166. Johnson, W.P.; Tong, M.; Li, X. On colloid retention in saturated porous media in the presence of energy barriers: The failure of alpha, and opportunities to predict eta. *Water Resour. Res.* **2007,** *43* (12), W12S13; 10.1029/2006WR005770.

167. Johnson, W.P.; Li, X.; Yal, G. Colloid retention in porous media: Mechanistic confirmation of wedging and retention in zones of flow stagnation. *Environ. Sci. Technol.* **2007,** *41* (4), 1279-1287; 10.1021/es061301x.

168. Johnson, W.P. and Li, X. Comment on breakdown of colloid filtration theory: Role of the secondary energy minimum and surface charge heterogeneities. *Langmuir* **2005,** *21* (23), 10895-10895; 10.1021/la050850y.

169. Bradford, S.A.; Torkzaban, S.; Walker, S.L. Coupling of physical and chemical mechanisms of colloid straining in saturated porous media. *Water Res.* **2007,** *41* (13), 3012-3024; 10.1016/j.watres.2007.03.030.

170. Bradford, S.A.; Simunek, J.; Bettahar, M.; van Genuchten, M.T.; Yates, S.R. Significance of straining in colloid deposition: Evidence and implications. *Water Resour. Res.* **2006,** *42* (12), W12S15; 10.1029/2005WR004791.

171. Elimelech, M. and O'Melia, C.R. Effect of Particle-Size on Collision Efficiency in the Deposition of Brownian Particles with Electrostatic Energy Barriers. *Langmuir* **1990,** *6* (6), 1153-1163.

172. Henry, C.; Minier, J.; Lefevre, G.; Hurisse, O. Numerical Study on the Deposition Rate of Hematite Particle on Polypropylene Walls: Role of Surface Roughness. *Langmuir* **2011,** *27* (8), 4603-4612; 10.1021/la104488a.

173. Huang, X.F.; Bhattacharjee, S.; Hoek, E.M.V. Is Surface Roughness a "Scapegoat" or a Primary Factor When Defining Particle-Substrate Interactions? *Langmuir* **2010,** *26* (4), 2528-2537; 10.1021/la9028113 ER.

174. Mitik-Dineva, N.; Wang, J.; Truong, V.K.; Stoddart, P.; Malherbe, F.; Crawford, R.J.; Ivanova, E.P. Escherichia coli, Pseudomonas aeruginosa, and Staphylococcus aureus Attachment Patterns on Glass Surfaces with Nanoscale Roughness. *Curr. Microbiol.* **2009,** *58* (3), 268-273; 10.1007/s00284-008-9320-8.

175. Morales, V.L.; Gao, B.; Steenhuis, T.S. Grain Surface-Roughness Effects on Colloidal Retention in the Vadose Zone. *Vadose Zone Journal* **2009,** *8* (1), 11-20; 10.2136/vzj2007.0171.

176. Zan, Q.F.; Wang, C.; Dong, L.M.; Cheng, P.; Tian, J.M. Effect of surface roughness of chitosan-based microspheres on cell adhesion. *Appl. Surf. Sci.* **2008,** *255* (2), 401-403; 10.1016/j.apsusc.2008.06.074 ER.

177. Mendez-Vilas, A.; Bruque, J.M.; Gonzalez-Martin, M.L. Sensitivity of surface roughness parameters to changes in the density of scanning points in multi-scale AFM studies. Application to a biomaterial surface. *Ultramicroscopy* **2007,** *107* (8), 617-625; 10.1016/j.ultramic.2006.12.002.

178. Katainen, J.; Paajanen, M.; Ahtola, E.; Pore, V.; Lahtinen, J. Adhesion as an interplay between particle size and surface roughness. *J. Colloid Interface Sci.* **2006,** *304* (2), 524-529; 10.1016/j.jcis.2006.09.015.

179. Khan, S.P.; Auner, G.G.; Newaz, G.M. Influence of nanoscale surface roughness on neural cell attachment on silicon. *Nanomedicine* **2005,** *1* (2), 125-9.

180. Henry, C.; Minier, J.; Lefevre, G. Numerical Study on the Adhesion and Reentrainment of Nondeformable Particles on Surfaces: The Role of Surface Roughness and Electrostatic Forces. *Langmuir* **2012,** *28* (1), 438-452; 10.1021/la203659q.

181. Darbha, G.K.; Schaefer, T.; Heberling, F.; Luettge, A.; Fischer, C. Retention of Latex Colloids on Calcite as a Function of Surface Roughness and Topography. *Langmuir* **2010,** *26* (7), 4743-4752; 10.1021/la9033595.

182. Roy, A.; Bhattacharjee, K.; Lenk, H.P.; Mahapatra, D.P.; Dev, B.N. Surface roughness of ion-bombarded Si#100# surfaces: Roughening and smoothing with the same roughness exponent. *Nuclear Instruments & Methods in Physics Research Section B-Beam Interactions with Materials and Atoms* **2008,** *266* (8), 1276-1281; 10.1016/j.nimb.2007.10.045 ER.

183. Shellenberger, K. and Logan, B.E. Effect of molecular scale roughness of glass beads on colloidal and bacterial deposition. *Environ. Sci. Technol.* **2002,** *36* (2), 184-189; 10.1021/es015515k ER.

184. Cooper, K.; Gupta, A.; Beaudoin, S. Simulation of the adhesion of particles to surfaces. *J. Colloid Interface Sci.* **2001,** *234* (2), 284-292; 10.1006/jcis.2000.7276.

185. Cooper, K.; Ohler, N.; Gupta, A.; Beaudoin, S. Analysis of contact interactions between a rough deformable colloid and a smooth substrate. *J. Colloid Interface Sci.* **2000,** *222* (1), 63-74.

186. Markov, B. and Loginov, A. Use of Hilbert–Huang transformation in the measurement of the roughness of surfaces. *Measurement Techniques* **2012,** , 1-4.

187. Komvopoulos, K. Surface engineering and microtribology for microelectromechanical systems. *Wear* **1996,** *200* (1), 305-327.

188. Yan, W. and Komvopoulos, K. Contact analysis of elastic-plastic fractal surfaces. *J. Appl. Phys.* **1998,** *84* (7), 3617-3624.

189. Eichenlaub, S.; Gelb, A.; Beaudoin, S. Roughness models for particle adhesion. *J. Colloid Interface Sci.* **2004,** *280* (2), 289-298; 10.1016/j.jcis.2004.08.017.

190. Tamai, H.; Nagai, Y.; Suzawa, T. Interfacial Electrical Studies on the Deposition of Polymer Latexes Onto Fabrics and the Removal of these Deposited Latexes .6. Latex Deposition on Fibers .6. Deposition State and Interaction Energy. *J. Colloid Interface Sci.* **1983,** *91* (2), 464-471.

191. Darbha, G.K.; Fischer, C.; Michler, A.; Luetzenkirchen, J.; Schaefer, T.; Heberling, F.; Schild, D. Deposition of Latex Colloids at Rough Mineral Surfaces: An Analogue Study Using Nanopatterned Surfaces. *Langmuir* **2012,** *28* (16), 6606-6617; 10.1021/la3003146.

192. Darbha, G.K.; Fischer, C.; Luetzenkirchen, J.; Schäfer, T. Site-specific retention of colloids at rough rock surfaces. *Environ. Sci. Technol.* **2012,** *46* (17), 9378-9387.

193. Bai, R.B. and Zhang, X. Polypyrrole-coated granules for humic acid removal. *J. Colloid Interface Sci.* **2001,** *243* (1), 52-60.

194. Bai, R.B. and Tien, C. Effect of deposition in deep-bed filtration: Determination and search of rate parameters. *J. Colloid Interface Sci.* **2000,** *231* (2), 299-311.

195. Dabros, T.; Adamczyk, Z.; Czarnecki, J. Transport of Particles to a Rotating-Disk Surface Under an External Force-Field. *J. Colloid Interface Sci.* **1977,** *62* (3), 529-541; 10.1016/0021-9797(77)90104-7.

196. Bendersky, M. and Davis, J.M. DLVO interaction of colloidal particles with topographically and chemically heterogeneous surfaces. *Journal of Colloid And Interface Science* **2011,** *353*, 87-97.

197. Kunert, C.; Harting, J.; Vinogradova, O.I. Random-Roughness Hydrodynamic Boundary Conditions. *Phys. Rev. Lett.* **2010,** *105* (1), 016001; 10.1103/PhysRevLett.105.016001.

198. Neto, C.; Evans, D.; Bonaccurso, E.; Butt, H.; Craig, V. Boundary slip in Newtonian liquids: a review of experimental studies. *Reports on Progress in Physics* **2005,** *68* (12), 2859-2897; 10.1088/0034-4885/68/12/R05.

199. Vinogradova, O. and Yakubov, G. Surface roughness and hydrodynamic boundary conditions. *Physical Review E* **2006,** *73* (4), 045302; 10.1103/PhysRevE.73.045302.

200. Vinogradova, O.I. and Belyaev, A.V. Wetting, roughness and flow boundary conditions. *Journal of Physics-Condensed Matter* **2011,** *23* (18), 184104; 10.1088/0953-8984/23/18/184104.

201. Zhu, Y.X. and Granick, S. Limits of the hydrodynamic no-slip boundary condition. *Phys. Rev. Lett.* **2002,** *88* (10), 106102; 10.1103/PhysRevLett.88.106102.

202. Bonaccurso, E.; Butt, H.J.; Craig, V.S.J. Surface roughness and hydrodynamic boundary slip of a newtonian fluid in a completely wetting system. *Phys. Rev. Lett.* **2003,** *90* (14), 144501; 10.1103/PhysRevLett.90.144501.

203. Pit, R.; Hervet, H.; Leger, L. Direct experimental evidence of slip in hexadecane: Solid interfaces. *Phys. Rev. Lett.* **2000,** *85* (5), 980-983; 10.1103/PhysRevLett.85.980.

204. Degennes, P. Wetting - Statics and Dynamics. *Rev. Mod. Phys.* **1985,** *57* (3), 827-863; 10.1103/RevModPhys.57.827.

205. Vinogradova, O. Slippage of water over hydrophobic surfaces. *Int. J. Miner. Process.* **1999,** *56* (1-4), 31-60; 10.1016/S0301-7516(98)00041-6.

206. Mongruel, A.; Chastel, T.; Asmolov, E.S.; Vinogradova, O.I. Effective hydrodynamic boundary conditions for microtextured surfaces. *Physical Review E* **2013,** *87* (1), 011002; 10.1103/PhysRevE.87.011002.

207. Derksen, J.J. Drag on random assemblies of spheres in shear-thinning and thixotropic liquids. *Phys. Fluids* **2009,** *21* (8), 083302; 10.1063/1.3200946.

Chapter 3
Non-linear, non-monotonic impact of surface roughness on colloidal particle deposition during granular media filtration at favorable conditions

3.1 Overview

Surface roughness can impact colloidal particle deposition on surfaces such as porous media. In this study, it was hypothesized that the relationship between particle deposition and media surface roughness is non-linear, non-monotonic. Column tests were conducted using two sizes of colloidal particles (1.0 and 4.5 μm diameter polystyrene microspheres), two sizes of glass beads (0.707 to 0.841 mm and 0.5 to 0.595 mm diameter) and three different levels of surface roughness. All of the experiments were conducted at a loading rate of 1.5 m/h and favorable conditions for deposition (i.e., microspheres were suspended in 100 mM KCl). The normalized effluent concentration (C/C_0) was used to evaluate the difference between various operational conditions whereas spatial distribution of attached particles and total mass recovery in the packed column were utilized to verify the experimental observations. The experiments demonstrated that surface roughness can not only enhance particle deposition, but also decrease it. Classic colloid filtration theory (CFT), chemical heterogeneity, and hydrophobicity fail to explain this non-linear, non-monotonic impact of surface roughness on particle deposition; particularly decreased deposition resulting from increased surface roughness. Consideration of the fluid flow field, shear lift force and particle rolling can assist in explaining the experimental observations reported herein. Overall, this work demonstrates a minimum particle deposition efficiency that is unique to each combination of sizes of colloidal particle, collector, and collector roughness.

3.2 Introduction

A thorough understanding of the physical and chemical mechanisms of particle removal by granular media filtration is required for better evaluation and optimization of particle and microorganism removal by filtration in engineered and natural (e.g., subsurface) systems (1-5). In the past few decades, numerous experimental and theoretical studies have been conducted to investigate the effects of multiple factors affecting particle deposition. These include: the properties of particles and filtration media (6, 7), physico-chemical (or biological) interactions between particles and media (8, 9), and system operational conditions (10, 11). Among these, the morphology of media surfaces (i.e. roughness) is a particularly important factor (12-14) that remains unaddressed in CFT (15-17).

It is widely believed that media surface roughness can enhance colloidal particle deposition on surfaces; numerous examples of this effect exist in the literature. Tamai (1983) (18) examined the deposition behavior of polystyrene latex particles on polyamide and polyacrylonitrile fibers and found that the colloidal particles preferably attached along surface grooves with roughness rather than on open smooth planes. Bai and Zhang (2000; 2001) (19, 20) coated glass beads with polypyrrole and observed that particle deposition on the relatively rough, coated surfaces was considerably higher than on the uncoated, smooth beads. Similarly, Shellenberger and Logan (2002) (21) investigated the deposition of latex microspheres and two strains of bacteria (*E. coli* and *Dechlorosoma sp* KJ.) suspended in a high ionic strength solution and observed 50% higher deposition on rough glass beads as compared to smooth ones; several other similar examples exist (22, 23).

In contrast, several studies have also reported that surface roughness did not enhance particle or bacterial deposition in packed columns or on flat plate surfaces. For example, Morales et al. (2009) (24) reported that surface roughness resulted in a 20% increase in particle removal by small media with an effective size of 0.3-0.4 mm, but not by media with 0.8-1.2 mm effective size. Similarly, Shellenberger and Logan (2002) (21) did not observe any differences in particle removal when high ionic strength suspensions of latex microspheres were passed through rough and smooth media. Moreover, Chen et al (2010) investigated

nano-scale roughness on stainless steel/aluminum plates and reported less particle deposition on rough surfaces relative to smooth ones. Several other studies have reported similar outcomes (12, 13, 25).

Within the framework of CFT, it has been suggested that particle deposition is governed by DLVO forces, which are the sum of Lifshtz-van der Waals attraction forces and electrostatic double layer repulsive forces (26). It is believed that only a few nanometers of surface roughness can reduce the magnitude of interaction energy substantially thereby enhancing particle deposition because of longer separation distances created by roughness features (27-30). Surface charge heterogeneity, attachment within the secondary energy minimum, and hydration and hydrophobicity have also been used to explain contributions of surface roughness to particle deposition (31-34). Other factors that may also help to interpret contributions of surface roughness to particle deposition include straining (35, 36), grain to grain contact (37), the "shadow effect" (38) and others (39, 40). While all of these factors may be able to qualitatively explain surface roughness impacts on particle deposition in specific situations, none have been proven broadly applicable.

In the present study, a non-linear, non-monotonic relationship between surface roughness and colloidal particle deposition on surfaces was hypothesized. Column tests were conducted using two colloidal particles (1.0 and 4.5 μm diameter polystyrene carboxylated microspheres), two sizes of glass beads (Medium A: 0.707 to 0.841 mm and Medium B: 0.5 to 0.595 mm) and three levels of surface roughness (Treatment 0 – smooth, Treatment 1 – moderately rough, and Treatment 2 – roughest). All of the experiments were conducted at a loading rate of 1.5 m/h, with the microspheres suspended in a background electrolyte solution of 100 mM KCl (i.e., favorable conditions for particle deposition).

3.3 Materials and Methods

3.3.1 Colloidal particles

Two sizes of carboxylated, fluorescent-dyed polystyrene microspheres (Fluoresbrite YG microspheres, Polysciences Inc., Warrington, PA) microspheres were used: 1.0 μm and 4.5 μm diameter. These sizes were verified by dynamic light scattering (Zetasizer NanoZS Malvern). The stock suspensions of 1.0 μm and 4.5 μm microspheres contained 4.99 x 10^{10} and 4.99 x 10^{8} microspheres/mL, respectively. The density of the microspheres was 1.045g/mL.

Prior to introducing the microspheres into the filtration column, the 1.0 μm and 4.5 μm microsphere stock suspensions were diluted to achieve influent concentrations (C_0) of 5.7 x 10^{7} and 1.0 x 10^{6} particles/mL, respectively, with pH of 6.5-6.7. The microspheres were suspended in 100 mM KCl, thereby creating favorable conditions for particle deposition. The colloid suspensions were sonicated in a water bath for 30 minutes before and during the experiment to prevent particle aggregation. This was confirmed using epifluorescence microscopy before and after the experiments.

3.3.2 Granular porous media and surface modification

Two sizes of spherical soda-lime glass beads (Class V, MO-SCI Corporation, Rolla, MO) were used as model collectors. The beads were size-fractioned with nylon sieves (U.S standard size of 20-25 and 30-35) and had diameters of 0.707 to 0.841 mm (Medium A) and 0.5 to 0.595 mm (Medium B). Prior to modification, the glass beads had smooth surfaces (less than 2 nm of roughness). The glass beads were first soaked in 2% Extran™ (VWR, Canada) for 30 minutes and then sonicated for 15 minutes to remove metal and organic impurities. The beads were extensively rinsed with deionized (DI) water and then soaked in 12N HCl (Fisher Scientific, Canada) for 12 hours, after which they were washed with Milli-Q™ water and baked at 550˚C overnight.

Hydrofluoric acid (BDH, Canada) was used to etch the glass surfaces (41) to achieve varying levels of surface roughness. The etching rate is related to HF acid concentration and reaction

time. Two different acid concentrations and etching durations were employed to generate roughness at two different scales. Micro-scale roughness was achieved by soaking the glass bead in 8% HF acid for 30 minutes (Treatment 1 – moderately rough), whereas macro-scale roughness was achieved by soaking in 36% HF acid for 12 hours (Treatment 2 - roughest). During the etching process, a magnetic bar was continuously used to maintain uniform etching conditions. After etching, the modified glass beads were extensively rinsed with Milli-Q^{TM} water until the rinse water reached a pH of 6.72-6.92. The rinsed beads were then baked at 550 ˚C for 12 hours to remove any residuals or impurities.

3.3.3 Characterization of media surface properties

The surface topography of the etched glass beads was assessed using Scanning Electron Microscopy (SEM) (JEOL 6380LV) with 3-Dimensional fractographic analysis. The glass bead samples were coated with 10 nm of pure gold for electric conduction and mounted on a steel plate for measurement. In contrast to more commonly used SEM approaches, the sample images were collected from two different viewpoints located on the same plane with 6 º to 8 º differences in angularity. By knowing the parallax distance, the microscope magnification, and the tilting angle, the pair of SEM topographic images could be automatically merged by the stereophotogrammetry software to generate 3-D images of the glass beads, which provide a detailed view of the surface roughness on these curved surfaces (42). Mercury intrusion porosimetry (MIP) (Porous Materials, Inc.) was also used to evaluate the pore volume distribution and total surface area on the surface of the glass beads (43, 44).

3.3.4 Electrokinetic Characterization of colloidal particles and collectors

Microelectrophoresis (ZetaSizer Nano ZS, Malvern) was used to characterize the electrokinetic properties of the polystyrene microspheres in the background electrolyte solution (100mM KCl) used during column experiments. The electrophoretic mobility was measured in triplicate at 22 ±1˚C using particle suspensions of 1.0 x10^6 for 4.5 μm particles/mL and 2.3 x10^8 for 1.0 μm particles/mL, respectively. Zeta-potentials were calculated from the measured electrophoretic motilities using Smoluchowski's equation (45).

Cleaned glass beads were wet packed at a bed depth of 3 cm and rinsed extensively with DI water and then equilibrated with background electrolyte solution (100mM KCl). Measured at a fixed pH value (5.7-5.8), cleaned glass beads (7 g) were sonicated for 20 min in 12 mL of background electrolyte solution (100mM KCl). The supernatant from each sonicated sample was then diluted 10 times with the background electrolyte solution (100mM KCl). The electrophoretic mobility of the supernatant was then measured and used to calculate the chemical potentials on the glass bead surfaces using the Smoluchowski equation (46).

3.3.5 Column experiments

Bench scale column tests were conducted by pumping the colloidal particle suspensions through an adjustable-height glass chromatography column (GE health care, C16/20) with 1.6 cm inner diameter. The glass beads were wet-packed to a height of 15.0 ± 0.1 cm with vibration to maximize compaction and minimize air entrapment and formation of preferential pathways for fluid flow and associated particle transport. Using a standard gravimetric method, the porosities of the packed media were determined to be 0.38 and 0.37 for Medium A and B, respectively (47, 48).

To ensure that the packed media were saturated with the background electrolyte solution (100mM KCl), 30 pore volumes of particle-free background electrolyte were pumped through the packed bed at a constant loading rate (1.5m/h) prior to introducing microspheres to the column influent. Then, 6 pore volumes of the colloidal particle suspension were passed through the column. The seed suspension was continuously sonicated to prevent particle aggregation and maintain a constant influent concentration. All experiments were conducted in duplicate.

Column effluent samples were collected every minute in 5 mL glass tubes using a fraction collector (Spectra/Chrom CF-1, Houston, USA). The microsphere concentrations in the effluent samples were determined by measuring UV absorbance (HP model 8453 UV-spectrophotometer) at 280 nm and 220 nm for the 4.5 μm and 1.0 μm particles respectively (9). To ensure uniform microsphere suspensions, the column effluent samples were sonicated

for 3 minutes and then vortexed for 15 seconds prior to measuring absorbance. The particle concentrations were then calculated using a calibration curve (Appendix A).

Destructive sampling was conducted after every experiment to determine the spatial distribution of microspheres within the packed column and to perform a mass balance to evaluate any microsphere loss within the system. After each experiment, the packed media were removed from the column in seven discrete segments (six 2 cm segments and one 3 cm segment). Each segment was placed in a glass tube (20 ml) containing 10 mL of Milli-Q^{TM} water and the mass of the medium was recorded. The glass tubes were sonicated for 15 minutes and then vortexed for 30 seconds at 2000 rmp to release attached microspheres and obtain a homogeneous supernatant. A 1 mL sample of supernatant was collected from each tube and the microsphere concentration was enumerated using a previously described method (49). Samples were diluted with background electrolyte solution as necessary.

3.3.6 Determination of deposition coefficiency and attachment efficiency

The transport and deposition of colloidal particles in porous media have been modeled by Eulerian (50) and Lagrangian (51) methods to predict particle attachment efficiency (α) during physico-chemical filtration. Using normalized (C/C_0) steady-state particle breakthrough curves, the deposition coefficient (k_d) and the particle attachment efficiency (α) were calculated by:

$$k_d = \frac{3(1-\varepsilon)}{2d_c\varepsilon}\alpha\eta_0 v \tag{3-1}$$

$$\alpha = -\frac{2d_c}{3(1-\varepsilon)L\eta_0}\ln(C/C_0) \tag{3-2}$$

where the ε is the porosity of the medium, d_c is the collector diameter, η_0 is the single collector contact efficiency, v is the fluid velocity, and L is the bed depth (52).

3.4 Results

3.4.1 Media surface roughness

The surface roughness of the smooth and modified (etched) glass beads was evaluated using SEM and 3-D fractographic analysis. Media surface characteristics are summarized in Table 3- 1 and representative images depicting modifications in surface roughness on Medium A and B are presented in Figure 3-1. These images demonstrate that both types of beads had the roughest surfaces after Treatment 2 (the longest period of etching). The surface asperities on the modified glass beads included both macro-and micro-scale roughness which indict relatively large and small morphology variations as compared to the approaching particles that covered the entire media surface. In contrast, Treatment 1 (the shorter etching period) created "moderate roughness" comprised of micro-scale roughness features with relatively few macro-scale asperities. Untreated, smooth glass beads did not have macro-scale asperities and only minimal micro-scale roughness (< 20-30 nanometers). The root mean square height (R_q) of unmodified smooth beads of Medium A and B was 11.5 ±7.6nm and 8.3 ±3.9nm respectively. Treatment 1 (moderate roughness) resulted in surface roughness (R_q) of 185.9 ±37.8nm and 154.3 ±28.3nm on Medium A and B respectively. Treatment 2 (roughest surface) resulted in surface roughness (R_q) of 579.6 ±76.5nm and 694.2 ±89.9 nm on Medium A and B, respectively.

	130X Magnification	*3-Dimensional view*		*130X Magnification*	*3-Dimensional view*
Medium A-T_0	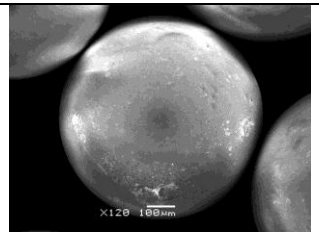	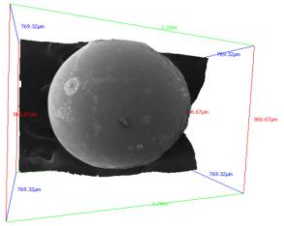	Medium B-T_0	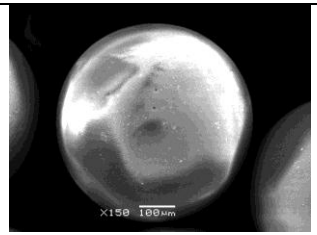	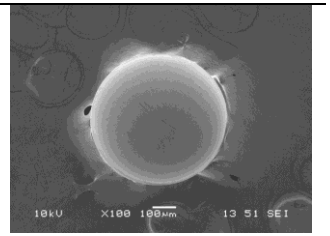
Medium A-T_1	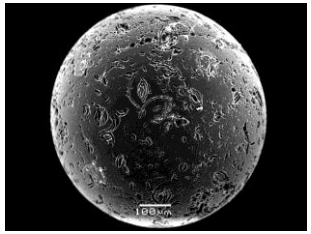	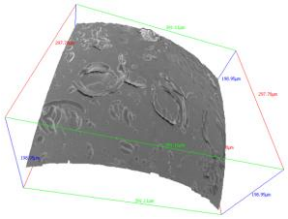	Medium B-T_1	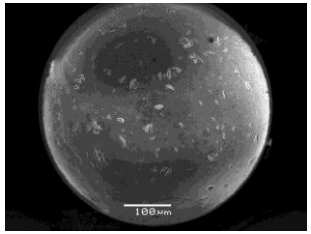	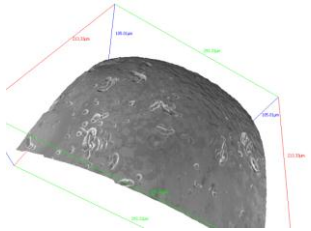
Medium A-T_2	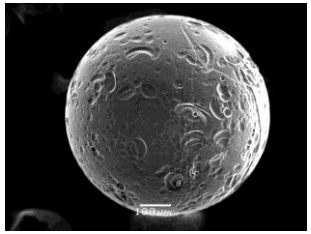	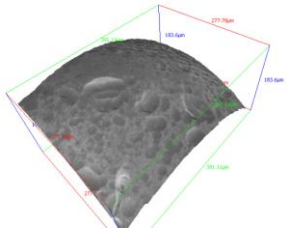	Medium B-T_2	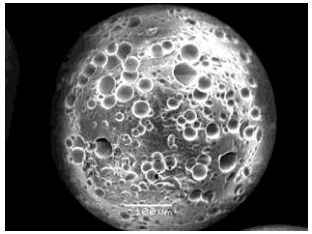	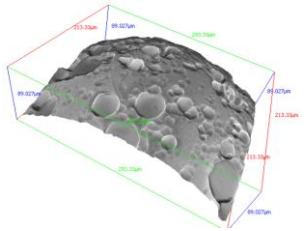

Figure 3-1. Representative 2-D and 3-D SEM images of Medium A and Medium B (US standard, Mesh 20-25 and Mesh 30-35) with no treatment - smooth (T0), Treatment 1 – moderate roughness (T1) and Treatment 2 – roughest (T2).

3.4.2 Media cumulative surface area and cumulative pore volume (CPV)

Although SEM images provide quantitative information regarding media surface roughness, they cannot describe media characteristics relevant to packing in a filter column. Surface roughness modifications can also impact "bulk properties" associated with pack beds, such as total surface area and CPV. Mercury intrusion porosimetry results for the total surface area and CPV of the media used in the column experiments are presented in Table 3-1. These results indicate that as roughness generated during the chemical etching process in the present investigation increased, CPV and total surface area also increased, regardless of media size.

Cumulative pore volume (CPV) is the pore space on the media surface, and is sometimes referred to as media porosity. It should be distinguished from the more typical use of "porosity", which refers to void spaces in the pack bed and is more dependent on the physical size of the media and packing method (i.e., bed porosity). Two filter columns packed in the same manner, but with media of differing roughness may have the same bed porosity but different CPV. In the present investigation, packed bed porosity was the same in all filter columns containing the same size of media, regardless of media roughness (Table 3-1). In contrast, the CPV of smooth Media A and B increased by 10.7% and 24.0% respectively after Treatment 1, and 39.3% and 39.6% respectively after Treatment 2 (Table 3-1).

Table 3-1. Characterization of physical and chemical properties of glass beads

Media type-Treatment	*Media size*	*Roughness (R_q)*	*Porosity*	*Cumulative pore volume*	*Total surface area*	*Zeta potential*
	(μm)	(nm)	-	(ml/g)	(m^2/g)	(mV)
Medium A-T_0	710-840	11.5 ±7.6	0.38	0.0184	0.0016	-20.3 ±6.6
Medium A-T_1		185.9 ±37.8	0.38	0.0206	0.0019	-17.9 ±8.3
Medium A-T_2		579.6 ±76.5	0.38	0.0303	0.003	-19.6 ±7.3
Medium B-T_0	500-550	8.3 ±3.9	0.37	0.0329	0.0022	-23.9 ±5.3
Medium B-T_1		154.3 ±28.3	0.37	0.0433	0.0028	-19.4 ±7.8
Medium B-T_2		694.2 ±89.9	0.37	0.0547	0.0034	-21.2 ±6.3

3.4.3 Zeta potentials and DLVO interaction energy

Accurate calculation of the DLVO interaction energy between the particles and media with unevenly distributed roughness is difficult because it requires very precise measurements of surface roughness; however, the range of the DLVO interaction energies can be estimated. The zeta potentials of the 1.0 μm and 4.5 μm microspheres suspended in 100 mM KCl background electrolyte solution were -20.3±6.6 and -17.5±8.9 mv respectively. The chemical potentials of the glass beads are listed in Table 3-1. Although surface roughness was relatively evenly distributed herein, the range of the DLVO interaction energies associated with the roughness still needed to be estimated. Here, the minimum of the range was calculated by assuming smooth media. The maximum of the range was calculated by assuming the roughness was 1) represented by the average root mean square roughness size (e.g., R_q = 0.5 μm) and 2) distributed uniformly on the media surface with 100% coverage. These estimated interaction energies suggest that the high ionic strength of the background electrolyte solution decreased the energy barriers between the microspheres and the glass bead media surfaces by electrostatic double layer compression; accordingly, the system conditions favored microsphere deposition on the media surfaces without the presence of large interaction energy barriers.

3.4.4 Column experiments

Representative microsphere breakthrough curves are presented in Figure 3-2. Effluent particle concentration (C; mean of initial concentration values) was normalized by the initial microsphere concentration (C_0) in the feed suspension (C/C_0) and plotted against the number of pore volumes of the suspension that had passed through the filter column. Error bars indicate one standard deviation. The average value of the effluent concentration measured between PV = 2.0 and 6.0 was used to calculate microsphere/particle deposition using Equations 3-2 and 3-3 (Appendix A).

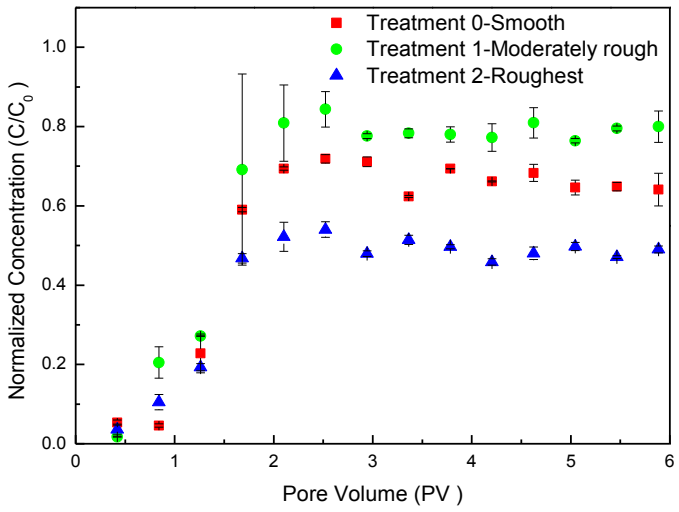

Figure 3-2. Representative (a) normalized effluent 4.5 µm microsphere concentration curves for particle passage through Medium A (0.71 to 0.84 mm glass beads with porosity = 0.38) with no treatment (Treatment 0 - smooth) (■), Treatment 1 – moderately rough (•) and Treatment 2 – roughest (▲).

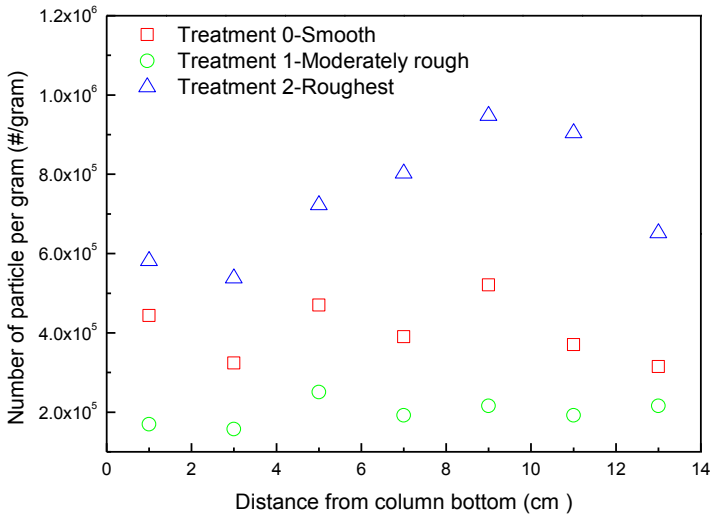

Figure 3-3. Representative spatial retained particle distributions (open symbol) for particle retention in Medium A (0.770 to 0.850 mm glass beads with porosity = 0.38) with no treatment (Treatment 0 - smooth) (□), Treatment 1 – moderately rough (○) and Treatment 2 – roughest (△).

Destructive sampling of the filter beds confirmed microsphere retention on the media surfaces and reasonable mass balance within the system, thereby validating the particle deposition outcomes from the breakthrough curves. Specifically, the normalized filter effluent microsphere concentrations during the column tests (Figure 3-3) and the fraction of microspheres retained on the media during the column tests (Figure 3-4) were added to obtain total mass recovery during the column tests. Mass recoveries of the 4.5 μm microspheres were consistently close to 100%; mean recovery (± standard deviation) was 98.68 %± 4.6%. Mass recovery of the 1.0 μm ranged between 85 and 99%, with mean recovery (± standard deviation) of 89.7% ± 8.04%. The slightly lower recovery associated with 1.0 μm microspheres was because the chemical bonding between the small particles and the media surfaces was stronger than that between the big particle and the media surface. The extensive washing procedure may not be able to remove all the small particles bonded to the media (11, 53).

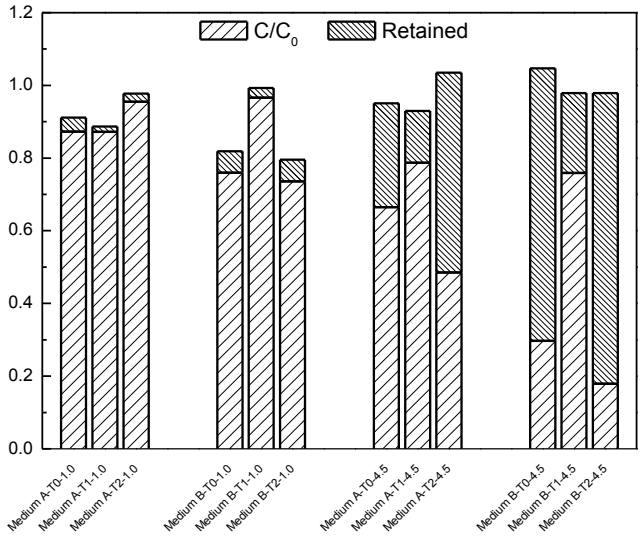

Figure 3-4. Normalized filter effluent microsphere concentration, ratio of retained microspheres, and overall microsphere recovery during column tests conducted with 1.0 and 4.5 μm in 100 mM KCl passing through Medium A (0.710 to 0.850 mm glass beads with porosity = 0.38) and Medium B (0.5 to 0.595 mm glass beads with porosity = 0.37) at a loading rate of 1.5m/h

According to CFT, less particle deposition should occur on the larger diameter media than on the smaller media at the same operational conditions; this is due to fewer available attachment sites and interception (3). Consistent with CFT, particle deposition rate for Medium A (0.71 to 0.84 mm glass beads) was lower than for Medium B (0.5 to 0.595 mm glass beads) (Figure 3-5). CFT also suggests that, all other factors and being equal, the deposition/removal efficiency of 1.0 μm particles would be lower than that of 4.5 μm particles because particles near 1.0 μm in size would be near a minimum contact efficiency with collectors due to the relative cumulative contributions of diffusion, sedimentation and inertia (3, 52). The experimental results reported in Figure 3-5 are also consistent with this theory. Specifically, compared to deposition of 1.0 μm microspheres, the deposition of rate 4.5 μm microspheres on the smooth media was 300% and 445% higher for medium A and B. The particle attachment efficiencies (α) calculated for the smooth beads (Treatment 0) during the present investigation ranged from 0.7 to 1.1 (Figure 3-6), and were close to the theoretically calculated attachment efficiency (α = 1.0) that would be expected according to CFT for the experimental conditions employed herein (i.e., particles suspended in a high ionic strength electrolyte favoring particle deposition because of absence of an energy barrier). The observed agreement between the experimental results obtained with smooth beads in the present study and theoretical expectation based on CFT highlights the applicability of CFT for such experimental conditions (4, 54).

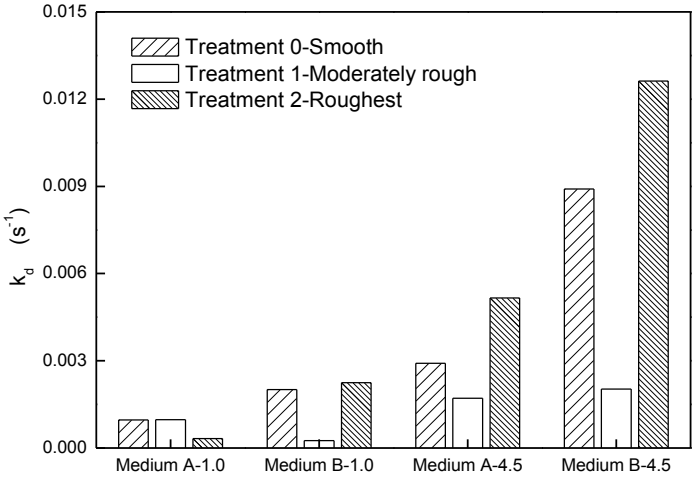

Figure 3-5. Particle deposition rates k_d (s^{-1}) for 1.0 and 4.5 μm microspheres in Medium A (0.770 to 0.850 mm glass beads with porosity = 0.38) with no treatment (Treatment 0 - smooth), Treatment 1 – moderately rough and Treatment 2 – roughest.

In contrast, the impacts of media surface roughness on particle removal during filtration are underscored in Figure 3-2. Examination of the normalized concentration plateaus in Figure 3-2 indicates 79% removal of 4.5 μm microspheres by the roughest medium (Treatment 2), 67% removal by the smooth medium (Treatment 0), and 49% removal by the moderately rough medium (Treatment 1). The microsphere removal performance data in Figure 3-2 are supported by the microsphere recovery data presented in Figure 3-3, which were obtained from destructive sampling of the filter beds. These data demonstrate the greatest retention of 4.5 μm microspheres by the most rough medium (Treatment 2), followed by the smooth medium, and the least retention of microspheres by the moderately rough medium (Treatment 1).

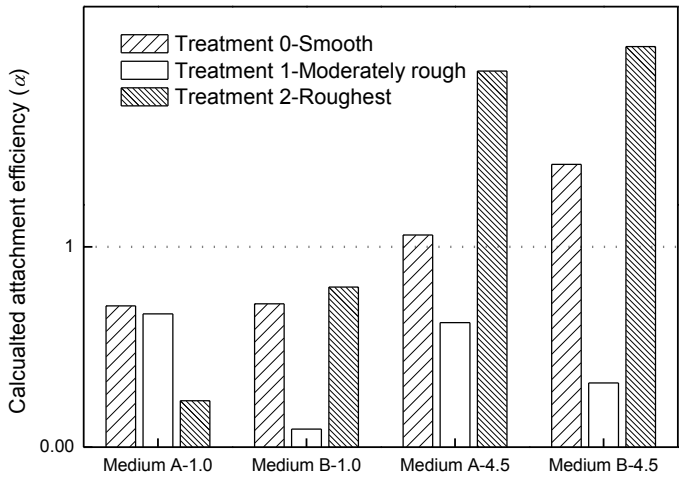

Figure 3-6. Particle attachment efficiency (α) for 1.0 and 4.5 µm microspheres in Medium A (0.770 to 0.850 mm glass beads with porosity = 0.38) with no treatment (Treatment 0 - smooth), Treatment 1 – moderately rough and Treatment 2 – roughest. The single collector efficiency was determined using Equation 17(52)**.**

In most cases as shown in Figure 3-5, the highest rate of microsphere deposition occurred on the roughest medium (Treatment 2), followed by the smooth medium (Treatment 0), with the lowest rate of microsphere deposition occurring on the moderately rough medium (Treatment 1). The only exception to this trend was the situation in which the 0.710 to 0.850 mm glass beads (Medium A) were removing 1.0 µm microspheres. In this case, microsphere removal by the smooth (Treatment 0) and moderately rough (Treatment 1) media was similar, while less microsphere deposition was observed on the roughest medium (Treatment 2). These results are supported by the destructive sampling of the filter beds, which indicated the same trends in microsphere retention (mass recovery) by the various media in the filter columns.

3.5 Discussion and Conclusions

In the present investigation, CFT failed to explain particle attachment efficiency results from experiments in which rough media were utilized. As evident in Figure 3-6, α values calculated for modified glass beads with surface roughness (i.e., either Treatment 1 or 2) demonstrated substantial deviation in attachment efficiency (α) from unity (1.0) relative to the smooth glass beads (Treatment 0); thereby violating a key tenet of CFT, which is $\alpha = 1.0$ at favorable conditions for particle deposition.(3, 40, 55) Therefore, the data presented herein demonstrate that media roughness is an important factor that should be considered as CFT evolves and is further developed with the goal of being more practically relevant. Notably, the results in Figures 3-4 to 3-6 clearly demonstrate a non-linear, non-monotonic impact of surface roughness on colloidal particle deposition during filtration. These data further suggest that the same level of roughness may have different impacts on particle removal for different combinations of particle and collector sizes; accordingly, optimal levels of roughness may exist to maximize or minimize particle removal by filtration for different combinations of particle and collector sizes. Specifically, the results from the present study indicated that when the ratio of particle diameter (d_p) to media/collector diameter (d_c) was greater than 0.0015, the roughest surface (Treatment 2) achieved the greatest level of microsphere deposition whereas the moderately rough surface (Treatment 1) achieved the lowest level of microsphere deposition. If the ratio was smaller than 0.0015, the roughest surface had the lowest level of microsphere deposition and the smooth surface had the highest. A d_p/d_c ratio of 0.0015 appeared to be critical in the present investigation, above and below which apparent trends in the impact of roughness on particle deposition during filtration reversed.

Increases in particle deposition due to increased roughness on media surfaces (relative to smooth media) can be explained by lower interaction action energies that result in more attractive DLVO forces (27, 56, 57). The increased cumulative pore volume and total surface area associated with larger scale roughness such as Treatment 2 may also result in more pore space around collectors that may enhance the transport of particles to collector surfaces (58). At favorable conditions for particle deposition where the negative energy barrier is small or

absent, the entire media surface is more attractive to the colloids. Rough media with greater surface area will also provide more particle attachment sites on collector surfaces relative to smooth media (59, 60). Furthermore, it is also possible that surface roughness may increase the number of sites available for physical attachment, such as grain-to-grain contact and straining locations between each individual collector (24, 37).

In the experiments reported herein, it was also observed that increasing relative media surface roughness (Treatment 1) could not only also result in increased particle deposition on surfaces, but also decreased particle deposition relative to smooth media (Treatment 0). Here, higher filter effluent particle concentrations, lower particle deposition rates, and lower attachment efficiencies were observed for the moderately rough medium (Treatment 1) relative to the smooth medium (Treatment 0). Correspondingly, less colloidal particle retention occurred within the packed column containing the moderately rough medium (Treatment 1). While CFT can be used to interpret increased particle deposition in the presence of roughness from the perspectives of lower interaction energy, deeper secondary energy minimum and additional "shadow effect," it cannot explain decreased deposition caused by media surface roughness (38, 61).

Chemical heterogeneity and hydrophobicity have been commonly used to explain differences between observed data and those that would be expected according CFT (57, 59, 62). Here, to test if chemical heterogeneity contributed to the relatively lower particle deposition that was observed with moderate roughness (Treatment 1), the glass beads were examined after destructive sampling using fluorescence microscopy (Appendix A). This examination demonstrated that the colloidal particles were uniformly attached on the media surfaces with moderate roughness (as well as all of the other surfaces, smooth and roughest), thereby excluding media surface chemical heterogeneity as a potential cause of the differences between the observed levels of colloid deposition on rough surfaces and those that would be expected according CFT. To investigate if the chemical etching changed the hydrophobicity of the media surfaces, additional column tests were conducted using smooth glass beads dipped in 1% HF acid for 30 seconds (Treatment 3). Due to the low HF concentration and short exposure time, the media surfaces after this treatment were regarded to have the same

hydrophobicity as after Treatments 1 and 2, but without roughness features. No significant differences between microsphere deposition on the medium with Treatment 3 and the smooth medium (Treatment 0) were found (Appendix A), thereby suggesting that media surface hydrophobicity also did not cause of the differences between the observed levels of colloid deposition on rough surfaces and those that would be expected according CFT. This result is not surprising given that the carboxylated microspheres used in this investigation are very hydrophilic; accordingly, hydrophobic interactions between the microspheres and media surface should be negligible (63).

Mechanisms associated with flow velocity conditions (64, 65), the shear lift force (66-68), and particle rolling (69, 70) contribute to reduced particle deposition (relative to smooth surfaces) when a colloidal particle interacts with media surface roughness features; accordingly, these may help to explain the experimental outcomes observed herein. For example, it has been demonstrated that micro- and macro-scale roughness impact the magnitude and direction of flow velocity in the near-surface region (64, 71). Roughness also affects how the surrounding flow field should be described. Specifically, in the presenence of surface roughness, a slip boundary condition for the flow field should be applied on the bottom of surface, instead of non-slip condition that is applied for smooth surfaces. The slip boundary condition will lead to a higher velocity profile for the streamlines, which will prevent colloid attachment and result in lower attachment efficiency. The direction of flow component will also affect particle deposition. Yang et al. (1999) compared particle deposition trends in parallel plate and stagnation point flow chambers and found that the stagnation point flow chamber always resulted in a higher particle deposition rate (64). In contrast to particle transport in the parallel plate system, mass transport of the particles in the stagnation point chamber was always toward the surface. Surface roughness can alter particle velocities such that particles are driven either toward or away from target surfaces. As a result, in some cases, colloids possibly travel longer distances along collector surfaces, resulting in less mass transport to media surfaces.

The shear lift force exerted on a particle moving along a straight channel in shear flow is considered as a force perpendicular to the surface (66, 67). In the direction tangent to the

curvature of the velocity profile, the shear lift force is able to cause particle migration away from the surface. The interfacial force between an approaching particle and a collector normally has been simplified to the interaction between a sphere and a flat wall by assuming that the collector is much larger than the particle (72). In reality, collector surfaces have curvature due to their spherical (or other) shape and the micro- and macro-scale curvature caused by surface roughness. This curvature will generate a shear lift force on the particle when it is close to the collector surface. In the current framework of CFT, the shear lift force has been ignored (52). When collector surfaces are rough, the overall shear lift force perpendicular to the surfaces could be greater than the shear lift force caused by the curved smooth surface alone. As a result of the net increase in shear lift force, particle deposition on rough surfaces could be less than on smooth surfaces.

Particle rolling may also contribute to potential decreases in particle deposition on rougher surfaces relative to smoother ones (69). Caused by the coordinated formation and breakage of receptor-ligand bonds, rolling can be initiated even at very low flow rates and laminar flow conditions (e.g., Reynolds number <0.001) for selected colloidal particle in this study. In conjunction with the shear lift force and surface roughness, particle rolling can act to decrease particle deposition. Surface roughness can also increase flow velocity with more force components driving the particle away from the surface.

All of these factors: surface roughness, flow velocity, shear lift and particle rolling can contribute to relatively less particle deposition on surfaces; none of them are currently considered in CFT, however. Particle deposition during granular media filtration is a process in which a dynamic equilibrium between the physico-chemical forces that favor and preclude particle attachment to collector surfaces should be reached (11, 73). This work demonstrated a non-linear, non-monotonic impact of surface roughness on colloidal particle deposition during filtration. The results of this study underscore the need for further description of the forces and mechanisms that govern this non-linear, non-monotonic impact of media surface roughness on particle deposition and filtration performance.

3.6 References

1. Ma, H.L.; Pedel, J.; Fife, P.; Johnson, W.P. Hemispheres-in-Cell Geometry to Predict Colloid Deposition in Porous Media (vol 43, pg 8573, 2009). *Environ. Sci. Technol.* **2010,** *44* (11), 4383-4383; 10.1021/es1009373 ER.

2. Tufenkji, N. Modeling microbial transport in porous media: Traditional approaches and recent developments. *Adv. Water Resour.* **2007,** *30* (6-7), 1455-1469; 10.1016/j.advwatres.2006.05.014.

3. Yao, K.M.; Habibian, M.M.; O'Melia, C.R. Water and Waste Water Filtration - Concepts and Applications. *Environ. Sci. Technol.* **1971,** *5* (11), 1105-&.

4. Nelson, K.E. and Ginn, T.R. Colloid filtration theory and the Happel sphere-in-cell model revisited with direct numerical simulation of colloids. *Langmuir* **2005,** *21* (6), 2173-2184; 10.1021/la048404i.

5. Rajagopalan, R. and Tien, C. Trajectory Analysis of Deep-Bed Filtration with Sphere-In-Cell Porous-Media Model. *AICHE J.* **1976,** *22* (3), 523-533.

6. Bradford, S.A.; Torkzaban, S.; Walker, S.L. Coupling of physical and chemical mechanisms of colloid straining in saturated porous media. *Water Res.* **2007,** *41* (13), 3012-3024; 10.1016/j.watres.2007.03.030.

7. Johnson, W.P.; Pazmino, E.; Ma, H. Direct observations of colloid retention in granular media in the presence of energy barriers, and implications for inferred mechanisms from indirect observations. *Water Res.* **2010,** *44* (4), 1158-1169; 10.1016/j.watres.2009.12.014.

8. Emelko, M.B. and Tufenkji, N. Transport and fate of colloids and microbes in granular aqueous environments. *Water Res.* **2010,** *44* (4), 1027-1027; 10.1016/j.watres.2010.02.005.

9. Tufenkji, N.; Miller, G.F.; Ryan, J.N.; Harvey, R.W.; Elimelech, M. Transport of Cryptosporidium oocysts in porous media: Role of straining and physicochemical filtration. *Environ. Sci. Technol.* **2004,** *38* (22), 5932-5938; 10.1021/es049789u.

10. Huck, P.; Coffey, B.; Emelko, M.; Maurizio, D.; Slawson, R.; Anderson, W.; Van den Oever, J.; Douglas, I.; O'Melia, C. Effects of filter operation on Cryptosporidium removal. *Journal American Water Works Association* **2002,** *94* (6), 97-111.

11. Amirtharajah, A. and Raveendran, P. Detachment of Colloids from Sediments and Sand Grains. *Colloids and Surfaces A-Physicochemical and Engineering Aspects* **1993,** *73*, 211-227.

12. Chen, G.; Bedi, R.S.; Yan, Y.S.; Walker, S.L. Initial Colloid Deposition on Bare and Zeolite-Coated Stainless Steel and Aluminum: Influence of Surface Roughness. *Langmuir* **2010,** *26* (15), 12605-12613; 10.1021/la101667t.

13. Mitik-Dineva, N.; Wang, J.; Truong, V.K.; Stoddart, P.; Malherbe, F.; Crawford, R.J.; Ivanova, E.P. Escherichia coli, Pseudomonas aeruginosa, and Staphylococcus aureus Attachment Patterns on Glass Surfaces with Nanoscale Roughness. *Curr. Microbiol.* **2009,** *58* (3), 268-273; 10.1007/s00284-008-9320-8.

14. Bradford, S.A. and Torkzaban, S. Colloid transport and retention in unsaturated porous media: A review of interface-, collector-, and pore-scale processes and models. *Vadose Zone Journal* **2008,** *7* (2), 667-681; 10.2136/vzj2007.0092.

15. Elimelech, M.; Jia, X.; Gregory, J.; Williams, R. *Particle deposition & aggregation: measurement, modelling and simulation.* Butterworth-Heinemann: 1998; .

16. Tien, C. and Ramarao, B.V. *Granular filtration of aerosols and hydrosols.* Access Online via Elsevier: 2011; .

17. Masliyah, J.H. and Bhattacharjee, S. *Electrokinetic and colloid transport phenomena.* John Wiley & Sons: 2006; .

18. Tamai, H.; Nagai, Y.; Suzawa, T. Interfacial Electrical Studies on the Deposition of Polymer Latexes Onto Fabrics and the Removal of these Deposited Latexes .6. Latex Deposition on Fibers .6. Deposition State and Interaction Energy. *J. Colloid Interface Sci.* **1983,** *91* (2), 464-471.

19. Bai, R.B. and Tien, C. Effect of deposition in deep-bed filtration: Determination and search of rate parameters. *J. Colloid Interface Sci.* **2000,** *231* (2), 299-311.

20. Bai, R.B. and Zhang, X. Polypyrrole-coated granules for humic acid removal. *J. Colloid Interface Sci.* **2001,** *243* (1), 52-60.

21. Shellenberger, K. and Logan, B.E. Effect of molecular scale roughness of glass beads on colloidal and bacterial deposition. *Environ. Sci. Technol.* **2002,** *36* (2), 184-189; 10.1021/es015515k ER.

22. Zan, Q.F.; Wang, C.; Dong, L.M.; Cheng, P.; Tian, J.M. Effect of surface roughness of chitosan-based microspheres on cell adhesion. *Appl. Surf. Sci.* **2008,** *255* (2), 401-403; 10.1016/j.apsusc.2008.06.074 ER.

23. Vanhaecke, E.; Remon, J.P.; Moors, M.; Raes, F.; Derudder, D.; Vanpeteghem, A. Kinetics of Pseudomonas-Aeruginosa Adhesion to 304 and 316-L Stainless-Steel - Role of Cell-Surface Hydrophobicity. *Appl. Environ. Microbiol.* **1990,** *56* (3), 788-795.

24. Morales, V.L.; Gao, B.; Steenhuis, T.S. Grain Surface-Roughness Effects on Colloidal Retention in the Vadose Zone. *Vadose Zone Journal* **2009,** *8* (1), 11-20; 10.2136/vzj2007.0171.

25. Barnes, L.; Lo, M.; Adams, M.; Chamberlain, A. Effect of milk proteins on adhesion of bacteria to stainless steel surfaces. *Appl. Environ. Microbiol.* **1999,** *65* (10), 4543-4548.

26. Hogg, R.; Healy, T.W.; Fuersten.Dw Mutual Coagulation of Colloidal Dispersions. *Transactions of the Faraday Society* **1966,** *62* (522P), 1638-&; 10.1039/tf9666201638.

27. Bhattacharjee, S.; Ko, C.H.; Elimelech, M. DLVO interaction between rough surfaces. *Langmuir* **1998,** *14* (12), 3365-3375.

28. Huang, X.F.; Bhattacharjee, S.; Hoek, E.M.V. Is Surface Roughness a "Scapegoat" or a Primary Factor When Defining Particle-Substrate Interactions? *Langmuir* **2010,** *26* (4), 2528-2537; 10.1021/la9028113 ER.

29. Eichenlaub, S.; Gelb, A.; Beaudoin, S. Roughness models for particle adhesion. *J. Colloid Interface Sci.* **2004,** *280* (2), 289-298; 10.1016/j.jcis.2004.08.017.

30. Suresh, L. and Walz, J.Y. Direct measurement of the effect of surface roughness on the colloidal forces between a particle and flat plate. *J. Colloid Interface Sci.* **1997,** *196* (2), 177-190.

31. Adamczyk, Z.; Nattich, M.; Barbasz, J. Deposition of colloid particles at heterogeneous and patterned surfaces. *Adv. Colloid Interface Sci.* **2009,** *147*, 2-17.

32. Tufenkji, N. and Elimelech, M. Breakdown of colloid filtration theory: Role of the secondary energy minimum and surface charge heterogeneities. *Langmuir* **2005,** *21* (3), 841-852; 10.1021/la048102g.

33. Elimelech, M. Indirect Evidence for Hydration Forces in the Deposition of Polystyrene Latex Colloids on Glass Surfaces. *Journal of the Chemical Society-Faraday Transactions* **1990,** *86* (9), 1623-1624; 10.1039/ft9908601623.

34. Dorobantu, L.S.; Bhattacharjee, S.; Foght, J.M.; Gray, M.R. Analysis of Force Interactions between AFM Tips and Hydrophobic Bacteria Using DLVO Theory. *Langmuir* **2009,** *25* (12), 6968-6976; 10.1021/la9001237 ER.

35. Johnson, W.P.; Ma, H.L.; Pazmino, E. Straining Credibility: A General Comment Regarding Common Arguments Used to Infer Straining As the Mechanism of Colloid Retention in Porous Media. *Environ. Sci. Technol.* **2011,** *45* (9), 3831-3832; 10.1021/es200868e ER.

36. Bradford, S.A.; Simunek, J.; Bettahar, M.; van Genuchten, M.T.; Yates, S.R. Significance of straining in colloid deposition: Evidence and implications. *Water Resour. Res.* **2006,** *42* (12), W12S15; 10.1029/2005WR004791.

37. Li, X.Q.; Lin, C.L.; Miller, J.D.; Johnson, W.P. Role of grain-to-grain contacts on profiles of retained colloids in porous media in the presence of an energy barrier to deposition. *Environ. Sci. Technol.* **2006,** *40* (12), 3769-3774; 10.1021/es052501w.

38. Ko, C.H. and Elimelech, M. The "shadow effect" in colloid transport and deposition dynamics in granular porous media: Measurements and mechanisms. *Environ. Sci. Technol.* **2000,** *34* (17), 3681-3689; 10.1021/es0009323.

39. Dorobantu, L.S.; Bhattacharjee, S.; Foght, J.M.; Gray, M.R. Atomic force microscopy measurement of heterogeneity in bacterial surface hydrophobicity. *Langmuir* **2008,** *24* (9), 4944-4951; 10.1021/la7035295 ER.

40. Elimelech, M.; Chen, J.Y.; Kuznar, Z.A. Particle deposition onto solid surfaces with micropatterned charge heterogeneity: The "hydrodynamic bump" effect. *Langmuir* **2003,** *19* (17), 6594-6597; 10.1021/la034516i.

41. Buhler, J.; Steiner, F.P.; Baltes, H. Silicon dioxide sacrificial layer etching in surface micromachining. *J Micromech Microengineering* **1997,** *7* (1), R1-R13; 10.1088/0960-1317/7/1/001.

42. Azevedo, C.R.F. and Marques, E.R. Three-dimensional analysis of fracture, corrosion and wear surfaces. *Eng. Failure Anal.* **2010,** *17* (1), 286-300; 10.1016/j.engfailanal.2009.06.010.

43. Washburn, E.W. Note on a method of determining the distribution of pore sizes in a porous material. *Proc. Natl. Acad. Sci. U. S. A.* **1921,** , 115-116.

44. Webb, P.A. and Orr, C. *Analytical methods in fine particle technology.* Micromeritics Instrument Corp: 1997; .

45. Hunter, R.J. Foundations of colloid science (POD). **2000,** .

46. Tufenkji, N. and Elimelech, M. Deviation from the classical colloid filtration theory in the presence of repulsive DLVO interactions. *Langmuir* **2004,** *20* (25), 10818-10828; 10.1021/la0486638.

47. Crittenden, J.C.; Trussell, R.R.; Hand, D.W.; Howe, K.J.; Tchobanoglous, G. *MWH's Water Treatment: Principles and Design.* Wiley. com: 2012; .

48. Allen, T. *Particle Size Measurement: Volume 2: Surface Area and Pore Size Determination.* Springer: 1997; Vol. 2, .

49. Emelko, M.; Huck, P.; Douglas, I. Cryptosporidium and microsphere removal during late in-cycle filtration. *Journal American Water Works Association* **2003,** *95* (5), 173-182.

50. Song, L. and Elimelech, M. Dynamics of Colloid Deposition in Porous-Media - Modeling the Role of Retained Particles. *Colloids and Surfaces A-Physicochemical and Engineering Aspects* **1993,** *73*, 49-63.

51. Tien, C. Hydrosol deposition in porous media: the effect of surface interactions. *Advanced Powder Technology* **2000,** *11* (1), 9-56.

52. Tufenkji, N. and Elimelech, M. Correlation equation for predicting single-collector efficiency in physicochemical filtration in saturated porous media. *Environ. Sci. Technol.* **2004,** *38* (2), 529-536; 10.1021/es034049r.

53. Kim, J.K. and Lawler, D.F. Particle detachment during hydraulic shock loads in granular media filtration. *Water Science and Technology* **2006,** *53* (7), 177-184; 10.2166/wst.2006.222 ER.

54. Ryan, J.N. and Elimelech, M. Colloid mobilization and transport in groundwater. *Colloids and Surfaces A-Physicochemical and Engineering Aspects* **1996,** *107*, 1-56.

55. Elimelech, M. and O'Melia, C.R. Effect of Particle-Size on Collision Efficiency in the Deposition of Brownian Particles with Electrostatic Energy Barriers. *Langmuir* **1990,** *6* (6), 1153-1163.

56. Mendez-Vilas, A.; Bruque, J.M.; Gonzalez-Martin, M.L. Sensitivity of surface roughness parameters to changes in the density of scanning points in multi-scale AFM studies. Application to a biomaterial surface. *Ultramicroscopy* **2007,** *107* (8), 617-625; 10.1016/j.ultramic.2006.12.002.

57. Walz, J.Y. The effect of surface heterogeneities on colloidal forces. *Adv. Colloid Interface Sci.* **1998,** *74*, 119-168.

58. Wan, J.M. and Wilson, J.L. Colloid Transport in Unsaturated Porous-Media. *Water Resour. Res.* **1994,** *30* (4), 857-864; 10.1029/93WR03017.

59. Duval, J.F.L.; Leermakers, F.A.M.; van Leeuwen, H.P. Electrostatic interactions between double layers: Influence of surface roughness, regulation, and chemical heterogeneities. *Langmuir* **2004,** *20* (12), 5052-5065; 10.1021/la030404f.

60. Vermeltfoort, P.B.J.; van der Mei, H.C.; Busscher, H.J.; Hooymans, J.M.M.; Bruinsma, G.M. Physicochernical factors influencing bacterial transfer from contact lenses to surfaces with different roughness and Wettability. *Journal of Biomedical Materials Research Part B-Applied Biomaterials* **2004,** *71B* (2), 336-342; 10.1002/jbm.b.30100.

61. Kuznar, Z.A. and Elimelech, M. Direct microscopic observation of particle deposition in porous media: Role of the secondary energy minimum. *Colloids and Surfaces A-Physicochemical and Engineering Aspects* **2007,** *294* (1-3), 156-162; 10.1016/j.colsurfa.2006.08.007 ER.

62. Tang, H.; Cao, T.; Liang, X.; Wang, A.; Salley, S.O.; McAllister,James,,II; Ng, K.Y.S. Influence of silicone surface roughness and hydrophobicity on adhesion and colonization of Staphylococcus epidermidis. *Journal of Biomedical Materials Research Part a* **2009,** *88A* (2), 454-463; 10.1002/jbm.a.31788.

63. Harvey, R.W.; Metge, D.W.; Mohanram, A.; Gao, X.; Chorover, J. Differential effects of dissolved organic carbon upon re-entrainment and surface properties of groundwater bacteria and bacteria-sized microspheres during transport through a contaminated, sandy aquifer. *Environ. Sci. Technol.* **2011,** *45* (8), 3252-3259.

64. Yang, J.L.; Bos, R.; Poortinga, A.; Wit, P.J.; Belder, G.F.; Busscher, H.J. Comparison of particle deposition in a parallel plate and a stagnation point flow chamber. *Langmuir* **1999,** *15* (13), 4671-4677; 10.1021/la981607k.

65. Neto, C.; Evans, D.; Bonaccurso, E.; Butt, H.; Craig, V. Boundary slip in Newtonian liquids: a review of experimental studies. *Reports on Progress in Physics* **2005,** *68* (12), 2859-2897; 10.1088/0034-4885/68/12/R05.

66. Darbha, G.K.; Fischer, C.; Michler, A.; Luetzenkirchen, J.; Schaefer, T.; Heberling, F.; Schild, D. Deposition of Latex Colloids at Rough Mineral Surfaces: An Analogue Study Using Nanopatterned Surfaces. *Langmuir* **2012,** *28* (16), 6606-6617; 10.1021/la3003146.

67. Derksen, J.J. and Larsen, R.A. Drag and lift forces on random assemblies of wall-attached spheres in low-Reynolds-number shear flow. *J. Fluid Mech.* **2011,** *673*, 548-573; 10.1017/S0022112010006403.

68. Krishnan, G.P. and Leighton, D.T. Inertial Lift on a Moving Sphere in Contact with a Plane Wall in a Shear-Flow. *Phys. Fluids* **1995,** *7* (11), 2538-2545; 10.1063/1.868755.

69. King, M.R. and Hammer, D.A. Multiparticle adhesive dynamics: Hydrodynamic recruitment of rolling leukocytes. *Proc. Natl. Acad. Sci. U. S. A.* **2001,** *98* (26), 14919-14924; 10.1073/pnas.261272498.

70. Greenberg, A.W. and Hammer, D.A. Cell separation mediated by differential rolling adhesion. *Biotechnol. Bioeng.* **2001,** *73* (2), 111-124; 10.1002/bit.1043.

71. Sedmik, R.I.P.; Borghesani, A.F.; Heeck, K.; Iannuzzi, D. Hydrodynamic force measurements under precisely controlled conditions: Correlation of slip parameters with the mean free path. *Phys. Fluids* **2013,** *25* (4), 042103; 10.1063/1.4801096.

72. Elimelech, M. and O'Melia, C.R. Effect of Particle-Size on Collision Efficiency in the Deposition of Brownian Particles with Electrostatic Energy Barriers. *Langmuir* **1990,** *6* (6), 1153-1163.

73. O'Melia, C.R. Particles, Pretreatment, and Performance in Water Filtration. *J. Environ. Eng. -ASCE* **1985,** *111* (6), 874-890.

.

Chapter 4

Impact of nano-scale surface roughness on colloidal particle deposition. I. Experiments in a parallel plate system

4.1 Overview

An experimental (Part I) and numerical simulation (Part II) investigation of the impact of nano-scale roughness of contact surfaces on particle deposition at high ionic strength conditions favoring particle deposition was conducted. The experimental portion of this two-part study is presented here. The impacts of different nano-scale quartz surface roughness sizes (10, 20, 50, 200 and 400 nm) on deposition kinetics of three sizes (0.55, 0.98 and 1.76 μm) of polystyrene microspheres suspended in 100 mM KCl were examined. A non-linear, non-monotonic relationship between surface roughness and particle deposition flux was observed. A critical roughness size associated with a minimum deposition flux was identified. When the roughness size was less than the critical depth, particle deposition decreased with increased roughness size. When the roughness size was greater than the critical size, particle deposition increased with increased roughness size. Nano-scale roughness size had a significant impact on the deposition of (e.g. 0.55μm) particles, which was mainly dominated by diffusion. Deposition of larger (e.g. 1.76 μm) particles was predominantly governed by gravity, without a significant impact of nano-scale roughness.

4.2 Introduction

The deposition of colloidal- and nano-scale particles on surfaces is critical to numerous natural and engineered environmental, health, and industrial applications. These include protection of public health by protecting drinking water supplies through understanding pathogen transport in the subsurface(1, 2) and in engineered drinking water filters(3-5), improved screening of ambient air quality through enhanced ion mobility measurement(5), control of chronic contamination of processed food supplies(6), improved medical screening and treatment by improved cell separation and detection(7, 8), improved health protection and assessment via understanding of nano-particle deposition in the respiratory system(9, 10), assessing and improving pipeline inefficiencies due to particle formation/accumulation(11), improved semiconductor manufacturing by enhanced surface cleaning and particle removal(12, 13) to name a few. Despite the wide range of applications for which particle deposition on surfaces is replied upon, this process remains inadequately described both conceptually and mathematically, thereby precluding application of predictive models for improved application understanding or enhancement. This investigation focuses on definitively demonstrating a non-linear, non-monotonic effect of nano-scale surface roughness on particle deposition to ultimately contribute to enabling better quantitative description of particle deposition on surfaces.

Particle deposition on surfaces can be generally considered as comprised of two steps: particle transport to and attachment on surfaces(14, 15). The deposition of colloids under the influence of external forces including Van der Waals forces (VDW), electrostatic double layer forces (EDL), gravity and hydrodynamic retardation forces etc. can be quantitatively described using Eulerian methods by solving the Convection-Diffusion Equation. Commonly utilized models for quantifying these solutions are based on the theoretical assumptions that 1) colloidal particles and contact surfaces are smooth and chemically homogenous and 2) colloid attachment is predominately governed by chemical interactions between the particles and surfaces that are independent of the flow field(16-18). Unfortunately, existing models often fail to predict particle deposition in real systems, with predictions that are frequently off by several orders of magnitude(19-21, 21-23). The discrepancies are likely caused by the

assumptions made in the models. For instance, the assumption that colloidal particles and contact surfaces are smooth is not accurate in real systems which will certainly influence local flow field and particle deposition. Indeed, roughness on contact surfaces has been shown to affect particle deposition(24-26). Therefore, it must be considered in developing models for describing particle deposition. (15, 27-29).

The effect of surface roughness on particle deposition is very complex because there exist several relative length scales between roughness, particle, and filtration media which also influence the local flow field and thus particle deposition mechanisms. Its complexity is also evidenced by the inconsistent and even contradictory experimental observations from numerous case studies Therefore, the associated mechanisms are still poorly understood and described(24, 26, 30-32). Surface roughness, with depths as small as a few hundred nanometers, can significantly enhance particle deposition in some cases(33-36). For example, Chen et al. (2010) coated stainless steel and aluminum alloys with zeolite to increase surface roughness and achieved up to 50% more colloid deposition in most cases(37). Darbha et al. (2010) also reported a positive correlation between calcite surface roughness and the number of attached colloidal particles;(25) they also found that surface roughness-enhanced particle deposition was more significant for smaller particles (0.3 μm) as compared to larger (2 μm) ones(38). Zan et al. (2008) investigated opportunities for enhancing orthopadeic stainless steel affinity to host bone tissue and also found that more colloidal particles (here, mouse osteoblasts) attached on rough surfaces than on smooth ones(39).

Contradictory results regarding the impact of surface roughness on particle deposition have also been reported, however. For example, Tang et al. (2009) investigated the adhesion and colonization of *Staphylococcus epidermidis* on silicon and reported that rougher surfaces did not promote bacterial adhesion and colonization when surface roughness size was below a certain threshold (i.e. 200 nm)(40). Similarly, Chen et al. (2010) found that surface roughness resulted in increased particle deposition in most cases; however, two exceptions were noted in which the rough surface (zeolite coated stainless steel and an unpolished aluminum plate) had less particle deposition than a smooth surface comprised of the same material and exposed to the same operational conditions(37). Consistent with these studies, a

non-linear, non-monotonic impact of surface roughness on colloidal particle deposition (i.e., the potential for both decreased and increased deposition) was recently proposed by Jin and Emelko (2014) in packed bed filtration columns in which (1.0 μm and 4.5 μm) glass beads were modified by hydrofluoric acid etching to yield different levels of micro-scale surface roughness(74).

Existing models for particle deposition on surfaces cannot adequately describe particle deposition in the presence of surface roughness. It has been suggested that differences in particle deposition in the presence of surface roughness may be attributable to changes in DLVO interaction energy (26, 41), chemical heterogeneity on charged surfaces(42, 43), hydrophobicity between particles and subsurfaces(40), straining(23), or rolling (7, 44). Quantitative evaluations of these hypotheses are lacking, however.

The present investigation focused on systematically evaluating the effect of surface roughness on colloidal particle deposition on surfaces using laboratory experiments(Part I) and mathematical modeling simulations(Part II). To achieve this goal, experimental data that were not confounded by other factors (e.g, media grain size and distribution, media composition, media shape, porosity, hydrophobicity, chemical heterogeneity, etc.) were required. Accordingly, a parallel plate chamber was designed because the flow field is well understood which allows accurate evaluation of its impact on particle deposition. Homogeneous roughness features at targeted depths on plate surfaces are carefully ensured through nano-fabrication techniques explained later. Particle deposition on these surfaces was monitored by microscopic technique and image analysis. This paper (Part I) focuses on interpretation and discussion of the experimental results; including a simple quantitative demonstration of the non-linear, non-monotonic impact of surface roughness on particle deposition. A key component of this work was to develop and conduct rigorous quality assurance experiments to exclude any impacts on enumerated particle deposition from potentially pre-attached particles on re-used slide surfaces or differences in initial particle concentration in the influent suspension entering the chamber. In an accompanying paper (Part II), a theoretical model that quantitatively describes colloidal particle deposition

behavior in the presence of micro-scale surface roughness was developed and verified by comparing with experimental results (Part II).

4.3 Materials and Methods

4.3.1 Theoretical Approach

Particle deposition on rough surfaces is a complex mass transfer phenomenon requiring integration of surface chemistry and fluid mechanics principles. The overall goal of this work was better understand roughness effects on particle deposition and their relevance to natural and engineered filtration processes, however, a tractable sub-subset of operational conditions had to be selected for this proof-of-concept demonstration. First, favorable conditions for particle deposition were investigated. At these conditions, the EDL force is ignored/ minimized by using a high concentration electrolyte (e.g., 100 mM KCl) solution. Second, gravity effects were minimized by using colloidal particles with density close to water (i.e., (1.045 ± 0.005g/ml). However, gravity effects on particle deposition were still observed in some cases. As would be expected, gravity effects became evident for some particles after they had travelled some distance from the chamber inlet, therefore those data were excluded from the quantitative evaluation and model development described herein. Given the extensive number of data points collected prior to any evidence of these impacts (as detailed below), further study to incontrovertibly exclude gravity effects was not necessary. Finally, convective interaction was also ignored based of an evaluation of the relative contributions of Brownian convection and diffusion (represented by the dimensionless number N) as described in, as described in Equation 4-1. This evaluation enabled the development of an analytical solution to the Convective-Diffusion equation. Specifically, the Smoluchowski-Levich approximation was used which assumes 1) hydrodynamic interactions between the particle and the surface are counterbalanced by attractive VDW forces, 2) particles move with the undisturbed fluid velocity, and 3) all other external colloidal and external forces and interception are absent or negligible(16). It is generally valid when $N>>1.0$, which is the case herein. In the absence of external forces including gravity, interception, and colloidal and

hydrodynamic interactions, the analytical solution for Sherwood number (*Sh*) representing the ratio of convective to diffusive mass transport can be described by Equation 4-2.

$$N = \frac{3Vb}{2D_\infty} = \frac{Peb^3}{a^3} \tag{4-1}$$

$$Sh = \frac{1}{\Gamma(4/3)}\left(\frac{2Pe}{9\bar{x}}\right)^{1/3} \tag{4-2}$$

$$Pe = \frac{3V_m a_p^3}{2b^2 D_\infty} \tag{4-3}$$

Here, N is the dimensionless ratio of the relative contributions of Brownian convection and diffusion, V the average flow velocity , b the half channel height, a the particle radius, D_∞ the particle diffusion coefficient in bulk solution, and Pe the dimensionless Peclet number (described by Equation 4-3) that evaluates the relative contributions of convection and diffusion and is calculated from the Stokes-Einstein equation. *Sh* is the dimensionless flux of particles to the surface and $\bar{x} = x/b$, where x is the distance to the inlet from the point of entry in the parallel plate chamber.

When particles deposit during the initial or "clean bed" period of filtration, particle-particle interactions in the colloidal suspension, multilayer-colloidal deposition, and blocking effects are negligible and the dominating factor that governs particle deposition is particle-surface interaction(16). The deposition rate (number of colloidal per unit area per unit time or deposition flux *J*) is described by slope of particle accumulation over time (Equation 4-4). The dimensionless Sherwood number (*Sh*) can be calculated by estimating *J* (Equation 4-5)(45).

$$J = \frac{N^*/A}{t} \tag{4-4}$$

$$Sh = \frac{J * a_p}{C_0 D_\infty} \tag{4-5}$$

In these equations, N^* is number of colloids deposited at each location during a given time interval t, A is the microscopic image area, and C_0 is the initial colloidal particle concentration.

4.3.2 Colloidal particle characterization

Carboxylated fluorescent (441nm excitation, 486 nm emission) polystyrene microspheres (Polysciences Inc., PA) with diameter 0.55 ± 0.017μm, 0.98 ± 0.047 μm and 1.76 ± 0.31 μm were utilized; their concentrations in the stock suspensions were 3.64x 10^{11}, 4.55 x 10^{10} and 5.68 x10^{9} particles/mL, respectively. The reported density of the microspheres was 1.045 ± 0.005 g/mL. Influent microsphere suspensions were made by diluting stock suspensions in 100mM KCl (VWR, Canada). They were sonicated for 30 minutes before each experiment to ensure all particles were disaggregated.

Electrokinetic properties of the microspheres in the electrolyte solution (100mM KCl) were obtained using Dynamic Light Scattering (DLS) (Zetasizer nano range, Malvern, UK). Using Smoluchowski's equation, the measured electrophoretic mobility was converted to zeta potential of particle in the KCl solution. To confirm that no particle aggregation occurred in the stock suspensions despite its high ionic strength, the particle size distribution of each colloid was measured using DLS before and after the deposition experiments. These measurements did not indicate any changes in particle size distribution over the two hour experimental period, thereby confirming negligible particle aggregation in the stock microsphere suspension during the deposition experiments. The measured physical/chemical parameters for the selected particle solution and also the corresponding dimensionless numbers are listed below (Table 4-1).

Table 4-1. Physical/chemical characterization of colloidal particles in 100 mM KCl

Particle diameter (*μ*m)	*Measured Particle size* (*μ*m) (mean ±std. dev.)	*Zeta-potential* (*mV*) (mean ±std. dev.)	*Initial concentration* (*particle/ml*)	*Peclet number*	*Reynolds number*	*Gravity number*
0.525	0.55 ±0.017	-18.5 ±6.3	$7.28*10^{7}$	$1.68*10^{-4}$	0.0167	0.00257
1.03	0.98 ±0.047	-24.9 ±3.1	$5.71*10^{7}$	$1.72*10^{-3}$	0.0167	0.0264
1.76	1.76 ±0.31	-21.6 ±2.2	$1.14*10^{7}$	$1.78*10^{-2}$	0.0167	0.273

4.3.3 Quartz slide pre-treatment

Quartz microscope slides with less than 2 nm of surface roughness were utilized during the particle deposition experiments (Ted Pella Inc., Redding, USA). The slides were sonicated in acetone, cleaned using the RCA 1 method(46), and then rinsed with isopropyl alcohol. The clean slides were extensively rinsed with DI water then blown dry with pure N_2 gas.

A nano-fabrication method using CsCl self-assembly was employed to generate different roughness sizes on the quartz slide surfaces(47). Briefly, CsCl was evaporated at a pressure of 6 μTorr in a humid chamber and deposited onto the slide surfaces, forming isolated hemispheres by kinetic dissolution and deposition at the solid/solution boundary(48). Subsequently, the slides were exposed in a humid chamber at a relative humidity of 22% and a temperature of 21 ℃ for 10 minutes. The spherical shapes of thin layers of CsCl (10 nm) were used as a mask to pattern the quartz surface using reactive ion etching (RIE) with a constant etch rate of 25 nm/minute to create surface roughness at targeted depths of 10 nm, 20 nm, 50 nm, 100 nm, 200 nm and 400 nm. After the nano-fabrication process, the modified slides were rinsed with Milli-Q^{TM} water and then analytical grade acetone. They were dried with N_2 gas.

The modified quartz slides were characterized by streaming potential analysis (Surpass Anton Paar, VA, USA) for their zeta potentials, contact angle measurement (Axisymmertic drop shape analysis-profile, University of Waterloo, Canada) for their hydrophilic properties, and Atomic Force Microscopy (AFM) (XE-NSOM, Park Systems, Korea) for their surface topology. The measured peoperties are listed in Table 4-2. Because each slide surface was etched rather than coated, the composition and chemical properties of the modified and unmodified slides remained consistent. The modified and unmodified quartz slide surfaces were negatively charged with similar magnitudes of zeta potentials. The modified and smooth slides were both hydrophilic, with contact angles ranging from 20˚ to 25˚ at the conditions investigated. The contact angles increased with increased scales of nano-scale roughness, indicting that the roughest slides were the most hydrophilic; however, it should be noted that these changes were not substantial. The AFM images demonstrate that the nano-

fabrication process generated roughness in the shape of hemispherical columns uniformly distributed over the entirety of each quartz slide surface. They also confirm that longer RIE etching times produced deeper surface roughness. The achieved absolute height of the roughness features generally met the targeted values.

The arithmetic average roughness (R_a) and the root mean square roughness (R_q) were measured (Table 4-2). These values are different from the absolute roughness size (peak to peak values of roughness elements). That is because the R_a and R_q calculations also include the distance between roughness elements. Triplicate AFM measurements of the height of roughness features in a 20 μm x 20 μm section of each slide were employed to obtain R_a and R_q.

Table 4-2. Quartz slide characteristics

Target roughness (nm)	*Measured R_a (nm)* (mean ±std. dev.)	*Measured R_q (nm)* (mean ±std. dev.)	*Water Contact angle (deg)* (mean ±std. dev.)	*Zeta-potential (mV)* (mean ±std. dev.)
10	4.3 ±0.5	5.6 ±0.5	31.2 ±6.8	-18.3 ±3.5
20	1.9 ±0.2	2.8 ±0.3	27.2 ±5.5	-21.5 ±6.7
50	10.7 ±1.8	14.6 ±1.8	29.4 ±4.3	-16.2 ±5.1
100	30.3 ±2.9	35.9 ±3.3	26.2 ±7.1	-14.9 ±5.8
200	53.5 ±7.6	65.1 ±6.4	21.9 ±4.2	-13.6 ±7.4
400	60.7 ±9.1	81.4 ±7.8	18.3 ±3.5	-15.3 ±5.2

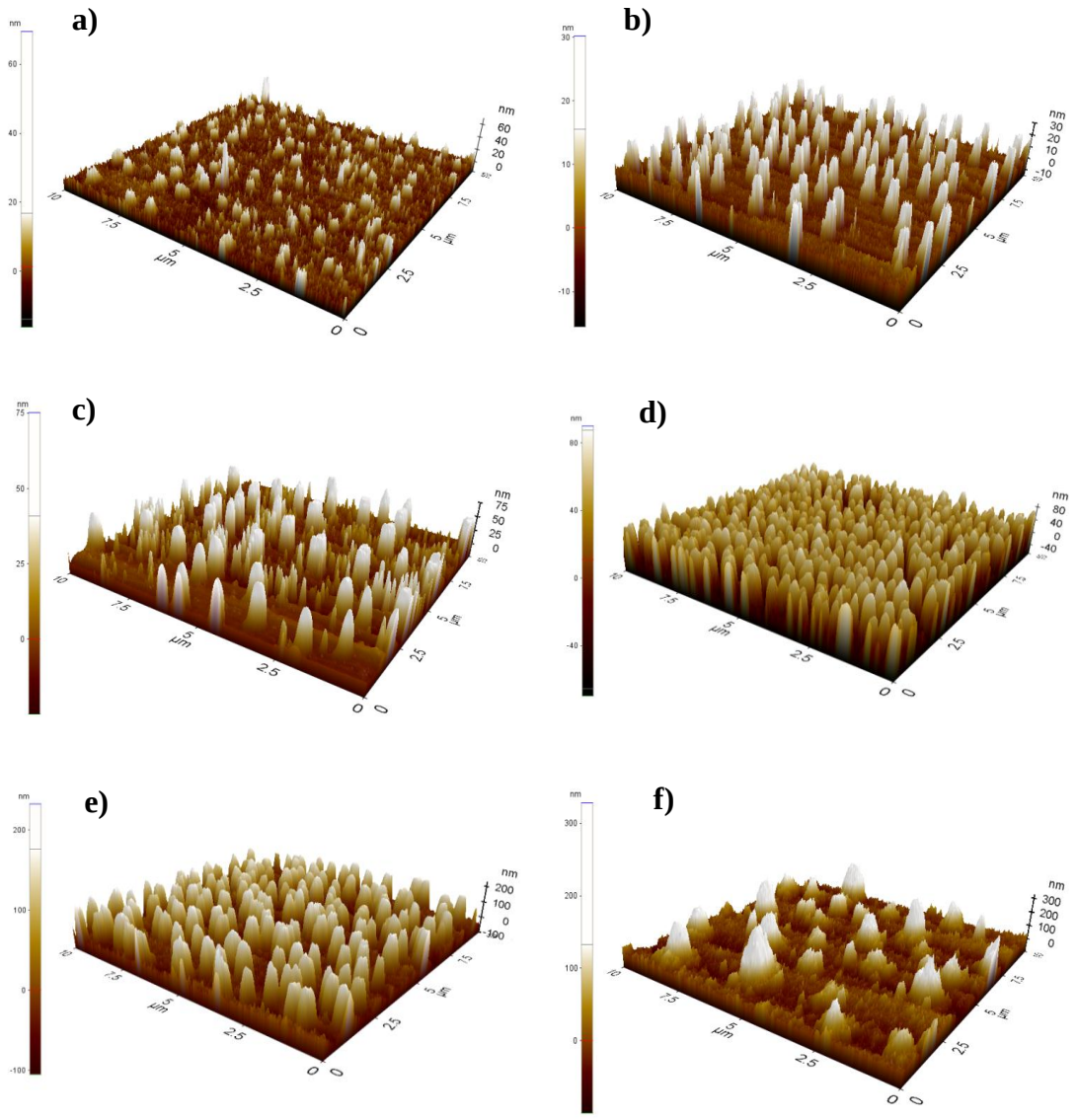

Figure 4-1. AFM profiles of representative modified slides with roughness sizes of a) 10nm, b) 20 nm, c) 50nm, d) 100nm, e) 200nm, and f) 400 nm.

4.3.4 Experimental Setup

The colloidal particle deposition experiments were conducted in a vacuum-sealed parallel plate flow chamber (GlycoTech, MA, USA) with inner dimensions of 5x1 cm (Figure 4-2(a)). The parallel plate chamber was firmly bonded on the quartz slides and installed on the stage of an automated inverted fluorescence microscope (Eclipse Ti, Nikon, Canada). Images were

continuously acquired during each experiment at 9 locations along the flow direction from the inlet to the outlet of the chamber, with 5 replicated measurements (labeled as Location 1-5 in Figure 4-4) in the cross-flow direction at each location (Figure 4-2(b)). All cross-flow measurements at each location along the flow path were treated as replicates because the distances between points were several orders of magnitude greater than the size of particles so each point could be considered independent and obtained at identical experimental conditions.

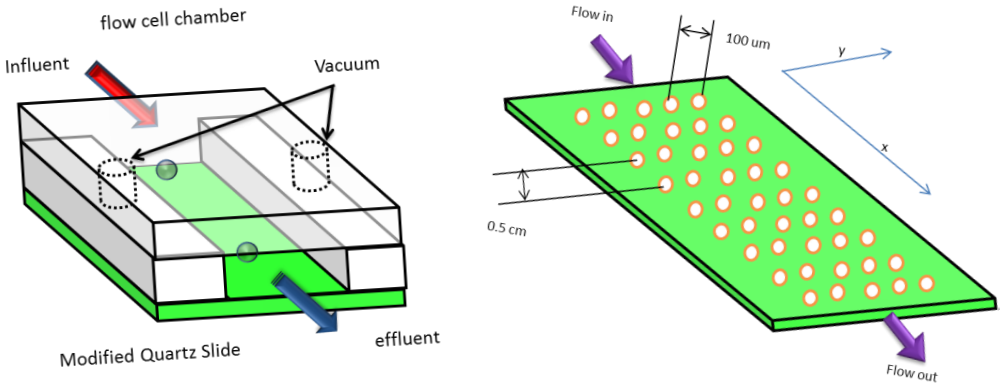

Figure 4-2. Schematic of experimental set-up. a) Parallel plate chamber attached to quartz slide (left). b) Sampling locations on the quartz slide (right).

The use of the parallel plate chamber enabled particle deposition to be easily monitored and modeled as long as key assumptions were met, as discussed above. Multiple colloid sizes of environmental relevance and a relatively long (i.e., 4 cm as opposed to 2 cm, which is commonly reported in the literature) parallel plate chamber were utilized with the recognition that at some point the role of gravity within the chamber would likely confound the ability to attribute deposition to surface roughness as opposed to deposition due to the combined effect of surface roughness and gravity. More specifically, the aim of the experimental configuration was to enable the collection of a data set in the zone where flow and roughness related diffusion-convection effects were essentially constant (i.e., at points within the chamber that were a relatively short distance away from the inlet) and gravity effects were reasonably insignificant such that the bulk colloid concentration in the zone of interest within

the chamber was essentially constant and unchanged from that entering the chamber. According to Adamczyk and van de Ven (1981)(16, 17, 45), at some point along the flow path particle deposition profiles reach a plateau because particles accumulate in the zone above the bottom surface in the chamber, resulting in a higher particle concentration than in other part parts of the chamber, thereby hindering their deposition and resulting in a particle concentration gradient between the bulk suspension and the zone near the bottom surface within the chamber. The experimental configuration and exhaustive collection of data enabled reasonable assessment of the where in the chamber (i.e., the distance along the flow path) the contributions of gravity to particle deposition became significant and thereby allowed identification of a dimensionless distance within the chamber beyond which data could be excluded from analysis due to contributions from gravity.

During each experiment, the parallel plate chamber was first primed to prevent bubble entrapment. Specifically, it was placed in a vertical orientation and particle free 100 mM KCl was pumped through it using a syringe pump (ID: 55-333, Harvard Apparatus, Canada) at a flow rate of 100 μL/min for 15 minutes. The chamber was then placed on the monitor stage (PRIOR Scientific, MA, USA) and the flow rate was adjusted to the desired value for 30 minutes to ensure steady flow conditions within the chamber. After the flow stabilized, the colloidal particle suspension was pumped through the chamber at a rate of 10.0 μL/min, corresponding to a mean loading rate of 6.7 $x10^{-5}$ m/s. All experiments were conducted at pH of 6.5–6.9 and 22–24˚C.

Microsphere deposition on the quartz slides was imaged at 40X magnification every 5 minutes during the 120-minute duration of each experiment. This was achieved by focusing on the bottom surface of the parallel plate chamber. A relatively long exposure time (1 second) was used to distinguish between deposited and moving particles. Moving particle appeared as streaks, whereas deposited particles appeared as discreet spheres that remained in a fixed location in subsequent images.

4.3.5 Image Analysis

An image analysis program was developed in MatLab® to enumerate deposited particles. To ensure maximum accuracy, the program had to a) confirm that particles remained in a fixed location after being deposited; b) count particles accurately despite lens curvature, which meant counting in blurred image areas or areas containing over-bright particles due to lens curvature; and c) exclude aggregated particles from the count. Local Hessian matrices were computed for each pixel in each image, and the determinant of each matrix was calculated. A probability density function of the matrix determinants was then constructed and the cell centroids were identified using nonmaximal suppression and statistical analysis on the constructed probability density function. Aggregated and moving particles were excluded by setting the threshold for particle size and shape in the enumeration code. To confirm the accuracy of the microsphere enumeration program, selected images were manually counted and compared to the counts obtained with the automated system. Representative initial and enumerated images are presented in Figure 4-3(a) and (b), respectively.

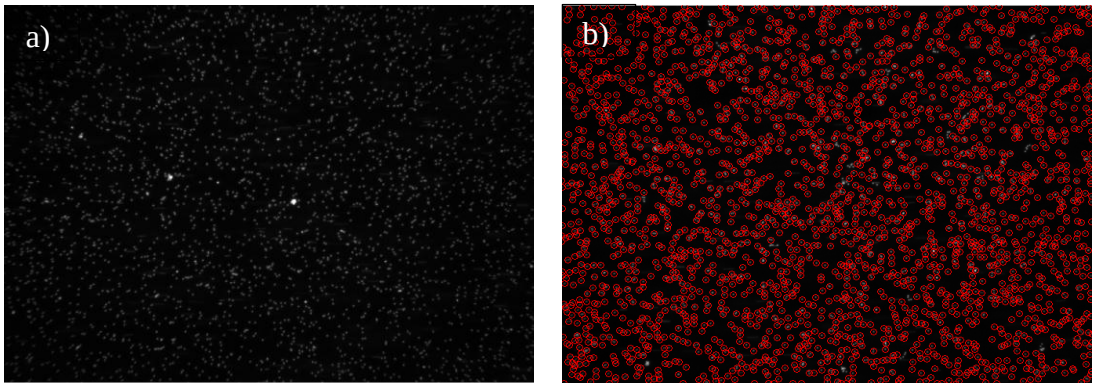

Figure 4-3. Representative images of a) an initial image of deposited particles and b) an enumerated image depicting microsphere deposition on a quartz slide.

To determine particle flux to the target surface, the number of deposited particles at each location was tracked over time. A representative plot of cumulative number of attached particles per unit area (image) as a function of time is presented in Figure 4-4. This figure demonstrates that the number of deposited particles increased linearly with time within the

first two hours, indicating non-impeded deposition (i.e., negligible blocking). Excluding the first 10 minutes during which the system was primed, a linear relationship (R^2 >0.999) in particle deposition over time was observed at all locations during the experiments. The slope of each individual curve was used to assess particle deposition (*J* and *Sh*) using Equation 4-3 and 4-4.

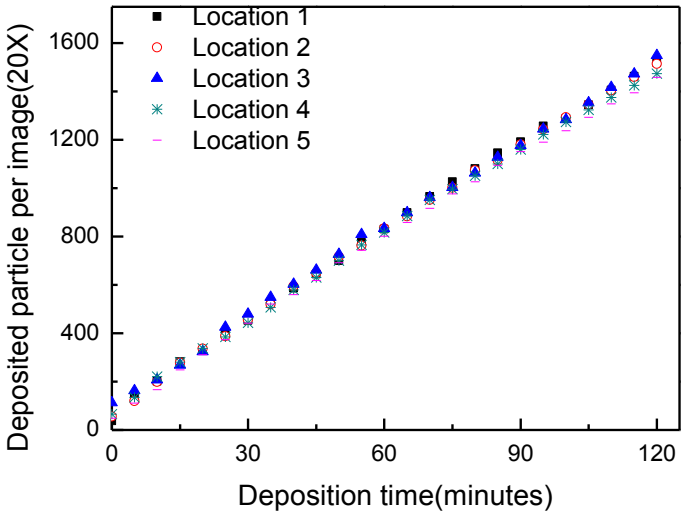

Figure 4-4. Representative plot of the number of polystyrene particles deposited over time in the parallel plate chamber at five locations across the width of the chamber.

4.3.6 Experimental design

This study involved three phases of experimentation. The Phase I and II experiments focused on quality assurance (QA), while the Phase III experiments were designed to assess the impact of surface roughness on particle deposition. It should be noted that the QA experiments were considered critical to incontrovertibly demonstrating the impact of surface roughness on particle deposition. Most such experimental investigations do not report confirmatory data demonstrating consistency except for roughness between all experimental surfaces(18, 37, 45, 49); accordingly, when particle deposition data from other studies are examined, it is difficult to attribute observed outcomes exclusively to impacts of surface roughness. Here, details of the experimental surfaces evaluated by streaming potential

analysis, contact angle evaluation and AFM, are reported as discussed above. Potential impacts from the washing protocol used to clean the experimental parallel plate chamber (Phase I) and the initial concentration of particles utilized during the deposition experiments (Phase II) were investigated to ensure that experimental outcomes observed during experimental Phase III were exclusively attributable to surface roughness.

During Phase I, an initial particle deposition experiment was conducted using 0.55 μm microspheres (initial concentration = 7.28×10^7 particles/mL). After running each deposition experiment, the quartz slide was cleaned and the same experiment was repeated. The slide cleaning protocol involved dipping the slide in Milli-Q™ water and removing it very slowly, owing from the pulling force at liquid/air/solid contact lines(50). After dipping the slide 10 times, the slide was immersed in acetone and sonicated for 15 minutes to remove all residual polystyrene, which dissolves in acetone. The slide was then extensively rinsed with Milli-Q™ water and blown dry with N_2 gas. Each slide was examined by fluorescence microscopy. The cleaning method was able to consistently achieve >98% removal of attached particles from the slide surface. This experimental phase was critical to ensuring that particle deposition monitored during Phase III occurred during the clean-bed period, with negligible particle-particle interactions.

During Phase II, different initial concentrations of representative microspheres (i.e., 0.98 μm) were utilized during the particle deposition experiments. The initial microsphere concentration investigated was 5.7×10^7 particles/mL and represented a 100% particle load in the influent suspension. The other investigated initial particle concentrations were 50% and 20% particle concentrations/loads. Theoretically, the dimensionless particle flux to the surface (*Sh*) should not be impacted by the initial influent particle concentration; however, in practice it is independent of influent particle concentration if particle deposition is being monitored during clean bed operation and if the particles do not aggregate during the experiments. In this study, influent particle suspensions were always made immediately before the experiments were conducted. They were also consistently sonicated prior to the experiments to avoid microsphere aggregation. This experimental phase was critical to

ensuring that Phase III experiments were conducted during clean bed particle deposition with negligible particle-particle interactions and without particle aggregation.

The Phase III investigation was comprised of 18 experiments, utilizing six targeted surface roughness sizes and three particle sizes (0.55, 0.98 and 1.76 μm microspheres) to evaluate the concurrent effects of particle size and roughness size on the particle deposition. The influent particle suspensions contained $7.28x10^7$ and $5.7x10^7$ and$1.14x10^7$ particles/mL of 0.55, 0.98, and 1.76 μm particles, respectively.

4.4 Results and discussion

4.4.1 Phase I and Phase II Results

Particle deposition (*Sh*) along the nine sampling locations along the distance from the chamber inlet to the outlet during the Phase I experiments is presented in Figure 4-5 (a). Five measurements were collected at each distance along the width of the slide (as depicted in the Figure 4-5). No differences in particle deposition (*Sh*) in experiments conducted before and after slide cleaning were observed. These results demonstrated that the cleaning method used during these and subsequent experiments effectively remove retained particles and returned the quartz slide surfaces to a clean bed condition so that they could be re-used. The duplicate deposition data were compared to results obtained using the analytical solution for particle deposition (Equation 4-2). As the selected particle size was relatively small (0.55 μm), *N* was 17402 and >>1.0, indicting that this key assumption of the analytical solution was satisfied for the experimental conditions applied herein. As demonstrated in Figure 4-5(a), excellent agreement between the experimental data and the analytical solution for dimensionless particle deposition (*Sh*) was obtained, as would be expected when the assumptions of the analytical solution were met. This agreement also confirmed the effectiveness of our experimental set-up, images acquisition and image analysis protocol for evaluating the particle deposition behavior.

Particle deposition (*Sh*) along the nine sampling locations along the distance from the chamber inlet to the outlet during the Phase II experiments is presented in Figure 4-5(b). Particle deposition (*Sh*) after concentration normalization did not vary between the triplicate experiments. These results suggested that the deposited particles were effectively enumerated with the developed image analysis protocol. Moreover, the data demonstrated that the initial particle concentration did not impact particle flux to the surface; accordingly a higher initial particle concentration could be utilized to shorten the duration of experiments during Phase III.

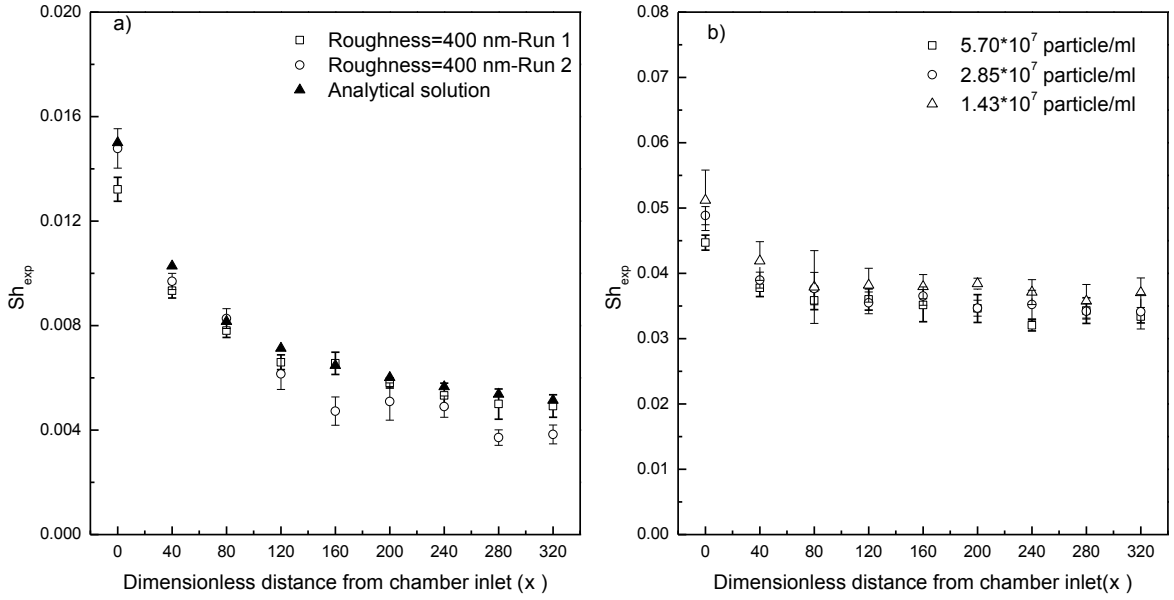

Figure 4-5. Representative plot of deposition curves for a) cleaning test with operational conditions: 400nm roughness, colloidal particle diameter: 0.55 µm, initial particle concentration: $7.28*10^7$ particle per ml; and b) concentration test using smooth slides, colloidal particle diameter: 0.98 µm, initial particle concentrations: $5.7*10^7$, $2.85*10^7$ and $1.425*10^7$ particles/mL, flow rate: 10µL/min, ionic strength: 100mM KCl, pH~6.9, and temperature: 22°C.

The Phase I and II experiments demonstrated that neither the quartz slide wash protocol, particle aggregation due to high ionic strength in the stock suspension, nor influent particle concentration affected clean bed conditions on the quartz slides between experiments. They

validated the appropriateness of the experimental set-up, operational procedures and the automated code for particle enumeration. The large number of experimental data (1125 images per experiment) enabled demonstration of the accuracy in the particle flux data. Accordingly, these experiments contributed to ensuring that the results obtained during the Phase III experiments incontrovertibly demonstrated surface rough impacts on particle deposition.

4.4.2 Phase III Results

To definitively prove a non-linear, non-monotonic effect of surface roughness on particle deposition, a well-controlled experiment involving an experimental configuration in which the convective-diffusion equation could be readily described and several colloidal particle sizes could be investigated was required, because it has been well established that colloidal particle size impacts particle deposition on surfaces(17, 18). Three different particle sizes of environmental relevance and six roughness sizes were utilized because the different combinations of particle and roughness sizes were expected to yield different deposition outcomes (74). The observed flux of the smallest (0.55 μm) particles to the surface at the 9 locations (i.e., distances from the inlet) on the slides at the 6 roughness sizes is presented in Figure 4-6(a). Maximum particle deposition (Sh_{exp}) was observed at the inlet of the parallel plate chamber. Particle deposition then decreased asymptotically with increasing distance from the inlet to the chamber ($\bar{x}$). The corresponding analytical solution for particle deposition was calculated (Equation 4-2) and also plotted for comparison. As expected, with 10 nm of surface roughness, the observed Sh_{exp} values based on the experimental data were very similar to the analytical solution. The roughness size of 10 nm was small and not substantially different from a smooth surface; accordingly, the analytical solution predicted the particle deposition flux well. As expected, deposition fluxes eventually reached a plateau because of gravity; in this case this occurred at a dimensionless distance ($\bar{x}$) of 200. Therefore, the flux data collected at 200 and beyond were excluded from quantitative analysis.

As mentioned above, to minimize the gravity effect which is substantially impacted by particle size and density and thus alternatively determine the location of plateau for deposition curve, the density of the particle suspension was chosen to be close to the KCl solution. Before the cut-off distance, the cumulative gravity effect on concentration gradient is relatively small as compared to diffusion and convection. In contrast, numbers of suspended particle in bulk solution settled down at the vicinity of bottom surface after the cut-off distance and ultimately form a concentration gradient which could interfere the deposition rate. The cumulative gravity effect is gradually owing to the dynamic equilibriums among various mechanism including diffusion, convection, hydrodynamic, gravity and chemical related mechanisms. It is also changeling to predict the exact value of cut-off distance (200 for 0.55μm particle) for average flux calculation to exclude the cumulative gravity impact and also beyond the scope of this study. As the focus of this investigation is to identify the impact of nano-scale roughness on deposition, cut-off distance at dimensionless distance of 200 was applied to for subsequent data analysis and comparison for other sizes of colloids.

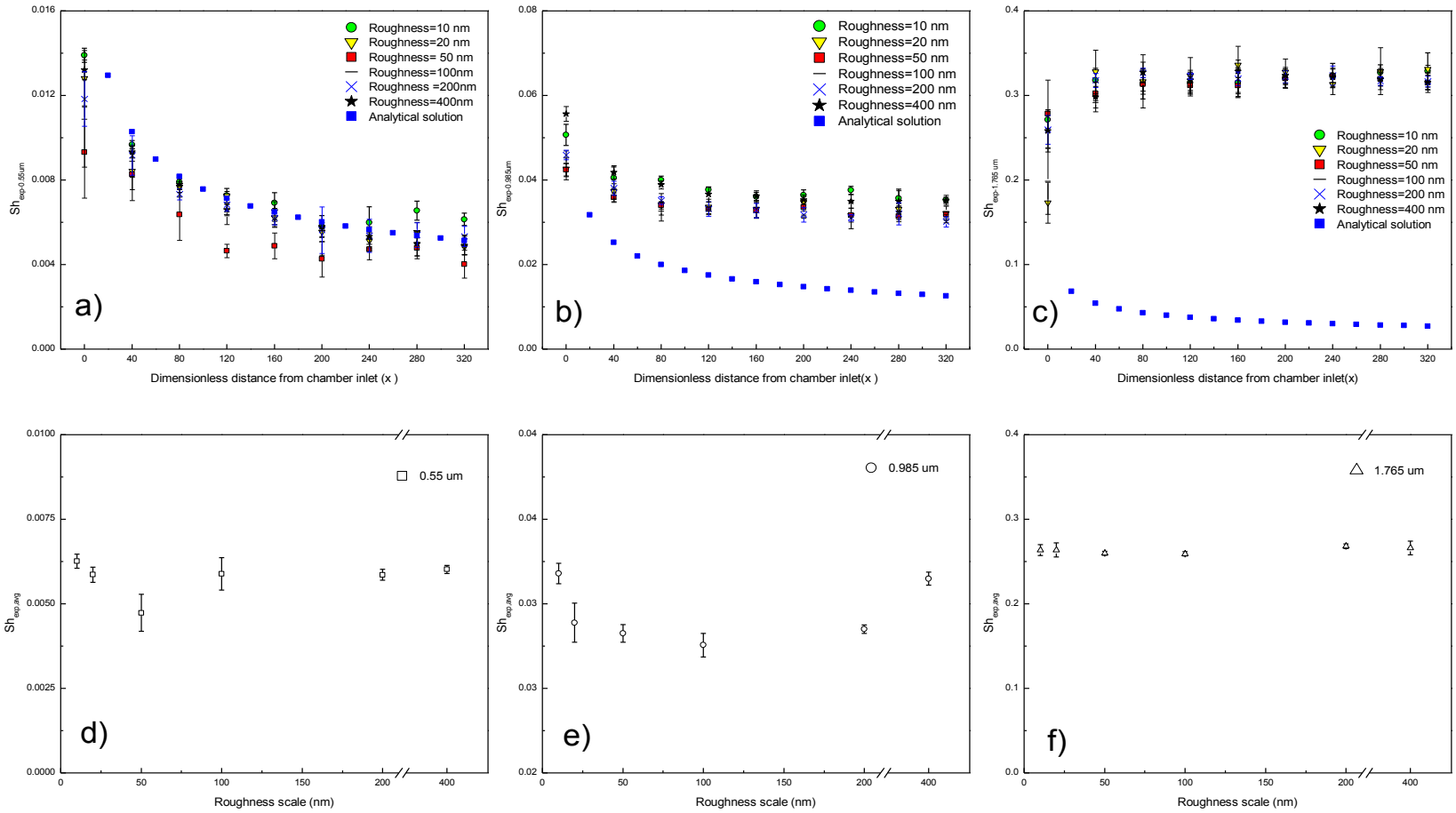

Figure 4-6. Dimensionless deposition rate (Sh_{exp}) and average dimensionless flux ($Sh_{exp,avg}$) of 0.55 µm a) and c), 0.98 µm b) and e), 1.76 µm c) and f) microsphere on quartz slides with different patterned roughness (10 nm, 20nm, 50 nm, 100nm, 200nm and 400nm respectively). The operational conditions: colloidal particle diameter: 0.55µm, initial particle concentration: 7.28*107 particle per ml respectively. Other conditions: flow rate: 10ul/min, Ionic strength: 100mM KCl, pH~6.9, Room temperature: 22˚C.

The deposition profiles for the larger (0.98 and 1.76 μm) colloids, as well as the associated analytical solutions for deposition, are presented in Figures 4-6(b) and (c), respectively. Like for the smaller colloids, Sh_{exp} decreased along $\bar{x}$; however, it was ~2 and ~7 times higher than the calculated analytical solution *Sh* for the 0.98 (Figure 4-6(b)) and 1.76 μm (Figure 4-6 (c)) colloids, respectively. As would be expected, greater deviation between the analytical solution and experimental data would be expected for larger sized colloids because gravity is inversely proportional to diffusion, but cubically proportional to particle sized (16). Notably, while the deposition profile (Sh_{exp}) for the 0.98 μm particles (Figure 4-6(b)) was similar to that of the 0,55 μm particles (Figure 4-6(a)), the trend in deposition flux along $\bar{x}$ was inversed for the 1.76 μm particles (Figure 4-6(c)); instead of decreasing with dimensionless distance in the flow direction, Sh_{exp} increased with $\bar{x}$ and then leveled off. Moreover, these data clearly demonstrated that total flux of particles to the surface increased with particle size. Overall, these observations and comparative differences in particle deposition profiles for the various sizes of colloids underscore the complex relationship between colloid and roughness size on particle deposition.

Close examination of Figures 4-6 (a-c) demonstrates a non-linear, non-monotonic impact of surface roughness on particle deposition. More specifically, deposition (Sh_{exp}) of a particle of given size at a specific point in the chamber (i.e. distance along the flow path) varied non-linearly with roughness size. The observed non-linear, non-monotonic effect of surface roughness on particle deposition can be more clearly and definitively demonstrated by examining the average dimensionless deposition flux Sh_{avg} for a given combination of particle and roughness size. This was done by averaging the Sh_{exp} values for each slide determined between 0.5 and 2.5 cm ($\bar{x}$ = 40 and 200) using Equation 4-6

$$Sh_{\exp,avg} = \frac{\sum_{\bar{x}_1}^{\bar{x}_n} Sh_{\bar{x}_i} * (\bar{x}_{i+1} - \bar{x}_i)}{\bar{x}_n - \bar{x}_1} \qquad (4\text{-}6)$$

in which $Sh_{\bar{x}_i}$ is the observed flux at $\bar{x}_i$ on the deposition curves, n = 5, $\bar{x}_1$ = 40 and $\bar{x}_n$ = 200.

The Sh_{exp} values for the first sampling location ($\bar{x}$ = 0) were excluded from the calculation because flow likely had not reached steady state at the entrance of the parallel plate chamber. The Sh_{exp} for sampling locations where the Sh_{exp} reached a plateau ($\bar{x}$ > 200) were also excluded because of the likely concentration gradient near the contact surface that was discussed above, which would violate the fundamental assumption of clean bed filtration(15, 51, 52). While this effect merits further study, it was beyond the scope of the present work and fortunately did not preclude definitive demonstration of a non-linear, non-monotonic effect of surface roughness on particle deposition.

The average dimensionless deposition flux $Sh_{exp,avg}$ at the various surface roughness sizes investigated herein is presented for each particle size (0.55, 0.98, and 1.76 μm) in Figures 4-6(d), (e), and (f), respectively. These figures demonstrate that, regardless of particle size, as surface roughness size increased, particle deposition flux first decreased to a minimum value and then increased and finally leveled off. The minimum level of particle deposition or "sag effect" depends on particle size and a "critical roughness size" below which, *increases* in nano-scale surface roughness result in decreased particle deposition and above which, *increases* in nano-scale surface roughness results in increased particle deposition that ultimately plateaus. For example, the maximum $Sh_{exp,avg}$ for the 0.55 μm particles was obtained at the smallest roughness size (10 nm); the deposition minimum was observed at a critical roughness size of 50 nm (Figure 4-6(d)) and the maximum measured Sh_{avg} was 32% larger than the minimum value. This difference in particle deposition was significantly (p=.0021) and highlights the significant impact of nano-scale roughness on 0.55 μm particle deposition. Similarly, the maximum Sh_{avg} for the 0.98 μm particles was also observed at the 10nm roughness size; however, the deposition minimum was observed at a critical roughness size of 100 nm (Figure 4-6(e)). While a "sag effect" was also observed with these particles, the difference between maximum and minimum Sh_{avg} values was only 12.5%. Nonetheless, the greatest differences in 0.98 μm particle deposition fluxes to surfaces with different levels

of nano-scale roughness were still significantly different (p=0.0001) at the conditions investigated.

The relationship between particle deposition flux and surface roughness size for the 1.76 μm particles was different from those of the other particles (Figure 4-6(f)). In this case, there was no clearly apparent "sag effect" and the difference between the maximum and minimum values of Sh_{avg} was only 1.4 %, which was not statistically significant (p=0.268). Not surprisingly, none of the differences between 1.76 μm particle deposition fluxes to surfaces with different levels of nano-scale roughness were significantly different at the conditions investigated. An increase in flow rate would likely have an additional synergistic impact resulting in an apparent sag effect for these larger size particles. Further, changes in operational conditions such as the flow rate and/or ionic strength would undoubtedly result in different particle deposition profiles and should be the focus of future study.

The present investigation is consistent with others that have demonstrated that the deposition of smaller particles on surfaces is more sensitive to nano-scale surface roughness than that of larger particles(25, 34). While enhanced particle deposition in the presence of surface roughness has been widely reported(39, 49, 53), some studies have reported decreased deposition associated with surface roughness (37, 40). Notably, the present investigation demonstrates a significant non-linear, non-monotonic relationship or "sag effect" between particle deposition and surface roughness size; this relationship is unique to different combinations of particle and roughness size for a given set of operational conditions (e.g., flow rate, ionic strength, etc.). The results presented herein are also consistent with the experimental data obtained from column tests conducted with glass beads (74). In contrast to those results from packed column studies, the experiments presented herein were more exhaustive and conducted with an experimental configuration (i.e., parallel plate chamber with extensive sampling) that enabled definitive evidence of the non-linear, non-monotonic impacts of nano-scale surface roughness on colloidal particle deposition on collector surfaces and subsequent mathematical model development (presented in the associated Part II paper 76).

4.5 Mechanistic Implications

The well-controlled operational conditions applied in the present investigation minimized and essentially excluded confounding impacts of surface chemical heterogeneity, surface hydrophobicity, and the secondary energy minimum on particle deposition. The use of 100mM KCl compressed the electric double layer (κ^{-1} = 0.3 nm) around the colloidal particles and contact surface, thereby minimizing the impact of the secondary energy minimum. Contact angle measurements on the contact surfaces with different levels of roughness did not indicate substantial differences in surface hydrophobicity. Microscopic evaluation of all modified quartz slide contact surfaces did not reveal any indication of surface chemical heterogeneities, as well extensive particle aggregation or blocking at specific locations was not observed. Chemical heterogeneity(33, 42), the secondary energy minimum(54, 55)and hydrophobicity (40, 56) are commonly recognized, chemically-based mechanisms that can influence particle deposition behavior; however, they clearly did not result in the non-linear, non-monotonic relationship between the particle deposition and the surface roughness that was observed in the present investigation.

Enhanced particle deposition in the presence of surface roughness had been extensively discussed in the literature(25, 37, 57). It has been widely accepted that the presence of surface roughness can reduce the magnitude of interaction energy curves; previous modeling studies have suggested that repulsive electrostatic forces decay more rapidly than attractive van der Waals force over distance from target surfaces (19, 58). Accordingly, the energy barrier can be substantially reduced, even if only 4% of a surface is covered by roughness (59). Particle size is also relevant to particle deposition; the critical roughness scale that results in the minimal interaction energy that favors particle deposition may vary with the particle size(36, 60). The increased distance between particles and deposition surfaces that is attributed to roughness elements makes net interaction energy more favorable for particle attachment on surfaces(26, 59, 60). Accordingly, quantitative description of DLVO interaction energy should be modified to reflect the impact of surface roughness and its non-linear, non-monotonic impact on particle deposition, as demonstrated herein. This is discussed in the paper (Part II) that accompanies this one.

In addition to recommended changes in the calculation of DLVO forces, the hydrodynamic retardation functions that describe the repulsive wall effects on approaching particles should also be modified to include the effect of surface roughness(52). Originally developed in 1960s(61-64), hydrodynamic retardation functions have been successfully applied to describe the hydrodynamic retardation effect of approaching particle due to the wall effects. It is recently recognized; however, that for rough surfaces, the effective surface plain is located at an intermediate position between the top and bottom of the asperities; the position of this intermediate plane is controlled by the density of the roughness elements(65, 66). Accordingly, hydrodynamic retardation should be scaled down depending on the height of roughness asperities. The presence of surface roughness can reduce the retardation effect and enhance particle transport, bringing particles closer to target surfaces, thereby potentially enhancing deposition. The quantitative analysis of the expected extent of enhanced particle deposition due to surface roughness is discussed in the accompanying paper (Part II).

Decreased particle deposition in the presence of surface roughness can also be the result of the changes in hydrodynamics. When surface roughness is present, the absolute scales and direction of flow change accordingly(67, 68). A slip boundary condition (or partial-slip boundary condition) should be used instead of the no-slip boundary that is commonly used and only applicable to smooth surfaces. Depending on the coverage and scale of surface roughness, the flow velocity on the contact surface may be increased and lead to more particle deposition from convection. The presence of roughness can also change the flow direction around the roughness features and simultaneously enhance particle detachment. Ko et al. (2000) (69) reported the "shadow effect" to explain decreased particle deposition caused by the surface roughness. They hypothesized that surface roughness could alter the tangential component of fluid flow around roughness features and "guide" the approaching particle away from the surface, creating a "shadow zone" for particle attachment. Similarly, Yang et al. (1999) (18) reported that the changes in flow direction due to surface asperities could decrease particle deposition.

The shear lift force could be another factor that contributes to decreased particle deposition associated with surface roughness(70, 71). When a particle approaches a target surface, it

experiences a lift force that "pushes" the particle away from the surface, due to the relative translation velocity between the particle and the streamlines in the viscous flow(70, 71). If the particle is already resting on the surface, the shear lift force is always present to contribute to driving it away from the surface(72). Leighton and Acrivos (1985) found that surface roughness could impact the scale of shear lift force when the particle attached to the surface(72). Derksen and Larsen (2011) demonstrated that surface roughness (in the form of attached spheres) could increase the shear lift force by 3.6 times as compared to the lift force on smooth surfaces; moreover, the shear lift force was independent of *Re* when $Re<0.1$ and could be significant even at low *Re*.(73) Therefore, shear lift forces will not only "push" approaching particles away from target surfaces, but also "shear off" attached particles, thereby leading to decreased particle deposition. The net force exerted on the colloidal particles determines the final fate of particle as attached and removed from suspension or detached and migrate back the bulk solution. Appropriate consideration of all of these factors will better enable quantitative explanation of the observed critical roughness size or "sag effect" for particle deposition on surfaces described herein.

4.6 Conclusions

To systemically evaluate and definitively demonstrate the impacts of surface roughness on particle deposition at high ionic strength conditions favoring particle deposition, a two part investigations (experimental, Part I and numerical simulation, Part II) was conducted. The Part I investigation is presented in this paper. The deposition kinetics of polystryrene microspheres suspended in 100mM KCl on quartz slides with nano-scale surface roughness were examined. A non-linear, non-monotonic relationship between surface roughness and particle deposition flux was observed. A critical roughness size that contributed to a minimal deposition flux for each combination of particle and roughness size was identified experimentally. When the roughness size was greater than critical roughness, increased roughness resulted in increased particle deposition; in contrast, increasing roughness at sizes smaller than the critical roughness size resulted in decreased particle deposition. The effect of roughness on particle deposition was most significant for small colloids (e.g. 0.55 μm) whose

deposition was mainly dominated by diffusion. This paper also underscored the importance of methodology of used to evaluate particle deposition behavior on target surfaces by underscoring the importance of rigorous quality assurance and the importance of adequate data collection so as to assure appropriate mechanistic evaluation of outcomes (e.g., the importance of reproducibility in data and exclusion of confounding factors such as gravity).

A straightforward analytical solution to the convective-diffusion equation was utilized herein to help interpret the experimental outcomes. The data presented herein underscore the inadequacy of current models of particle deposition that assume smooth collector surfaces. The development of a modified analytical solution to describe particle deposition behavior in the presence of surface roughness is presented in the Part II paper in which formula modifications for different mechanisms (flow field, hydrodynamic retardation, and DLVO interaction energy) due to the presence of the roughness are discussed and a numerical model is developed to simulate the non-linear, non-monotonic effect of the surface roughness on the particle deposition observed in the parallel-plate chamber experiments.

4.7 References

1. Mccarthy, J.F. and Zachara, J.M. Subsurface Transport of Contaminants - Mobile Colloids in the Subsurface Environment may Alter the Transport of Contaminants. *Environ. Sci. Technol.* **1989,** *23* (5), 496-502.

2. Mesquita, M.M.F.; Stimson, J.; Chae, G.-.; Tufenkji, N.; Ptacek, C.J.; Blowes, D.W.; Emelko, M.B. Optimal preparation and purification of PRD1-like bacteriophages for use in environmental fate and transport studies. *Water Res.* **2010,** *44* (4), 1114-1125; 10.1016/j.watres.2009.11.017.

3. Emelko, M.B.; Huck, P.M.; Coffey, B.M. A review of Cryptosporidium removal by granular media filtration. *Journal American Water Works Association* **2005,** *97* (12), 101-+.

4. Betancourt, W.Q. and Rose, J.B. Drinking water treatment processes for removal of Cryptosporidium and Giardia. *Vet. Parasitol.* **2004,** *126* (1–2), 219-234; http://dx.doi.org/10.1016/j.vetpar.2004.09.002.

5. Edzwald, J.K. *Water Quality & Treatment: A Handbook on Drinking Water.* McGraw-Hill New York: 2011; .

6. Barnes, L.; Lo, M.; Adams, M.; Chamberlain, A. Effect of milk proteins on adhesion of bacteria to stainless steel surfaces. *Appl. Environ. Microbiol.* **1999,** *65* (10), 4543-4548.

7. Greenberg, A.W. and Hammer, D.A. Cell separation mediated by differential rolling adhesion. *Biotechnol. Bioeng.* **2001,** *73* (2), 111-124; 10.1002/bit.1043.

8. Santos, J.P.; Hontanon, E.; Ramiro, E.; Alonso, M. Performance evaluation of a high-resolution parallel-plate differential mobility analyzer. *Atmos. Chem. Phys.* **2009,** *9* (7), 2419-2429.

9. Ehara, K.; Hagwood, C.; Coakley, K.J. Novel method to classify aerosol particles according to their mass-to-charge ratio - Aerosol particle mass analyser. *J. Aerosol Sci.* **1996,** *27* (2), 217-234; 10.1016/0021-8502(95)00562-5.

10. Mainelis, G.; Willeke, K.; Baron, P.; Grinshpun, S.; Reponen, T. Induction charging and electrostatic classification of micrometer-size particles for investigating the electrobiological properties of airborne microorganisms. *Aerosol. Sci. Technol.* **2002,** *36* (4), 479-491; 10.1080/027868202753571304.

11. Young, J. and Leeming, A. A theory of particle deposition in turbulent pipe flow. *J. Fluid Mech.* **1997,** *340*, 129-159; 10.1017/S0022112097005284.

12. Nijhawan, S.; McMurry, P.H.; Campbell, S.A. Particle transport in a parallel-plate semiconductor reactor: Chamber modification and design criterion for enhanced process cleanliness. *Journal of Vacuum Science & Technology A-Vacuum Surfaces and Films* **2000,** *18* (5), 2198-2206; 10.1116/1.1288193.

13. Liu, B. and Ahn, K. Particle Deposition on Semiconductor Wafers. *Aerosol. Sci. Technol.* **1987,** *6* (3), 215-224; 10.1080/02786828708959135.

14. Ryan, J.N. and Elimelech, M. Colloid mobilization and transport in groundwater. *Colloids and Surfaces A-Physicochemical and Engineering Aspects* **1996,** *107*, 1-56.

15. Yao, K.M.; Habibian, M.M.; O'Melia, C.R. Water and Waste Water Filtration - Concepts and Applications. *Environ. Sci. Technol.* **1971,** *5* (11), 1105-&.

16. Adamczyk, Z. and Vandeven, T.G.M. Deposition of Particles Under External Forces in Laminar-Flow through Parallel-Plate and Cylindrical Channels. *J. Colloid Interface Sci.* **1981,** *80* (2), 340-356; 10.1016/0021-9797(81)90193-4.

17. Bowen, B. and Epstein, N. Fine Particle Deposition in Smooth Parallel-Plate Channels. *J. Colloid Interface Sci.* **1979,** *72* (1), 81-97; 10.1016/0021-9797(79)90184-X.

18. Yang, J.L.; Bos, R.; Poortinga, A.; Wit, P.J.; Belder, G.F.; Busscher, H.J. Comparison of particle deposition in a parallel plate and a stagnation point flow chamber. *Langmuir* **1999,** *15* (13), 4671-4677; 10.1021/la981607k.

19. Adamczyk, Z. and Weronski, P. Application of the DLVO theory for particle deposition problems. *Adv. Colloid Interface Sci.* **1999,** *83* (1-3), 137-226; 10.1016/S0001-8686(99)00009-3.

20. Knappett, P.S.K.; Emelko, M.B.; Zhuang, J.; McKay, L.D. Transport and retention of a bacteriophage and microspheres in saturated, angular porous media: Effects of ionic strength and grain size. *Water Res.* **2008,** *42* (16), 4368-4378; 10.1016/j.watres.2008.07.041.

21. Johnson, W.P.; Tong, M.; Li, X. On colloid retention in saturated porous media in the presence of energy barriers: The failure of alpha, and opportunities to predict eta. *Water Resour. Res.* **2007,** *43* (12), W12S13; 10.1029/2006WR005770.

22. Elimelech, M. and Song, L. Theoretical investigation of colloid separation from dilute aqueous suspensions by oppositely charged granular media. *Separations Technology* **1992,** *2* (1), 2-12; http://dx.doi.org.proxy.lib.uwaterloo.ca/10.1016/0956-9618(92)80001-T.

23. Johnson, W.P.; Ma, H.L.; Pazmino, E. Straining Credibility: A General Comment Regarding Common Arguments Used to Infer Straining As the Mechanism of Colloid

Retention in Porous Media. *Environ. Sci. Technol.* **2011,** *45* (9), 3831-3832; 10.1021/es200868e ER.

24. Henry, C.; Minier, J.; Lefevre, G. Numerical Study on the Adhesion and Reentrainment of Nondeformable Particles on Surfaces: The Role of Surface Roughness and Electrostatic Forces. *Langmuir* **2012,** *28* (1), 438-452; 10.1021/la203659q.

25. Darbha, G.K.; Schaefer, T.; Heberling, F.; Luettge, A.; Fischer, C. Retention of Latex Colloids on Calcite as a Function of Surface Roughness and Topography. *Langmuir* **2010,** *26* (7), 4743-4752; 10.1021/la9033595.

26. Huang, X.F.; Bhattacharjee, S.; Hoek, E.M.V. Is Surface Roughness a "Scapegoat" or a Primary Factor When Defining Particle-Substrate Interactions? *Langmuir* **2010,** *26* (4), 2528-2537; 10.1021/la9028113 ER.

27. Tufenkji, N. and Elimelech, M. Correlation equation for predicting single-collector efficiency in physicochemical filtration in saturated porous media. *Environ. Sci. Technol.* **2004,** *38* (2), 529-536; 10.1021/es034049r.

28. Tien, C. and Ramarao, B.V. *Granular filtration of aerosols and hydrosols.* Access Online via Elsevier: 2011; .

29. Ma, H.L.; Pedel, J.; Fife, P.; Johnson, W.P. Hemispheres-in-Cell Geometry to Predict Colloid Deposition in Porous Media (vol 43, pg 8573, 2009). *Environ. Sci. Technol.* **2010,** *44* (11), 4383-4383; 10.1021/es1009373 ER.

30. Mendez-Vilas, A.; Bruque, J.M.; Gonzalez-Martin, M.L. Sensitivity of surface roughness parameters to changes in the density of scanning points in multi-scale AFM studies. Application to a biomaterial surface. *Ultramicroscopy* **2007,** *107* (8), 617-625; 10.1016/j.ultramic.2006.12.002.

31. Zembala, M. Electrokinetics of heterogeneous interfaces. *Adv. Colloid Interface Sci.* **2004,** *112* (1-3), 59-92; 10.1016/j.cis.2004.08.001.

32. Suresh, L. and Walz, J.Y. Direct measurement of the effect of surface roughness on the colloidal forces between a particle and flat plate. *J. Colloid Interface Sci.* **1997,** *196* (2), 177-190.

33. Walz, J.Y. The effect of surface heterogeneities on colloidal forces. *Adv. Colloid Interface Sci.* **1998,** *74,* 119-168.

34. Shellenberger, K. and Logan, B.E. Effect of molecular scale roughness of glass beads on colloidal and bacterial deposition. *Environ. Sci. Technol.* **2002,** *36* (2), 184-189; 10.1021/es015515k ER.

35. Hoek, E.M.V.; Bhattacharjee, S.; Elimelech, M. Effect of membrane surface roughness on colloid-membrane DLVO interactions. *Langmuir* **2003,** *19* (11), 4836-4847; 10.1021/la027083c.

36. Henry, C.; Minier, J.; Lefevre, G.; Hurisse, O. Numerical Study on the Deposition Rate of Hematite Particle on Polypropylene Walls: Role of Surface Roughness. *Langmuir* **2011,** *27* (8), 4603-4612; 10.1021/la104488a.

37. Chen, G.; Bedi, R.S.; Yan, Y.S.; Walker, S.L. Initial Colloid Deposition on Bare and Zeolite-Coated Stainless Steel and Aluminum: Influence of Surface Roughness. *Langmuir* **2010,** *26* (15), 12605-12613; 10.1021/la101667t.

38. Darbha, G.K.; Fischer, C.; Michler, A.; Luetzenkirchen, J.; Schaefer, T.; Heberling, F.; Schild, D. Deposition of Latex Colloids at Rough Mineral Surfaces: An Analogue Study Using Nanopatterned Surfaces. *Langmuir* **2012,** *28* (16), 6606-6617; 10.1021/la3003146.

39. Zan, Q.F.; Wang, C.; Dong, L.M.; Cheng, P.; Tian, J.M. Effect of surface roughness of chitosan-based microspheres on cell adhesion. *Appl. Surf. Sci.* **2008,** *255* (2), 401-403; 10.1016/j.apsusc.2008.06.074 ER.

40. Tang, H.; Cao, T.; Liang, X.; Wang, A.; Salley, S.O.; McAllister,James,,II; Ng, K.Y.S. Influence of silicone surface roughness and hydrophobicity on adhesion and colonization of Staphylococcus epidermidis. *Journal of Biomedical Materials Research Part a* **2009,** *88A* (2), 454-463; 10.1002/jbm.a.31788.

41. Hoek, E.M.V. and Agarwal, G.K. Extended DLVO interactions between spherical particles and rough surfaces. *J. Colloid Interface Sci.* **2006,** *298* (1), 50-58; 10.1016/j.jcis.2005.12.031.

42. Rizwan, T. and Bhattacharjee, S. Particle Deposition onto Charge-Heterogeneous Substrates. *Langmuir* **2009,** *25* (9), 4907-4918; 10#1021/la804075g ER.

43. Dorobantu, L.S.; Bhattacharjee, S.; Foght, J.M.; Gray, M.R. Atomic force microscopy measurement of heterogeneity in bacterial surface hydrophobicity. *Langmuir* **2008,** *24* (9), 4944-4951; 10.1021/la7035295 ER.

44. King, M.R. and Hammer, D.A. Multiparticle adhesive dynamics: Hydrodynamic recruitment of rolling leukocytes. *Proc. Natl. Acad. Sci. U. S. A.* **2001,** *98* (26), 14919-14924; 10.1073/pnas.261272498.

45. Sjollema, J. and Busscher, H. Deposition of Polystyrene Particles in a Parallel Plate Flow Cell .1. the Influence of Collector Surface-Properties on the Experimental Deposition Rate. *Colloids and Surfaces* **1990,** *47,* 323-336; 10.1016/0166-6622(90)80081-E.

46. Kern, W. The evolution of silicon wafer cleaning technology. *J. Electrochem. Soc.* **1990,** *137* (6), 1887-1892.

47. Liu, W.; Ferguson, M.; Yavuz, M.; Cui, B. Porous TEM windows fabrication using CsCl self-assembly. *Journal of Vacuum Science & Technology B* **2012,** *30* (6), 06F201; 10.1116/1.4751550.

48. Green, M. and Tsuchiya, S. Mesoscopic hemisphere arrays far use as resist in solid state structure fabrication. *J. Vac. Sci. Technol. B* **1999,** *17* (5), 2074-2083; 10.1116/1.590875.

49. Darbha, G.K.; Fischer, C.; Luetzenkirchen, J.; Schäfer, T. Site-specific retention of colloids at rough rock surfaces. *Environ. Sci. Technol.* **2012,** *46* (17), 9378-9387.

50. Suarez, C.; Noordmans, J.; van der Mei, H.; Busscher, H. Removal of colloidal particles from quartz collector surfaces as stimulated by the passage of liquid-air interfaces. *Langmuir* **1999,** *15* (15), 5123-5127.

51. Logan, B.E.; Jewett, D.G.; Arnold, R.G.; Bouwer, E.J.; O'Melia, C.R. Clarification of Clean-Bed Filtration Models. *Journal of Environmental Engineering-Asce* **1995,** *121* (12), 869-873.

52. Elimelech, M.; Jia, X.; Gregory, J.; Williams, R. *Particle deposition & aggregation: measurement, modelling and simulation.* Butterworth-Heinemann: 1998; .

53. Elimelech, M. and O'Melia, C.R. Effect of Particle-Size on Collision Efficiency in the Deposition of Brownian Particles with Electrostatic Energy Barriers. *Langmuir* **1990,** *6* (6), 1153-1163.

54. Tufenkji, N. and Elimelech, M. Breakdown of colloid filtration theory: Role of the secondary energy minimum and surface charge heterogeneities. *Langmuir* **2005,** *21* (3), 841-852; 10.1021/la048102g.

55. Hahn, M.W.; Abadzic, D.; O'Melia, C.R. Aquasols: On the role of secondary minima. *Environ. Sci. Technol.* **2004,** *38* (22), 5915-5924; 10.1021/es049746d.

56. Dorobantu, L.S.; Bhattacharjee, S.; Foght, J.M.; Gray, M.R. Analysis of Force Interactions between AFM Tips and Hydrophobic Bacteria Using DLVO Theory. *Langmuir* **2009,** *25* (12), 6968-6976; 10.1021/la9001237 ER.

57. Shellenberger, K. and Logan, B.E. Effect of molecular scale roughness of glass beads on colloidal and bacterial deposition. *Environ. Sci. Technol.* **2002,** *36* (2), 184-189; 10.1021/es015515k.

58. Bhattacharjee, S.; Ko, C.H.; Elimelech, M. DLVO interaction between rough surfaces. *Langmuir* **1998,** *14* (12), 3365-3375.

59. Walz, J.Y. and Sun, N. Effects of surface roughness on van der Waals and electrostatic contributions to particle-particle interactions and particle adhesion. *Particles of Surfaces 7: Detection, Adhesion and Removal* **2002,** , 151-169.

60. Saiers, J.E. and Ryan, J.N. Colloid deposition on non-ideal porous media: The influences of collector shape and roughness on the single-collector efficiency. *Geophys. Res. Lett.* **2005,** *32* (21), L21406; 10.1029/2005GL024343.

61. Brenner, H. The Slow Motion of a Sphere through a Viscous Fluid Towards a Plane Surface. *Chem. Eng. Sci.* **1961,** *16* (3-4), 242-251; 10.1016/0009-2509(61)80035-3.

62. Goren, S.L. and O'Neill, M.E. Hydrodynamic Resistance to a Particle of a Dilute Suspension when in Neighbourhood of a Large Obstacle. *Chemical Engineering Science* **1971,** *26* (3), 325-&; 10.1016/0009-2509(71)83008-7.

63. Goldman, A.J.; Cox, R.G.; Brenner, H. Slow Viscous Motion of a Sphere Parallel to a Plane Wall .I. Motion through a Quiescent Fluid. *Chemical Engineering Science* **1967,** *22* (4), 637-&; 10.1016/0009-2509(67)80047-2.

64. Goldman, A.J.; Cox, R.G.; Brenner, H. Slow Viscous Motion of a Sphere Parallel to a Plane Wall .2. Couette Flow. *Chemical Engineering Science* **1967,** *22* (4), 653-&; 10.1016/0009-2509(67)80048-4.

65. Kunert, C.; Harting, J.; Vinogradova, O.I. Random-Roughness Hydrodynamic Boundary Conditions. *Phys. Rev. Lett.* **2010,** *105* (1), 016001; 10.1103/PhysRevLett.105.016001.

66. Vinogradova, O.I. and Belyaev, A.V. Wetting, roughness and flow boundary conditions. *Journal of Physics-Condensed Matter* **2011,** *23* (18), 184104; 10.1088/0953-8984/23/18/184104.

67. Zhu, Y.X. and Granick, S. Limits of the hydrodynamic no-slip boundary condition. *Phys. Rev. Lett.* **2002,** *88* (10), 106102; 10.1103/PhysRevLett.88.106102.

68. Bonaccurso, E.; Butt, H.J.; Craig, V.S.J. Surface roughness and hydrodynamic boundary slip of a newtonian fluid in a completely wetting system. *Phys. Rev. Lett.* **2003,** *90* (14), 144501; 10.1103/PhysRevLett.90.144501.

69. Ko, C.H. and Elimelech, M. The "shadow effect" in colloid transport and deposition dynamics in granular porous media: Measurements and mechanisms. *Environ. Sci. Technol.* **2000,** *34* (17), 3681-3689; 10.1021/es0009323.

70. Saffman, P.G. Lift on a Small Sphere in a Slow Shear Flow. *J. Fluid Mech.* **1965,** *22*, 385-&; 10.1017/S0022112065000824.

71. Cherukat, P. and Mclaughlin, J.B. The Inertial Lift on a Rigid Sphere in a Linear Shear-Flow Field Near a Flat Wall. *J. Fluid Mech.* **1994,** *263*, 1-18; 10.1017/S0022112094004015.

72. Leighton, D. and Acrivos, A. The Lift on a Small Sphere Touching a Plane in the Presence of a Simple Shear-Flow. *Zeitschrift Fur Angewandte Mathematik Und Physik* **1985,** *36* (1), 174-178; 10.1007/BF00949042.

73. Derksen, J.J. and Larsen, R.A. Drag and lift forces on random assemblies of wall-attached spheres in low-Reynolds-number shear flow. *J. Fluid Mech.* **2011,** *673*, 548-573; 10.1017/S0022112010006403.

74. Jin, C. and Emelko, M.B. Non-linear, non-monotonic impact of surface roughness on colloidal particle deposition during granular media filtration at favorable conditions. *Environ. Sci. Technol.* **2014,** *to be submitted*

75. Jin, C.; Glawdel, T.; Ren, C.; Emelko, M.B. Non-Linear, non-monotonic impact of nano-scale surface roughness on colloidal particle deposition. I. Experiments in a parallel plate system. *Langmuir* **2014,** *to be submitted*

76. Jin, C.; Glawdel, T.; Ren, C.; Emelko, M.B. Non-Linear, non-monotonic impact of nano-scale roughness on particle deposition: II. Numerical modeling. *Langmuir* **2014,** *to be submitted*

Chapter 5

Non-Linear, non-monotonic impact of nano-scale roughness on particle deposition: II. Numerical modeling

5.1 Overview

This is the second of a two-part investigation of the impact of nano-scale surface roughness on particle deposition at high ionic strength conditions favoring particle deposition. In the preceding paper, a non-linear, non-monotonic relationship between particle deposition and surface roughness was demonstrated and a critical roughness size associated with a minimum deposition flux was identified. Here, an Eulerian model describing colloidal particle deposition influenced by nano-scale surface roughness is developed. The model incorporates numerical modifications to the flow field profile, hydrodynamic retardation functions, and DLVO interaction energy; the influence of each component on particle deposition is quantitatively evaluated. The importance of gravity and the boundary condition for deposition in the Convective-Diffusion equation is also discussed. The numerical solutions to the model were validated by comparison to the experimental data reported in our preceding paper (60). The present work provides a mathematical framework that enables better quantitative description of particle deposition on real surfaces for numerous applications (e.g., natural and engineered filtration, semi-conductor manufacturing, pipeline efficiency optimization, prevention of food contamination, cell separation and detection, air quality assessment, etc.) because it includes the effect of collector surface roughness on particle deposition.

5.2 Introduction

The physico-chemical process of particle transport and attachment on collector surfaces (deposition), has been studied in the context of various natural and engineered systems, including filtration, since the 1960s; mathematical models have been developed to simulate this process(1-4). Existing models are able to predict particle deposition on surfaces when the following assumptions are satisfied(3, 5-7): 1) the contact surface is completely smooth, 2) there is no interaction energy barrier between the approaching particle and the target surface, 3) diffusion is the dominant mechanism governing particle transport to the target surface, 4) there are no particle-to-particle interactions in the suspension, and 5) blocking on the target surface is insignificant (i.e., clean bed filtration). As a result, existing models are typically inadequate for describing or predicting particle deposition in real-world applications, such as drinking water filtration processes. One reason why it is difficult to apply currently available models for particle deposition to real-world applications is because most surfaces commonly present in natural and engineered systems are not perfectly smooth, having at least some degree of surface roughness, at the nano-scale or larger.

Enhanced particle deposition attributed to surface roughness has been frequently reported(8-10); however, decreased particle deposition has also been attributed to surface roughness in a few cases(11, 12). In our Part I paper (60), the influence of the surface roughness on particle deposition was systematically studied through experiments conducted in a parallel plate chamber with plates patterned by different roughness sizes. A non-linear, non-monotonic relationship between surface roughness size and particle deposition was observed and the existence of a critical roughness size associated with a minimum deposition flux was identified for the conditions investigated.

The ultimate goal of our work is to develop a theoretical model that 1) describes colloidal particle deposition in the presence of surface roughness and 2) simulates particle deposition in systems with different geometries such as stagnation point flow chambers(13), rotating disks (4, 14), and spherical collectors(15-18) to name a few. The first critical step to achieving that goal was to establish a mathematical framework applicable to describing

particle deposition behavior in the presence of surface roughness in a parallel plate chamber. The Convective-Diffusion Equation was utilized to develop that mathematical framework.

Here, a model predicting particle deposition in a parallel plate chamber was developed to incorporate the impact of surface roughness on particle deposition. Accordingly, an appropriate description of surface roughness geometry was developed and associated impacts on the flow field were described. Relative to commonly utilized approaches for modeling particle deposition that assume smooth surfaces(6, 7, 19), this required modifications to 1) hydrodynamic retardation functions, and boundary conditions for the 2) flow field and 3) convective-diffusion (C-D) equation. DLVO forces in the presence of surface roughness also required appropriate representation(20-23). Chemical heterogeneity and surface hydrophobicity were negligible in the system(60) and were therefore excluded from the model. As well, the shear lift force associated with the employed loading rate of 6.67×10^{-5} m/s was negligibly small compared to DLVO forces and Brownian motion; therefore, it also was also excluded from the model.

5.3 Mathematical modeling

In this section, parallel plate chamber geometry impacted by nano-scale surface roughness is described. The approaches utilized to represent the flow field, hydrodynamic retardation, DLVO forces, flow field boundary conditions, and convective-diffusion equation boundary conditions are also described and integrated to yield a C-D model describing particle deposition on rough surfaces. The model is then validated by comparing the numerical solutions to analytical solution and the experimental results reported in Jin et al. (2014)(61).

5.3.1 Parallel plate chamber geometry and implications to flow fields.

Controlled by the conservation law, the mass transport of a particle in a suspension can be expressed as

$$\frac{\partial c}{\partial t} + \nabla \cdot J = Q \qquad (5\text{-}1)$$

where j is the particle flux vector, Q is the particle reaction rate, c is the particle concentration, and t is reaction time. At steady state ($\P c/\P t = 0$) and in absence of chemical reactions, the general continuity equation can be simplified to

$$\nabla \cdot j = 0 \tag{5-2}$$

Under the influence of convection, diffusion and external forces that can act as extra sources or sinks of momentum, the particle flux in a fixed Cartesian coordinate system (x,y,z) can be defined as

$$j_x = -D_x \frac{\partial c}{\partial x} + uc + \frac{D_x F_x}{k_b T} c \tag{5-3}$$

$$j_y = -D_y \frac{\partial c}{\partial y} + vc + \frac{D_y F_y}{k_b T} c \tag{5-4}$$

$$j_z = -D_z \frac{\partial c}{\partial z} + wc + \frac{D_z F_z}{k_b T} c \tag{5-5}$$

where T is the absolute temperature; k_b is Boltzmann's constant; c is the particle concentration; j_x, j_y and j_z are the particle flux vectors; D_x, D_y and D_z are the respective components of the diffusion tensor; u, v and w are the respective components of the fluid velocity; F_x, F_y and F_z are the respective components of the external forces. In this coordinate system, x is the flow direction (along the length of the chamber), y is the direction of chamber width, and z is the direction of chamber height. To solve the C-D equation so that the concentration of particles in time and space can be determined within the system, the particle velocity, net forces acting on the approaching particle, and the associated boundary conditions need to be determined.

Here, the fluid velocity field in the parallel plate chamber was assumed to be distant from the entrance of the chamber, allowing for a completely developed parabolic velocity profile. When the plate surface is chemically homogenous and smooth, the undisturbed fluid velocity (u, v, w) in the Cartesian coordinate system (u, v, w) can be expressed as

$$u = \frac{3}{2} V_{avg} \frac{z}{b}\left(2 - \frac{z}{b}\right) \quad (5\text{-}6)$$

$$v = 0 \quad (5\text{-}7)$$

$$w = 0 \quad (5\text{-}8)$$

where V_{avg} is the average fluid velocity and b is half of the channel height.

Inclusion of surface roughness effects necessitates changes in the boundary conditions used to calculate fluid flow fields(24). When target surfaces are assumed to be smooth, the no-slip boundary condition is applied to the target surface to determine flow velocity. When target surfaces cover by roughness, accurate flow field representation requires replacement of the non-slip boundary condition with slip or partial-slip boundary conditions(24-26), depending on the height and total coverage of roughness elements. Alternatively, the "effective target surface" can be regarded as a hydrodynamically equivalent smooth plane located between the top and bottom of roughness elements(6). The no-slip boundary condition for the "effective target surface" is still valid, but just moving from the top of roughness element to the bottom. When >50% of a surface is rough, the "effective target surface" can be considered as the plane at the bottom of the roughness elements and the velocity profile can be scaled by roughness size(24, 27)[28]. As a result, the velocity component that is parallel to the direction of flow in the chamber should be higher for rough surfaces as compared to smooth ones(25).

In the presence of surface roughness, the no-slip boundary condition for smooth surfaces should be modified with consideration of roughness size and extent of coverage. Based on the AFM measurements of the modified quartz surfaces employed during the present experiments, surface roughness coverage was >50%. The no-slip boundary condition was accordingly applied at the bottom of the roughness elements. The separation distance between the approaching particle and the surface was modified with dimensionless slip-length r_{slip} and the flow velocity above the roughness elements (u_{slip}) was approximated as

$$u_{slip} = \frac{3}{2} V_{avg} \frac{(z + r_{slip})}{b}\left(2 - \frac{z + r_{slip}}{b}\right) \quad (5\text{-}9)$$

The effect of the slip boundary condition on particle deposition flux was evaluated by simulating particle diffusion-convection with different slip lengths. A 1.0 μm particle size was selected and the associated *Pe* number was 0.1. The gravity, DLVO interaction, and hydrodynamic retardation functions were turned "off" by setting the Gr and DLVO interaction to 0 and the r_{slip}=0. Different values of r_{slip} (0.001, 0.01,0.1 and 1) were used.

In this investigation, the parallel plate chamber was situated in a manner parallel to the ground. The flow field inside of the chamber was wide enough to neglect edge effects in the y-direction. It was also assumed that particle concentration did not change in the y-direction. The fluid velocities in the y- and z-directions were negligible (i.e., $v = 0$ and $w = 0$), so the general equation for particle flux to the surface could be simplified to two dimensions and described by

$$j_x = -D_x \frac{\partial c}{\partial x} + uc + \frac{D_x F_x}{k_b T} c \qquad (5\text{-}10)$$

$$j_z = -D_z \frac{\partial c}{\partial z} + \frac{D_z F_z}{k_b T} c \qquad (5\text{-}11)$$

A schematic representation of the parallel plate chamber system with rough surface features is shown in Figure 5-1. In this system, the fluid velocity field was assumed to be laminar, steady and incompressible; and the suspended colloidal particles passing through the chamber were treated as smooth spherical particles. The roughness features added to the target surface were created using materials identical to those comprising the smooth slide surface; so, they had the same chemical potential, hydrophobicity, and Hamaker constant as the smooth surfaces (61). Particle-particle interactions and blocking effects were demonstrated as negligible in the system(61); as a result, particle deposition was driven by particle-surface interactions, thereby satisfying clean bed theory.

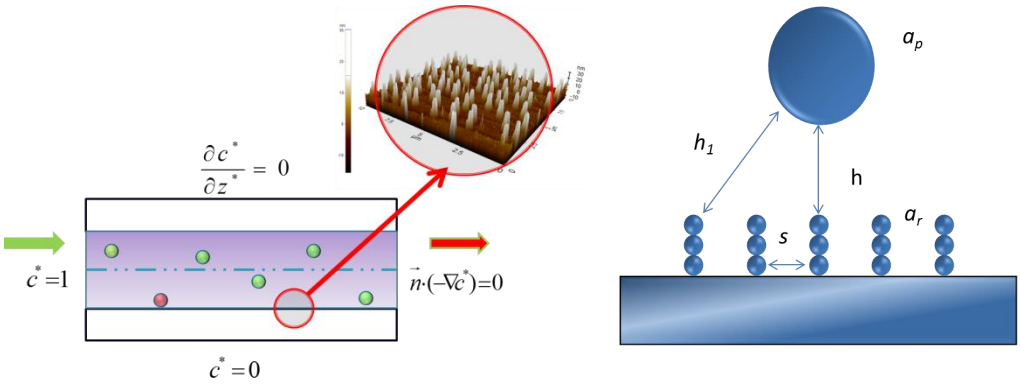

Figure 5-1. a). Parallel plate chamber system schematic and AFM image for rough surface, b) Schematic representation of roughness features on the target surface

5.3.2 DLVO interaction energy under the effect of roughness

Classic DLVO theory has been used to describe the long-range interfacial forces between particles (or particles and surfaces) influenced by electrostatic and van der Waals forces(28). It was originally developed assuming smooth and chemically homogenous surfaces(2, 29). Interaction energies between particles (or particles and surfaces) can be calculated by integrating the net force acting on the particle or surface over distance. They can be used to determine if particles will attach to or detach from target surfaces in aqueous systems.

Surface roughness effectively increases the effective distance between an approaching particle and the contact surface(28). The associated decrease in the repulsive electrostatic double layer (EDL) force is greater than the decrease in attractive van der Waals forces(22). The interaction energy barrier for rough surfaces can be reduced substantially when both particle and collector surfaces are negatively charged(21, 30). The presence of surface roughness requires specialized approaches for calculation of DLVO interaction energies(21, 22, 28, 31, 32).

Two approaches have been used to calculate interactions energies in the presence of surface roughness: surface element integration (SEI)(22, 23) and pairwise summation (PS)(32, 33). When the SEI method is used, the particles and the target surface can have arbitrary surface morphology features(23, 30, 34). Given an analytical expression (or numerical results) for the unit area interaction energy (dU) between two infinite flat plates, the exact interaction

energy between an approaching particle and the surface can be determined by integrating *dU* over the entire surface. The SEI method is robust for quantitatively investigating the impacts of different surface morphologies over short or long separation distances(31). The SEI method can provide good quantification of DLVO forces acting upon surfaces with roughness features; however, the method is computationally demanding.

In the PS method, rough surfaces can be treated as smooth plates covered by spherical asperities with smooth surfaces. Total interaction energy is then calculated as the sum of energies between the particle and the smooth plate and between the particle and the asperities(21, 28). The PS method can provide accurate analytical solutions if the target surface has uniform surface chemical potential and the asperities are spread within certain distances between each other(28, 35). The PS method is also computationally efficient. The PS method was selected for use in the present study because of its prediction accuracy and computational efficiency.

Nano-fabrication was used to create roughness features with simple, uniform geometry as depicted in Figure 5-1. The roughness features on the target surface were measured using AFM(61). The roughness elements were regarded as spheres with a diameter of a_r and were assembled vertically on the plate, which was the bottom surface of the chamber. All roughness elements were evenly distributed on the surface. The surface to surface distance between the roughness elements was *s*.

The total interaction energy between an approaching particle and the bottom surface with the roughness elements was determined by:

$$\begin{aligned} F_{Total}^{\ DLVO} &= F_{Total}^{\ VDW} + F_{Total}^{\ EDL} \\ &= -\nabla U_{Total}^{\ DLVO} \\ &= -\nabla \cdot (U_{Total}^{\ VDW} + U_{Total}^{\ EDL}) \end{aligned} \qquad \textbf{(5-12)}$$

where $F_{Total}^{\ DLVO}$ is the sum of the van der Waals force ($F_{Total}^{\ VDW}$) and the EDL force ($F_{Total}^{\ EDL}$) between the particle and surface; $U_{Total}^{\ DLVO}$ is the total interaction energy, $U_{Total}^{\ VDW}$ and

U_{Total}^{EDL} are the total VDW/EDL interaction energy accounting for all the contributions from roughness elements (21, 36, 37) and the bottom plate.

5.3.3 Electrostatic double layer force

To determine the changes in the interaction energy curves after including the impact of the surface roughness, the measured roughness size and surface chemical potentials were used in the numerical simulation. At the high ionic strength (100 mM KCl) used herein, the inverse Debye length (κ), used for estimating how far electrostatic effects persist, is given by

$$\kappa = \left(\frac{2e^2ci^2}{\varepsilon_0 \varepsilon kT}\right)^{1/2} \tag{5-13}$$

where e is the charge of an electron; i is the ion valence; c is the ion number concentration; ε_0 and ε are the relative permittivity of vacuum and water, respectively; and T is the temperature.

When $\kappa^{-1}a_p > 25$ (a_p is particle size), the total EDL interaction energy between the particle and the rough surface can be well approximated by the PS method(33). Here, the Debye length is small (ranging from 1 to 3 nm) relative to particle size because of the high ionic strength of the electrolyte in which the particles were suspended. Thus, the net EDL interaction energy was approximated as

$$U_{Total}^{EDL} = U_{PS}^{EDL} + \sum_{i=1}^{n} U_{PR}^{EDL} \tag{5-14}$$

where U_{PS}^{EDL} represents the EDL interaction energy between the particle and the plate surface and U_{PR}^{EDL} represents the EDL interaction energy between the particle and a given roughness element (i) on the surface.

When the chemical potential between the particle and surface is constant and does not exceed -25mV, the linearized Poisson-Boltzmann equation can be used in the electrostatic force calculation. The classic Hogg-Healy-Fuerstenau (HHF) expression(29) describes the

potential energy of interaction between dissimilar spherical colloidal particles, using the linear (Debye-Hückel) approximation for low surface potentials; it was utilized here to describe the EDL interaction between the approaching particle and the spherical component of the roughness asperities as

$$U_{ij}^{EDL} = \frac{\pi\varepsilon\varepsilon_0 a_i a_j}{(a_i + a_j)}[2\psi_i\psi_j \ln(\frac{1+\exp(-\kappa H)}{1-\exp(-\kappa H)}) + (\psi_i^2 + \psi_j^2)\ln(1-\exp(-2\kappa H))] \quad (5\text{-}15)$$

where U_{ij}^{EDL} is the EDL interaction between two spheres *i* and *j*; ψ_1 and ψ_i are the respective chemical potentials and *H* is the dimensionless surface-to-surface distance. U_{PS}^{EDL} is calculated by assuming the bottom surface is spherical with diameter much greater than the particle size, so

$$U_{PS}^{EDL} = \pi\varepsilon\varepsilon_0 a_p[2\psi_P\psi_S \ln(\frac{1+\exp(-\kappa H)}{1-\exp(-\kappa H)}) + (\psi_P^2 + \psi_S^2)\ln(1-\exp(-2\kappa H))] \quad (5\text{-}16)$$

5.3.4 van der Waals force

According to the PS method, the attractive van der Waals force is the sum of VDW interaction energies between the particle and all of the surface roughness elements; it is formulated as

$$U_{Total}^{VDW} = U_{PS}^{VDW} + \sum_{i=1}^{n} U_{PR}^{VDW} \quad (5\text{-}17)$$

where U_{PS}^{VDW} is the VDW interaction energy between the particle and the bottom surface and U_{PR}^{VDW} is the VDW interaction energy between the particle and a roughness element on the surface(28, 32).

Assuming there is no chemical heterogeneity on the surface and the Hamaker constant between the particle and plate surfaces is not changing, the individual un-retarded VDW interaction energy between two spheres (an approaching particle and a roughness element) can be expressed as

$$U_{ij}^{VDW} = -\frac{A_{ij}}{6}\left[\frac{2a_i a_j}{R_{ij}^2-(a_i+a_j)^2} + \frac{2a_i a_j}{R_{ij}^2-(a_i+a_j)^2+4a_i a_j} + \ln\left(\frac{R_{ij}^2-(a_i+a_j)^2}{R_{ij}^2-(a_i+a_j)^2+4a_i a_j}\right)\right] \quad (5\text{-}18)$$

where R_{ij} is the center-to-center distance between the two spheres, and A_{ij} is the Hamaker constant between the i^{th} and j^{th} spherical objects.

The approach for calculating sphere–plate interaction energy is valid for small separation distances and was described by Gregory (1981)(38) as

$$U_{SP}^{VDW} = -\frac{Aa_P}{6h}\left(\frac{1}{1+14h/\lambda}\right) \quad (5\text{-}19)$$

Where λ is the characteristic wavelength of electron oscillation. In the system used herein, the external forces exerted on the approaching particle included gravity and buoyancy (F_G), the corresponding shear lift force (F_{SL}), the electrostatic double layer force (F_{EDL}) and the van der Waals force (F_{VDW}). They must be defined to solve the general continuity equation (Equation 5-2). As described earlier, F_{SL} is negligible in the present investigation. F_{VDW} and F_{EDL} were described above. F_G is described below.

5.3.5 Gravity

The net effect of gravitational and buoyancy forces on the suspended particles is defined as

$$\vec{F}_G = \frac{4}{3}\pi a_p^3(\rho_p - \rho_w)\vec{g} \quad \textbf{(5-20)}$$

where a_p was the particle diameter, ρ_p and ρ_w are the densities of the colloidal particle and the fluid, respectively, and g is gravitational acceleration(6).

5.3.6 Hydrodynamic retardation functions

Surface roughness reduces hydrodynamic retardation(27, 39) -models of particle deposition on rough surfaces must reasonably account for this impact. To do so, hydrodynamic retardation functions for smooth surfaces should be first considered and then modified. In the

vicinity of a surface, the velocity field of an approaching particle is altered due to the hydrodynamic disturbances caused by the surface; in this case, the bounding walls of the parallel plate chamber. The dimensionless hydrodynamic retardation functions $f_1(H)$, $f_2(H)$ and $f_3(H)$ and are used in describing particle velocity (u) from the fluid motion as

$$u_x = f_3(H)u \tag{5-21}$$

$$u_z = f_1(H)\, f_2(H)v \tag{5-22}$$

where H is the dimensionless surface-to-surface distance(40-43).

In addition to approaching particle velocity, hydrodynamic retardation functions also affect the forces that act upon a particle approaching a surface; these are particularly important to consider at short and long separation distances that are relevant to particle attachment and detachment respectively. The hydrodynamic retardation functions $f_1(H)$ and $f_4(H)$ also affect the diffusion tensors (D) between the approaching particle and the surface and are described as

$$D_x = f_4(H)D_\infty \tag{5-23}$$

$$D_z = f_1(H)D_\infty \tag{5-24}$$

where D_∞ is the Stoke-Einstein diffusion coefficient(6, 44).

Table 5-1. Analytical solutions for the hydrodynamic retardation functions when the dimensionless distance (*H*) approaches 0 or ∞

Hydrodynamic retardation functions	*When H approaches 0*	*When H approaches ∞*
$f_1(H)$	$H\left(1+\frac{1}{5}H\ln\left(\frac{1}{H}\right)+0.971264H\right)^{-1}$	$\left(1+\frac{9}{8(H+1)}\right)^{-1}$
$f_2(H)$	3.2295	$\left(1-\frac{9}{8(H+1)}\right)^{-1}$
$f_3(H)$	$\left(0.66-0.2693\ln(H)\right)^{-1}$	$1-\frac{5}{16(H+1)^3}$
$f_4(H)$	$-\left(0.5\ln(H)-1\right)^{-1}$	$1-\frac{9}{16(H+1)}$

Calculation of the analytical solution for the hydrodynamic retardation functions over the entire simulation domain is computationally intensive for numerical simulation(17, 45). Approximations for the analytical solutions for hydrodynamic retardation functions ($f_{1\text{-}4}$) were required for the investigation described herein. They have been approximated for particle attachment and detachment scenarios that are associated with dimensionless distance approaching 0 or ∞ (Table 5-1); approximations for the entire simulation domain have also been suggested(40-42, 46, 47). None of the existing simplified hydrodynamic retardation functions is able to precisely match the analytical solution over the entire simulation domain, especially at the asymptotic limits (0 and ∞). To overcome this issue, two methods have been utilized to simplify the computation: 1) approximation of the hydrodynamic retardation function values(13, 48) using fitted parameters and 2) separation of the domain into several subdomains and subsequent numerical approximation for each domain(45).

In the present study, hydrodynamic retardation functions (f_i) were calculated as a blend of asymptotic solutions described by

$$f_i = \left[\frac{\left(f_{i0}f_{i\infty}\right)^n}{{f_{i0}}^n + {f_{i\infty}}^n}\right]^{1/n} \qquad (5\text{-}25)$$

where n is a fitting parameter, f_{i0} are the analytical solutions for f_{1-4} when the dimensionless distance is approaching 0 and $f_{i\infty}$ are the analytical solution for f_{1-4} when the dimensionless distance is approaching infinity. The determined values of n for f_{1-4} in Equation 5-25 are 5, 20, 15 and 10 respectively. These new approximations for f_i were used over the entire simulation domain. Here, f_{1-4} (Equation 5-25) are reduced to the analytical solution when H approaches both asymptotic limits. The new approximated solutions for f_i obtained using Equation 5-25 were compared to a numerical solution for particle deposition on ideal collectors from dilute flowing suspensions from Elimelech's work (1994)(13) and other solutions previously reported in the liaterature(17, 45, 48, 49) (Figures 5-2(a), (b), (c) and (d)). The new approximated hydrodynamic retardation functions best fit the exact numerical solution with no more than 2% relative difference over the entire simulation domain. The maximum relative differences between the other reported solutions and the numerical solution over the entire simulation domain were 37.5% for Masliyah and Bjattacharjee (2006)(48), 6.8% for Elimelech(1994)(50), and 299.3% for Johnson and Tong(2006)(51). The advantages of the simplified hydrodynamic functions used in this study are that they 1) are reduced to the analytical solution at the asymptotic limits; 2) match the analytical solution with greatest accuracy relative to other reported approximations; 3) are appropriate for use with rough surfaces; and 4) are simple and computationally efficient relative to other reported approximations.

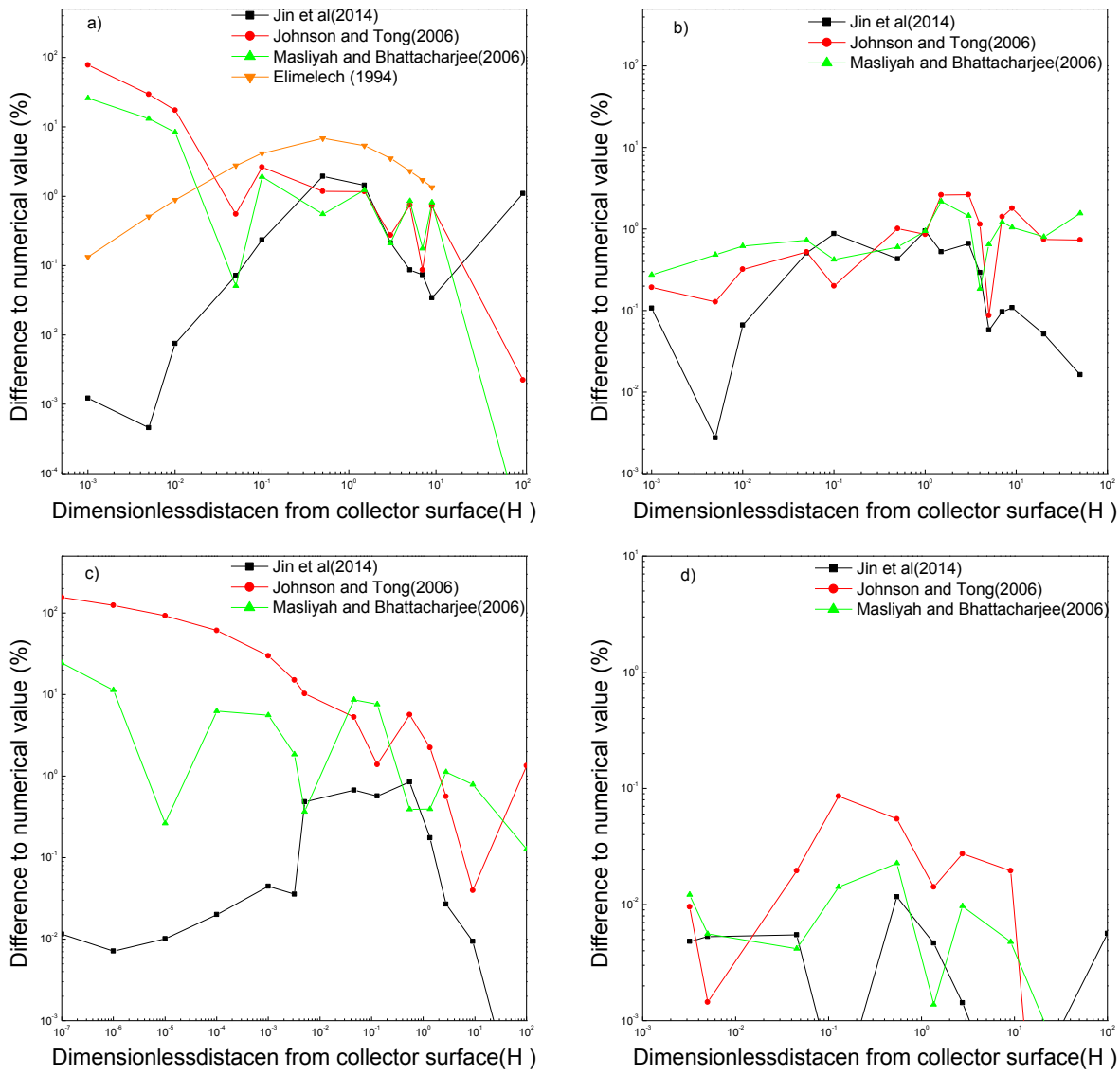

Figure 5-2. Comparison of the new developed and reported hydrodynamic retardation functions $f_1(H)$, $f_2(H)$, $f_3(H)$ and $f_4(H)$ to the numerical solution reported by Elimelech (1994)(50)

It should be recalled that all f_i were originally developed based on assumptions that an approaching particle and target surface are smooth with uniform and homogeneous chemical properties. To be relevant to the present investigations, the f_i required modification to account for the presence of surface roughness, with scaling based on absolute surface roughness size and coverage extent(27, 39). The modifications presented here are valid when surface

roughness is smaller than approaching particle diameter(52), as in this study. Notably, they are applicable to numerous manufacturing, health, and environmental scenarios in which inert particles or microbial particles including pathogenic viruses, bacteria, and protozoa may be depositing on relatively smooth surfaces such as sand grains with nano-scale.

When >50% of a surface is rough, it can be regarded as hydrodynamically equivalent to a smooth surface (no-slip wall) located at the bottom of the roughness features. The hydrodynamic retardation function that now accounts for surface roughness can be described by

$$f_i(H) = f_{i-new}(H') = f_{i-new}(H + r_{slip}) \tag{5-26}$$

$$r_{slip} = r_{roughness} / a_p \tag{5-27}$$

where H is the dimensionless distance and $r_{roughness}$ is the absolute height of roughness elements, a_p is particle radius, r_{slip} is the dimensionless slip length due to the presence of roughness, $f_i(H)$ are the original hydrodynamic retardation functions and f_{i-new} are the modified hydrodynamic retardation functions accounting for the presence of surface roughness. Maximum hydrodynamic retardation should occur at $H = 0$ for a smooth surface and at $H = r_{slip}$ for a rough surface (as shown in Figure 5-3); of course, these functions should also be the same as those for smooth surfaces when $r_{roughness} = 0$.

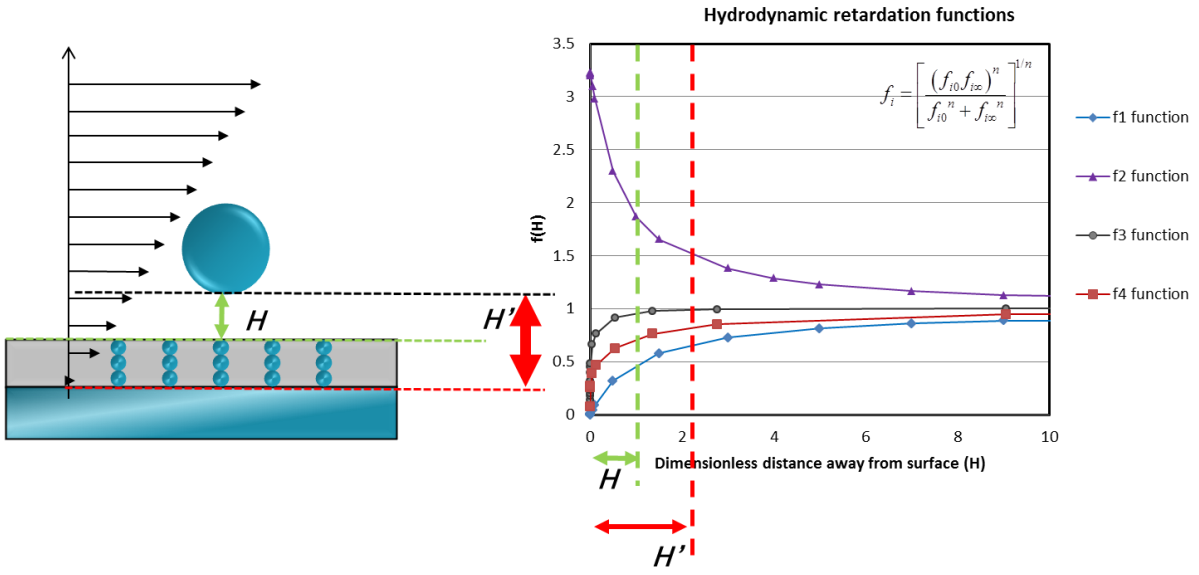

Figure 5-3. Impacts of nano-scale roughness on hydrodynamic retardation functions on the left; and the corresponding values of hydrodynamic retardation functions due to the original(Smooth surface) and modified 'effective target surface'(Rough surface) on the right

5.3.7 Particle transport equations and boundary conditions

The non-dimensional form of the particle transport (i.e., convection-diffusion) equation in a Cartesian coordinate system is

$$\nabla \cdot j = \frac{\partial j_x}{\partial x} + \frac{\partial j_z}{\partial z} = 0 \tag{5-28}$$

where

$$j_x = -D_\infty f_4(h)\frac{\partial c}{\partial x} + \frac{3}{2}V_{avg}\frac{z}{b}\left(2 - \frac{z}{b}\right)f_3(h)c + f_4(h)\frac{D_\infty F_x}{k_b T}c \tag{5-29}$$

$$j_z = -D_\infty f_1(h)\frac{\partial c}{\partial z} + f_1(h)\frac{D_\infty F_z}{k_b T}c \tag{5-30}$$

Numerical methods are frequently used to solve Equations 5-28 to 5-30 because of the number of variables involved. To simplify these equations and to reduce computation, pertinent dimensionless parameters are provided in Table 5-2.

Table 5-2. Dimensionless parameters and constants used in the scaled convection-diffusion equation

Dimensionless parameter	*Expression*
Scaled surface to surface distance	$H = z^* - 1$
Scaled particle radius	$a_p^* = \frac{a_p}{b}$
Scaled distance along the flow direction	$x^* = \frac{x}{b}$
Scaled vertical distance	$z^* = \frac{z}{a_p}$
Scaled concentration	$c^* = \frac{c}{c_\infty}$
Dimensionless Peclet number	$Pe = \frac{3}{2}\frac{V_{avg} a_p^3}{b^2 D_\infty}$
Diffusion coefficient	$D_\infty = \frac{k_b T}{6\pi\mu a_p}$
Scaled gravitational force	$Gr = \frac{\vec{F}_g * a_p}{k_b T}$
Scaled DLVO force	$DLVO = -\frac{d\Psi}{dy} * \frac{a_p}{k_b T}$

After the parameters are converted to the dimensionless forms, the particle transport equation and the corresponding boundary conditions are expressed as (All the variables are expressed in Table 5-2)

$$\frac{\partial}{\partial x^*}\left[f_4(h) a^{*2} \frac{\partial c^*}{\partial x^*} + Pe(h+1)\left(2 - (h+1)a^*\right) f_3(h) c^* + f_4(H) F_x^* a^* c^* \right] + \frac{\partial}{\partial h}\left[f_1(h) \frac{\partial c^*}{\partial z^*} + f_1(h) F_z^* c^* \right] = 0 \qquad (5\text{-}31)$$

$$c^* = 1 \qquad \partial\Omega \in Boundary1 \qquad (5\text{-}32)$$

$$c^* = 0 \qquad \partial\Omega \in Boundary2 \qquad (5\text{-}33)$$

$$\frac{\partial c^*}{\partial z^*} = 0 \qquad \partial\Omega \in Boundary3 \qquad (5\text{-}34)$$

$$\vec{n} \cdot (-\nabla c^*) = 0 \qquad \partial\Omega \in Boundary4 \qquad (5\text{-}35)$$

As shown in Figure 5-4, the inlet (Boundary 1) of the simulation domain was regarded as the bulk concentration. Convective flux was used for the outlet (Boundary 4) of the simulation domain. The upper surface (Boundary 3) was treated as the insulating boundary, with no particle attachment. In the present study, high ionic strength and associated DLVO forces resulted in net attraction between the approaching particles and the bottom surface (Boundary 2), which was treated as a perfect sink.

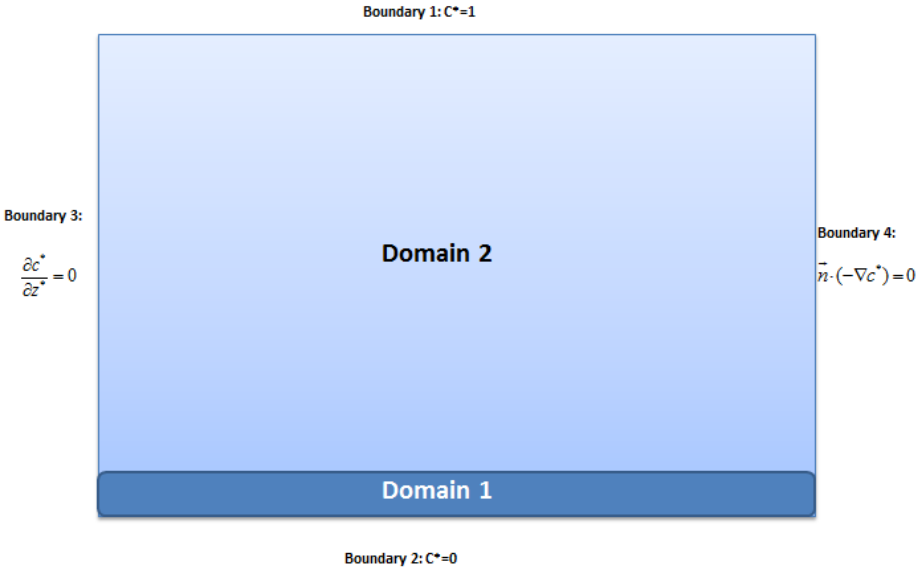

Figure 5-4. Schematic of simulation domain and boundary conditions in the parallel plate chamber

Two approaches for the perfect sink boundary condition on the bottom surface (Boundary 2) were utilized. The first approach involved setting the particle concentration to zero when the dimensionless vertical distance was zero ($c^* = 0$ when $h = 0$) (13, 53). The dimensionless flux of particles (Sherwood number, *Sh*) to the bottom surface was calculated at the primary interaction energy minimum, which is usually defined at a cut-off dimensionless distance by (δ), avoiding numerical singularity. It is described by

$$Sh\left(x^*\right)=\frac{j_z a_p}{D_\infty c_\infty}=f_1\left(h\right)\left(\frac{\partial c^*}{\partial z^*}-F_z^* c^*\right)_{h=\delta} \qquad \text{at } h=\delta \qquad (5\text{-}36)$$

where j_z is the dimensionless deposition flux on z direction, c_∞ is the bulk concentration, F_z^* is the scaled force in the z direction. Here, Equation 5-36 accounted for the effect of all external forces including the VDW force, the EDL force and gravity acting upon the approaching particle.

The second approach utilized for the perfect sink boundary condition was to presume that the particle concentration was zero at the primary interaction energy minimum ($c^* = 0$ when $h = \delta$)(6). The dimensionless flux of particles (*Sh*) to the bottom surface was then calculated by

$$Sh\left(x^*\right)=\frac{j_z a_p}{D_\infty c_\infty}=f_1\left(h\right)\left(\frac{\partial c^*}{\partial z^*}\right)_{h=\delta} \qquad \text{at } h=\delta \qquad (5\text{-}37)$$

The overall flux of particles to the surface in the *x* direction (flow direction) over distance x^* was calculated as the average Sherwood number ($\overline{Sh}$) described by

$$\overline{Sh}=\frac{1}{L^*}\int_0^{L^*} Sh\left(x^*\right)dx^* \qquad \text{at } h=\delta \qquad (5\text{-}38)$$

5.3.8 Numerical methodology

The numerical solution of the Convective-Diffusion Equation with four boundary conditions was solved using the finite element method (FEM) in the commercial simulator COMSOL® 3.5a (COMSOL, Inc., Canada). Exponentially distributed quadrilateral meshes were utilized to discretize the computational domain. Highly refined meshes were used for regions with a high concentration gradient or a large tensor of applied forces. The interfacial interactions caused by DLVO forces and the hydrodynamic retardation functions changed substantially near the bottom surface; therefore, a sub-region (Domain 1) close to the bottom surface was defined with a large number of mesh elements (250 x 600). The total number of the mesh elements employed in the simulations was 330,000; 150,000 of which were exponentially mapped within Domain 1. The size of the smallest mesh in Domain 1 was 10^{-5} in

dimensionless height, a value three orders of magnitude smaller than the Debye length at the ionic strength used this study. This enabled accurate determination of any flux change due to the high concentration gradient or large force tensor in the vicinity of the bottom surface. Dirichlet boundary conditions were applied to Domains 1 and 2. On Boundary 1, the Heaviside step function was applied to avoid numerical error associated with infinity in the left corner (0, 0) of Domain 1. To implement the second setting for the perfect sink boundary condition (Equation 37), the initial point of simulation domain in COMSOL® was moved from (0,0) to the location of the primary interaction energy at (δ,0).

5.3.9 Analytical solution

To validate the numerical solution obtained by simulation, solutions developed herein were compared to analytical solutions. The analytical solution for dimensionless local mass transfer can be expressed as

$$Sh = \frac{1}{\Gamma(4/3)}\left(\frac{2Pe}{9x^*}\right)^{1/3} \qquad (5\text{-}39)$$

where $Pe = \frac{3V_m a_p^3}{2b^2 D_\infty}$ is the dimensionless Peclet number, a is the particle radius, b is the half channel height, D_∞ is the diffusion coefficient, v is the flow rate, $x^* = x/b$, x is the distance to the inlet in the parallel plate chamber(6). To implement the proper settings in COMSOL® to obtain the analytical solution, all of the external forces applied on the particle other than Brownian motion were "turned off " (set to 0) and f_{1-4} were set to 1.0. The simulation domain was set to the dimensions of the parallel plate chamber: 4cm x 1cm x 125μm (length x width x height)(61). Five sizes of particles (diameter) of 0.125, 0.25, 0.5, 0.915 and 1.765μm) were injected to the parallel plate chamber at a flow rate of 10 μl/min during the simulation, yielding a loading rate of 6.67×10^{-5} m/s. Mass balance in the simulation domain was checked for each experiment by integrating flux over the entire domain.

Deposition of representative particles on the bottom surface (*Sh*) was plotted over dimensionless distance $\bar{x}$ (Figure 5-5) in which the filled symbols represent the analytical

solution and the open symbols are the numerical solutions. The inserted figure shows the dependence of average $\overline{Sh}$ number on *Pe*, where the circles represent numerical solutions and the solid triangles represent calculated analytical solutions. Mass recoveries within the simulation domain were close to 100%, suggesting no mass loss due to meshing or the applied boundary conditions. The numerical solutions obtained using the model developed herein were in excellent agreement with the analytical solutions for all conditions investigated (Figure 5-5).

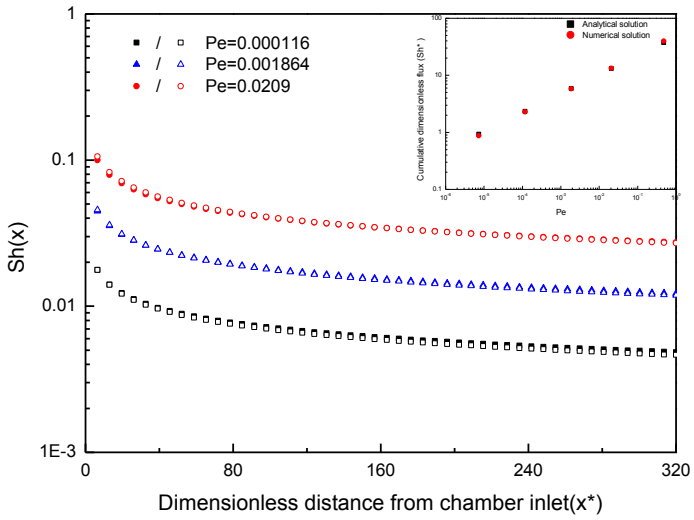

Figure 5-5. Comparison of developed numerical solution with analytical solution(6)

5.4 Results and Discussion

5.4.1 Impacts of roughness on DLVO interaction energies

The functions used to calculate DLVO interaction energy in this study were first validated by comparing simulation results when the roughness was set to zero to published data(54). The calculated DLVO interaction energy as a function of separation distance was plotted (Appendix D). The calculated data in the present study and the reported data had excellent agreement, validating the numerical methods and applied formulae for DLVO interaction energy that were used herein.

To simulate DLVO interaction energy in the presence of surface roughness, the surface was characterized by the roughness features of roughness elements radius (a_r) and distance between each individual roughness elements (s). The roughness parameter values and chemical potentials between the particles and surface are listed in Table 5-3. The DLVO interaction energies at the primary energy minimum (δ = 1 nm) are depicted for different particle and roughness sizes in Figure 5-6. The data in this figure demonstrate that with increasing roughness, the absolute value of DLVO interaction energy decreased, reached a minimum and then increased. This is because as roughness increased, the impact of the bottom surface on the particle decreased and the impact of the roughness elements on the particle increased. These results are consistent with those of Henry et al. (2011) for negatively charged particles and surfaces(21) and Jin and Emelko (2014) who conducted column tests and suggested non-linearity of surface roughness impacts on particle deposition(60). Here, a "critical roughness size" was associated with the minimial interaction energies. Although the critical roughness size was different for particles of different sizes, it was still observed for all particle sizes (Figure 5-6).

Table 5-3. physical and chemical characteristics of slide surfaces with different roughness size

Target roughness (nm)	a_r (nm)	s (nm)	R_a (nm) Mean ±Std.Dev.	R_q (nm) Mean ±Std.Dev.	*Chemical potential* (mV) Mean ±Std.Dev.
10	1.5	50	4.2 ±0.5	5.6 ±0.56	-18.3 ±3.5
20	3.5	800	1.9 ±0.2	2.8 ±0.3	-21.5 ±6.7
50	9	800	10.6 ±1.8	14.6 ±1.8	-16.2 ±5.1
100	16	400	30.3 ±2.9	35.9 ±3.3	-14.9 ±5.8
200	30	800	53.5 ±7.6	65 ±6.4	-13.6 ±7.4
400	50	2000	60.7 ±9.1	81.4 ±7.8	-15.3 ±5.2

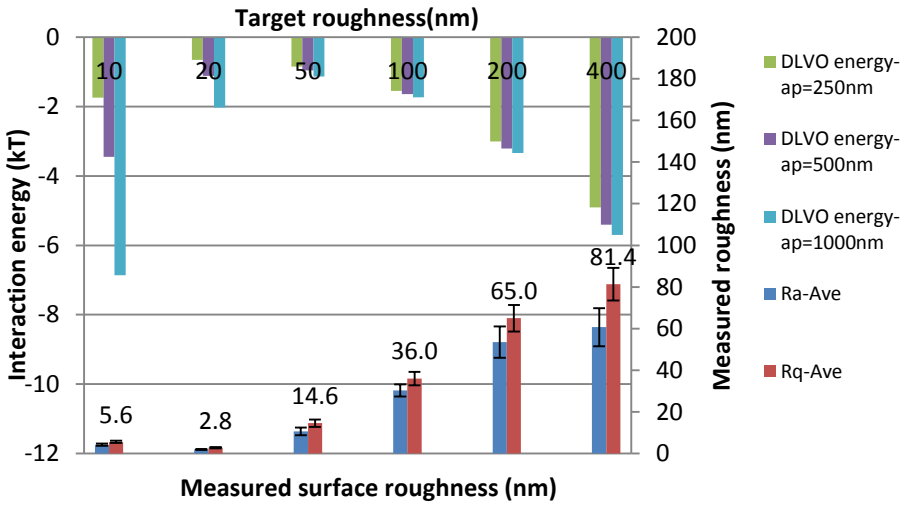

Figure 5-6. Measured surface roughness R_a and R_q and corresponding DLVO interaction energy for three particle sizes (0.55, 0.985 and 1.765 µm)

All of the calcualted interaction energies were negative and without the presence of energy barriers. The net DLVO force on the particle, the derivative of the interaction energy over the distance(13), was positive in all cases during the present investigation, indicating net attraction between the approaching particle and the target surface. According to classic DLVO theory, greater attractive forces lead to higher particle deposition flux(5), which is what was observed experimentally(61).

5.4.2 Impact of roughness on flow field profile

In Figure 5-7(a), particle deposition (*Sh*) for different slip lengths (r_{slip}) (calculated with the corresponding analytical solutions) was plotted over the dimensionless distance in the direction of flow. Although introducing the slip length increased the flow velocity on the top of the roughness elements, deposition flux was not changed substantially. As a result, significant differences in deposition were not observed between the different slip lengths utilized herein (Figure 5-7(a)).

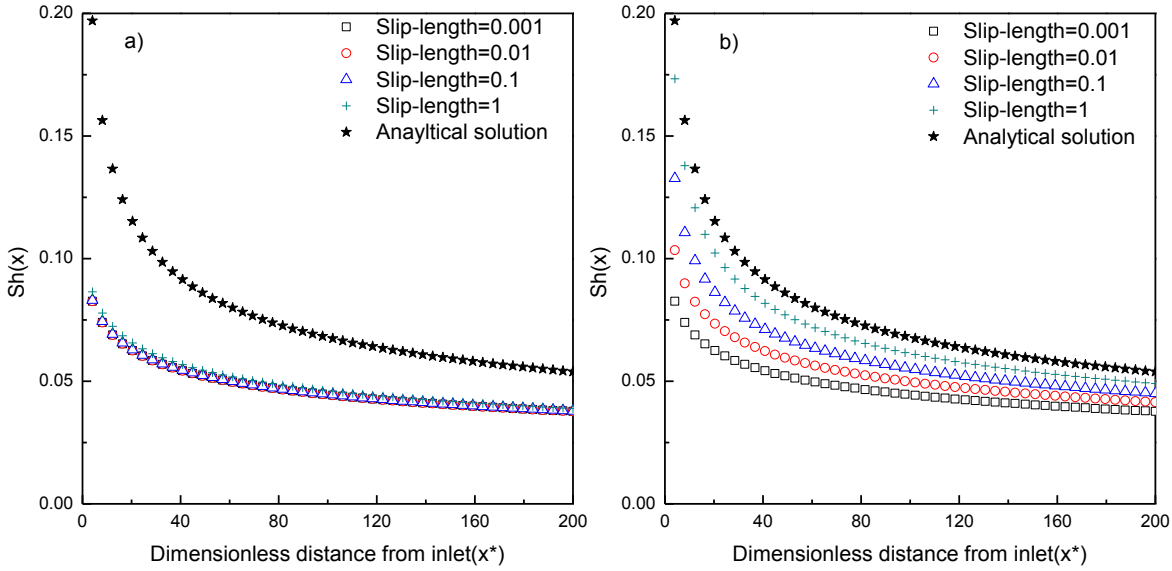

Figure 5-7. a) Particle deposition fluxes for different flow fields associated with different slip-lengths (particle size 1.0 µm, Pe=0.1, Gr=0; b) Particle deposition flux calculated using the analytical solution and numerical simulations with different slip-lengths associated with changes in hydrodynamic retardation functions (particle size 1.0 µm, Pe=0.1, and Gr=0.

5.4.3 Effect of roughness on hydrodynamic retardation functions

To account for surface roughness impacts on the hydrodynamic retardation functions, a hydrodynamically equivalent plane on the bottom of the roughness elements was used as the effective target surface. For a selected particle size of 1.0 µm, the calculated Peclet number was 0.1. Dimensionless slip lengths were set at 0.001, 0.01, 0.1 and 1. The effect of the hydrodynamic retardation functions was evaluated with exclusion of DLVO interaction and gravity by setting the Hamaker constant, chemical potential and gravity effect on the particles

to zero. Flow streamlines were not affected because the employed roughness sizes were smaller than the particle radius. Particle deposition (*Sh*) was calculated for different slip lengths and plotted against the dimensionless distance in the direction of flow (Figure 5-7(b)); consistent with the analytical solution, these simulations demonstrated exponential decay in particle deposition (*Sh*) with the increasing dimensionless distance (x^*). The smaller dimensionless slip length (r_{slip}) associated with very small roughness size (<1nm) led to the lowest particle deposition flux on the bottom surface because of a substantial retardation effect. Larger slip-lengths (larger roughness sizes) caused less hydrodynamic retardation and resulted in more particle deposition flux on the bottom surface. The highest level of particle deposition flux (*Sh*) observed from the investigated numerical simulations was observed when r_{slip} was equal to 1. This particle deposition profile was also very similar to that obtained with the analytical solution, thereby indicting that the hydrodynamic retardation effect became insignificant when the approaching particle was at a distance further than one particle radius from the contact surface.

Here, particle deposition flux was more sensitive to the smaller (0.001μm) roughness features as compared to larger ones (1μm). When the slip length increased from 0.001 (essentially smooth surface) to 0.01 and then 0.1 (rough surface), particle deposition flux (*Sh*) increased by 11.2% and 23.8% respectively (at a corresponding x^* of 100). In contrast, particle deposition flux only increased by 15% when the slip length increased from 0.1 to 1.0, which demonstrates that it was less sensitive to changes in slip length (r_{slip}) at values above 0.1. Based on the observations above, it can be concluded that when the roughness size was smaller than particle radius, increased roughness size led to more particle flux to the bottom surface, though the relative increase in particle deposition is non-linear, non-monotonic with respect to roughness size.

5.4.4 Effect of gravity on particle deposition

The gravity effect is related to particle size and the difference in density between a particle and the solution in which it is suspended. The effect of gravity was included in the Convection-Diffusion equation. It was represented by the dimensionless number *Gr*. In

studies of deposition phenomena, colloidal particles with densities close to that of water are commonly selected(55-58). The influence of gravity on these particles is often considered to be small, particularly for particles smaller than 1.0 μm; accordingly, to simplify model simulation, the gravity effect is sometimes ignored. Gravity was found to substantially impact particle deposition in the present investigation(44); however, and ignoring it would lead to erroneous outcomes.

The density of the colloidal particles used in the associated experiments was 1.045 ± 0.005g/mL. To evaluate the effect of gravity on particle deposition and to better match the experimental data with the developed numerical solutions, three values of particle density (1.04, 1.045 and 1.05 g/ml) were utilized in calculating *Gr*. The effect of the associated different *Gr* values was demonstrated by the simulations using particles of 0.55 and 1.765 μm that were expected to be the particle sizes the least and most impacted by gravity during our associated experimental investigation(61).

Figure 5-8 (a) and 8 (b) show the effect of different *Gr* on the deposition flux of particles with radius of 0.55 and 1.765 μm, respectively. The deposition fluxes of the particles with a diameter of 0.55 μm were similar when different density values were used (Figure 5-8 (a)). In contrast, and as was expected, the deposition fluxes of 1.765 μm particles increased with increased particle density (Figure 5-8 (b)).

The 0.55 and 1.765 μm particle concentration distributions in the vertical (*y*) direction above the representative point of x^*=100 (along the centerline of the domain) were plotted in Figures 5-8(c) and (d), respectively. In the Figure 5-8(c), the dimensionless 0.55μm particle concentration decreased from 1.0 in the bulk solution to 0 on the bottom surface along the centerline, without any particle accumulation resulting in concentrations greater than the bulk concentration. The deposition of 0.55μm particles was dominated by diffusion, so relatively small changes in density did not impact the deposition flux significantly.

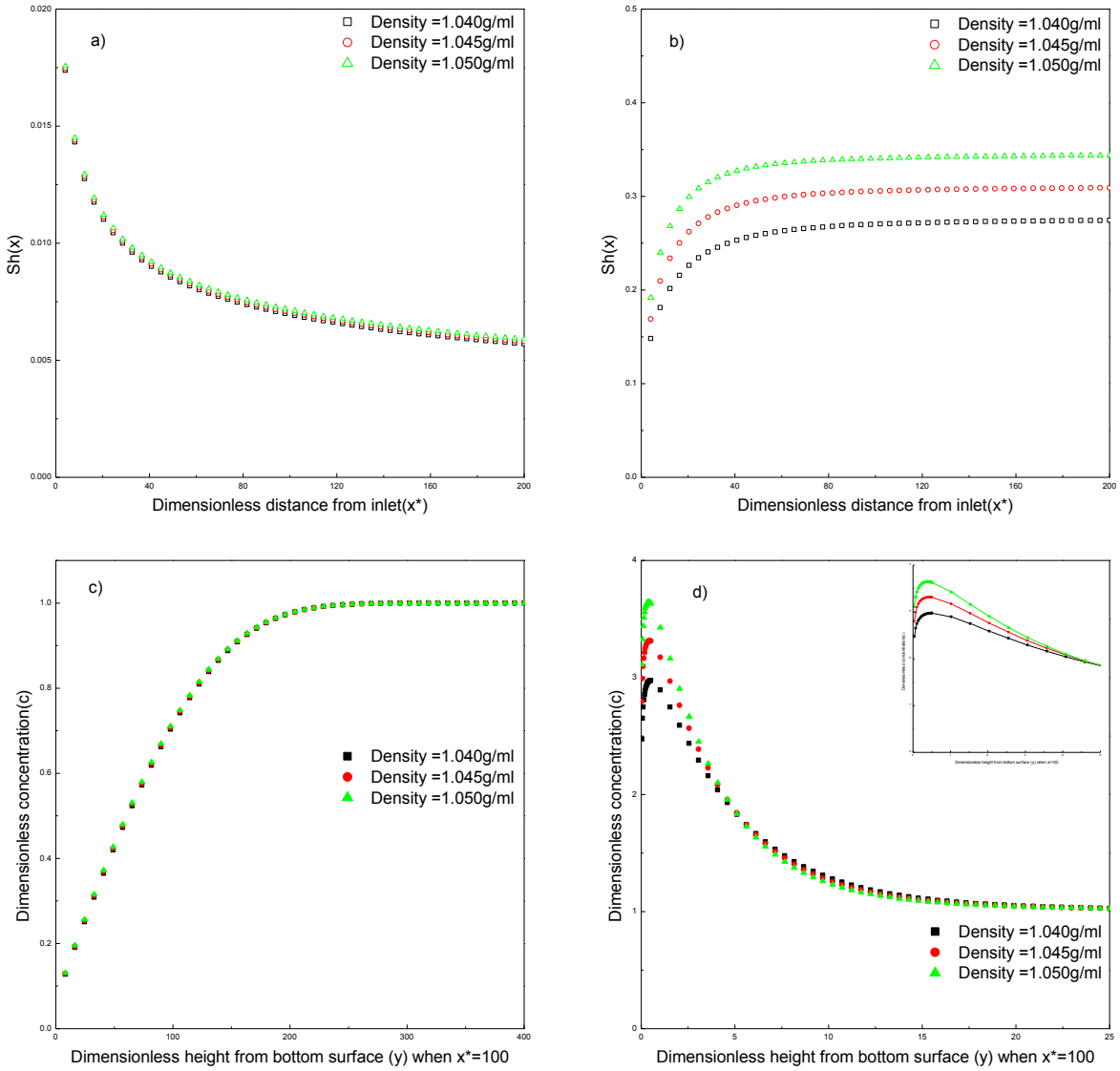

Figure 5-8. Deposition flux of particles with different density (0.04, 0.045 and 0.05 g/ml) along dimensionless distance in the chamber a) for 0.55 μm particles; and b) 1.765 μm particles. Dimensionless particle distribution along the vertical distance from the bottom surface in the center line of the parallel plate chamber, x=100 in the simulation domain c) for 0.55 μm particles; and d) for 1.765 μm particles.

In contrast, the different densities significantly influenced the deposition flux of the larger (1.765μm) particles. Specifically, the flux increased by 13.04 % and 25.97% when the density was increased from 1.040 to 1.045 and to 1.050 g/mL, respectively. Along the

centerline, the dimensionless particle concentration increased from 1.0 to ~3.6 and then decreased to 0 on the bottom surface. Colloidal particles accumulated above the bottom surface due to gravity. As would be expected, larger values of *Gr* resulted in more particle accumulation during the simulations. Between the particle accumulation zone and the bottom surface, dynamic equilibrium was achieved between diffusion and gravity.

As expected, the effect of gravity on particle deposition increased with increasing particle size, with minimal impact on the particles whose transport is dominated by diffusion (e.g., 0.55μm). Gravity had more effect on the larger particles and deposition flux was sensitive to small differences in particle density (e.g., 0.005 g/ml). These analyses underscore that gravity effects should not necessarily be ignored when modeling particle deposition and therefore, precisely measured particle size and density data can be critical to ensuring that numerical simulations such as the one developed herein can adequately describe experimental observations.

5.4.5 Perfect sink boundary condition

Here, a perfect sink boundary condition was applied to the bottom surface. Therefore, it was assumed that particles migrate to the primary energy minimum where they particle were regarded as attached to the target surface and simultaneously removed from the simulation domain(13). Identifying the primary energy minimum location/distance is important for the particle flux calculation when using the Convective-Diffusion Equation(5, 19) It determines where the perfect sink boundary conditions should be implemented(6). A distance of 1 nm above the target surface has been commonly selected as the primary energy minimum distance(13, 59); however, the location of the primary energy minimum can be extended to 100nm or more depending on the chemical potential of both the target surface and colloids, surface morphology, hydrodynamic conditions, *etc*(5). The area between the primary energy minimum distance and the surface (i.e., the area under the impact of short range forces) was not investigated herein.

Two methods to implement the perfect sink boundary condition were introduced in the numerical methodology section. The two methods were examined in this study to find an

optimal approach for implementing the perfect sink boundary condition. Particles with radius of 1.0 μm were evaluated. As well, the target surface was assumed to be smooth without any roughness features. The corresponding *Pe* number was 0.1 and the *Gr* was set as 0. Different locations of the primary interaction energy minimum were examined, including fixed distances of 0.1,1, 10, 100 and 1000 nm from the target surface. To ensure reasonable simulation accuracy, extensive meshing was applied.

The simulated dimensionless flux along the flow direction using different δ is shown in Figure 5-9. Figure 5-9 (a) presents the simulated particle flux obtained using Equation 5-37 whereas Figure 5-9 (b) presents the simulated flux using Equation 5-36. When the perfect sink condition was set by Equation 5-37, the simulations indicated increased particle deposition flux with increases in δ. In contrast, the simulated flux rarely changed when δ was increased from 0.1 to 1000 nm when Equation 5-36 was used to set the boundary condition.

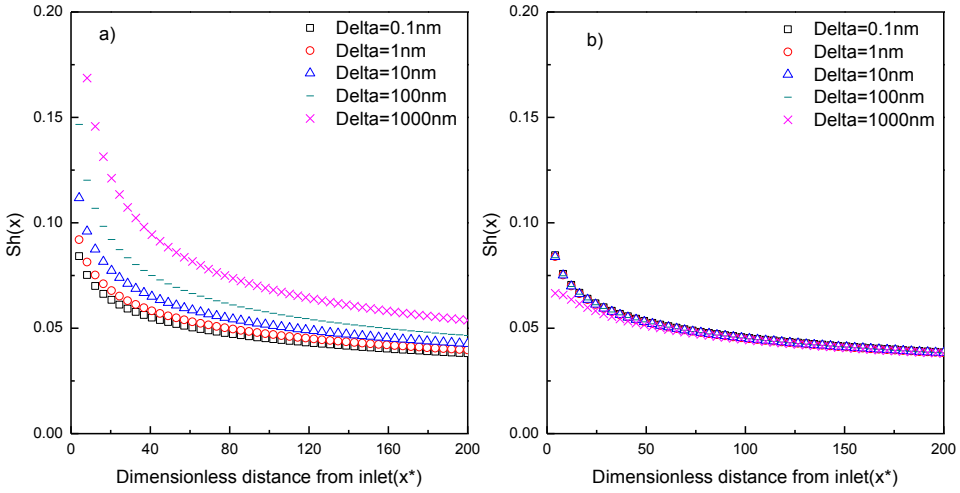

Figure 5-9. Deposition flux due to different methods for the prefect sink boundary condition a) Adamczyk and Van der ven (1981) boundary condition(6)**, and b) Elimelech (1994) boundary condition**(50)**. In both cases the selected particle size:1.0 μm, Pe=0.1, and Gr=0.**

Mass recoveries using the two methods were also examined. The mass recoveries obtained using Equation 5-37 were greater than 0.99, which satisfied the mass conservation law. To implement the Equation 5-37, the starting point of the simulation domain was moved to the corresponding δ, where the greatest DLVO force was exerted upon the particle (when $H = \delta$).

Although the calculated DLVO force could be much larger than Brownian motion under certain circumstances, it still had a finite value. In contrast, mass was not conserved when Equation 5-36 was used. As the zero concentration plane was set at $H = 0$, the calculated DLVO force approached negative infinity when the dimensionless distance H approached zero. With the limited number of mesh elements, the infinite force tensor could not be simulated and the accuracy of the numerical method could not be ensured when H approached zero. Therefore, because of good mass recovery and sensitivity to the primary minimum energy location, Equation 5-37 was selected for use herein to implement the perfect sink boundary conditions.

5.4.6 Summary of nano-scale roughness impacts on particle flux to surfaces

When nano-scale surface roughness was present on the target surface, the calculated DLVO interaction energy curve, the flow field profiles, and the hydrodynamic retardation functions required modification as discussed above. The effect of the three factors was assessed individually by model simulations and can be summarized as:

1) In the presence of the nano-scale surface roughness, both the bottom surface and the roughness element interacted with the particle. Increasing the roughness size (from 0 to the particle radius) resulted in decreased DLVO interaction energy at first, then it reached a minimum point, and then it increased. The minimum value of the DLVO interaction energy was achieved at a “critical roughness size”;

2) The presence of surface roughness changed the flow field; however, for the loading rate used in the present experiments, the changes in flow field did not cause significant changes in the particle deposition flux;

3) When surface roughness coverage exceeds 50%, the slip length should be included in the hydrodynamic retardation functions. The slip length is directly proportional to roughness size. Slip length and hydrodynamic retardation were inversely related, so larger slip lengths led to greater particle deposition flux. Particle deposition flux varied more when slip length was small (small roughness). It became less sensitive to the change of the slip length when the roughness was close to the particle radius in size;

4) In addition to the factors modified to incorporate the effect of nano-scale roughness into the model, two factors that are independent of surface roughness, gravity and the perfect sink boundary condition, were also important. Often regarded as negligible, the gravity effect significantly impacted particle deposition flux, especially that of large particles. Relatively small variations in particle density could also cause significant changes in the deposition flux of particles greater than 1.0 μm in size;

5) The perfect sink boundary condition was set using the approach of Adamczyk and Van der ven(1981) (Equation 5-37) because setting (δ, 0) as the initial point of the simulation domain instead of (0, 0) enabled excellent mass conservation and also could reflect the flux change due to different values of primary energy minimum locations; and

6) The model developed herein was able to describe the deposition behavior of particles on rough surfaces under the combined influence of DLVO forces, hydrodynamic retardation and gravity. It was able to demonstrate changes in the deposition flux in association with changes in surface roughness, including the minimum deposition flux at a critical roughness size that was observed in the experiments. When the roughness size was smaller than the critical size, increasing roughness resulted in decreased deposition flux because the particles were influenced by the relatively high hydrodynamic retardation effect and a decreasing DLVO interaction. When the roughness size was larger than the critical size, the increase of the roughness enhanced the deposition process because of reduced hydrodynamic retardation and an increasing DLVO interaction energy.

5.4.7 Comparison between the numerical solution and experimental data

The simulation results using the model developed in this study were compared to experimental data. Three sets of experimental results were selected for each particle size: patterned slides with nano-scale roughness of 10 and 400 nm were selected as the two extreme conditions (smoothest and roughest). The slide with a roughness size generating the minimum deposition flux for each particle size was selected and the specific roughness size was regarded as the critical roughness size (for the corresponding particle size). The critical roughness size changed with particle size. The deposition flux data monitored between 0.5

cm and 2.5 cm along the flow direction on the plate were utilized, thereby excluding entrance disturbance effects and cumulative gravity effects in the parallel plate chamber. The zeta potential, particle size, temperature, loading rate, and roughness features measured in the experiments were used for the model calculations.

Figure 5-10 (a), (b), and (c) show the dimensionless particle flux (Sh_{exp} and Sh_{num}) along the dimensionless distance (from 0.5 to 2.5 cm). The solid circles with the error bars represent the experimental data and the open circles represent the simulated results. The developed model was able to simulate the experimental results obtained at favorable conditions for deposition (i.e., high ionic strength) with the best-fitted primary energy minimum distance δ in the presence of the nano-scale surface roughness. Modifications to the Convection-Diffusion Equation that incorporated the effect of surface roughness on the flow field, hydrodynamic retardation functions, and DLVO forces were validated. The model was able to describe the changes in particle deposition flux caused by changes in surface roughness.

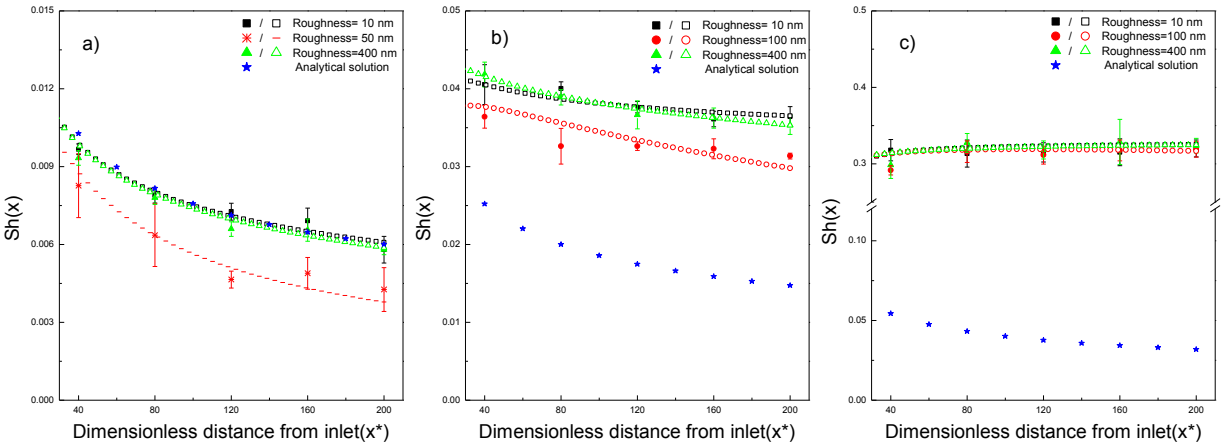

Figure 5-10. Comparisons between the experimental data and simulated numerical solution with best-fitted δ for the prefect sink boundary condition. The selected particle sizes were a) 0.5 μm, b) 1.0 μm, and c) 1.83 μm.

The best-fitted δ values were used due to the difficulty in pre-determining the exact primary energy minimum location because it would require a comprehensive analysis including the

short-range forces, hydrophobicity and chemical heterogeneity etc. and was not the focus of current study. At present there are no quantitative studies that describe the comprehensive effect of long and short range forces between colloidal particles and the contact surface. Therefore, only long-range forces such as van der Waals, EDL and hydrodynamic forces were included in the model developed herein. However, the trend of δ changing with the roughness size could be deduced. Given the variation of the DLVO interaction energy with the roughness size, the DLVO interaction would reach the minimum value at the critical roughness size. If a fixed magnitude of attractive force were required to remove the particles from the bulk solution, the perfect sink boundary would be less distant from the surface to obtain the same level of attractive force. Therefore, a smaller value of δ should be used in the simulations for the critical roughness size. For example, for the 0.55μm particles, the best-fitted δ for the roughness size of 10, 50 and 400 nm were 1, 0.25 and 1, respectively.

5.5 Conclusions

The numerical solutions presented herein show excellent agreement with the experimental results obtained in previous study(Jin et al, 2014) using the best-fitted δ(61). This study also validated the effectiveness of modifications to the flow field, the hydrodynamic retardation functions, and the calculated DLVO forces to incorporate the effect of the nano-scale surface roughness on particle deposition. The importance of the gravity effect was demonstrated, underscoring the importance of including precise measurements of particle size and density in modeling simulations. It was also demonstrated that the location of the perfect sink boundary was critical to the numerical results. Research on short-range forces is needed to pre-determine δ for the prefect sink boundary. The next stage of this going-on study is to apply the developed mathematical framework to granular media filtration modeling as a numerical methodology including a quantitative description of the roughness effect is still unavailable.

5.6 References

1. Bowen, B. and Epstein, N. Fine Particle Deposition in Smooth Parallel-Plate Channels. *J. Colloid Interface Sci.* 1979, *72* (1), 81-97; 10.1016/0021-9797(79)90184-X.

2. Hull, M. and Kitchene.Ja Interaction of Spherical Colloidal Particles with Planar Surfaces. *Transactions of the Faraday Society* 1969, *65* (563P), 3093-&.

3. Marshall, J.K. and Kitchene.Ja Deposition of Colloidal Particles on Smooth Solids. *J. Colloid Interface Sci.* 1966, *22* (4), 342-&.

4. Dabros, T.; Adamczyk, Z.; Czarnecki, J. Transport of Particles to a Rotating-Disk Surface Under an External Force-Field. *J. Colloid Interface Sci.* 1977, *62* (3), 529-541; 10.1016/0021-9797(77)90104-7.

5. Adamczyk, Z. and Weronski, P. Application of the DLVO theory for particle deposition problems. *Adv. Colloid Interface Sci.* 1999, *83* (1-3), 137-226; 10.1016/S0001-8686(99)00009-3.

6. Adamczyk, Z. and Van de ven, T.G.M. Deposition of Particles Under External Forces in Laminar-Flow through Parallel-Plate and Cylindrical Channels. *J. Colloid Interface Sci.* 1981, *80* (2), 340-356; 10.1016/0021-9797(81)90193-4.

7. Yang, J.L.; Bos, R.; Poortinga, A.; Wit, P.J.; Belder, G.F.; Busscher, H.J. Comparison of particle deposition in a parallel plate and a stagnation point flow chamber. *Langmuir* 1999, *15* (13), 4671-4677; 10.1021/la981607k.

8. Chen, G.; Bedi, R.S.; Yan, Y.S.; Walker, S.L. Initial Colloid Deposition on Bare and Zeolite-Coated Stainless Steel and Aluminum: Influence of Surface Roughness. *Langmuir* 2010, *26* (15), 12605-12613; 10.1021/la101667t.

9. Darbha, G.K.; Schaefer, T.; Heberling, F.; Luettge, A.; Fischer, C. Retention of Latex Colloids on Calcite as a Function of Surface Roughness and Topography. *Langmuir* 2010, *26* (7), 4743-4752; 10.1021/la9033595.

10. Mitik-Dineva, N.; Wang, J.; Truong, V.K.; Stoddart, P.; Malherbe, F.; Crawford, R.J.; Ivanova, E.P. Escherichia coli, Pseudomonas aeruginosa, and Staphylococcus aureus Attachment Patterns on Glass Surfaces with Nanoscale Roughness. *Curr. Microbiol.* 2009, *58* (3), 268-273; 10.1007/s00284-008-9320-8.

11. Zan, Q.F.; Wang, C.; Dong, L.M.; Cheng, P.; Tian, J.M. Effect of surface roughness of chitosan-based microspheres on cell adhesion. *Appl. Surf. Sci.* 2008, *255* (2), 401-403; 10.1016/j.apsusc.2008.06.074 ER.

12. Darbha, G.K.; Fischer, C.; Michler, A.; Luetzenkirchen, J.; Schaefer, T.; Heberling, F.; Schild, D. Deposition of Latex Colloids at Rough Mineral Surfaces: An Analogue Study Using Nanopatterned Surfaces. *Langmuir* 2012, *28* (16), 6606-6617; 10.1021/la3003146.

13. Elimelech, M. Particle Deposition on Ideal Collectors from Dilute Flowing Suspensions - Mathematical Formulation, Numerical-Solution, and Simulations. *Separations Technology* 1994, *4* (4), 186-212; 10.1016/0956-9618(94)80024-3.

14. Prieve, D.C. and Lin, M.M.J. Adsorption of Brownian Hydrosols Onto a Rotating-Disk Aided by a Uniform Applied Force. *J. Colloid Interface Sci.* 1980, *76* (1), 32-47.

15. Yao, K.M.; Habibian, M.M.; O'Melia, C.R. Water and Waste Water Filtration - Concepts and Applications. *Environ. Sci. Technol.* 1971, *5* (11), 1105-&.

16. Tufenkji, N. and Elimelech, M. Correlation equation for predicting single-collector efficiency in physicochemical filtration in saturated porous media. *Environ. Sci. Technol.* 2004, *38* (2), 529-536; 10.1021/es034049r.

17. Ma, H.L.; Pedel, J.; Fife, P.; Johnson, W.P. Hemispheres-in-Cell Geometry to Predict Colloid Deposition in Porous Media (vol 43, pg 8573, 2009). *Environ. Sci. Technol.* 2010, *44* (11), 4383-4383; 10.1021/es1009373 ER.

18. Tien, C. Hydrosol deposition in porous media: the effect of surface interactions. *Advanced Powder Technology* 2000, *11* (1), 9-56.

19. Sjollema, J. and Busscher, H. Deposition of Polystyrene Particles in a Parallel Plate Flow Cell .1. the Influence of Collector Surface-Properties on the Experimental Deposition Rate. *Colloids and Surfaces* 1990, *47,* 323-336; 10.1016/0166-6622(90)80081-E.

20. Bendersky, M. and Davis, J.M. DLVO interaction of colloidal particles with topographically and chemically heterogeneous surfaces. *Journal of Colloid And Interface Science* 2011, *353,* 87-97.

21. Henry, C.; Minier, J.; Lefevre, G.; Hurisse, O. Numerical Study on the Deposition Rate of Hematite Particle on Polypropylene Walls: Role of Surface Roughness. *Langmuir* 2011, *27* (8), 4603-4612; 10.1021/la104488a.

22. Huang, X.F.; Bhattacharjee, S.; Hoek, E.M.V. Is Surface Roughness a "Scapegoat" or a Primary Factor When Defining Particle-Substrate Interactions? *Langmuir* 2010, *26* (4), 2528-2537; 10.1021/la9028113 ER.

23. Hoek, E.M.V. and Agarwal, G.K. Extended DLVO interactions between spherical particles and rough surfaces. *J. Colloid Interface Sci.* 2006, *298* (1), 50-58; 10.1016/j.jcis.2005.12.031.

24. Neto, C.; Evans, D.; Bonaccurso, E.; Butt, H.; Craig, V. Boundary slip in Newtonian liquids: a review of experimental studies. *Reports on Progress in Physics* 2005, *68* (12), 2859-2897; 10.1088/0034-4885/68/12/R05.

25. Pit, R.; Hervet, H.; Leger, L. Direct experimental evidence of slip in hexadecane: Solid interfaces. *Phys. Rev. Lett.* 2000, *85* (5), 980-983; 10.1103/PhysRevLett.85.980.

26. Zhu, Y. and Granick, S. Limits of the hydrodynamic no-slip boundary condition. *Phys. Rev. Lett.* 2002, *88* (10), 106102; 10.1103/PhysRevLett.88.106102.

27. Kunert, C.; Harting, J.; Vinogradova, O.I. Random-Roughness Hydrodynamic Boundary Conditions. *Phys. Rev. Lett.* 2010, *105* (1), 016001; 10.1103/PhysRevLett.105.016001.

28. Walz, J.Y. and Sun, N. Effects of surface roughness on van der Waals and electrostatic contributions to particle-particle interactions and particle adhesion. *Particles of Surfaces 7: Detection, Adhesion and Removal* 2002, , 151-169.

29. Hogg, R.; Healy, T.W.; Fuersten.Dw Mutual Coagulation of Colloidal Dispersions. *Transactions of the Faraday Society* 1966, *62* (522P), 1638-&; 10.1039/tf9666201638.

30. Eichenlaub, S.; Gelb, A.; Beaudoin, S. Roughness models for particle adhesion. *J. Colloid Interface Sci.* 2004, *280* (2), 289-298; 10.1016/j.jcis.2004.08.017.

31. Hoek, E.M.V.; Bhattacharjee, S.; Elimelech, M. Effect of membrane surface roughness on colloid-membrane DLVO interactions. *Langmuir* 2003, *19* (11), 4836-4847; 10.1021/la027083c.

32. Suresh, L. and Walz, J.Y. Direct measurement of the effect of surface roughness on the colloidal forces between a particle and flat plate. *J. Colloid Interface Sci.* 1997, *196* (2), 177-190.

33. Kemps, J.A.L. and Bhattacharjee, S. Interactions between a solid spherical particle and a chemically heterogeneous planar substrate. *Langmuir* 2005, *21* (25), 11710-11721; 10.1021/la051292q ER.

34. Duval, J.F.L.; Leermakers, F.A.M.; van Leeuwen, H.P. Electrostatic interactions between double layers: Influence of surface roughness, regulation, and chemical heterogeneities. *Langmuir* 2004, *20* (12), 5052-5065; 10.1021/la030404f.

35. Elimelech, M. and O'Melia, C.R. Effect of Particle-Size on Collision Efficiency in the Deposition of Brownian Particles with Electrostatic Energy Barriers. *Langmuir* 1990, *6* (6), 1153-1163.

36. Henry, C.; Minier, J.; Lefevre, G. Numerical Study on the Adhesion and Reentrainment of Nondeformable Particles on Surfaces: The Role of Surface Roughness and Electrostatic Forces. *Langmuir* 2012, *28* (1), 438-452; 10.1021/la203659q.

37. Walz, J.Y. The effect of surface heterogeneities on colloidal forces. *Adv. Colloid Interface Sci.* 1998, *74*, 119-168.

38. Gregory, J. Approximate expressions for retarded van der waals interaction. *J. Colloid Interface Sci.* 1981, *83* (1), 138-145; http://dx.doi.org/10.1016/0021-9797(81)90018-7.

39. Vinogradova, O.I. and Belyaev, A.V. Wetting, roughness and flow boundary conditions. *Journal of Physics-Condensed Matter* 2011, *23* (18), 184104; 10.1088/0953-8984/23/18/184104.

40. Brenner, H. The Slow Motion of a Sphere through a Viscous Fluid Towards a Plane Surface. *Chem. Eng. Sci.* 1961, *16* (3-4), 242-251; 10.1016/0009-2509(61)80035-3.

41. Goldman, A.J.; Cox, R.G.; Brenner, H. Slow Viscous Motion of a Sphere Parallel to a Plane Wall .I. Motion through a Quiescent Fluid. *Chemical Engineering Science* 1967, *22* (4), 637-&; 10.1016/0009-2509(67)80047-2.

42. Goldman, A.J.; Cox, R.G.; Brenner, H. Slow Viscous Motion of a Sphere Parallel to a Plane Wall .2. Couette Flow. *Chemical Engineering Science* 1967, *22* (4), 653-&; 10.1016/0009-2509(67)80048-4.

43. O'Neill, M.E. A Sphere in Contact with a Plane Wall in a Slow Linear Shear Flow. *Chemical Engineering Science* 1968, *23* (11), 1293-&; 10.1016/0009-2509(68)89039-6.

44. Spielman, L.A. and Fitzpatrick, J.A. Theory for particle collection under London and gravity forces. *J. Colloid Interface Sci.* 1973, *42* (3), 607-623.

45. Nelson, K.E. and Ginn, T.R. Colloid filtration theory and the Happel sphere-in-cell model revisited with direct numerical simulation of colloids. *Langmuir* 2005, *21* (6), 2173-2184; 10.1021/la048404i.

46. Happel, J. and Brenner, H. *Low Reynolds number hydrodynamics: with special applications to particulate media.* Springer: 1965; Vol. 1, .

47. Cox, R.G. and Brenner, H. The slow motion of a sphere through a viscous fluid towards a plane surface—II Small gap widths, including inertial effects. *Chemical Engineering Science* 1967, *22* (12), 1753-1777; http://dx.doi.org/10.1016/0009-2509(67)80208-2.

48. Masliyah, J.H. and Bhattacharjee, S. *Electrokinetic and colloid transport phenomena.* John Wiley & Sons: 2006; .

49. Nelson, K.E. and Ginn, T.R. New collector efficiency equation for colloid filtration in both natural and engineered flow conditions. *Water Resour. Res.* 2011, *47* (5).

50. Elimelech, M. Particle deposition on ideal collectors from dilute flowing suspensions: Mathematical formulation, numerical solution, and simulations. *Separations Technology* 1994, *4* (4), 186-212.

51. Johnson, W.P. and Tong, M. Observed and simulated fluid drag effects on colloid deposition in the presence of an energy barrier in an impinging jet system. *Environ. Sci. Technol.* 2006, *40* (16), 5015-5021; 10.1021/es060450c.

52. Vinogradova, O. Slippage of water over hydrophobic surfaces. *Int. J. Miner. Process.* 1999, *56* (1-4), 31-60; 10.1016/S0301-7516(98)00041-6.

53. Prieve, D.C. and Ruckenstein, E. Rates of Deposition of Brownian Particles Calculated by Lumping Interaction Forces into a Boundary-Condition. *J. Colloid Interface Sci.* 1976, *57* (3), 547-550.

54. Tufenkji, N.; Redman, J.A.; Elimelech, M. Interpreting deposition patterns of microbial particles in laboratory-scale column experiments. *Environ. Sci. Technol.* 2003, *37* (3), 616-623; 10.1021/es025871i.

55. Tufenkji, N. and Elimelech, M. Spatial distributions of Cryptosporidium oocysts in porous media: Evidence for dual mode deposition. *Environ. Sci. Technol.* 2005, *39* (10), 3620-3629; 10.1021/es048289y.

56. Passmore, J.M.; Rudolph, D.L.; Mesquita, M.M.F.; Cey, E.E.; Emelko, M.B. The utility of microspheres as surrogates for the transport of E. coli RS2g in partially saturated agricultural soil. *Water Res.* 2010, *44* (4), 1235-1245; 10.1016/j.watres.2009.10.010.

57. Johnson, W.P.; Pazmino, E.; Ma, H. Direct observations of colloid retention in granular media in the presence of energy barriers, and implications for inferred mechanisms from indirect observations. *Water Res.* 2010, *44* (4), 1158-1169; 10.1016/j.watres.2009.12.014.

58. Bradford, S.A.; Kim, H.N.; Haznedaroglu, B.Z.; Torkzaban, S.; Walker, S.L. Coupled Factors Influencing Concentration-Dependent Colloid Transport and Retention in Saturated Porous Media. *Environ. Sci. Technol.* 2009, *43* (18), 6996-7002; 10.1021/es900840d.

59. Sjollema, J. and Busscher, H. Deposition of Polystyrene Latex-Particles Toward Polymethylmethacrylate in a Parallel Plate Flow Cell. *J. Colloid Interface Sci.* 1989, *132* (2), 382-394; 10.1016/0021-9797(89)90253-1.

60. Jin, C. and Emelko, M.B. Non-linear, non-monotonic impact of surface roughness on colloidal particle deposition during granular media filtration at favorable conditions. *Environ. Sci. Technol.* **2014,** *to be submitted*

61. Jin, C.; Glawdel, T.; Ren, C.; Emelko, M.B. Non-Linear, non-monotonic impact of nano-scale surface roughness on colloidal particle deposition. I. Experiments in a parallel plate system. *Langmuir* **2014,** *to be submitted*

62. Jin, C.; Glawdel, T.; Ren, C.; Emelko, M.B. Non-Linear, non-monotonic impact of nano-scale roughness on particle deposition: II. Numerical modeling. *Langmuir* **2014,** *to be submitted*

63. Jin, C.; Glawdel, T.; Ren, C.; Emelko, M.B. Modeling particle deposition on rough spherical collectors in absence of an energy barrier. *Environ. Sci. Technol.* **2014,** *to be submitted*

Chapter 6
Modeling particle deposition on rough spherical collectors in absence of an energy barrier

6.1 Overview

A mathematical framework for describing particle deposition on spherical collector surfaces with nano-scale roughness in absence of an energy barrier was developed. In comparison to available models of physico-chemical filtration of colloidal particles, the present model incorporates recently developed numerical approaches that provide improved description of flow field profile, hydrodynamic retardation, and DLVO forces. The influence of each of these contributions to particle deposition on rough spherical collector surfaces was quantitatively evaluated. The impacts of particle size, particle loading rate (i.e., approach velocity), and background electrolyte solution ionic strength on particle deposition were evaluated at several roughness sizes. A non-linear, non-monotonic impact of surface roughness on particle deposition has been demonstrated. Here, that relationship was further explored and it is demonstrated that the non-linear, non-monotonic impact of nano-scale roughness on collector surfaces roughness on particle deposition is consistently observed, regardless of particle size, particle loading rate, and background electrolyte solution ionic strength. The relative magnitude of this impact depended on the combination of operational parameters, as would be expected. This work demonstrates that incorporation of surface roughness into the Convection-Diffusion equation, with accurate representation of its associated impacts on the flow field, hydrodynamic retardation, and DLVO forces can contribute to better, more realistic description of particle deposition during physico-chemical filtration in porous media and other systems with non-smooth collector surfaces. When determining the particle size associated with the minimum deposition in a granular media filtration system, not only should particle size be considered (as it is in most contemporary modeling approaches), but roughness attributes such as roughness size and distribution also should be taken into the consideration. Without a doubt, where applicable, these

considerations may contribute to explaining discrepancies between model-based expectations and experimental outcomes.

6.2 Introduction

Over the past three decades, tremendous research effort has focused on improved understanding of colloidal and nano-particle transport and deposition phenomena in a variety of natural and industrial environments (1-5). Particle deposition on target (or collector) surfaces can be numerically described by Eulerian or Lagrangian methods assuming the collectors have ideal geometries such as spheres (6), cylinders (7), rotation disks (8), or parallel plates (7, 9, 10). To model particle deposition behavior on collector surfaces within the framework of classic DLVO theory, the sum of van der Waals forces (VDW) and electrostatic double layer forces (EDL), and the physical and chemical interactions between the particle and collector surfaces have been described and applied to experimental scenarios with moderate success, which typically has depended on how well the experimental scenarios met the fundamental assumptions of the models (6, 11, 12).

Classic filtration theory can provide reasonable prediction of particle deposition on smooth surfaces when the particle and collector surface are oppositely charged (13); however, in many cases, model predictions have failed to describe experimental observations. Significant discrepancies between theoretical predictions and experimental outcomes have been reported when particles and collectors are similarly charged and a large interaction energy barrier is present (6, 14-16). In contrast to theoretical models that predict a sharp decrease in particle deposition flux when ionic strength is below a certain critical concentration (6, 17, 18), experimental investigations have frequently demonstrated gradually decreasing particle deposition flux with decreasing background electrolyte solution ionic strength (6). Often, the predicted particle deposition flux at low ionic strength was several orders of magnitude lower than that actually observed experimentally (19-22). As a result, fitting parameters such as attachment efficiency (α) have been introduced to describe experimental results when limited theoretical explanation is available from current theory (1, 23). Existing filtration theory is un-realistically sensitive to changes in ionic strength and chemical potential, thereby

rendering many model predictions of particle deposition flux inappropriate as they are too strongly influenced by the shape and magnitude of particle-surface interaction energy profiles.

It has been suggested that the discrepancies in particle deposition between theoretical predictions and experimental outcomes can be explained by considerations of a) roughness on particle and collector surfaces (6); b) chemical charge heterogeneity (24, 25) and deposition due to the secondary energy minima (26, 27); c) hydrophobicity (28, 29) and short range forces(30, 31); and d) physical mechanisms, such as straining (32, 33), wedging(16), and blocking(14, 34). Regardless of the exact factors that contribute to these discrepancies, a critical consideration is that some of the original assumptions (e.g., smooth collector surfaces) on which many of traditional and current models of particle deposition are based are not realistic for most natural and engineered applications. Improvements in the understanding of surface chemistry effects such as chemical heterogeneity, secondary energy minimum, and hydrophobicity and associated modifications to particle deposition models have helped to explain the discrepancies between model predictions and experimental observations (5, 35); however, in many cases the discrepancies are still substantial and preclude the use of these modeling approaches in practice.

Several studies have recently reported that collector surface roughness features are able to significantly alter the shape and magnitude of particle-surface interaction energy profiles (30, 31, 36-38, 70). Enhanced particle deposition due to collector surface roughness has been frequently reported (10, 39-41). Decreased particle deposition regarding the presence of surface roughness has also been reported in a few cases (42-44). Despite this experimental evidence, a mathematical framework for describing the presence of surface roughness and comprehensively quantifying its contributions to particle deposition in spherical geometry (as is required for packed bed applications) is currently lacking (11, 12, 23), thereby precluding effective application of particle deposition models to many natural and engineered systems in which surface roughness is ubiquitous (5, 13, 16, 16, 19, 32).

In this paper, a mathematical model was developed using an Eulerian approach to describe particle deposition on spherical collectors with nano-scale surface roughness in absence of an energy barrier (i.e., at favorable conditions for particle deposition). Clean bed filtration conditions were assumed; accordingly, particle-particle interactions and blocking effects were considered negligible (68-70). The classic Happel sphere-in-cell model was used to describe the flow field profile around the collector. In comparison to available models of physico-chemical filtration of colloidal particles, the present model incorporates recently implemented and developed numerical approaches that provide improved description of the flow field profile, hydrodynamic retardation, and DLVO forces (Jin et al,2014 of two). The influence of each these contributions to particle deposition on rough spherical collector surfaces was quantitatively evaluated. Several scenarios were simulated using the developed model to demonstrate the impact of particle size, particle loading rate (i.e., approach velocity), and background electrolyte solution ionic strength on particle deposition at several roughness sizes.

6.3 Model development

System geometry will affect the flow field and force balance acting upon a particle approaching a collector surface. Accordingly, modeling particle deposition in porous media systems, such as granular media filtration processes and the subsurface transport requires description of particle deposition on spherical collector surfaces. Modeling the deposition flux on spherical collectors with roughness requires description of not only roughness size, but also roughness distribution on the surface. Detailed representation of surface roughness topography can be achieved with Fourier transform (45) or fractal analysis (46) approaches; however, integration of these approaches with Convective-Diffusion models becomes exceedingly computationally intensive. As a result, simplifying assumptions for reasonable representation of collector surface roughness are desirable. In the following sections, a simplified geometric representation of surface roughness on spherical collectors was developed and previously reported numerical approaches that provided improved description

of the flow field profile, hydrodynamic retardation, and DLVO forces in parallel plates systems (Jin et al,2014) were modified and applied for packed bed systems(69,70).

6.3.1 Simplified geometric representation of collector surface roughness

A previously described approach for describing collector surface roughness is utilized in this investigation (Jin et al,2014)(69,70). Briefly, rough surfaces were described as a smooth bottom surface with protruding roughness features represented by three stacked spheres with radius a_r. The roughness elements were uniformly distributed on the collector surface with a distance of s between elements; they covered more than 50% of the collector surface. The absolute size of the roughness elements ($6a_r$) was assumed to be smaller than the diameter of any approaching particle (i.e., "nano-scale roughness").

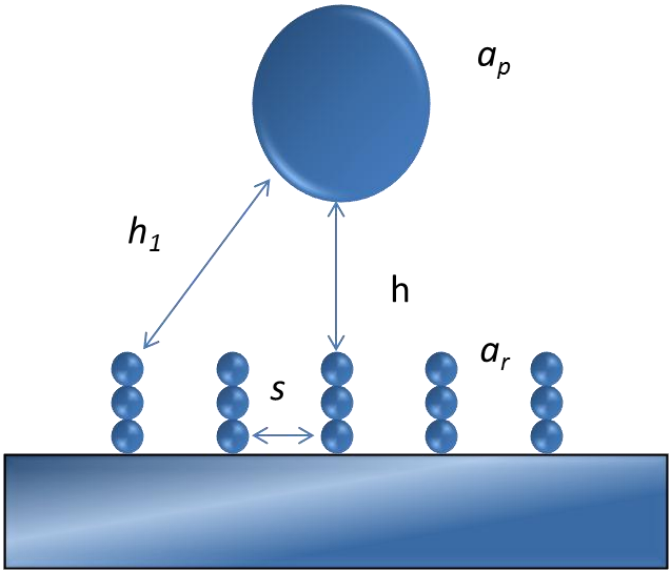

Figure 6-1. General schematic of spherical collector surface roughness ("rough sphere")

6.3.2 Mass transfer in spherical geometry.

At steady state and in absence of chemical reactions, the general convection-diffusion equation for particle mass transfer due to diffusion, convection and external forces can be expressed as

$$\nabla\cdot(\boldsymbol{u}C)=\nabla\cdot(D\cdot\nabla C)-\nabla\cdot\left(\frac{\boldsymbol{D}\cdot\boldsymbol{F}}{kT}C\right) \qquad (6\text{-}1)$$

where T is the absolute temperature, k_b is Boltzmann's constant, c is the particle concentration, D is the diffusion tensor, and F represents external forces that can act as sources or sinks of momentum. Equation 6-1 can be solved numerically when the flow velocity field, diffusion tensor and external forces are known. In spherical geometry, the full expression of Convective-Diffusion equation is described as

$$\begin{aligned}
&\frac{\partial c}{\partial \theta}\left\{ N_R{}^2 f_4(H)\frac{\partial c}{\partial \theta} + N_R{}^2 f_4(H)cot\theta - f_4(H)F_G^* sin\theta N_R - \frac{N_{Pe}}{2} f_3(H)V_\theta N_R \right\} \\
&+\frac{\partial c}{\partial H}\left\{ f_1(H)\frac{\partial c}{\partial H} + \left[2N_R f_1(H) + \frac{\partial f_1(H)}{\partial H} + f_1(H)\left(\frac{\partial \varphi}{\partial H} + F_G^* cos\theta \right) - f_1(H) f_2(H) V_r \frac{N_{Pe}}{2} \right] \right\} \\
&= \boldsymbol{c}\{ \left[\left(2N_R f_1(H) + \frac{\partial f_1(H)}{\partial H} \right)\left(\frac{\partial \varphi}{\partial H} + F_G^* cos\theta \right) + f_1(H)\frac{\partial^2 \varphi}{\partial H^2} + \frac{f_1(H)\partial F_G^* cos\theta}{\partial H} - 2 f_4(H) N_R cos\theta F_G^* \right] \\
&-\frac{N_{Pe}}{2}\left[2N_R f_1(H) f_2(H)V_r + \frac{\partial f_1(H)}{\partial H} f_2(H)V_r + \frac{\partial f_2(H)}{\partial H} f_1(H)V_r + f_1(H) f_2(H)\frac{\partial V_r}{\partial H} + 2N_R f_3(H)cot\theta V_\theta \right] \}
\end{aligned} \tag{6-2}$$

A list of the non-dimensional parameters used in Equation 6-2 and adapted from Jin et al. (2014) is provided in Table A-2(69,70). To solve Equation 6-2 numerically, the implemented boundary conditions were

$$C\ (H = 0, \theta) = 0 \tag{6-3}$$

$$C\ (H \sim, \theta) = 1 \tag{6-4}$$

$$\left(\frac{\partial c}{\partial \theta}\right)_{\theta=0} = 0 \tag{6-5}$$

When the Peclet number was small (Pe < 0.1), the implemented boundary condition were

$$v_r C - D_r \frac{\partial C}{\partial r} = -UC_0 cos\theta \, at\, r = b, ? \le \theta \le \quad \pi \tag{6-6}$$

$$\frac{\partial C}{\partial r} = 0 ? at\, r = b \quad \pi \le \theta \le \pi \tag{6-7}$$

To avoid the continuity issue for numerical simulation, the new boundary condition over the entire out boundary was described as

$$\lim_{\theta \to 0.5\pi} \frac{\partial C}{\partial r} = \lim_{\theta \to 0.5\pi} \left[\frac{U}{D_r} \left(C_0 - C \right) cos\theta \right] = 0 \tag{6-8}$$

The complete form of the convective-diffusion equation derived from first principals (Appendix D) was utilized to describe particle deposition in the present investigation (Appendix D). In contrast to other versions (Elimelech et al. 1998) (17) commonly utilized as a foundation for modeling particle and microorganism deposition on porous media (13, 23, 47-49), Equation 6-2 included three extra terms in red font $N_R{}^2 f_4(H) \frac{\partial^2 c}{\partial \theta^2}$, $N_R{}^2 f_4(H) cot\theta \frac{\partial c}{\partial \theta}$ and $\frac{f_1(H) \partial F_G^* cos\theta}{\partial H}$ that were assumed negligible (17). In the present work, the first two terms were included in the simulation for completeness. The third term was equal to zero and was thus removed from the simulation.

6.3.3 Particle deposition flux

When the dimensionless particle concentration is determined using Equations 6-2 to 6-8, the particle flux perpendicular to the collector surface $J^*(H_\delta, \theta)$ can be calculated at a cut off distance δ by implementing the perfect sink boundary condition. The overall particle deposition flux perpendicular to the collector surface can be integrated over the entire surface (0-2π) to evaluate the total rate of particle contact with a single collector (I) (Appendix D). Normalized by the rate of particle flow toward the projected area of the collector, the overall contact efficiency or single collector efficiency (η) is defined as

$$\eta = \frac{I}{\pi a_c^2 U c} \tag{6-9}$$

When diffusion is the dominant mechanism of particle transport to the collector surface, the single collector efficiency can be described analytically (13) as

$$\eta_D = 4.0 * A_s^{1/3} (\frac{D_\infty}{2Ua_c})^{2/3} \quad (6\text{-}10)$$

where A_s is a porosity-dependent parameter which was same as defined functions in Tien 2001' work(50) .

6.3.4 Flow field

In granular media filtration, packed beds are generally regarded as comprised of perfectly smooth spheres assembled by a simple cubic packing scheme (13). According to Happel's sphere-in-cell model, the collectors are assumed to be enveloped by a shell of fluid (13, 51) of thickness (b), which is related to the overall porosity (ε) of the packed bed (52) and described by

$$b = a_c(1-\varepsilon)^{1/3} \quad (6\text{-}11)$$

where a_c is the collector radius.

In the present investigation, the previously developed functions for flow field (50) were utilized to represent the flow field velocity profile under the assumptions of a) creeping flow of an incompressible fluid at steady state and b) no-slip boundary conditions with smooth surface. It should be noted that the stream function (Appendix D) is only valid within the envelope of Happel's sphere cell with thickness (b) described by Equation 6-11.

When collector surfaces are rough, traditional application of the no-slip boundary condition to the top of collector surfaces is inappropriate (53, 54,70). As detailed in Jin et al., 2014(69,70), when the size of surface roughness features is less than the approaching particle radius and the extent of surface coverage with roughness elements exceeds 50%, a no-slip boundary condition can be applied at the bottom of the roughness elements (7) and the modified flow field reflecting the presence of surface roughness can be approximated by slip-length (i.e., dimensionless roughness size) on top of the roughness elements (55, 56). Here,

the original assumptions implicit to Happel's sphere-in-cell model were not changed; however, the thickness of the fluid shell around the collector was scaled down by the size of the roughness elements. This enabled the use of dimensionless slip-length (r_{slip}) to describe the flow field velocity component on top of the roughness elements as

$$V_{\theta}^{'}(r) = V_{\theta}(r + r_{slip}) \tag{6-12}$$

$$r_{slip} = r_{Roughness} / r_{particle} \tag{6-13}$$

where the $V_{\theta}^{'}(r)$ was the modified radial velocity component. When $r_{Roughness}$ was equal to zero, indicating no roughness on the collector surface, the velocity component was equal to that of a smooth surface.

To quantitatively evaluate the change in particle deposition due to the changed flow field in the presence of the surface roughness, the DLVO interaction (U_{Total}^{DLVO}) and gravity components of the model were set to zero during these simulations. The hydrodynamic retardation functions for smooth collector surfaces were used and a particle loading rate of 10^{-3} m/s was applied. The particle and collector radii were 200 nm and 200 μm, respectively. The porosity of the packed media calculated from the Happel's sphere-in-cell approximation for the flow field profile was 0.38. Dimensionless slip lengths of 0 to 1.0 were used to reflect the different roughness sizes.

6.3.5 Hydrodynamic retardation functions

Surface roughness reduces hydrodynamic retardation; therefore, the associated descriptive functions must be appropriately modified (55, 57). Analogous to the concept of the slip-length modification for the flow field, slip-length can also be used in describing the influence of surface roughness on hydrodynamic retardation. Proposed by Vinogradova and Belyaev (2011)(57), a hydrodynamically equivalent plane between the top and bottom of the roughness elements can be assumed as the new target surface for the calculation of the effective hydrodynamic retardation functions. The effectiveness of the slip-length for rough surfaces was validated using high-speed dynamic AFM (57). Slip-length was also utilized for

describing surface roughness in a parallel plate experimental system (Jin et al., 2014) and it was found that the numerical solutions had good agreement to the experimental results (Jin et al., 2014)(69,70). Here, slip-length was also utilized to describe changes in the hydrodynamic retardation functions due to the presence of surface roughness.

The classic hydrodynamic retardation functions and the slip-length modifications for rough surfaces were developed on a planar surface for laminar flow without considering curvature (58-61). In spherical geometry, the functions are still valid because of the relative size between the approaching particle and collector. For 0.1-10 μm colloidal particles collectors and spherical collectors typically >200 μm, a simplifying assumption of planar collector surfaces is reasonable (17).

Assuming >50% surface coverage with roughness on the collectors, the previously defined slip-length in Equation 6-13 could be used to represent the corresponding slip-length (r_{slip}) for hydrodynamic retardation. When roughness size was set as 0, the hydrodynamic retardation functions were the same as those applicable to a smooth surface.

The new hydrodynamic retardation functions were expressed as

$$f_i(h) = F_i(h + r_{slip}) \tag{6-14}$$

where $f_i(h)$ represents the original individual hydrodynamic retardation functions $f_{1-4}(h)$ and $F_i(h)$ represented the modified hydrodynamic retardation functions $F_{1-4}(h)$ that include consideration of collector surface roughness (70).

To quantitatively evaluate the change in particle deposition due to the changed hydrodynamic retardation effect in the presence of the surface roughness, roughness elements were assumed to be evenly distributed along the collector surface with >50% coverage. The DLVO interaction energy, gravity, and slip-length in the flow field components of the model were set to zero during these simulations. A particle loading rate of 10^{-3} m/s was applied and the particle and collector radii were 200 nm and 200 μm, respectively. The porosity of the packed media calculated from the Happel's sphere-in-cell approximation for the flow field

profile was 0.38. Dimensionless slip lengths of 0 to 1.0 were used to reflect the different roughness sizes.

6.3.6 DLVO force modifications for approaching particles

To describe changes in DLVO interaction energies between the approaching particle and collector surface, a recently reported, computationally efficient approach for approximating these interaction energies was applied(69,70). In brief, particle-surface total DLVO interaction energies in the presence of surface roughness were approximated by the pairwise summation method under the assumptions of constant chemical potential (38, 62). The selected chemical potentials for the particle and collector surfaces were in the range of ±25 mV to satisfy the linear approximation of the Poisson-Boltzmann equation for the EDL force calculation. The determined EDL interaction can be expressed analytically as described by Hogg et al. (1966) (63). Ionic strengths ranging from 1mM to 100mM KCl were selected for the numerical simulations; the corresponding Debye-Hückel lengths ranged from 0.963 nm to 9.63 nm respectively.

The total interaction energy arising from VDW and EDL forces (U_{Total}^{DLVO}) by the pairwise summation method can be described as

$$\begin{aligned} U_{Total}^{DLVO} &= U_{Total}^{VDW} + U_{Total}^{EDL} \\ &= U_{PS}^{VDW} + \sum_{i=1}^{n} U_{PR}^{VDW} + U_{PS}^{EDL} + \sum_{i=1}^{n} U_{PR}^{EDL} \end{aligned} \tag{6-15}$$

where the U_{PS}^{VDW} and U_{PS}^{EDL} represent the VDW and EDL interaction energies between the approaching particle and bottom surface and U_{PR}^{VDW} and U_{PR}^{EDL} represent the VDW and EDL interaction between the particle and the roughness elements on the surface.

In this study, the un-retarded VDW interaction energy using Hamaker's approach was used to evaluate the VDW interaction energy between the approaching particle to the rough surface (U_{PS}^{VDW} and U_{PR}^{VDW}). The linear approximation of the Poisson-Boltzmann equation

was used to assess the EDL interaction energy between the approaching particle and rough surface (U_{PS}^{EDL} and U_{PR}^{EDL}) individually(36, 38, 64).

$$U_{PS}^{VDW} = -\frac{Aa_P}{6h}\left(\frac{1}{1+14h/\lambda}\right) \tag{6-16}$$

$$U_{ij}^{VDW} = -\frac{A_{ij}}{6}\left[\frac{2a_ia_j}{R_{ij}^2-(a_i+a_j)^2} + \frac{2a_ia_j}{R_{ij}^2-(a_i+a_j)^2+4a_ia_j} + \ln\left(\frac{R_{ij}^2-(a_i+a_j)^2}{R_{ij}^2-(a_i+a_j)^2+4a_ia_j}\right)\right] \tag{6-17}$$

$$U_{PS}^{EDL} = \pi\varepsilon\varepsilon_0 a_p\left[2\psi_P\psi_S\ln\left(\frac{1+\exp(-\kappa H)}{1-\exp(-\kappa H)}\right) + (\psi_P^2+\psi_S^2)\ln(1-\exp(-2\kappa H))\right] \tag{6-18}$$

$$U_{ij}^{EDL} = \frac{\pi\varepsilon\varepsilon_0 a_i a_j}{(a_i+a_j)}\left[2\psi_i\psi_j\ln\left(\frac{1+\exp(-\kappa H)}{1-\exp(-\kappa H)}\right) + (\psi_i^2+\psi_j^2)\ln(1-\exp(-2\kappa H))\right] \tag{6-19}$$

where *i* and *j* represent the rough sphere and approaching particle, R_{ij} is the center-to-center distance between two spheres, A_{ij} is the Hamaker constant between *i* and *j* in a solution, λ is the characteristic wavelength, ψ_1 and ψ_i are the respective chemical potentials of the two spheres, and *h* and *H* respectively are the true and dimensionless surface-to-surface distances.

To meet the requirement for applying the linear approximation of the Poisson-Boltzmann equation to the EDL interactions, the chemical potentials for the colloidal particle and collector surface were assumed to be 20 mV and -20mV respectively. As a result, for all simulations, the net force between the colloidal particle and collector was attractive and without an interaction energy barrier. The overall size of surface roughness was evaluated from 0 nm to 600 nm. Other parameters were kept identical to those in Figure 6-2. The VDW and EDL force formulas used to calculate DLVO interaction energies in this study were validated by comparing the simulation results to published data (65). In these validation experiments, the size of the rough sphere (a_r) was set to 0 (i.e., a smooth sphere) and s was 100 nm. Gravity effects were excluded during all of the simulations.

6.3.7 Numerical methods

The numerical solution of Equation 6-2 with all boundary conditions was solved by the finite element method using a commercial simulator COMSOL 3.5a® (COMOSL, Inc., Canada). The simulation domain was discretized using quadrilateral meshing. Highly refined meshes were required at the regions with high concentration gradients or large tensors of applied forces. Because a steep particle concentration gradient existed in the vicinity of the collector surface, extremely fine mesh elements smaller than the Debye-Hückel length (e.g., 10^{-4} in dimensionless size) were utilized at the bottom of the collector surface. Therefore, the simulation domain was divided into two domains: 1 and 2. The sub-region close to the bottom surface was defined as Domain 1. It was meshed by larger numbers of meshing elements to guarantee accurate numerical simulation. The total number of mesh elements employed in the simulation was 400,000, 70% of which were mapped within Domain 1. Neumann boundary conditions were applied on the boundaries of Domains 1 and 2.

6.3.8 Model validation

Validation of the Convection-Diffusion model developed in COMSOL® (including selected formulas, boundary conditions and finite element calculations) involved comparing the numerical solutions with published numerical results. Figure A-10(Appendix D) shows a representative plot of results from simulations using the developed model. It depicts dimensionless particle deposition flux (*Sh*) as a function of location (θ) on the spherical collector at a flow rate of 10^{-5} m/s. The particle deposition flux (*Sh*) at different ionic strengths ranging from 10^{-6} to 10^{-4} mol/L and the no EDL interaction condition are plotted for comparison (Figure A-10). The solid lines represent numerical results for *Sh* (Figure A-10) previously reported by Elimelech and Song (1992) (13). The open circles represent the calculated dimensionless particle deposition fluxes from simulations using the developed model. The two sets of data demonstrate excellent agreement and validate the current model by demonstrating that it is able to describe colloidal particle deposition on smooth collectors (i.e., in absence of collector surface roughness) in spherical geometry to yield the same results as a previously published model (13).

6.4 Results and discussion

6.4.1 Surface roughness effects on flow field profile

Figure 6-2 depicts the (a) tangential (v_θ) and (b) radial flow (v_r) velocity components as a function of the radial location on the spherical collector (θ). The tangential velocity for all simulated results using different slip lengths approaches zero when $\theta = 0$ or π and achieves maximum values when $\theta=0.5\pi$. Illustrated in Figure 6-2 (a), bigger dimensionless slip-lengths result in higher tangential flow velocity, indicating higher flow-derived shear forces. The radial flow velocity component also increases with increased slip-length (Figure 6-2 (b)) indicating higher particle flow velocity towards to the target surface, which alternatively leads to more particles available for attachment. Flow field changes that were attributable to surface roughness resulted in changes in particle deposition flux that followed patterns similar to those of the flow velocity components (i.e., v_θ and v_r). When surface roughness size (slip-length for a fixed particle size) increased, total particle deposition flux on the spherical collector surfaces increased (Figure 6-3(a)) due to changes in the flow velocity profile. The incremental changes in deposition flux due to flow field changes were relatively small when slip-length was smaller than 0.1, but they became more substantial at slip lengths greater than 0.1. Higher flow fields enable the fluids to carry more particles to the vicinity of spherical collector surface; therefore, for a fixed attachment efficiency (α), more available particles could result in more deposition flux.

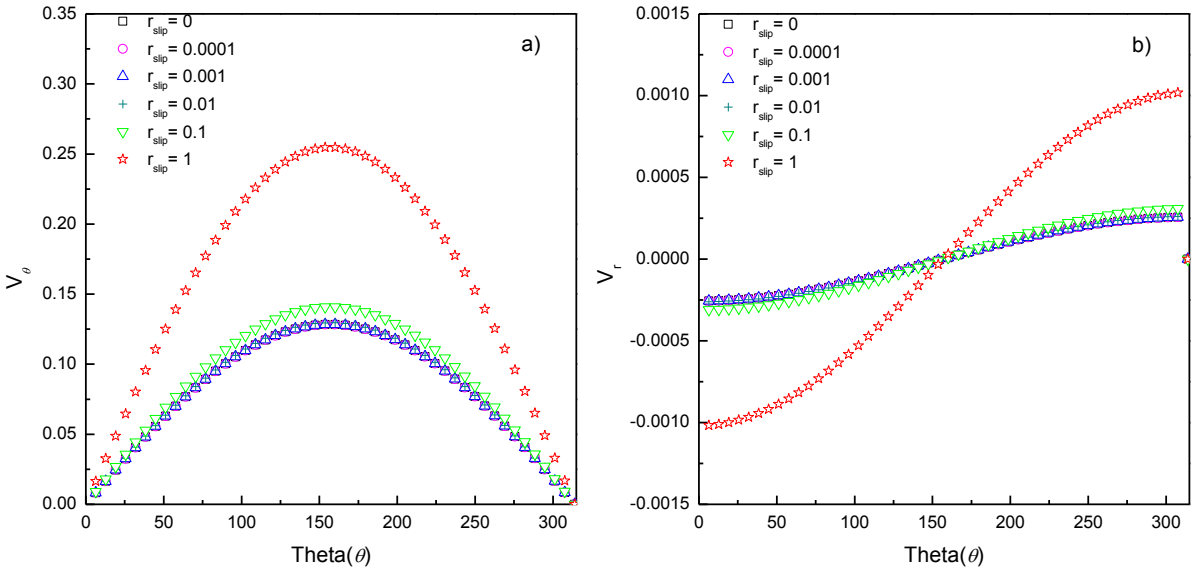

Figure 6-2. a) The tangential (v_θ) and b) radial (v_r) flow velocity components as a function of the radial location on a spherical collector (θ) at different slip-lengths. The particle and collector surface potentials = -0 mV and 0 mV respectively; particle radius = 200 nm; collector diameter = 200 μm; porosity = 0.38; temperature = 25 ˚C, Hamaker constant = $1x10^{-20}$ J; loading rate = 10^{-3} m/s; cut-off distance δ = 1 nm; and gravity number = 0. The curves correspond to the following flow field modified slip lengths: 0, 0.0001, 0.001, 0.01, 0.1 and 1.

6.4.2 Surface roughness effects on hydrodynamic retardation functions

Figure 6-3(b) depicts dimensionless particle deposition flux (*Sh*) due to different sizes of slip length (used to modify hydrodynamic retardation) as a function of the radial location on the spherical collector (θ). Increased slip-length resulted in increased total dimensionless particle deposition flux (area under the *Sh* curve). Here, due to the presence of surface roughness, the hydrodynamic retardation functions have less repulsive effect relative to that from a smooth surface. This enables approaching particles to more readily move closer to collector surfaces and to be removed from the bulk solution. The majority of the increase in particle flux occurs on the first half of the collector surface (i.e., the surface facing the flow) where θ is between 0 and 0.5π. These results are consistent with recently reported results describing particle deposition on rough surfaces in a parallel plate chamber (69,70). In both cases, the presence of surface roughness increased particle deposition flux by reducing the hydrodynamic retardation effect.

Assuming that the same slip-length can be used to modify the flow field profile and hydrodynamic retardation functions for a specific surface roughness element size, the deposition flux under the net effect of increased flow velocity and reduced hydrodynamic retardation is presented in Figure 6-3(c). In this figure, gravity and DLVO interaction effects were excluded and set to zero. The total increase in particle deposition flux ($\Delta Sh = Sh_{slip} - Sh_{slip=0}$) associated with concurrently applying the same slip-length to the flow field and that hydrodynamic retardation functions was not additive. Specifically, the total increase in particle deposition flux Figures 6-3 (c) was greater than the value obtained by adding the ΔSh from Figures 6-3 (a) and (b) for the corresponding slip-lengths. For example, when the slip-length increased from 0 to 1, the total particle deposition flux over the collector surface increased by 3.9% and 80.3% due to respective changes in the flow field and hydrodynamic retardation functions. The concurrent impact of these factors on total particle deposition flux (99.9%) in Figure 6-3(c) is significantly more than sum of individual contributions that the total particle deposition flux. The particle deposition fluxes have a positive relationship to the scales of roughness. Under the net effects of higher flow velocity and lower hydrodynamic retardation effects due to the presence of surface roughness, *Sh* are increased significantly.

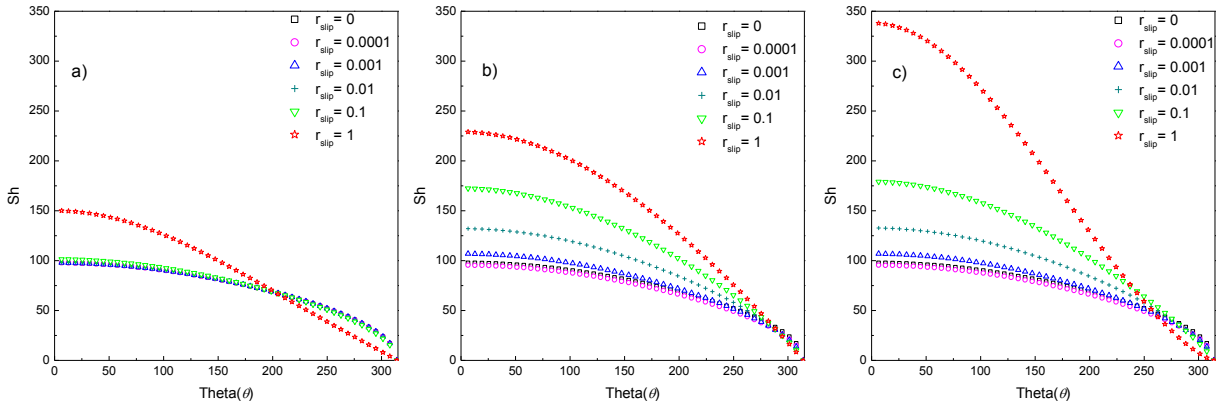

Figure 6-3. Particle deposition flux (*Sh*) changes as a function of different slip-lengths used to modify a) only the flow field around a spherical collector, b) only the hydrodynamic retardation functions and c) both the flow field and hydrodynamic retardation functions. The particle and collector surface potentials = -0 mV and 0 mV respectively; particle radius = 200 nm; collector diameter = 200 μm; porosity = 0.38;

temperature = 25 ˚C, Hamaker constant = $1x10^{-20}$ J; loading rate = 10^{-3} m/s; cut-off distance δ = 1 nm; and gravity number = 0. The curves correspond to the following flow field modified slip lengths: 0, 0.0001, 0.001, 0.01, 0.1 and 1.

6.4.3 Surface roughness effects on DLVO interaction energy

In Figure 6-4(a), the DLVO interaction energy curves between an approaching particle and collector surface with different roughness element sizes are presented as a function of the dimensionless separation distance (H). Notably, all of the calculated interaction energies are negative (indicating a net attractive force between the particle and collector surface); this is what would be expected in absence of an energy barrier to particle deposition. To quantitatively compare the interaction energies for different roughness sizes, the value of interaction energy at a cut off distance of 1 nm is presented in the inserted figure of Figure 6-4(a). When roughness element size increased from 0 to 600 nm, the absolute values of interaction energy first decreased to a minimum value and then increased. In this case, a critical roughness size around 60 nm resulted in the minimum absolute value of interaction energy. The magnitude of the attractive colloidal interactive force, which is the derivative of the interaction energy over the distance, decreased to a minimum and then increased correspondingly. According to DLVO theory, this greater attractive force should lead to higher particle deposition flux on the collector surface.

Dimensionless particle deposition flux on the collector surface as a function of the radial location on the spherical collector (θ) is presented in Figure 6-4(b) for different roughness features. Here, the gravity and slip-length effects for the flow field and the hydrodynamic retardation functions were "turned off" by setting the gravity number and roughness element a_r for hydrodynamic retardation functions to zero. All other physico-chemical parameters were identical to those in the Figure 6-3. The inserted figure describes the localized deposition flux for different roughness features when theta (θ) is equal to 100 º. Here, the overall and localized dimensionless particle deposition flux followed the same pattern as the change of the DLVO interaction energy along the radial distance from the spherical collector. Maximum deposition was achieved on the smooth surfaces when the roughness size was equal to zero. When the surface roughness size increased from 0 to 600 nm, the deposition

flux decreased to the minimum value, then it increased and reached a second maximum when the surface roughness increased beyond 60 nm and kept increasing until it reached the biggest roughness size investigated (600 nm). According to classic DLVO theory, the applied net forces on the approaching particle determine the final fate of particle deposition. A critical roughness size was identified through the simulation at 60 nm roughness and led to the minimum magnitude of applied force (Figure 6-4(a)) and accordingly, the minimum deposition flux (Figure 6-4(b)). This observation regarding the contribution of roughness to particle deposition is consistent to the experimental and numerical results obtained in parallel plate system, which indicated a non-linear, non-monotonic relationship between roughness size and particle deposition flux was observed when the DLVO interaction was the dominant mechanism driving deposition (69,70).

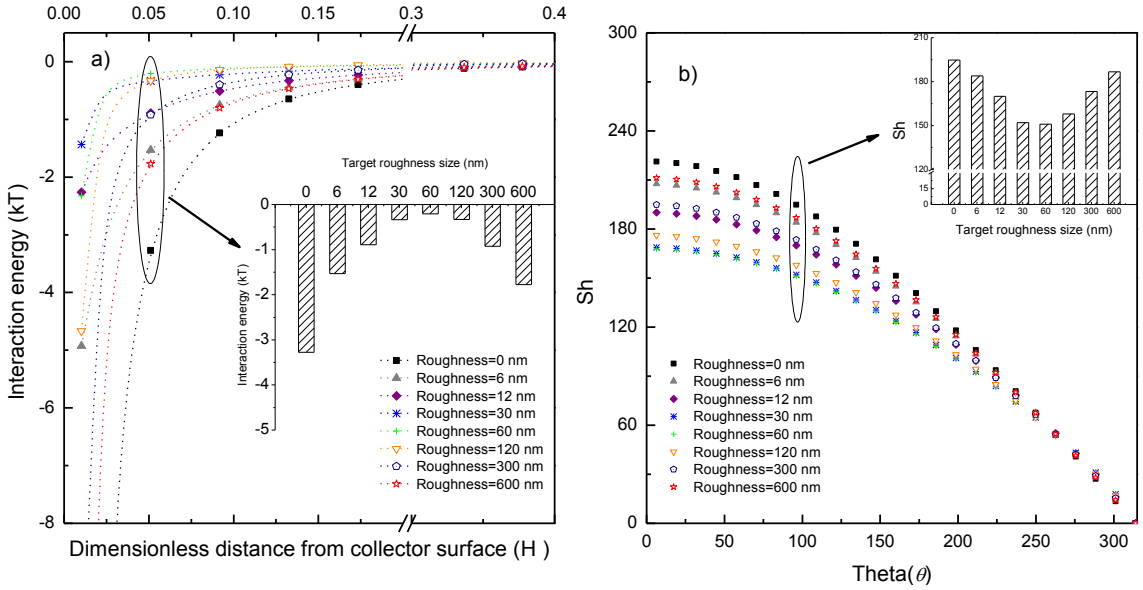

Figure 6-4. a) DLVO interaction energy curves and the absolute values of interaction energy at a cut-off distance of 1 nm for different roughness element sizes and b) particle flux for different roughness element size solely impacted by DLVO force and the corresponding flux at x*=100. Particle and collector surface potentials = -20mV and 20mV respectively; ionic strength = 100mM KCl; particle radius = 200nm; collector diameter = 200 µm; temperature = 25 ˚C; and Hamaker constant = $1x10^{-20}$ J. The curves correspond to rough spheres with radius a_r: 1, 2, 5, 10, 20, 50 and 100nm.

6.4.4 Surface roughness effects on particle deposition

In the previous sections, the effects of surface roughness on the flow field, hydrodynamic retardation effect, and the DLVO interaction energy on particle deposition flux on the spherical collectors were evaluated individually. Here, the responses of the particle deposition flux (*Sh*) to the spherical collector surfaces with different roughness due to all of the contributions explored above are assessed and discussed. The predicted deposition fluxes in the presence of the surface roughness using representative roughness values ranging from 0 to 60 nm are shown in Figure 6-5. The selected roughness sizes were limited to <100 nm to be consistent with the experimental assumption of roughness size that is smaller than approaching particle radius. All of the other physico-chemical parameters were identical to those utilized in Figure 6-4. In the simulations, a cut-off distance of 1nm was used for the closest location for attachment to avoid nonphysical divergence of VDW interactions at the contact surface. Preliminary calculations showed that the results did not change significantly when the cut-off distance was changing from 0.1 to 2 nm.

Particle deposition generally increased with increased nano-scale roughness at the conditions investigated; however, an overall non-linear, non-monotonic impact of surface roughness on particle deposition is demonstrated in Figure 6-5. When roughness size was smaller than 30 nm, particle deposition flux was not significantly enhanced by surface roughness. When the roughness size was greater than 30 nm, the increase in particle deposition flux was more pronounced. The slip-length for the flow field and the hydrodynamic retardation effect always have positive contributions to the deposition flux, whereas the DLVO interactions change non-linearly with roughness size, thereby having a non-linear, non-monotonic impact on the particle deposition flux. When the roughness was smaller than the critical roughness, DLVO interactions decreased with increased roughness size and counter-acted the enhanced deposition flux associated with increased flow velocity and reduced hydrodynamic retardation. When the roughness was greater than the critical size, the deposition flux increased substantially under the net effects from all of the mentioned forces acting upon the particle.

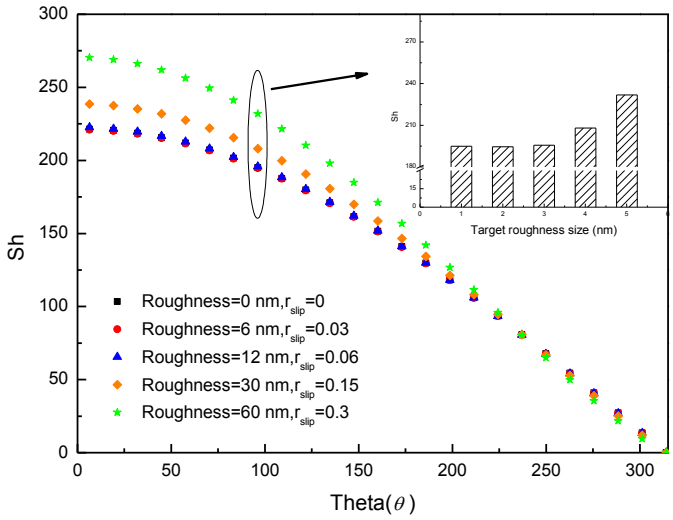

Figure 6-5. Particle deposition flux (*Sh*) for different roughness element sizes resulting from the concurrent impacts of modified flow field, hydrodynamic retardation functions and corresponding DLVO interactions. The curves correspond to rough spheres with radius a_r: 0, 1, 2, 5 and 10 nm respectively. Gravity number = 0; slip-length for flow field and hydrodynamic retardation functions = 0; particle and collector surface potentials = -20mV and 20mV respectively; ionic strength = 100mM KCl; particle radius = 200nm; collector diameter = 200 µm; temperature=25°C; and Hamaker constant = $1x10^{-20}$ J.

6.5 Evaluation of surface roughness impacts on particle deposition under different operational conditions.

Particle deposition flux on the spherical collector surfaces with different roughness sizes was evaluated as a function of particle loading rate, approaching colloidal particle size, and background electrolyte ionic strength. Selected roughness element sizes (6 nm, 30nm, 120 nm and 240 nm) were evaluated. Particle loading rates of 10^{-2}, 10^{-3}, 10^{-4} and 10^{-5} m/s were employed. Five sizes of particle radius (100nm, 200nm, 500nm, 750 nm and 1000 nm) were used to evaluate the effect of approaching particle size. Four levels of ionic strength (100mM, 50 mM 10mM and 1 mM KCl) satisfying the theoretical assumptions of pairwise summation method for DLVO interaction energy were evaluated. The effect of gravity was excluded from the simulations by setting approaching particle density to the density of water. The overall deposition flux on the entire collector surface (η) was calculated using Equation 6-9. The dimensionless particle deposition flux η/η_0 (the ratio of dimensionless flux under the

influence of all physico-chemical interactions to the flux impacted only by Brownian motion without consideration of DLVO interaction, gravity and hydrodynamic retardation effects - the Smoluchowshi-Levich approximation) was evaluated. The ratio η/η_0 was expected to be greater than 1.0 due to the attractive double layer force.

6.5.1 Effect of loading rate

Figure 6-6 depicts the cumulative particle deposition flux ratio (η/η_0) on a single spherical collector for different roughness element sizes as a function of different particle loading rates. To exclude the effect of EDL interactions, an ionic strength of 100 mM (the corresponding κ^{-1} was 0.96 nm) was chosen and the chemical potentials for the colloidal particle and collector were -20mV and +20 mV. The cut-off distance of 1 nm for flux determination from the model was chosen to avoid an unrealistic attractive force arising from VDW forces near the collector surface. The roughness size was between 6 nm and 240 nm with the roughness element radius between 1nm and 40 nm. The corresponding slip-lengths for the flow field and hydrodynamic retardation functions were between 0.003 and 1.2.

The estimated cumulative deposition flux ratio η/η_0 was always greater than unity, indicating that colloidal particle deposition was enhanced under the net effects of diffusion, convection, hydrodynamic retardation, and VDW and EDL interactions, as compared to the situation where particle deposition is solely diffusion dominated. Figure 6-6(a) depicts the cumulative deposition flux ratio as a function of different roughness sizes for various loading rates. At the same loading rate as shown in Figure 6-6(a), the roughness sizes examined had a positive impact on the cumulative deposition flux ratio η/η_0; specifically, bigger roughness size resulted in a higher η/η_0 ratio. The differences between the η/η_0 ratios obtained from simulations employing different roughness sizes on the collector are significant. For the same range of roughness sizes, the cumulative flux ratio was more sensitive when the loading rate was higher. At a lower loading rate (10^{-5} m/s), increased roughness element sizes on the spherical collectors only increased the η/η_0 ratio by 7 %. Here, the behavior of the colloidal particle was mainly dominated by pure convective and diffusive mechanisms (η_0) and the influence from the modified flow field, hydrodynamic retardation and DLVO forces was

relatively inconsequential. In contrast, when the loading rate increased to 10^{-2} m/s, convection became more significant to particle deposition and the cumulative flux ratio (η/η_0) increased 126% when the roughness size increased from 6 nm to 240 nm.

Figure 6-6(b) depicts the cumulative deposition flux ratio as a function of different loading rates for various roughness sizes. When the roughness is ranging from 6nm to 240 nm; however, the concurrent impact of loading rate and collector roughness size on approaching particle deposition was clearly non-linear and non-monotonic. While the loading rate is increasing from 10^{-5} to 10^{-2} m/s, the values of η/η_0 first decreased to a minimum value and then increased with the increased loading rate. A critical value of loading rate was observed for each roughness size; this contributed to the minimum value of η/η_0 that was observed in each scenario. Although, this critical value varied with different combinations of loading rate and roughness size, it was consistently observed.

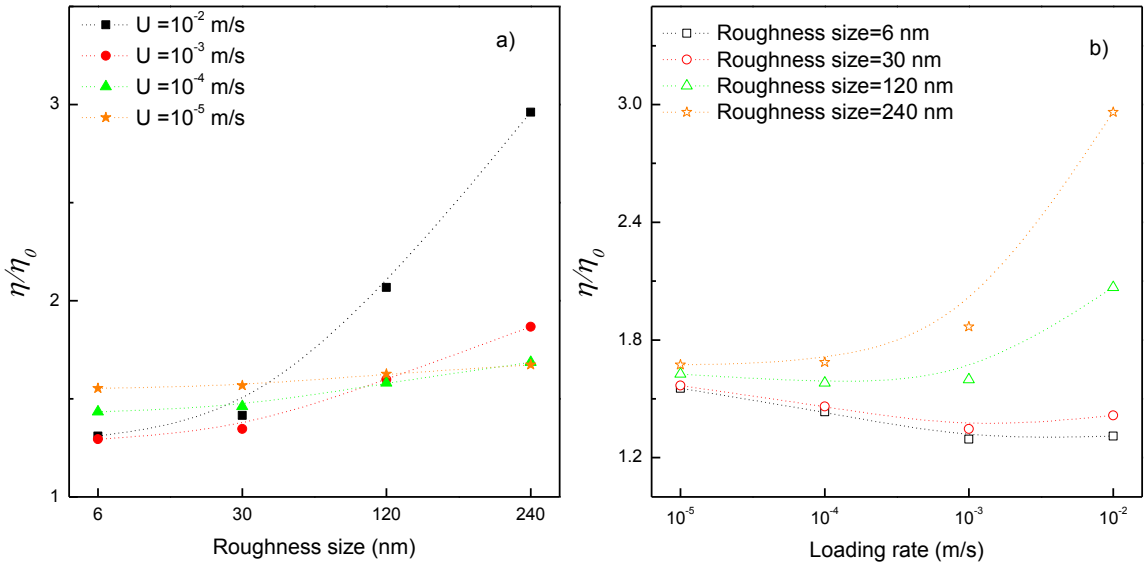

Figure 6-6. Cumulative particle deposition flux ratio (η/η_0) for a single spherical collector as a function of a) roughness size at different loading rates and b) loading rate at various roughness sizes. Gravity number = 0; particle and collector surface potentials = -20mV and 20mV respectively; ionic strength = 100mM KCl; particle radius = 200nm; collector diameter = 200 µm; temperature = 25 ˚C; Hamaker constant = 1x10^{-20} J; and porosity = 0.38. The curves correspond to rough spheres with radius a_r: 1, 5, 20 and 40 nm respectively.

6.5.2 Effect of particle size

The cumulative particle deposition flux ratio η/η_0 is plotted as a function of particle radius for different collector surface roughness sizes (Figure 6-7). Deposition of particles sized 100nm, 200nm, 500nm, 750 nm and 1000 nm in ***radius*** was simulated at a loading rate of 10^{-4} m/s. All of the η/η_0 ratios were greater than 1, indicating enhanced particle deposition by the net effect of flow field, hydrodynamic retardation and DLVO forces.

The contribution of particle size to cumulative particle deposition flux ratio η/η_0 was similar to that observed for loading rate. For a given particle size, rougher collector surfaces generally retained more particles at the conditions investigated. The extent of this enhanced deposition was greater for larger sized particles, as shown in Figure 6-7(a). For example, when roughness size increased from 6 to 240 nm, the η/η_0 ratio increased by 10.0% and 58.8% for 100 and 1000 nm particles, respectively. Bigger particles were also more sensitive to changes in roughness. Deposition of small particles were dominated by diffusion whereas bigger particles experienced a relatively lower degree of diffusion and changes in convection (flow field) and hydrodynamic retardation contributed governed the significant increases in deposition as a result of increased collector surface roughness; regardless of approaching particle size, but especially for larger particles.

Figure 6-7(b) depicts the cumulative deposition flux ratio for various roughness sizes as a function of particle radius. Notably, a minimum particle deposition flux was observed for particles approximately 1 μm in size (radius of ~500 nm); this is consistent with the well-known minimum deposition flux for smooth surfaces (1, 23, 66), with which the model developed herein shows excellent agreement (results not shown for smooth surfaces). Here, the values of η/η_0 varied considerably for different roughness element sizes, particularly for the larger 1.5 and 2.0 μm (750 and 1000 nm in radius) sized particles investigated.

When roughness size was small (6nm and 30 nm), the shape of deposition curves for different particle sizes followed a pattern similar to that of a smooth surface. In contrast, when the roughness size was relatively large (e.g., 120 nm and 240 nm), the "sag effect" (68) associated with the minimum values of η/η_0 was less pronounced, though still very evident.

When the roughness features of media are taken into the consideration, the shape of deposition curves (and thus also the single collector efficiency curves) can be altered significantly. Notably, the amount of minimum deposition and its relationship to critical roughness size and particle radius can markedly shift as well. When determining the particle size associated with the minimum deposition in a granular media filtration system, not only should particle size be considered (as it is in most contemporary modeling approaches), but roughness attributes such as roughness size and distribution also should be taken into the consideration. Without a doubt, where applicable, these considerations may contribute to explaining discrepancies between model-based expectations of minimum particle deposition or removal efficiencies for particles near 1.0 μm in size experimental investigations in which these relationships were not observed (26, 32, 67).

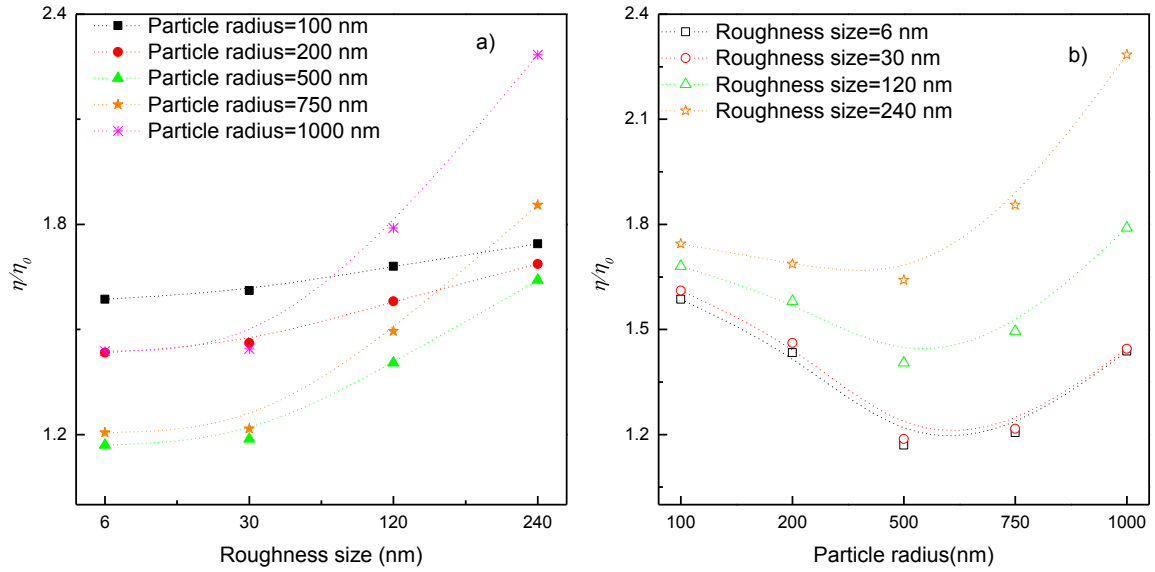

Figure 6-7. Cumulative particle deposition flux ratio (η/η_0) on a single spherical collector with a) different roughness element sizes as a function of different particle sizes and b) different particle size as a function of various roughness sizes. Gravity number = 0; particle and collector surface potentials = -20mV and 20mV respectively; ionic strength = 100mM KCl; loading rate = 10^{-4} m/s; collector diameter = 200 μm; temperature = 25°C; Hamaker constant = $1x10^{-20}$ J; porosity = 0.38. The curves correspond to rough spheres with radius a_r: 1, 5, 20 and 40 nm.

6.5.3 Effect of ionic strength

The cumulative particle deposition flux ratio η/η_0 is plotted as a function of bulk solution ionic strength for different collector surface roughness element sizes (Figure 6-8). Four levels of ionic strength (1mM, 10mM, 50 mM and 100mM KCl) were selected for the simulations. A 200 nm approaching particle radius and a 10^{-4} m/s loading rate were utilized. Other physico-chemical parameters were identical to those used in Figure 6-7.

For a given ionic strength, increased surface roughness consistently resulted in increased particle deposition at the conditions investigated (Figure 6-8(a)). When roughness increased from 6 to 240 nm, the values of η/η_0 ratio increased similarly, regardless the changes of ionic strength. The presence of roughness decreased the hydrodynamic retardation effect. Bigger roughness results in less retardation and therefore facilitates more particles to approach the vicinity of collector surfaces. Without the presence of an energy barrier (as was the case for all of the simulated scenarios), more deposition flux was expected.

For a given roughness size, particle deposition slightly decreased due to the more compressed double-layer and the reduced EDL force when ionic strength increased from 1 mM to 100mM (Figure 6-8(b)). Nonetheless, the DLVO forces were always attractive across the range of investigated ionic strengths and, as would be expected, their impacts did not significantly affect particle deposition. With the changes in ionic strength, the Debye- Hückel length (κ^{-1}) increased from 1 nm to only 10 nm. Therefore, only a small number of colloidal particles were under the influence of the extended attractive double layer force and contributed to enhanced deposition; accordingly, a significant amount of deposition enhancement was not observed. This result is consistent with other reported data that indicate that the enhancement due to ionic strength is not significant when it is higher than the equivalent of 0.1mM KCl (13).

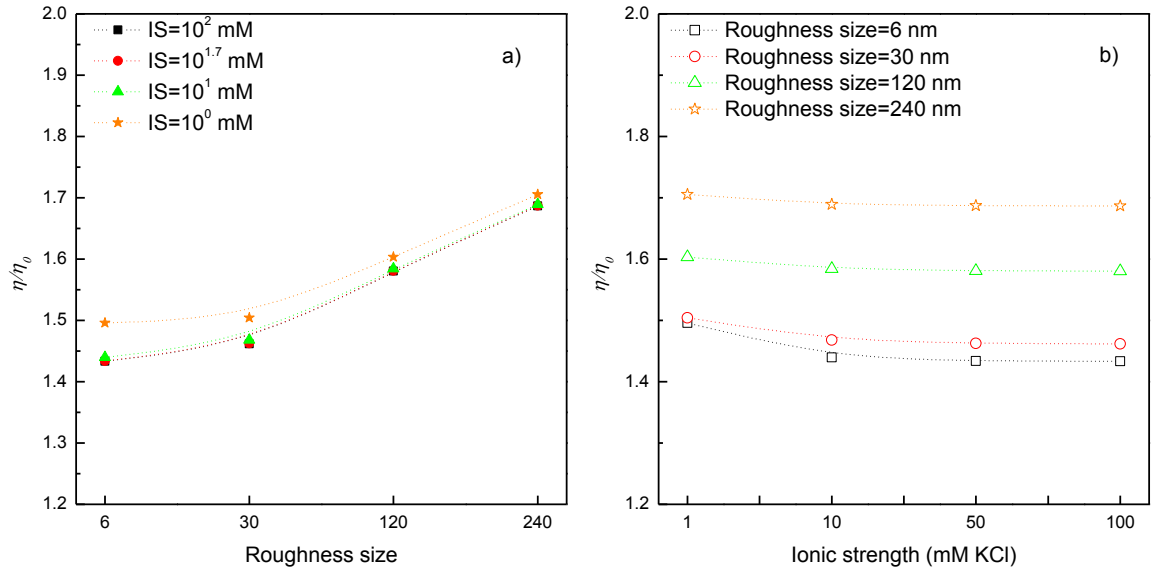

Figure 6-8. Cumulative particle deposition flux ratio (η/η_0) on a single spherical collector with a) different roughness element sizes as a function of various ionic strengths and b) different ionic strengths as a function of various roughness size. Gravity number = 0; particle and collector surface potentials = -20mV and 20mV respectively; loading rate = 10^{-4} m/s; particle radius = 200 nm; collector diameter = 200 μm; temperature = 25°C; Hamaker constant = $1x10^{-20}$ J; and porosity=0.38. The curves corresponded to the following radii of roughness spheres a_r: 1, 5, 20 and 40 nm respectively.

A non-linear impact of surface roughness on particle deposition has been demonstrated in the present study. Here, it is demonstrated that the non-linear, non-monotonic impact of nano-scale roughness on collector surfaces roughness on particle deposition is consistently observed, regardless of particle size, particle loading rate, and background electrolyte solution ionic strength. The relative magnitude of this impact depended on the combination of operational parameters. It is important to incorporate surface roughness into the Convection-Diffusion equation, with accurate representation of its associated impacts on the flow field, hydrodynamic retardation, and DLVO forces. When determining the particle size associated with the minimum deposition in a granular media filtration system, not only should particle size be considered, but roughness attributes such as roughness size and distribution also should be taken into the consideration. Without a doubt, where applicable, these considerations may contribute to explaining discrepancies between model-based expectations and experimental outcomes.

6.6 References

1. Yao, K.M.; Habibian, M.M.; O'Melia, C.R. Water and Waste Water Filtration - Concepts and Applications. *Environ. Sci. Technol.* **1971,** *5* (11), 1105-&.

2. Tufenkji, N.; Ryan, J.N.; Elimelech, M. The promise of bank filtration. *Environ. Sci. Technol.* **2002,** *36* (21), 422A-428A.

3. Tien, C. Hydrosol deposition in porous media: the effect of surface interactions. *Advanced Powder Technology* **2000,** *11* (1), 9-56.

4. Schijven, J.F. and Hassanizadeh, S.M. Removal of viruses by soil passage: Overview of modeling, processes, and parameters. *Crit. Rev. Environ. Sci. Technol.* **2000,** *30* (1), 49-127.

5. Adamczyk, Z. and Weronski, P. Application of the DLVO theory for particle deposition problems. *Adv. Colloid Interface Sci.* **1999,** *83* (1-3), 137-226; 10.1016/S0001-8686(99)00009-3.

6. Elimelech, M. Particle deposition on ideal collectors from dilute flowing suspensions: Mathematical formulation, numerical solution, and simulations. *Separations Technology* **1994,** *4* (4), 186-212.

7. Adamczyk, Z. and Vandeven, T.G.M. Deposition of Particles Under External Forces in Laminar-Flow through Parallel-Plate and Cylindrical Channels. *J. Colloid Interface Sci.* **1981,** *80* (2), 340-356; 10.1016/0021-9797(81)90193-4.

8. Prieve, D.C. and Lin, M.M.J. Adsorption of Brownian Hydrosols Onto a Rotating-Disk Aided by a Uniform Applied Force. *J. Colloid Interface Sci.* **1980,** *76* (1), 32-47.

9. Yang, J.L.; Bos, R.; Poortinga, A.; Wit, P.J.; Belder, G.F.; Busscher, H.J. Comparison of particle deposition in a parallel plate and a stagnation point flow chamber. *Langmuir* **1999,** *15* (13), 4671-4677; 10.1021/la981607k.

10. Chen, G.; Bedi, R.S.; Yan, Y.S.; Walker, S.L. Initial Colloid Deposition on Bare and Zeolite-Coated Stainless Steel and Aluminum: Influence of Surface Roughness. *Langmuir* **2010,** *26* (15), 12605-12613; 10.1021/la101667t.

11. Ma, H.L.; Pedel, J.; Fife, P.; Johnson, W.P. Hemispheres-in-Cell Geometry to Predict Colloid Deposition in Porous Media (vol 43, pg 8573, 2009). *Environ. Sci. Technol.* **2010,** *44* (11), 4383-4383; 10.1021/es1009373 ER.

12. Nelson, K.E. and Ginn, T.R. New collector efficiency equation for colloid filtration in both natural and engineered flow conditions. *Water Resour. Res.* **2011,** *47* (5).

13. Elimelech, M. and Song, L. Theoretical investigation of colloid separation from dilute aqueous suspensions by oppositely charged granular media. *Separations Technology* **1992,** *2* (1), 2-12; http://dx.doi.org.proxy.lib.uwaterloo.ca/10.1016/0956-9618(92)80001-T.

14. Jegatheesan, V.; Vigneswaran, S.; Lee, S.H. Deposition of submicron particles in deep bed filtration under unfavorable surface conditions. *Korean Journal of Chemical Engineering* **2005,** *22* (1), 142-146.

15. Hahn, M.W. and O'Melia, C.R. Deposition and reentrainment of Brownian particles in porous media under unfavorable chemical conditions: Some concepts and applications. *Environ. Sci. Technol.* **2004,** *38* (1), 210-220; 10.1021/es030416n.

16. Johnson, W.P.; Tong, M.; Li, X. On colloid retention in saturated porous media in the presence of energy barriers: The failure of alpha, and opportunities to predict eta. *Water Resour. Res.* **2007,** *43* (12), W12S13; 10.1029/2006WR005770.

17. Elimelech, M.; Jia, X.; Gregory, J.; Williams, R. *Particle deposition & aggregation: measurement, modelling and simulation.* Butterworth-Heinemann: 1998; .

18. Logan, B.E.; Jewett, D.G.; Arnold, R.G.; Bouwer, E.J.; Omelia, C.R. Clarification of Clean-Bed Filtration Models. *Journal of Environmental Engineering-Asce* **1995,** *121* (12), 869-873.

19. Knappett, P.S.K.; Emelko, M.B.; Zhuang, J.; McKay, L.D. Transport and retention of a bacteriophage and microspheres in saturated, angular porous media: Effects of ionic strength and grain size. *Water Res.* **2008,** *42* (16), 4368-4378; 10.1016/j.watres.2008.07.041.

20. Walshe, G.E.; Pang, L.; Flury, M.; Close, M.E.; Flintoft, M. Effects of pH, ionic strength, dissolved organic matter, and flow rate on the co-transport of MS2 bacteriophages with kaolinite in gravel aquifer media. *Water Res.* **2010,** *44* (4), 1255-1269; 10.1016/j.watres.2009.11.034.

21. Jewett, D.G.; Hilbert, T.A.; LoganM, B.E.; Arnold, R.G.; Bales, R.C. Bacterial transport in laboratory columns and filters: influence of ionic strength and pH on collision efficiency. *Water Res.* **1995,** *29* (7), 1673-1680; 10.1016/0043-1354(94)00338-8.

22. Ryan, J.N. and Elimelech, M. Colloid mobilization and transport in groundwater. *Colloids and Surfaces A-Physicochemical and Engineering Aspects* **1996,** *107*, 1-56.

23. Tufenkji, N. and Elimelech, M. Correlation equation for predicting single-collector efficiency in physicochemical filtration in saturated porous media. *Environ. Sci. Technol.* **2004,** *38* (2), 529-536; 10.1021/es034049r.

24. Rizwan, T. and Bhattacharjee, S. Particle Deposition onto Charge-Heterogeneous Substrates. *Langmuir* **2009,** *25* (9), 4907-4918; 10#1021/la804075g ER.

25. Nazemifard, N.; Masliyah, J.H.; Bhattacharjee, S. Particle deposition onto micropatterned charge heterogeneous substrates: Trajectory analysis. *J. Colloid Interface Sci.* **2006,** *293* (1), 1-15; 10.1016/j.jcis.2005.06.033 ER.

26. Tufenkji, N. and Elimelech, M. Breakdown of colloid filtration theory: Role of the secondary energy minimum and surface charge heterogeneities. *Langmuir* **2005,** *21* (3), 841-852; 10.1021/la048102g.

27. Hahn, M.W.; Abadzic, D.; O'Melia, C.R. Aquasols: On the role of secondary minima. *Environ. Sci. Technol.* **2004,** *38* (22), 5915-5924; 10.1021/es049746d.

28. Tang, H.; Cao, T.; Liang, X.; Wang, A.; Salley, S.O.; McAllister,James,,II; Ng, K.Y.S. Influence of silicone surface roughness and hydrophobicity on adhesion and colonization of Staphylococcus epidermidis. *Journal of Biomedical Materials Research Part a* **2009,** *88A* (2), 454-463; 10.1002/jbm.a.31788.

29. Vanhaecke, E.; Remon, J.P.; Moors, M.; Raes, F.; Derudder, D.; Vanpeteghem, A. Kinetics of Pseudomonas-Aeruginosa Adhesion to 304 and 316-L Stainless-Steel - Role of Cell-Surface Hydrophobicity. *Appl. Environ. Microbiol.* **1990,** *56* (3), 788-795.

30. Hoek, E.M.V. and Agarwal, G.K. Extended DLVO interactions between spherical particles and rough surfaces. *J. Colloid Interface Sci.* **2006,** *298* (1), 50-58; 10.1016/j.jcis.2005.12.031.

31. Huang, X.F.; Bhattacharjee, S.; Hoek, E.M.V. Is Surface Roughness a "Scapegoat" or a Primary Factor When Defining Particle-Substrate Interactions? *Langmuir* **2010,** *26* (4), 2528-2537; 10.1021/la9028113 ER.

32. Johnson, W.P.; Ma, H.L.; Pazmino, E. Straining Credibility: A General Comment Regarding Common Arguments Used to Infer Straining As the Mechanism of Colloid Retention in Porous Media. *Environ. Sci. Technol.* **2011,** *45* (9), 3831-3832; 10.1021/es200868e ER.

33. Bradford, S.A.; Torkzaban, S.; Walker, S.L. Coupling of physical and chemical mechanisms of colloid straining in saturated porous media. *Water Res.* **2007,** *41* (13), 3012-3024; 10.1016/j.watres.2007.03.030.

34. Johnson, P.R. and Elimelech, M. Dynamics of Colloid Deposition in Porous-Media - Blocking Based on Random Sequential Adsorption. *Langmuir* **1995,** *11* (3), 801-812.

35. Adamczyk, Z. Particle adsorption and deposition: role of electrostatic interactions. *Adv. Colloid Interface Sci.* **2003,** *100*, 267-347; 10.1016/S0001-8686(02)00062-3.

36. Henry, C.; Minier, J.; Lefevre, G. Numerical Study on the Adhesion and Reentrainment of Nondeformable Particles on Surfaces: The Role of Surface Roughness and Electrostatic Forces. *Langmuir* **2012,** *28* (1), 438-452; 10.1021/la203659q.

37. Walz, J.Y. and Sun, N. Effects of surface roughness on van der Waals and electrostatic contributions to particle-particle interactions and particle adhesion. *Particles of Surfaces 7: Detection, Adhesion and Removal* **2002,** , 151-169.

38. Suresh, L. and Walz, J.Y. Direct measurement of the effect of surface roughness on the colloidal forces between a particle and flat plate. *J. Colloid Interface Sci.* **1997,** *196* (2), 177-190.

39. Darbha, G.K.; Schaefer, T.; Heberling, F.; Luettge, A.; Fischer, C. Retention of Latex Colloids on Calcite as a Function of Surface Roughness and Topography. *Langmuir* **2010,** *26* (7), 4743-4752; 10.1021/la9033595.

40. Shellenberger, K. and Logan, B.E. Effect of molecular scale roughness of glass beads on colloidal and bacterial deposition. *Environ. Sci. Technol.* **2002,** *36* (2), 184-189; 10.1021/es015515k ER.

41. Henry, C.; Minier, J.; Lefevre, G.; Hurisse, O. Numerical Study on the Deposition Rate of Hematite Particle on Polypropylene Walls: Role of Surface Roughness. *Langmuir* **2011,** *27* (8), 4603-4612; 10.1021/la104488a.

42. Morales, V.L.; Gao, B.; Steenhuis, T.S. Grain Surface-Roughness Effects on Colloidal Retention in the Vadose Zone. *Vadose Zone Journal* **2009,** *8* (1), 11-20; 10.2136/vzj2007.0171.

43. Barnes, L.; Lo, M.; Adams, M.; Chamberlain, A. Effect of milk proteins on adhesion of bacteria to stainless steel surfaces. *Appl. Environ. Microbiol.* **1999,** *65* (10), 4543-4548.

44. Mitik-Dineva, N.; Wang, J.; Truong, V.K.; Stoddart, P.; Malherbe, F.; Crawford, R.J.; Ivanova, E.P. Escherichia coli, Pseudomonas aeruginosa, and Staphylococcus aureus Attachment Patterns on Glass Surfaces with Nanoscale Roughness. *Curr. Microbiol.* **2009,** *58* (3), 268-273; 10.1007/s00284-008-9320-8.

45. Eichenlaub, S.; Gelb, A.; Beaudoin, S. Roughness models for particle adhesion. *J. Colloid Interface Sci.* **2004,** *280* (2), 289-298; 10.1016/j.jcis.2004.08.017.

46. Komvopoulos, K. and Yan, W. A fractal analysis of stiction in microelectromechanical systems. *J. Tribol. -Trans. ASME* **1997,** *119* (3), 391-400; 10.1115/1.2833500.

47. Nazemifard, N.; Masliyah, J.H.; Bhattacharjee, S. Particle deposition onto charge heterogeneous surfaces: Convection-diffusion-migration model. *Langmuir* **2006,** *22* (24), 9879-9893; 10.1021/la061702q ER.

48. Chatterjee, R.; Mitra, S.K.; Bhattacharjee, S. Particle Deposition onto Janus and Patchy Spherical Collectors. *Langmuir* **2011,** *27* (14), 8787-8797; 10.1021/la201421n.

49. Song, L.; Johnson, P.; Elimelech, M. Kinetics of Colloid Deposition Onto Heterogeneously Charged Surfaces in Porous-Media. *Environ. Sci. Technol.* **1994,** *28* (6), 1164-1171; 10.1021/es00055a030.

50. Tien, C. and Ramarao, B.V. *Granular filtration of aerosols and hydrosols.* Access Online via Elsevier: 2011; .

51. Happel, J. Viscous flow in multiparticle systems: Slow motion of fluids relative to beds of spherical particles. *AICHE J.* **1958,** *4* (2), 197-201; 10.1002/aic.690040214.

52. Tien, C. and Payatakes, A.C. Advances in Deep Bed Filtration. *AICHE J.* **1979,** *25* (5), 737-759.

53. Zhu, Y.X. and Granick, S. Limits of the hydrodynamic no-slip boundary condition. *Phys. Rev. Lett.* **2002,** *88* (10), 106102; 10.1103/PhysRevLett.88.106102.

54. Bonaccurso, E.; Butt, H.J.; Craig, V.S.J. Surface roughness and hydrodynamic boundary slip of a newtonian fluid in a completely wetting system. *Phys. Rev. Lett.* **2003,** *90* (14), 144501; 10.1103/PhysRevLett.90.144501.

55. Kunert, C.; Harting, J.; Vinogradova, O.I. Random-Roughness Hydrodynamic Boundary Conditions. *Phys. Rev. Lett.* **2010,** *105* (1), 016001; 10.1103/PhysRevLett.105.016001.

56. Neto, C.; Evans, D.; Bonaccurso, E.; Butt, H.; Craig, V. Boundary slip in Newtonian liquids: a review of experimental studies. *Reports on Progress in Physics* **2005,** *68* (12), 2859-2897; 10.1088/0034-4885/68/12/R05.

57. Vinogradova, O.I. and Belyaev, A.V. Wetting, roughness and flow boundary conditions. *Journal of Physics-Condensed Matter* **2011,** *23* (18), 184104; 10.1088/0953-8984/23/18/184104.

58. Brenner, H. The Slow Motion of a Sphere through a Viscous Fluid Towards a Plane Surface. *Chem. Eng. Sci.* **1961,** *16* (3-4), 242-251; 10.1016/0009-2509(61)80035-3.

59. Goldman, A.J.; Cox, R.G.; Brenner, H. Slow Viscous Motion of a Sphere Parallel to a Plane Wall .I. Motion through a Quiescent Fluid. *Chemical Engineering Science* **1967,** *22* (4), 637-&; 10.1016/0009-2509(67)80047-2.

60. Goldman, A.J.; Cox, R.G.; Brenner, H. Slow Viscous Motion of a Sphere Parallel to a Plane Wall .2. Couette Flow. *Chemical Engineering Science* **1967,** *22* (4), 653-&; 10.1016/0009-2509(67)80048-4.

61. O'Neill, M.E. A Sphere in Contact with a Plane Wall in a Slow Linear Shear Flow. *Chemical Engineering Science* **1968,** *23* (11), 1293-&; 10.1016/0009-2509(68)89039-6.

62. Kemps, J.A.L. and Bhattacharjee, S. Interactions between a solid spherical particle and a chemically heterogeneous planar substrate. *Langmuir* **2005,** *21* (25), 11710-11721; 10.1021/la051292q ER.

63. Hogg, R.; Healy, T.W.; Fuersten.Dw Mutual Coagulation of Colloidal Dispersions. *Transactions of the Faraday Society* **1966,** *62* (522P), 1638-&; 10.1039/tf9666201638.

64. Walz, J.Y. The effect of surface heterogeneities on colloidal forces. *Adv. Colloid Interface Sci.* **1998,** *74*, 119-168.

65. Redman, J.A.; Walker, S.L.; Elimelech, M. Bacterial Adhesion and Transport in Porous Media: Role of the Secondary Energy Minimum. *Environ. Sci. Technol.* **2004,** *38* (6), 1777-1785; 10.1021/es034887l.

66. Rajagopalan, R. and Tien, C. Single Collector Analysis of Collection Mechanisms in Water Filtration. *Can. J. Chem. Eng.* **1977,** *55* (3), 246-255.

67. Bradford, S.A.; Simunek, J.; Bettahar, M.; van Genuchten, M.T.; Yates, S.R. Significance of straining in colloid deposition: Evidence and implications. *Water Resour. Res.* **2006,** *42* (12), W12S15; 10.1029/2005WR004791.

68. Jin, C. and Emelko, M.B. Non-linear, non-monotonic impact of surface roughness on colloidal particle deposition during granular media filtration at favorable conditions. *Environ. Sci. Technol.* **2014,** *to be submitted*

69. Jin, C.; Glawdel, T.; Ren, C.; Emelko, M.B. Non-Linear, non-monotonic impact of nano-scale surface roughness on colloidal particle deposition. I. Experiments in a parallel plate system. *Langmuir* **2014,** *to be submitted*

70. Jin, C.; Glawdel, T.; Ren, C.; Emelko, M.B. Non-Linear, non-monotonic impact of nano-scale roughness on particle deposition: II. Numerical modeling. *Langmuir* **2014,** *to be submitted*

Chapter 7

Conclusions

7.1 Overall significance of this work

An understanding of particle deposition on surfaces is critical to a wide range of applications including chemical and microbial fate and transport in the environment, chromatographic separation, semiconductor manufacturing, membrane fouling, enhanced oil recovery, and human health to name a few. The transport and fate of particles including microorganisms during physico-chemical filtration in natural and engineered aquatic environments remains essential for effective and sustainable drinking water treatment and wastewater reclamation, as well as understanding and assessing the risk of environmental contamination of water supplies. The development of models to predict particle deposition by physico-chemical filtration has been ongoing since the 1960's. What is now considered classical colloid filtration theory (CFT) was developed in the 1970's to predict particle removal during granular media filtration used for drinking water treatment. More recently, CFT has been applied to various applications related to subsurface particle and microbial transport and fate, including riverbank filtration, aquifer storage and recovery, bioremediation, and assessment of contaminant transport and fate.

The classical theory of colloidal stability developed by Derjaguin, Landau, Verwey, and Overbeek, collectively known as the DLVO theory, is typically used in CFT models to describe the interactions between particles and media grain (collector) surfaces. Traditionally used to evaluate the total interaction energy as a function of separation distance between a non-biological particle and a flat surface, DLVO theory considers the sum of repulsive electrostatic double layer and attractive van der Waals forces. Significant discrepancies between predictions of particle deposition from current CFT models and experimental observations have been reported. While several model variations of CFT have been reported, models focusing on integration of impacts of collector surface geometry and physically-based mechanisms such as hydrodynamics have been rarely reported.

The results of this study prove that factors like collector surface roughness should be considered when modeling particle transport and fate because they may substantially impact particle deposition – this type of significant impact was demonstrated herein for some cases of surface roughness. A non-linear, non-monotonic relationship between particle deposition and collector surface roughness was identified and confirmed through experiments and numerical modeling in a parallel plate chamber and a bed packed with a porous medium. A mathematical model framework incorporating surface roughness and associated effects of hydrodynamics on particle deposition was developed, verified, and shown to result in improved particle deposition prediction capacity.

7.2 Conclusions

Several key conclusions have been demonstrated from this work. They include:

1. There is a significant non-linear, non-monotonic relationship or "sag effect" between collector surface roughness size and particle deposition. Experimental observations in packed columns and a parallel plate chamber verified that the presence of roughness significantly impacted the deposition of colloidal particles. The well-controlled operational conditions applied in the present investigation minimized and essentially excluded the confounding impacts of surface chemical heterogeneity, surface hydrophobicity, a secondary energy minimum, particle aggregation and blocking effects.

   Depending on the physico-chemical conditions of the system, a dynamic equilibrium can be reached between the forces that favor and impair particle attachment to collector surfaces. Increases in particle deposition due to increased roughness on media surfaces (relative to smooth media) can be explained by lower interaction action energies that result in more attractive DLVO forces. Flow velocity conditions, the shear lift force, and particle rolling may help to explain the observed experimental observations as they can contribute to reduced particle deposition (relative to smooth surfaces) when a colloidal particle interacts with media surface

roughness features. The results of this study underscore the need for experimental investigation and mathematical modeling to further elucidate the forces and mechanisms that govern this non-linear, non-monotonic impact of media surface roughness on particle deposition.

2. The morphology (size and distribution) of collector surface roughness is significant to particle deposition.

3. The deposition of smaller particles on surfaces is more sensitive to surface roughness than that of larger particles in parallel plate chamber. In contrast, the deposition of bigger particles is more sensitive to surface roughness in porous media .

4. The effect of gravity cannot be excluded *a priori* during development of predictive mathematical models of clean bed colloidal particle deposition. This underscores the importance of including precise measurements of particle size and density in modeling simulations.

In the parallel plate experiments, the deposition flux curves along the flow direction showed different patterns for different sizes of particles. When diffusion dominated the deposition process (for smaller particles), maximum particle deposition (Sh_{exp}) was observed at the inlet of the parallel plate chamber. Particle deposition then decreased asymptotically with increasing distance from the inlet to the chamber (consistent with the analytical solution for particle deposition). When gravity dominated the deposition process (for larger particles), the deposition rate gradually increased with the distance from the chamber inlet and reached a plateau, while the minimum deposition flux was observed at the inlet of the chamber.

The observed deposition flux was not uniformly distributed across the entire length of the target surface because the magnitude of deposition rate was related to the distance to the inlet of parallel chamber. It was critical to determine the distance to the

chamber inlet when comparing deposition rates for different operational scenarios. As with most experimental work, quality assurance and control was critical for obtaining accurate and reproducible results. Well-controlled operational conditions (e.g. uniform flow rate, isolated spheres, adequate initial particle concentration, proper washing procedures to enable slide reuse, etc), precise measurements of particle deposition (e.g. on-line measurement without disturbance, enumeration program to exclude moving or aggregated particles) and appropriate number of acquired data were required.

5. Predictive mathematical modeling of clean bed colloidal particle deposition influenced by nano-scale surface roughness in absence of an energy barrier can be achieved using the convective-diffusion equation and classic CFT approaches. It requires incorporation of numerical modifications to appropriately flow field profile, hydrodynamic retardation functions, and DLVO interaction energy.

   The approaches used to represent the flow field, hydrodynamic retardation, DLVO forces, flow field boundary conditions, and convective-diffusion equation boundary conditions were individually validated by comparing simulation results to previously reported analytical solutions. The study in Chapter 5 was the first to use a slip flow boundary condition in filtration modeling. By implementing a dimensionless slip-length, the flow velocity at the contact surface increased and the hydrodynamic retardation effects decreased. The change in the flow field only slightly increased the deposition flux; however, the change in the hydrodynamic retardation functions significantly improved the deposition flux rate. It was found in the simulations that small-scale roughness (1 – 10% of the particle radius) enhanced the particle deposition flux significantly. Particle deposition flux was less sensitive to changes in roughness size when the roughness was greater than 10% of the particle radius.

6. The location of the perfect sink boundary is critical to achieving accurate numerical results from predictive mathematical models of clean bed colloidal particle deposition influenced by nano-scale surface roughness. Further research regarding short-range forces is needed to better determine the most appropriate cut-off distance (δ) for the prefect sink boundary.

7. Overall, this work demonstrated that nano-scale surface roughness and associated hydrodynamics can impact on particle deposition. These impacts can and should be incorporated into predictive mathematical models of clean bed colloidal particle deposition.

Chapter 8
Recommendations and future work

8.1 Recommendations

This thesis work focuses on how surface roughness impacts particle deposition on surfaces. Among numerous applications, this research is directly relevant to physico-chemical filtration in natural and engineered drinking water treatment; the experiments discussed herein were designed and conducted at operational conditions relevant to several water treatment applications including rapid sand filtration and subsurface filtration. Based on the results of this study, recommendations are made for further experimental work on particle removal (mass transfer) in packed bed filters and parallel plate chambers (Section 8.1.1), modeling studies focused on improved mechanistic understanding and mathematical representation of phyisco-chemical filtration processes (Section 8.1.2) and water treatment plant operations and maintenance (Section 8.1.3).

8.1.1 Experimental research recommendations

The following recommendations are for quality assurance when investigating particle deposition in parallel plate chamber investigations.

1. Quantitatively evaluate the size and distribution of surface roughness elements on the deposition surface.
2. Avoid particle/microorganism aggregation using methods that do not affect particle surface chemistry (e.g., brief sonication vs. surfactant addition) and confirm outcome (particle size distribution evaluation).
3. Accurately determinate particle density and size.
4. Select an appropriate initial particle concentration to avoid particle aggregation during the investigation to ensure accuracy of particle removal performance evaluation and reasonable experimental duration.

5. Thoroughly clean experimental apparatus to prevent carryover of attached particles between experiments.
6. Evaluate particle deposition at multiple locations along the direction of flow in the chamber because the extent of deposition will change along this distance.
7. Accurately enumerate deposited particles, taking care to exclude aggregated or moving particles;
8. Whenever possible, collect replicate samples and conduct replicate experiments to ensure adequate statistical power in making inferences from the data.
9. Characterize the physico-chemical properties of the target surface using methods such as SEM, AFM, contact angle measurement, and XRD.

The following recommendations are for quality assurance when investigating particle deposition in packed bed filters (i.e., column tests).

1. Characterize the physico-chemical properties of the selected media including surface roughness (size and distribution), hydrophobicity, porosity, angularity, and zeta potential.
2. Check the media packing by conducting a tracer test (using an inert tracer) before each experiment.
3. Avoid particle/microorganism aggregation using methods that do not affect particle surface chemistry (e.g., brief sonication vs. surfactant addition) and confirm outcome (particle size distribution evaluation).
4. Use suitable enumeration method for quantitative analysis of particle removal (*e.g.*, standard concentration curves and spectrophotometric enumeration for higher particle concentrations or manual enumeration using microscopy for low particle concentrations).

5. Quantify mass recovery (and associated mass loss) after each experiment by using destructive sampling to enumerate particles attached within the column.

8.1.2 Modeling recommendations

This research demonstrated that the presence of surface roughness and its associated implications to the flow velocity field, hydrodynamic retardation and DLVO forces should not be ignored when investigating particle deposition. The contributions of physical factors have to be taken into the consideration in the numerical models. The following recommendations are made for further investigating the contributions of other mechanisms (e.g. macroscale roughness, hydrophobicity *etc.*) on particle deposition using numerical modeling.

1. Discretize and mesh the simulation domain extensively where large gradients exist, using subdomains if necessary.
2. Validate the numerical methods/formulae before implementing these terms in the simulators (*e.g.*, linear approximation for the Poisson-Boltzmann equation for chemical potential).
3. Derive the governing equations from first principles (conservation law, *etc.*), including all terms (where possible) to minimize approximation.
4. Investigate and validate the contributions of individual terms using different numerical methods if possible (*e.g.* Eulerian and Lagrangian methods respectively).

Before implementing the models developed in this study, the following questions related to modeling the effect of surface roughness on particle deposition should be answered quantitatively.

1. What type of surface roughness is studied (e.g., nano-scale, micro-scale macro-scale)?

2. Where is the primary energy minimum (alternatively, the cut-off distance to the collector surface) located? This is needed to determine the overall particle flux deposition over the collector surface when surface roughness is present.
3. What are the exact values required for the dimensionless slip-length used to account for roughness-associated changes in flow field and hydrodynamic retardation functions?
4. What are the contributions of chemical heterogeneity and hydrophobicity on the magnitude of dimensionless slip-length?
5. What is the role of short range forces in the process of particle attachment?
6. Are all of the relevant forces/interactions/mechanisms included in the mathematical frameworks describing mass-transfer?

8.1.3 Recommendations in practice

Although this research focused on lab-scale studies, it is still directly relevant to water treatment practice because surface roughness is ubiquitous on filtration media (i.e., collectors) in natural and engineered systems. The scale of surface roughness (i.e., size of roughness elements) and its range of potential impacts on particle deposition are not necessarily negligible and should be considered when designing and evaluating physico-chemical filtration processes. The following recommendations are for water treatment research and practice.

1. Determinate the non-linear, non-monotonic relationship between collector surface roughness size and particle deposition efficiency at pilot-scale.
2. Use the non-linear, non-monotonic relationship between collector surface roughness size and particle deposition efficiency obtained at pilot-scale to determine optimal media characteristics (including roughness) for enhancing particle removal efficiency concurrently with operational targets.

3. Determinate the effect of various operational conditions (*e.g*. loading rate, temperature, chemical coagulant dosage, *etc*.) on the physico-chemical filtration using rough media.
4. Evaluate the impact of surface roughness in biological filtration systems.

8.2 Future research

Other than the recommendations provided in Section 8.1, further fundamental investigation is essential for understanding the particle deposition process. Classic DLVO theory should be improved to incorporate the presence of short range forces, chemical heterogeneity and hydrophobicity. The impact of these mechanisms is observed experimentally, but not well studied and characterized from a modeling perspective. A theoretical framework that includes all of the interactions and can well describe experimental observations is still missing, especially when the energy barrier to deposition is large.

Theoretical studies on the slip-length in the presence of surface roughness and hydrophobicity should be continued. The utilization of slip-length has been successful in representing the lubrication effect resulting from irregularities (roughness) on the collector surface. The practical utility of this approach now needs to be investigated at a broader range of operational conditions. Furthermore, parameters or indices that can represent not only micro-, but also macro-scale roughness are needed to incorporate the implications of complicated streamlines, straining and wedging on particle entrapment into models for particle deposition.

Existing filtration models including regression based models for single collector efficiency η can be further developed. Most of these models were developed based on fundamental assumptions that collector and particle surfaces are perfectly smooth and chemically homogenous. Surface roughness, chemical heterogeneity, and hydrophobicity have not been included in the associated model simulations. Fitting parameters such as α (attachment efficiency) have been introduced to interpret discrepancies between model predictions and experimental observations. As fundamental models develop and account for more interactions and mechanisms, these regression models should be updated and fitting

parameters should be re-examined. Further challenges to scaling-up single collector efficiency η to predict the filter efficiency λ exist; however, dispensing with unnecessarily restrictive and non-realistic assumptions is a reasonable step to advancing filtration process understanding and optimization.

Appendix A

Quality control experiments for column test

Quality control experiment was conducted in Chapter 3 to investigate if the chemical etching changed the hydrophobicity of the media surfaces, additional column tests were conducted with the media which was dipped in 1% HF acid for 30 seconds (Treatment 3). The other physical/chemical operational conditions were same as the one described in Figure 3-3. The sample collection time (time interval between two samples) was 20 seconds. As seen in Figure A-1, there were no significant differences between the microsphere deposition on the medium with Treatment 3 and the smooth medium, thereby suggesting that media surface hydrophobicity did not significantly contribute to the observed trends in particle deposition

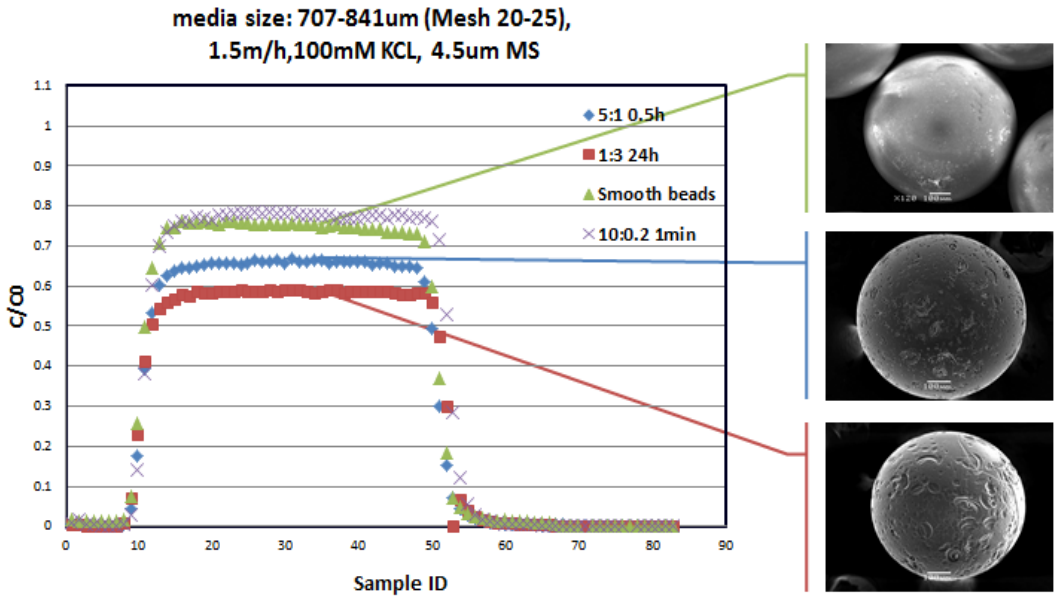

Figure A-1. Representative (a) normalized effluent 4.5 µm microsphere concentration curves for particle passage through Medium A (0.71 to 0.84 mm glass beads with porosity = 0.38) with no treatment (Treatment 0 - smooth) (■), Treatment 1 – moderately rough (▲), Treatment 2 – roughest (♦) and Treatment 3 (x).

The microsphere concentration in the effluent samples was determined by measuring UV absorbance (HP model 8453 UV-spectrophotometer) at 280 nm and 220 nm for the 4.5 μm and 1.0 μm particles respectively. The particle concentrations were then calculated using a calibration curve as shown in Figure A-2. Representative curve of the calibration curve for 4.5 μm colloidal particle was used here whose initial concentrations were ranging from 100-8000000 particle /ml. The y-axle was the detected absorbance through the samples whereas the x-axle was pre-determined particle concentration (particles/ml).

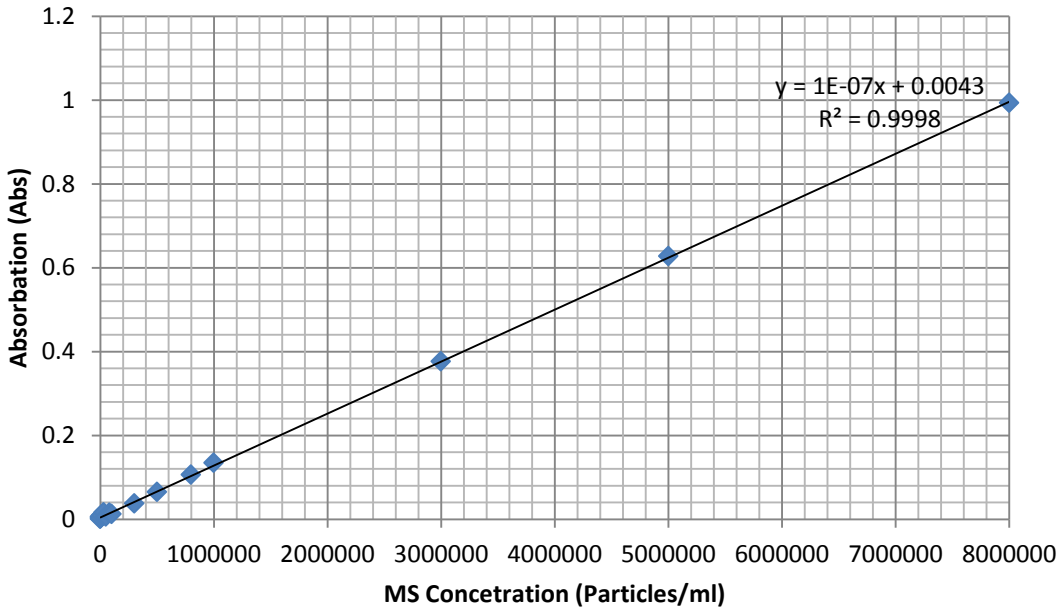

Figure A-2. Representative calibration curve using UV-spectrophotometer: colloidal particle: 4.5 μm, initial concentration: 100-8000000 particle/ ml, suspended solution: 100mM KCl, temperature: 22 ℃, detection wave length: 280 nm.

To quantitatively determine the physical propriety of modified glass beads, Mercury intrusion porosimetry (MIP) (Porous Materials, Inc.) was used to evaluate the pore volume distribution, total surface area and average pore size on the surface of the glass beads. Based on the premise that a non-wetting liquid (i.e. Mercury) will only intrude capillaries under pressure, information about the media characteristic can be determined quantitatively. The cumulative pore volume and cumulative surface area per gram for Medium A and B with all the surface modifications were presented in Figure A-3 and Figure A-4 respectively.

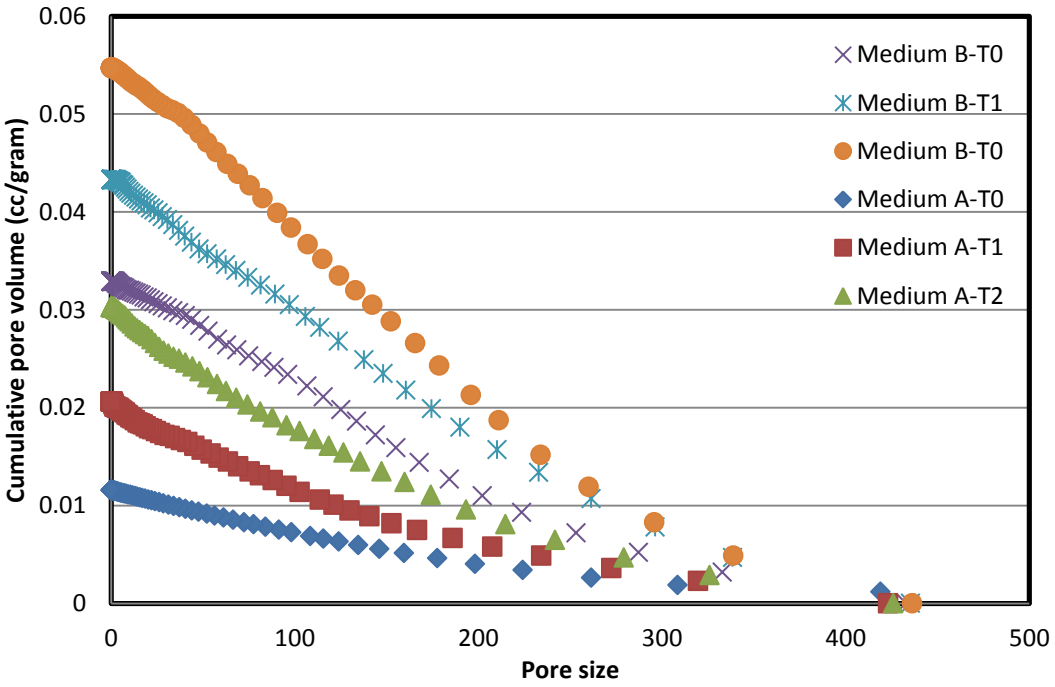

Figure A-3. Cumulative pore volume per gram for Medium A and B with all the surface modifications.

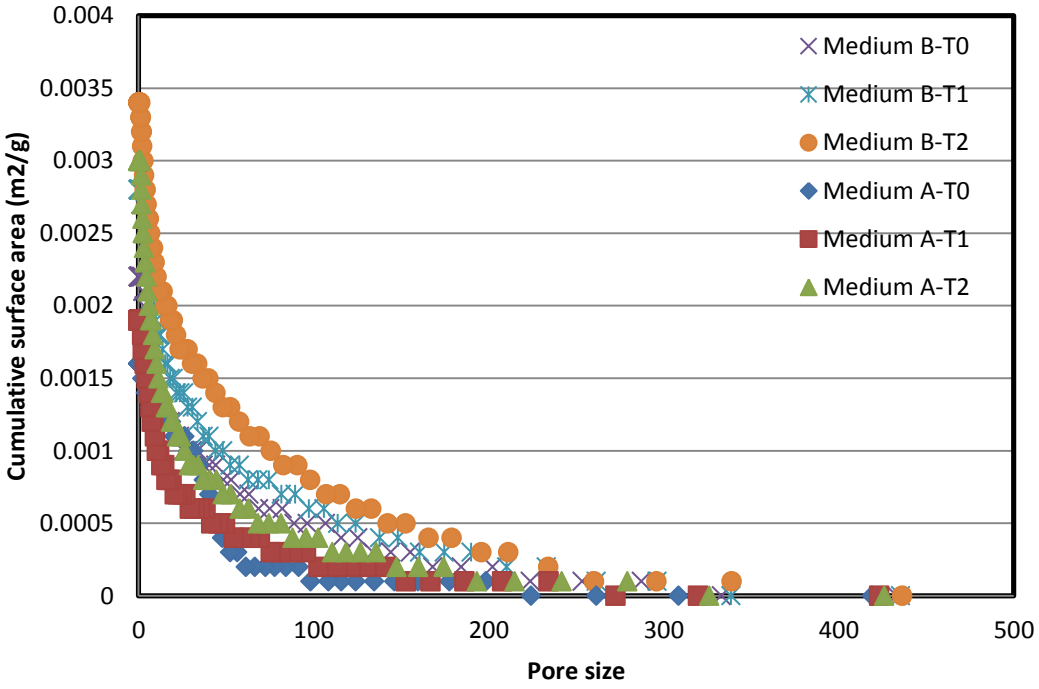

Figure A-4. Cumulative surface area per gram (m2/g) for Medium A and B with all the surface modifications.

To ensure the filtration column were packed consistently using different medium, measured by conductivity bromide concentration breakthrough curves were conducted before column test. Representative breakthrough curves were presented in Figure A-5.This figure portrays the breakthrough curves of 4 individual experiments, using different configuration such as media types and media size (Medium A-T0, Medium A-T1 Medium A-T2 and Medium A-T3).

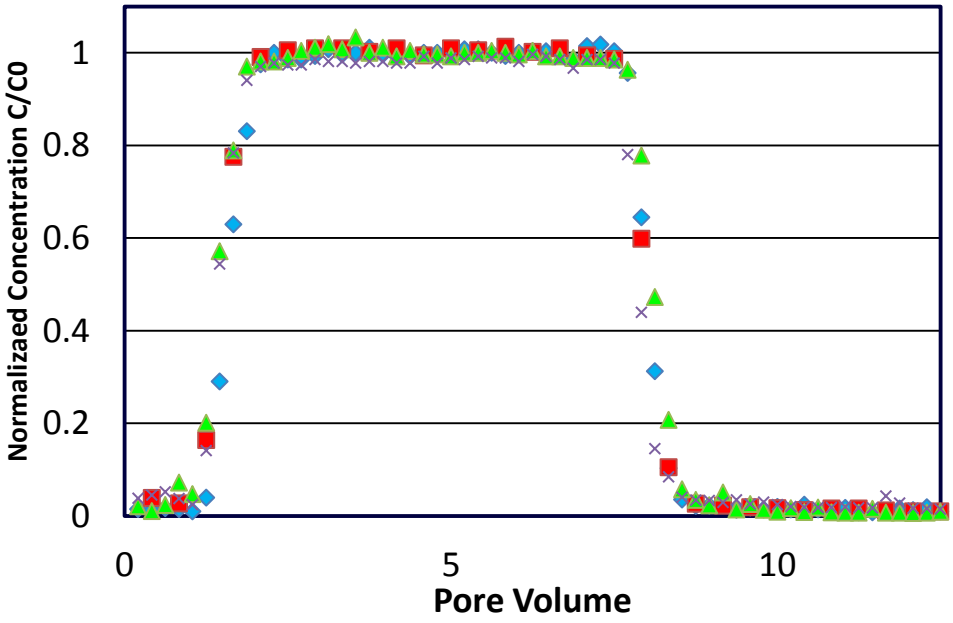

Figure A-5. Representative breakthrough curves (Treatment 0 - smooth) (■), Treatment 1 – moderately rough (▲), Treatment 2 – roughest (♦) and Treatment 3 (x).

As shown in the Figure A-5 the normalized concentration achieved a plateau after feeding about 2 pore Volume of stock. Because the inert bromide tracer is no reactive to the filter media, we assume they will barely be removed during the filtration process. This has been shown in the breakthrough curve as well because the plateau is at 1.0 which means no removal at all. The great overlap between the bromide tracer test indicted that all the column using the methods described in Chapter 3 were packed in the same manner without air trapping and preferential pathway.

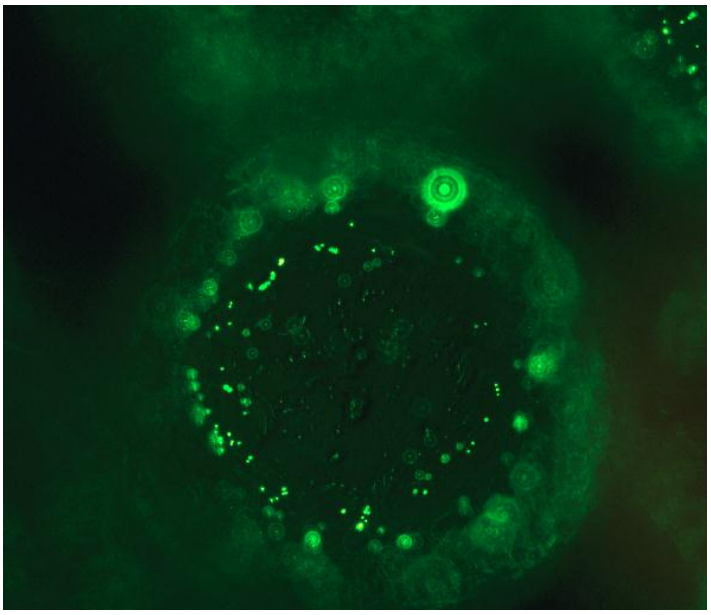

Figure A-6. Representative image of attached fluorescent particle on collector surface after column test

Table A-1. Determined experimental results: normalized concentration C/C_0 , mass recovery ratio, observed deposition rate (k_d) and attachment efficiency using Tufenkji and Elimelech's model (α) and ratio of particle size over media size. Experimental conditions are same as described in Figure 3-3.

Particle size	Experimental ID	C/C_0	Total mass retained	Mass recovery	Observed deposition rate (k_d)	Calculated TE equation	Calculated Attachment efficiency	Particle size /media size
μm		-	-	-	(s^{-1})		(α)	-
1.0	Medium A-T0-1.0	0.8729	0.0388	0.9117	0.001002	0.001115	0.706	0.001316
	Medium A-T1-1.0	0.872	0.0145	0.8865	0.0009444		0.666	0.001316
	Medium A-T2-1.0	0.955	0.0223	0.9773	0.0003284		0.232	0.001316
	Medium B-T0-1.0	0.76	0.0589	0.8189	0.002014	0.001501	0.716	0.001852
	Medium B-T1-1.0	0.966	0.0269	0.9929	0.000254		0.090	0.001852
	Medium B-T2-1.0	0.736	0.0597	0.7957	0.002249		0.800	0.001852
4.5	Medium A-T0-4.5	0.665	0.286	0.951	0.002910	0.002160	1.059	0.005921
	Medium A-T1-4.5	0.787	0.143	0.93	0.001709		0.622	0.005921
	Medium A-T2-4.5	0.485	0.55	1.035	0.005162		1.878	0.005921
	Medium B-T0-4.5	0.297	0.75	1.047	0.008907	0.003370	1.412	0.008333
	Medium B-T1-4.5	0.759	0.2198	0.9788	0.002023		0.321	0.008333
	Medium B-T2-4.5	0.179	0.80	0.979	0.012622		2.001	0.008333

Appendix B

Support information for parallel plate chamber experiments

A nano-fabrication method using CsCl self-assembly was employed to generate different roughness sizes on the quartz slide surfaces. Briefly, CsCl was evaporated at a pressure of 6 µTorr in a humid chamber and deposited onto the slide surfaces, forming isolated hemispheres by kinetic dissolution and deposition at the solid/solution boundary{{461 Green,M. 1999}}. Subsequently, the slides were exposed to air at a relative humidity of 22% and 21 ℃ for 10 minutes. The spherical shapes of thin layers of CsCl (10 nm) were used as a mask to pattern the quartz surface using reactive ion etching (RIE) with a constant etch rate of 25 nm/minute. This creates surface roughness at targeted sizes of 10 nm, 20 nm, 50 nm, 100 nm, 200 nm and 400 nm. The schematic of nano-fabrication process was presented in Figure A-7.

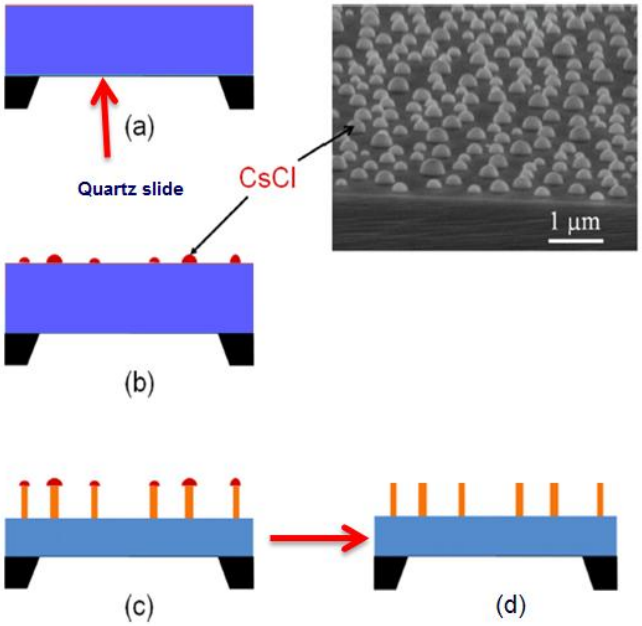

Figure A-7. Schematic process of nano- fabrication process to create target surface roughness on quartz slides, (a) slides cleaning with RCI1 method, (b) thermally evaporate CsCl film and allow it to self-assemble in the presence of moisture, (c) RIE etching to obtain traget surface roughness and (d) thoroughly cleaning

Water contact angles were measured to assess quartz slide surface hydrophobicity. The representative images for the water contact angle were shown in Figure A-8.

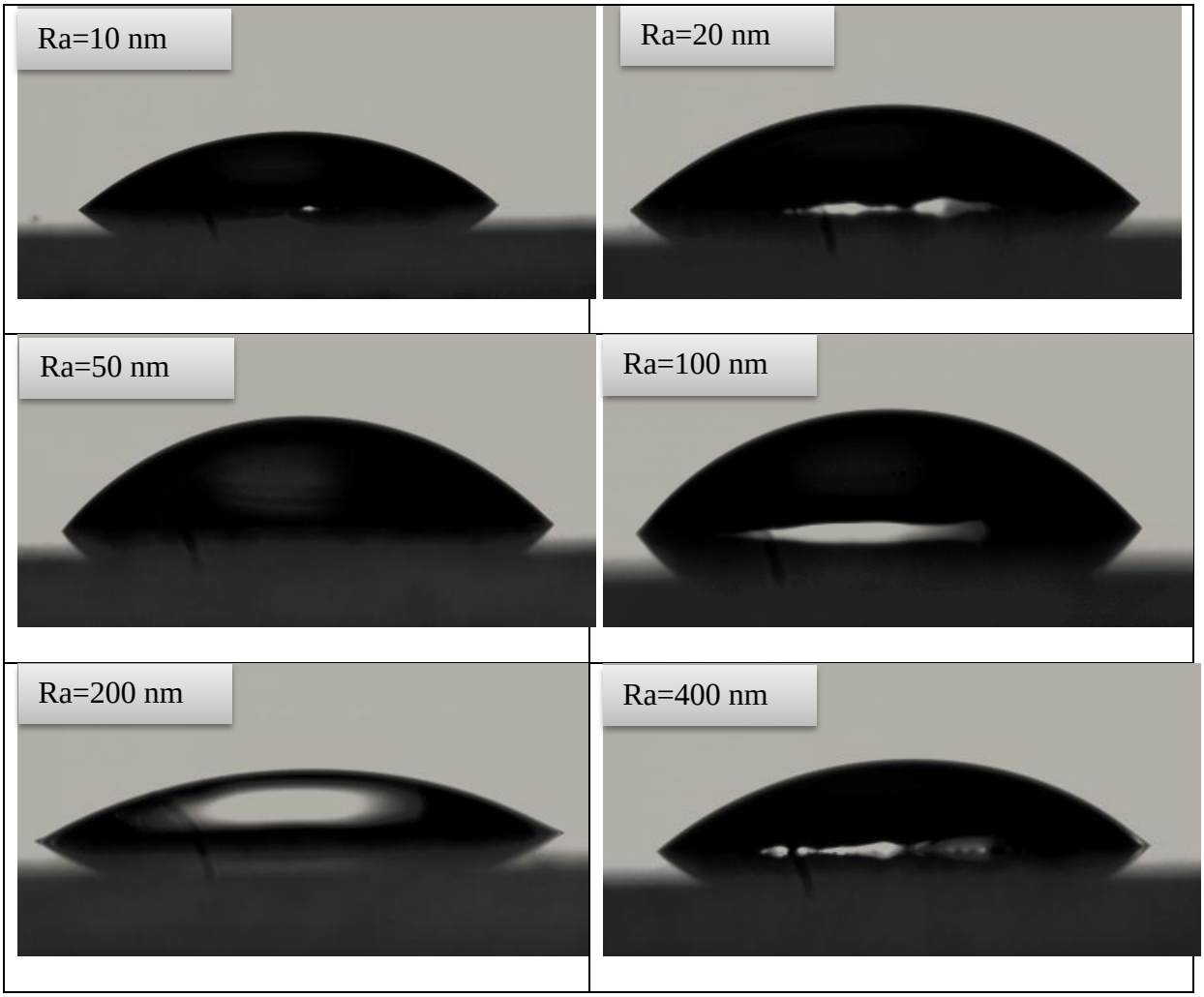

Figure A-8. The raw images of contact angle measurement for different roughness surface (10, 20, 50, 100, 200 and 400 nm), the suspended solution: 100mM KCl.

Appendix C

COMSOL simulation in parallel plate chamber

The numerical solution of the Convective-Diffusion Equation with the four boundary conditions was solved using the finite element method (FEM) in the commercial simulator COMSOL® 3.5a. Highly refined meshes were used for regions with a high concentration gradient or a large tensor of applied forces. The interfacial interactions caused by DLVO forces and the hydrodynamic retardation functions changed substantially near the bottom surface; therefore, a sub-region (Domain 1) close to the bottom surface was defined with a large number of mesh elements (250 x 600). The total number of the mesh elements employed in the simulations was 330,000; 150,000 of which were exponentially mapped within Domain 1. The interface of COMSOL with numerical solutions, variables, constant, boundary setting and subdomain setting (Domain 1 and 2) for parallel plate chamber is presented in Figure A- 9.

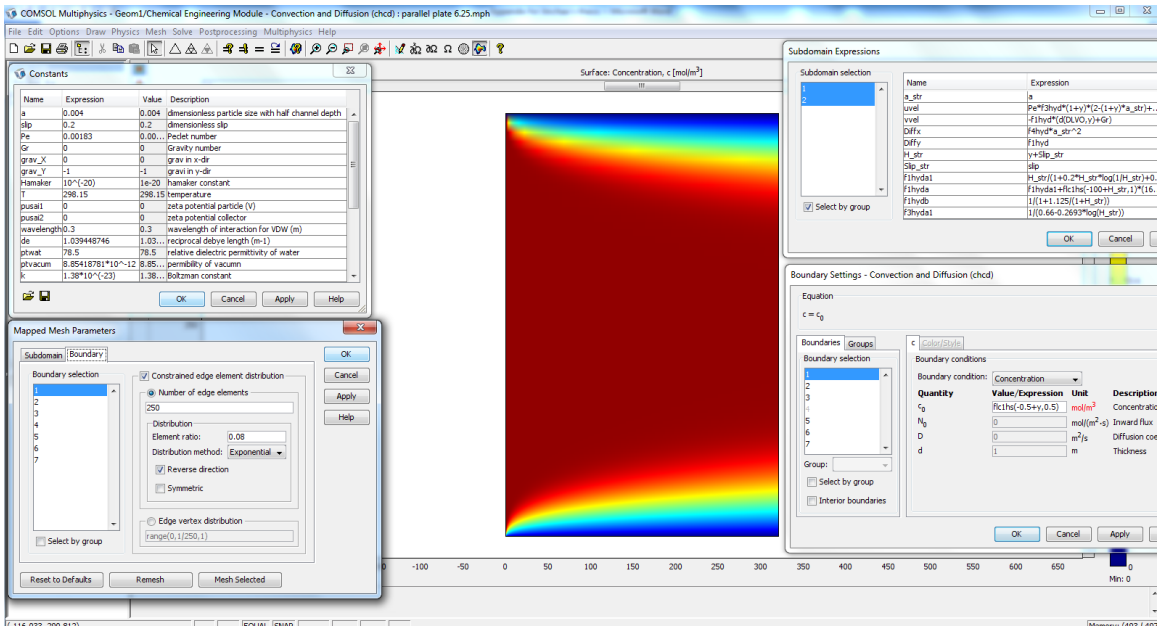

Figure A-9. The interface of COMSOL for numerical solution, constant, variable, boundary setting and subdomain setting in parallel plate chamber.

Appendix D

Derivation of Convection-Diffusion Equation in spherical geometry

The convective- diffusion equation calculation in spherical geometry:

$$\frac{\partial c}{\partial t} + \nabla \cdot J = Q$$

$$\frac{\partial c}{\partial t} + \nabla \cdot (\boldsymbol{u}C) = \nabla \cdot (D \cdot \nabla C) - \nabla \cdot \left(\frac{\boldsymbol{D} \cdot \boldsymbol{F}}{kT} C\right)$$

Application of this equation to coagulation or deposition phenomena shows that a steady is established after a short period of time. The steady state form of C-D equation will be shown as :

$$\nabla \cdot (\boldsymbol{u}C) = \nabla \cdot (D \cdot \nabla C) - \nabla \cdot \left(\frac{\boldsymbol{D} \cdot \boldsymbol{F}}{kT} C\right)$$

The particle velocity components are determined from the literatures as shown

$$u_r = f_1(H) f_2(H) v_r$$

$$u_\theta = f_3(H) v_\theta$$

The diffusion coefficient on perpendicular and tangential direction are determined as

$$D_r = f_1(H) D_\infty$$

$$D_\theta = f_4(H) D_\infty$$

The components of the convective –diffusive equations are calculated a below:

$$\nabla \cdot (\boldsymbol{u}C) = \nabla C \cdot \boldsymbol{u} + C \nabla \boldsymbol{u}$$

$$\nabla C \cdot \boldsymbol{u} = \frac{\partial c}{\partial r} u_r + \frac{\partial c}{\partial \theta} u_\theta$$

In spherical geometry:

$$C[\nabla \cdot \boldsymbol{u}] = \frac{1}{r^2}\frac{\partial}{\partial r}(r^2 u_r) + \frac{1}{r sin\theta}\frac{\partial}{\partial \theta}(sin\theta u_\theta)$$

$$= \frac{1}{r^2}\left[2r f_1(H) f_2(H) v_r + r^2 \frac{\partial f_1(H)}{\partial r} f_2(H) v_r + r^2 \frac{\partial f_2(H)}{\partial r} f_1(H) v_r \right.$$

$$\left. + r^2 f_1(H) f_2(H) \frac{\partial v_r}{\partial r}\right] + \frac{1}{r sin\theta}\left[\frac{\partial sin\theta}{\partial \theta} f_3(H) v_\theta + \frac{\partial v_\theta}{\partial \theta} sin\theta\right]$$

$$= \frac{2}{r} f_1(H) f_2(H) v_r + \frac{\partial f_1(H)}{\partial r} f_2(H) v_r + \frac{\partial f_2(H)}{\partial r} f_1(H) v_r + f_1(H) f_2(H) \frac{\partial v_r}{\partial r}$$

$$+ f_3(H) v_\theta \frac{cot\theta}{r} + \frac{1}{r} f_3(H) \frac{\partial v_\theta}{\partial \theta}$$

We also know that $v_\theta = sin\theta Y(r)$

$$\frac{\partial v_\theta}{\partial \theta} = Y(r) cos\theta = \frac{sin\theta Y(r) cos\theta}{sin\theta} = v_\theta cot\theta$$

$$f_3(H) v_\theta \frac{cot\theta}{r} + \frac{1}{r} f_3(H) \frac{\partial v_\theta}{\partial \theta} = \frac{2}{r} f_3(H) \frac{\partial v_\theta}{\partial \theta}$$

The $C[\nabla \cdot \boldsymbol{u}]$ is same as the terms derived in Elimelech, 1994.

$\nabla \cdot (D \cdot \nabla C)$ term:

$$\nabla C = \frac{\partial c}{\partial r} + \frac{\partial c}{\partial \theta}\frac{1}{r}$$

$$D \cdot \nabla C = \left[\frac{\partial c}{\partial r} f_1(H) + \frac{\partial c}{\partial \theta}\frac{1}{r} f_4(H)\right] D_\infty$$

$$\nabla \cdot (D \cdot \nabla C) = \frac{1}{r^2}\frac{\partial}{\partial r}\left(r^2 f_1(H)\frac{\partial c}{\partial r}\right) + \frac{1}{r sin\theta}\frac{\partial}{\partial \theta}\left(\frac{\partial c}{\partial \theta}\frac{1}{r} sin\theta f_4(H)\right)$$

$$= \frac{1}{r^2}\left[2r f_1(H)\frac{\partial c}{\partial r} + r^2 \frac{\partial f_1(H)}{\partial r}\frac{\partial c}{\partial r} + r^2 f_1(H)\frac{\partial^2 c}{\partial r^2}\right]$$

$$+ \frac{1}{r sin\theta}\frac{f_4(H)}{r}\left[\frac{\partial^2 c}{\partial \theta^2} sin\theta + cos\theta \frac{\partial c}{\partial \theta}\right]$$

$$= \frac{2}{r} f_1(H)\frac{\partial c}{\partial r} + \frac{\partial f_1(H)}{\partial r}\frac{\partial c}{\partial r} + f_1(H)\frac{\partial^2 c}{\partial r^2} + \frac{f_4(H)}{r^2}\frac{\partial^2 c}{\partial \theta^2} + \frac{f_4(H)}{r^2} cot\theta \frac{\partial c}{\partial \theta}$$

After comparison, the $\nabla \cdot (D \cdot \nabla C)$ is same as the terms derived in Elimelech. 1994.

$$\boldsymbol{D} = D_r + D_\theta$$

$$\boldsymbol{F} = F_r + F_\theta$$

$$\boldsymbol{D} \cdot \boldsymbol{F} = D_r F_r + D_\theta F_\theta = [f_1(H)F_r + f_4(H)F_\theta]\, D_\infty$$

$$\nabla \cdot \left(\frac{\boldsymbol{D} \cdot \boldsymbol{F}}{kT} C\right) = \nabla C \cdot \frac{\boldsymbol{D} \cdot \boldsymbol{F}}{kT} + C\nabla \cdot \frac{\boldsymbol{D} \cdot \boldsymbol{F}}{kT}$$

$$= \frac{D_\infty}{kT}\left\{\left(\frac{\partial c}{\partial r} + \frac{\partial c}{\partial \theta}\frac{1}{r}\right) \cdot (f_1(H)F_r + f_4(H)F_\theta)\right.$$

$$\left. + \boldsymbol{c}\left[\frac{1}{r^2}\frac{\partial}{\partial r}(r^2 f_1(H)F_r) + \frac{1}{r sin\theta}\frac{\partial}{\partial \theta}(sin\theta f_4(H)F_\theta)\right]\right\}$$

$$= \frac{D_\infty}{kT}\left\{\left[f_1(H)F_r\frac{\partial c}{\partial r} + f_4(H)F_\theta\frac{\partial c}{\partial \theta}\frac{1}{r}\right]\right.$$

$$+ \boldsymbol{c}\left[\frac{1}{r}2f_1(H)F_r + r^2\frac{\partial f_1(H)}{\partial r}F_r + r^2 f_1(H)\frac{\partial F_r}{\partial r}\right.$$

$$\left.\left. + \frac{1}{sin\theta}\frac{f_4(H)}{r}\left(\frac{\partial F_\theta}{\partial \theta}sin\theta + F_\theta cos\theta\right)\right]\right\}$$

$$= \frac{D_\infty}{kT}\left\{\left[f_1(H)F_r\frac{\partial c}{\partial r} + f_4(H)F_\theta\frac{\partial c}{\partial \theta}\frac{1}{r}\right]\right.$$

$$\left. + \boldsymbol{c}\left[\frac{2}{r}f_1(H)F_r + \frac{\partial f_1(H)}{\partial r}F_r + f_1(H)\frac{\partial F_r}{\partial r} + \frac{f_4(H)}{r}\frac{\partial F_\theta}{\partial \theta} + \frac{f_4(H)}{r}cot\theta F_\theta\right]\right\}$$

The $\nabla \cdot \left(\frac{\boldsymbol{D} \cdot \boldsymbol{F}}{kT} C\right)$ is same as the term derived in Elimelech, 1994

To make the equation dimensionless, we should notice that

$$r = a_c + a_p + y = r = a_c + a_p + Ha_p$$

Where a_c is the collector size, a_p is the particle diameter, y is the distance between particle surface to collector surface. To conduct the numerical simulation, several dimensionless groups have been introduced below to convert the Convective-Diffusion equation into the dimensionless form:

$$dr = a_p dH$$

$$v_\theta = \frac{1}{rsin\theta}\frac{\partial \varphi}{\partial r}$$

$$v_r = \frac{-1}{r^2 sin\theta}\frac{\partial \varphi}{\partial \theta}$$

$$N_R = \frac{a_p}{r}$$

$$V_r = \frac{v_r}{U}$$

$$V_\theta = \frac{v_\theta}{U}$$

$$N_{Pe} = \frac{2Ua_p}{D_\infty}$$

$$F_G^* = \frac{F_G a_p}{kT}$$

By doing the dimensionless transformation, the convective- diffusion equation could be written as following:

$$\nabla \cdot (\boldsymbol{u}C) = \frac{U}{a_p}\{\frac{\partial c}{\partial H} f_1(H) f_2(H) V_r + \frac{\partial c}{\partial \theta} \frac{f_3(H) V_\theta}{H + \frac{a_c + a_p}{a_p}}$$

$$+ \left[\frac{2}{H + \frac{a_c + a_p}{a_p}} f_1(H) f_2(H) V_r + \frac{\partial f_1(H)}{\partial H} f_2(H) V_r + \frac{\partial f_2(H)}{\partial H} f_1(H) V_r \right.$$

$$\left. + f_1(H) f_2(H) \frac{\partial V_r}{\partial H} + \frac{2}{H + \frac{a_c + a_p}{a_p}} f_3(H) cot\theta V_\theta \right] C\}$$

$$\nabla \cdot (D \cdot \nabla C) = \frac{D_\infty}{a_p^2}\{\frac{2}{H + \frac{a_c + a_p}{a_p}} f_1(H) \frac{\partial c}{\partial H} + \frac{\partial f_1(H)}{\partial H} \frac{\partial c}{\partial H} + f_1(H) \frac{\partial^2 c}{\partial H^2}$$

$$+ \frac{f_4(H)}{(H + \frac{a_c + a_p}{a_p})^2} \frac{\partial^2 c}{\partial \theta^2} + \frac{f_4(H)}{(H + \frac{a_c + a_p}{a_p})^2} cot\theta \frac{\partial c}{\partial \theta}\}$$

$$\nabla \cdot \left(\frac{\boldsymbol{D} \cdot \boldsymbol{F}}{kT} C \right) = \frac{D_\infty}{a_p^2 kT}\{f_1(H) \left(\frac{\partial \varphi}{\partial H} + F_G^* cos\theta \right) \frac{\partial c}{\partial H} - f_4(H) F_G^* sin\theta \frac{\partial c}{\partial \theta} \frac{1}{H + \frac{a_c + a_p}{a_p}}$$

$$+ \boldsymbol{c} \left[- \left(\frac{2}{H + \frac{a_c + a_p}{a_p}} f_1(H) + \frac{\partial f_1(H)}{\partial H} \right) \left(\frac{\partial \varphi}{\partial H} + F_G^* cos\theta \right) - f_1(H) \frac{\partial^2 \varphi}{\partial H^2} \right.$$

$$\left. - \frac{f_1(H) \partial F_G^* cos\theta}{\partial H} + \frac{2 f_4(H)}{H + \frac{a_c + a_p}{a_p}} cos\theta F_G^* \right]\}$$

Using all these variables, the particle transportation equation can be written as

$$\frac{N_{Pe}}{2}\left\{\frac{\partial c}{\partial H}f_1(H)f_2(H)V_r+\frac{\partial c}{\partial \theta}f_3(H)V_\theta N_R\right.$$
$$+\left[2N_R f_1(H)f_2(H)V_r+\frac{\partial f_1(H)}{\partial H}f_2(H)V_r+\frac{\partial f_2(H)}{\partial H}f_1(H)V_r\right.$$
$$\left.\left.+f_1(H)f_2(H)\frac{\partial V_r}{\partial H}+2N_R f_3(H)cot\theta V_\theta\right]C\right\}$$
$$=2N_R f_1(H)\frac{\partial c}{\partial H}+\frac{\partial f_1(H)}{\partial H}\frac{\partial c}{\partial H}+f_1(H)\frac{\partial^2 c}{\partial H^2}+{N_R}^2 f_4(H)\frac{\partial^2 c}{\partial \theta^2}$$
$$+{N_R}^2 f_4(H)cot\theta\frac{\partial c}{\partial \theta}+f_1(H)\left(\frac{\partial \varphi}{\partial H}+F_G^* cos\theta\right)\frac{\partial c}{\partial H}-f_4(H)F_G^* sin\theta\frac{\partial c}{\partial \theta}N_R$$
$$+\boldsymbol{c}\left[\left(2N_R f_1(H)+\frac{\partial f_1(H)}{\partial H}\right)\left(\frac{\partial \varphi}{\partial H}+F_G^* cos\theta\right)+f_1(H)\frac{\partial^2 \varphi}{\partial H^2}+\frac{f_1(H)\partial F_G^* cos\theta}{\partial H}\right.$$
$$\left.-2f_4(H)N_R cos\theta F_G^*\right]$$

The terms in the equation labeled as RED in the equation above are the terms which have been assumed to be 0.

To implement the C-D equation into COMSOl simulation within rectangular domain, the equation can be re-written as following:

$$\frac{\partial c}{\partial \theta}\left\{{N_R}^2 f_4(H)\frac{\partial c}{\partial \theta} + {N_R}^2 f_4(H)cot\theta - f_4(H)F_G^* sin\theta N_R - \frac{N_{Pe}}{2} f_3(H)V_\theta N_R\right\}$$

$$+\frac{\partial c}{\partial H}\left\{f_1(H)\frac{\partial c}{\partial H}\right.$$

$$\left.+\left[2N_R f_1(H) + \frac{\partial f_1(H)}{\partial H} + f_1(H)\left(\frac{\partial \varphi}{\partial H} + F_G^* cos\theta\right) - f_1(H)f_2(H)V_r\frac{N_{Pe}}{2}\right]\right\}$$

$$= \boldsymbol{c}\{\left[\left(2N_R f_1(H) + \frac{\partial f_1(H)}{\partial H}\right)\left(\frac{\partial \varphi}{\partial H} + F_G^* cos\theta\right) + f_1(H)\frac{\partial^2 \varphi}{\partial H^2}\right.$$

$$\left.+\frac{f_1(H)\partial F_G^* cos\theta}{\partial H} - 2f_4(H)N_R cos\theta F_G^*\right]$$

$$-\frac{N_{Pe}}{2}\left[2N_R f_1(H)f_2(H)V_r + \frac{\partial f_1(H)}{\partial H}f_2(H)V_r + \frac{\partial f_2(H)}{\partial H}f_1(H)V_r\right.$$

$$\left.+ f_1(H)f_2(H)\frac{\partial V_r}{\partial H} + 2N_R f_3(H)cot\theta V_\theta\right]\}$$

$$J^*(H,\theta) = -\frac{2f_1(H)}{N_{Pe}}\frac{\partial c}{\partial H} + f_1(H)f_2(H)V_r c - \frac{2f_1(H)}{N_{Pe}}[\frac{\partial \varphi}{\partial H} + F_G^* cos\theta]c$$

where boundary conditions of

C (H=0,θ)=0

C (H~∞,θ)=1

$$(\frac{\partial c}{\partial \theta})_{\theta=0} = 0$$

have been suggested (Elimelech, 1994); however, different boundary conditions were used for these simulations (Jin et al., 2014).

Note: more realistic boundary should be applied when the Peclect number are small (Elimelech 1992)

$$v_r C - D_r\frac{\partial C}{\partial r} = -UC_0 cos\theta \; at \; r = b, 0 \le \theta \le 0.5\pi$$

$$\frac{\partial C}{\partial r} = 0 \;\; at \; r = b, 0.5\pi \le \theta \le \pi$$

The new boundary conditions are continuous over the entire out boundary.

$$\lim_{\theta \to 0.5\pi} \frac{\partial C}{\partial r} = \lim_{\theta \to 0.5\pi} \left[\frac{U}{D_r} (C_0 - C) cos\theta \right] = 0$$

The local dimensionless flux is

$$J^*(H, \theta) = -\frac{2f_1(H)}{N_{Pe}} \frac{\partial c}{\partial H} + f_1(H) f_2(H) V_r c - \frac{2f_1(H)}{N_{Pe}} [\frac{\partial \varphi}{\partial H} + F_G^* cos\theta] c$$

The overall rate of particle deposition I can be expressed as

$$I = 2\pi r^2 \int_0^{\pi} J(H \to 0, \theta) sin\theta d\theta$$

The single collector efficiency is defined as

$$\eta = \frac{I}{\pi a_c^2 UC}$$

Table A- 2. Dimensionless groups and parameters used in the Convection-Diffusion Equation

Dimensionless group	*Expression*
Actual center-to-center distance between particle and collector	$r = a_c + a_p + y = r = a_c + a_p + Ha_p$
Radial velocity component of colloidal particle	$v_r = \frac{-1}{r^2 sin\theta}\frac{\partial \psi}{\partial \theta}$
Tangential velocity component of colloidal particle	$v_\theta = \frac{1}{r sin\theta}\frac{\partial \psi}{\partial r}$
Scaled surface-to-surface distance for h	$H = h / a_p$
Scaled particle ratio	$N_R = \frac{a_p}{r}$
Scaled radial velocity component of colloidal particle	$V_r = \frac{v_r}{U}$
Scaled tangential velocity component of colloidal particle	$V_\theta = \frac{v_\theta}{U}$
Peclet number	$N_{Pe} = \frac{2Ua_p}{D_\infty}$
Scaled gravity force	$F_G^* = \frac{F_G a_p}{kT}$
Scaled interaction energy	$\Phi = \frac{\varphi}{k_B T}$

Particle deposition flux. When the dimensionless particle concentration is determined, the particle flux perpendicular to the collector surface can be calculated. The prefect sink boundary condition was applied to the bottom surface where the approaching particle was simultaneously regarded as attached to the collector surface and removed from the simulation domain. To avoid the nonphysical divergence of DLVO forces, a cut-off separation distance (δ) was utilized to implement the perfect sink boundary condition (Jin et al) and set the concentration equal to zero such that

$$c^*\big|_{H=\delta} = 0$$

With consideration of external forces (e.g., gravity and buoyancy, shear lift force, electrostatic double layer force, and van der Waals forces), the non-dimensionless deposition flux at the collector surface can be evaluated as

$$j_r = -D_r \frac{\partial c}{\partial r} + u_r c + \frac{D_r F_r}{k_b T} c$$

To implement the prefect sink boundary conditions, the particle concentration was forced to zero when the H was set as zero ($c^* = 0$ when $H = 0$). To avoid mathematical singularity, a very small number (e.g. an arbitrary value of $2*10^{-5}$) rather than zero was utilized. The dimensionless flux of particles to the surface (J^*) was calculated at the primary interaction energy minimum of a cut-off distance δ by

$$J^*(H_\delta, \theta) = -\frac{2 f_1(H_\delta)}{N_{Pe}} \frac{\partial c}{\partial H} + f_1(H_\delta) f_2(H_\delta) V_r c - \frac{2 f_1(H_\delta)}{N_{Pe}} [\frac{\partial \varphi}{\partial H} + F_G^* cos\theta] c \quad \text{at } H = \delta$$

where the $J^*(H_\delta, \theta)$ is the dimensionless particle deposition flux, normalized as

$$J(H, \theta) = J^*(H_\delta, \theta) U c$$

The overall particle deposition flux perpendicular to the collector surface was integrated over the entire surface (0-2π) to evaluate the total rate of particle contact with a single collector (I), which is described by

$$I = 2\pi (r + \delta)^2 U c \int_0^\pi J^*(H_\delta \to 0, \theta) sin\theta d\theta$$

The total rate of particle contact with a single collector (I) divided by the rate of particle flow toward the projected area of the collector is the overall contact efficiency or single collector efficiency (η) and is defined as

$$\eta = \frac{I}{\pi a_c^2 U c}$$

When diffusion is the dominant mechanism of particle transport to the collector surface, the single collector efficiency can be described[13] analytically as

$$\eta_D = 4.0 * A_s^{1/3} (\frac{D_\infty}{2 U a_c})^{2/3}$$

where As is a porosity-dependent parameter defined as

$$A_s = 2(1 - p^5) / w$$

Total forces. Numerical solution required determination of the net-external forces on the approaching particle. In the present study, only the initial deposition stage (i.e., clean bed deposition) was evaluated; therefore, particle-particle and blocking impacts were negligible. The net radial force on the particle (F_{Total}) included the component of gravity, attractive van der Waals (VDW) forces, and repulsive electrostatic double layer (EDL) force between the particle and collector surface (bottom surface and roughness elements). It can be represented as

$$F_{Total} = F_{VDW} + F_{EDL} + F_G$$

where F_{VDW} and F_{EDL} represented VDW and EDL forces between the approaching particle and rough surface. The net VDW and EDL forces are commonly referred to as DLVO forces. F_G represents gravity. When roughness is commonly present on the target surface, the DLVO force component may be modified.

Flow field determination. For creeping flow of an incompressible fluid at steady state, the fluid velocity field can be determined in spherical coordinates by the following boundary conditions

$$E^4\psi = 0$$

$$V_r = 0 \qquad \text{when } r = a_c + b$$

$$\mu\left(\frac{\partial V_r}{r\partial\theta} + \frac{\partial V_\theta}{\partial V_r} - \frac{V_\theta}{r}\right) = 0 \qquad \text{when } r = a_c + b \qquad \textbf{)}$$

where r is the center-to-center distance between the approaching particle and collector, V_r and V_θ are the radial and tangential velocity components respectively, and ψ is the stream function. The radial and tangential flow field velocities can be respectively described as

$$v_r = \frac{-1}{r^2 sin\theta}\frac{\partial\psi}{\partial\theta}$$

$$v_\theta = \frac{1}{rsin\theta}\frac{\partial\psi}{\partial r}$$

Applying no-slip boundary conditions on the collector surface, the analytical solution for the stream function can be written as

$$\psi = A\left[k_1\left(\frac{a_c}{r}\right) + k_2\left(\frac{r}{a_c}\right) + k_3\left(\frac{r}{a_c}\right)^2 + k_4\left(\frac{r}{a_c}\right)^3\right]$$

where

$$A = Ua_c^{\,2}/2$$

$$p = a_c/b = (1-\varepsilon)^{1/3}$$

$$w = 2 - 3p + 3p^5 - 2p^6$$

$$k_1 = 1/w$$

$$k_2 = -(3+2p^5)/w$$

$$k_3 = (2+3p^5)/w$$

$$k_4 = -p^5/w$$

The stream function is only valid within the envelope of Happel's sphere cell with thickness (*b*) described.

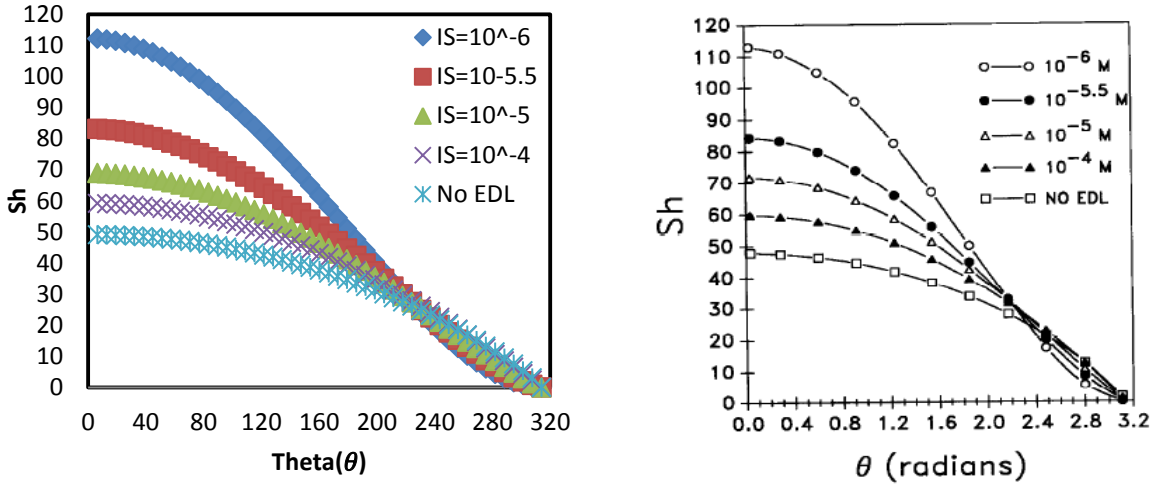

Figure A- 10. Dimensionless particle deposition flux (*Sh*) as a function of radial location on a spherical collector at a loading rate of 10^{-5} m/s. The figure on the right denotes previously reported values of *Sh* calculated by Elimelech and Song (1998). The symbols on the left represent the numerical solution of the Convective-Diffusion equation obtained using Equation 2.

Appendix E
COMSOL simulation in spherical geometry

The numerical solution of Equation 6-3 to 6-6 with all the boundary conditions was solved by finite element method using a commercial simulator COMSOL 3.5a (COMOSL, Inc, Canada). The simulation domain was discretized using quadrilateral meshing. For a good accuracy of the numerical solution, highly refined meshes were required at the regions with high concentration gradient or large tensor of applied forces. a sub-region (Domain 1) close to the bottom surface was defined and meshed by larger numbers of meshing element to guarantee good accuracy. Neumann boundary conditions were applied on the boundaries of Domain 1and 2 according to Equation 6-4 and 6-9.Typical meshing map is presented in Figure A-11 and representative result of particle concentration in the simulation domain is presented in Figure A-12.

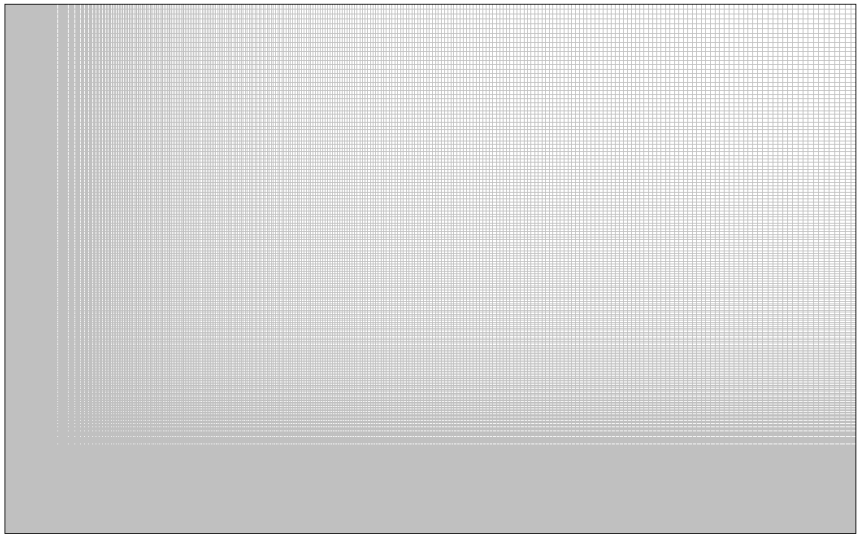

Figure A-11. Typical simulation domain after meshing in COMSOL for spherical geometry

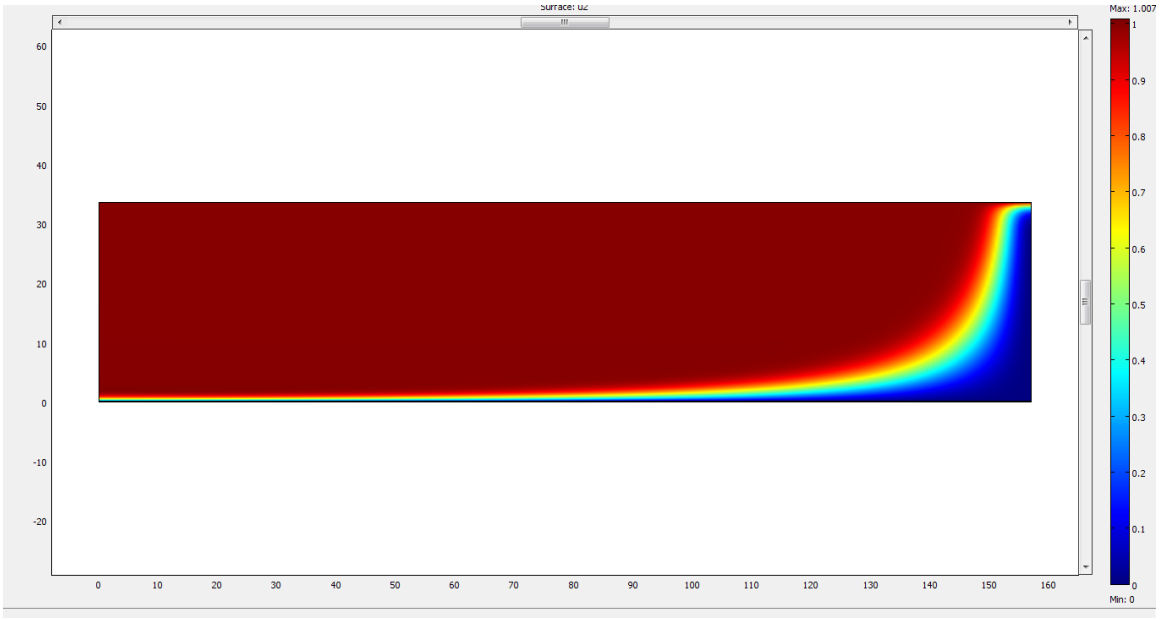

Figure A-12. Representative solution of particle deposition in spherical geometry. Parameters used in this figure are same as the one used in Figure 6-10.